



**UNIVERSIDAD DE CHILE  
FACULTAD DE CIENCIAS FÍSICAS Y MATEMÁTICAS  
DEPARTAMENTO DE GEOLOGÍA**

**PALEO-TERMOMETRÍA Y EVOLUCIÓN DEL SISTEMA HIDROLÓGICO DEL  
PARQUE NACIONAL TORRES DEL PAINE, PATAGONIA.**

**TESIS PARA OPTAR AL GRADO DE DOCTOR EN  
CIENCIAS MENCIÓN GEOLOGÍA**

**MARCELO ALBERTO SOLARI CORVALAN**

**PROFESOR GUÍA:  
FRANCISCO HERVE ALLAMAND**

**MIEMBROS DE LA COMISION:**

**GABRIEL VARGAS EASTON  
JACOBUS LE ROUX  
ALCIDES NOBREGA SIAL  
CLAUDIO LATORRE HIDALGO**

**SANTIAGO DE CHILE  
NOVIEMBRE 2010**

Resumen de la Tesis  
para optar al grado de  
Doctor en Ciencias Mención Geología.  
Por: Marcelo Alberto Solari Corvalán.  
Fecha de Examen: 05-11-2010  
Prof. Guía Sr. Francisco Herve

## PALEO-TERMOMETRÍA Y EVOLUCIÓN DEL SISTEMA HIDROLÓGICO DEL PARQUE NACIONAL TORRES DEL PAINE, PATAGONIA

Un conjunto de complejos morrénicos se distribuyen desde el margen este de la Cuenca de Drenaje de Torres del Paine hasta las cercanías del margen actual de los Campos de Hielo Patagónicos. Regionalmente se reconocen en el paisaje un conjunto de terrazas lacustres vinculadas a las fluctuaciones glaciares. Las evidencias geomorfológicas y sedimentarias lacustres encontradas apoyan la existencia de un único lago proglacial denominado en el presente estudio como Gran Paleo-Lago Tehuelche (GPT), mejoran la cronología de los eventos glaciares y permiten una comprensión de la evolución del sistema hidrológico de Torres del Paine.

Los avances glaciares previamente denominados por Marden (1993) como A, B y C, se desarrollaron durante el Último Máximo Glacial y alimentaron al GPT con aguas de fusión, permitiéndole al lago alcanzar su mayor extensión y altitud. El hallazgo de trombolitos en Laguna Amarga fue clave para determinar que el desagüe del GPT hacia el Seno de Última Esperanza se produjo hace 7110 años calibrados antes del presente (años cal AP) producto de la fusión de una gran barrera glacial existente durante el avance E, que posteriormente dio paso al complejo sistema hidrológico de ríos y lagos existente. Para dicho período, se proponen condiciones de mayor aridez en el sector de Laguna Amarga debido al descenso en las precipitaciones. Desde otra perspectiva, la temporalidad del avance E sumado a otras evidencias encontradas en Patagonia por otros investigadores, hacen referencia de un evento frío en Patagonia durante el Holoceno temprano. Mayores estudios deben realizarse en Patagonia para dilucidar si existe una relación con el evento frío ampliamente descrito en el Hemisferio Norte entre 8000 y 9000 años AP.

La regresión fría registrada en la Región de los Lagos (11.8-13.2 ka AP) respecto a los eventos de inversión fríos sincrónicos en Antártica y Torres del Paine (12.6-14.8 ka AP), se pueden explicar por la modulación de los Vientos Predominantes del Oeste (VPO) causada por el reforzamiento de los Vientos Tropicales del Este/ENSO y por la expansión hacia el norte de la celda atmosférica de Bajas Presiones Subpolar. Esta hipótesis muy preliminar busca recalcar la necesidad de comprender sobre la base de registros paleoclimáticos los reajustes espaciales y temporales de las diferentes células atmosféricas y la circulación oceánica, y con ello conceptualizar y modelar como la atmósfera y los océanos se comportan e interactúan frente a la una renovada teoría de forzamiento orbital propuesta por Davis y Bewer el año 2009.

Con posterioridad al desagüe del GPT, Lago Sarmiento y Laguna Amarga se transforman en cuencas endorreicas en las cuales se observan terrazas lacustres locales, las que entregan nuevas evidencias y aportan un conjunto de resultados de importancia paleoclimática regional.

Lago Sarmiento y Laguna Amarga actualmente están localizados al este de una de las mayores sombras orográficas de precipitaciones del mundo, generada al este del Campo de Hielo Patagónico Sur. Grandes colonias de trombolitos están presentes en Lago Sarmiento, mientras que extensas colonias de estromatolitos están presentes en Laguna Amarga. Basados en las características del sistema hidrológico de ambas cuencas, en conjunto con la estimación del balance isotópico y el análisis de las condiciones de equilibrio entre el agua y los carbonatos biológicamente inducidos, se concluyó que las microbialitas de Lago Sarmiento presentan mejores condiciones que Laguna Amarga para ser utilizadas como indicadores de paleo-temperaturas. Los trombolitos de Lago Sarmiento presentan una única especie mineral la cual precipita cerca de las condiciones de equilibrio isotópico y la variación de la temperatura controla el fraccionamiento isotópico de oxígeno en el lago. En los trombolitos se observan con claridad cuatro niveles lacustres, en los cuales fue posible cuantificar la temperatura:

- Hace 1215 años cal AP el nivel del lago fue 85 m s.n.m con una temperatura cercana a 9,3°C, y hace 600 Cal años AP el nivel descendió a 82 m s.n.m con una temperatura cercana a los 8,5°C. Estos períodos cálidos en el lago coinciden temporalmente con el Periodo Cálido Medieval (1200 a 800 años Cal AP) registrado ampliamente en el Hemisferio Norte, pero mayor cantidad de evidencias regionales son necesarias para establecer una correlación.
- Hace 183 años cal AP el nivel del lago fue de 80 m s.n.m con una temperatura de 7,7°C, representando un periodo de menor temperatura del lago coincidente con la Pequeña Edad de Hielo.
- La superficie de Lago Sarmiento disminuyó entre 1986 y 1999 debido a cambios en los patrones de precipitación y evaporación. Estos se relacionan probablemente con uno de los efectos del cambio climático detectado en el calentamiento troposférico al sur de Sudamérica en las últimas décadas, lo cual se asocia a la disminución de casi la totalidad de los grandes glaciares en los Campos de Hielo Patagónicos.

Un resultado importante de la tesis fue que la señal de  $\delta^{13}\text{C}$  en carbonatos es una herramienta efectiva para distinguir el proceso que produce su precipitación. Valores negativos de  $\delta^{13}\text{C}_{\text{VPDB}}$  son característicos de la precipitación inorgánica y valores positivos son característicos de la precipitación biológicamente inducida.

## AGRADECIMIENTOS

Mis agradecimientos a la Comisión Nacional de Investigación y Tecnología (CONICYT) por el financiamiento del presente estudio y por el apoyo parcial a los proyectos. En adición, deseo dar las gracias a A. Prieto quien realizó la importante recolección de muestras de agua en Lago Sarmiento financiado por el Proyecto FONDECYT 1070709: “Geological Connection between the Antarctic Peninsula and Patagonia” (ARTG-04) y “Geological and Paleontological Evolution of the Magellan and Larsen Basin, during the Mesozoic and Cenozoic” (ACT-105) financiados por el *Programa Bicentenario de Ciencia y Tecnología* (PBCT) de CONICYT y el *Instituto Antártico Chileno* (INACH) y liderados por la Doctora T. Torres. Agradezco particularmente a A. Airo por invitarme a participar en la campaña de terreno del año 2004, financiada por “National Science Foundation” de los Estados Unidos de America, en la cual el azar iniciado por mi zapato atrapado en el lodo me llevó a descubrir los estromatolitos de Laguna Amarga. Muchas gracias también al Laboratorio del Servicio Nacional de Geología y Minería (SERNAGEOMIN) y al Laboratorio de Difracción de Rayos X del Departamento de Física de la Universidad de Chile, por el apoyo analítico. Mi sincera gratitud a la Corporación Nacional Forestal (CONAF), por el soporte de terreno. Mi admiración para los guardaparques del Parque Nacional Torres del Paine, por la ayuda, las enseñanzas y su generosidad. Mis reconocimientos a mis compañeros de doctorado, con quienes compartí el aprendizaje de las aulas, los terrenos, la cotidianidad de la convivencia y muchísimas alegrías y experiencias de vida. Agradezco a Cristina Maureira por el apoyo y guía constante durante el doctorado. Gracias a J. Martinez por acogerme, y apoyarme en la investigación de los estromatolitos. Agradezco a los pasillos del Departamento de Geología y a la paciencia de los profesores por atender mis cuestionamientos e inquietudes, a Katja Deckart por ayudarme a construir las ecuaciones isotópicas y a Carlos Palacios por las frecuentes conversaciones científicas en temas de vinculados a la geobiología. Mi gratitud al Profesor Jacobus Le Roux y a Gonzalo Huerta por las enseñanzas y apoyo en terreno. Agradezco al Profesor Alcides Sial por su confianza en el presente estudio, por sus enseñanzas isotópicas y por acogerme en el laboratorio NEG-LABISE de la Universidad Federal de Pernambuco. Agradezco la guía de Francisco Hervé, la temeridad de creer en mis nuevas ideas doctorales, luego del periplo que viví en las cercanías del Faro Evangelista, las enseñanzas sobre la geología Antártica y Patagónica, el compartir su pasión por la naturaleza, la vida y el valor de la amistad. Por sobre todo, agradezco a mi compañera, amiga y esposa Daniella N., quien apoyó, compartió y se comprometió con la travesía de esta investigación, caminamos juntos en terreno y ahora caminamos junto a nuestro hijo por la vida. Gracias querida familia por entregarme el tiempo, paciencia y fuerza para finalizar mi tesis.

## **Cronología de publicaciones relacionadas a la tesis**

- Solari M. 2004. In the search of a paleoclimatic reconstruction between Antarctic Peninsula and Chilean Patagonia. Actas V Reunión de Investigación Antártica. Santiago de Chile, Octubre 2004. Comité Nacional de Investigaciones Antárticas.
- Solari M., Hervé F., and Martínez J., 2004. The presence of living stromatolites at Laguna Amarga, Torres del Paine National Park, Southernmost Chile. November 2004 GSA Denver Annual Meeting in Denver, Colorado, USA.
- Solari M., and Hervé F. 2005. The presence of living microbialites at Torres del Paine National Park, southernmost Chile. 9th INTERNATIONAL SYMPOSIUM ON BIOMINERALIZATION "From Paleontology to Materials Science", 6 - 9 December 2005 in Pucon, Chile.
- Solari, M., Airo A., Hervé F., Sial A.N. 2006. Avances en el estudio de la evolución paleo climática, lacustre y glacial, Torres del Paine, Patagonia, Chile. XI Congreso Geológico Chileno, Antofagasta, 7 al 11 de Agosto de 2006.
- Solari, M., Airo A., Hervé F., Sial A.N. 2006. Avances en el estudio de la evolución paleo climática, lacustre y glacial, Torres del Paine, Patagonia, Chile. II Simposio Latinoamericano Sobre Investigaciones Antárticas y VI Reunión Chilena de Investigación. Antártica, Concepción, 16 al 18 de agosto de 2006.
- Hervé H., Solari M., Hervé D. 2006. Towards the creation of Geoparks in Chile: present and future efforts. II seminario de "Minería y Monumentos Nacionales: Patrimonio Arqueológico, paleontológico e Histórico. Santiago, Chile, Septiembre 2006.
- Solari M., Le Roux J., and Huerta G., 2007. Sub-glacial deformation of lacustrine sediments and moraine at "El Canal" in the vicinity of Torres del Paine, Chile. Geosur 2007, An International Congress on the Geology and Geophysics of the Southern Hemisphere. Santiago de Chile, November 18-20 of 2007.
- Solari M., Airo A. 2007. Glacio lacustrine evolution and modern microbialites at Lago Sarmiento, del Toro and Laguna Amarga. Capitulo 3 en: the Field Trip Guide of the International Geological Congress on the Southern Hemisphere Punta Arenas, Chile 21/25 November 2007.
- Solari M. 2008. La importancia de comprender el registro climático en Sudamérica. Ecoengen. Revista de Medio Ambiente – FACEA UCENTRAL. N° 9. ISSN 0718-0454.
- Solari M.A., Hervé F, Le Roux J.P., Airo A, and Sial A.N. 2009. Climate change register in Lago Sarmiento and Laguna Amarga Microbialites, two Geosites in Torres del Paine, southern Chile. Resumen expandido publicado en XII Congreso Geológico Chileno, Santiago, 2 a 26 de Noviembre 2009.
- Airo, A., Ferrand, D., Lim, D.S., Christopher, M., Solari M.A., Lowe D.R., 2009. Environmental controls on the morphological development of microbialites at Lago Sarmiento, Chile. Submitted to PALAIOS.
- Solari M.A., Hervé F., Le Roux J.P., Airo A., Sial A.N. 2010. Paleoclimatic significance of lacustrine microbialites: A stable isotope case study of two lakes at Torres del Paine, southern Chile. *Palaeogeography, Palaeoclimatology, Palaeoecology*. doi:10.1016/j.palaeo.2010.07.016
- Solari M.A., Calderon M., Airo A., Le Roux J.P. and Hervé F. 2010, Accepted. Holocene and last Glacial variability of the Great Tehuelche Paleolake in the Torres del Paine National Park. *Andean Geology*.
- Solari M.A., Hervé F., Le Roux J.P., Airo A., Sial A.N. 2010. Water level and temperature reconstruction of two lakes at Torres del Paine, Southern Chile. PAGES 2010: II International symposium "Reconstructing Climate Variations in South America and the Antarctic Peninsula over the last 2000 years". Octubre 2010, Valdivia, Chile.



## ÍNDICE DE CONTENIDOS

<b>I. INTRODUCCION.....</b>	<b>1</b>
<b>I.1. INTRODUCCIÓN GENERAL.....</b>	<b>1</b>
I.1.1 HIPÓTESIS DEL GRAN PALEOLAGO TEHUELCHÉ. ....	1
I.1.2 HIPÓTESIS DE PALEOTERMOMETRÍA. ....	2
<b>I.2. OBJETIVOS. ....</b>	<b>2</b>
I.2.1 OBJETIVO GENERAL. ....	2
I.2.2 OBJETIVOS ESPECÍFICOS.....	2
<b>II. MARCO TEÓRICO.....</b>	<b>3</b>
<b>II.1. PALEOCLIMA.....</b>	<b>4</b>
II.1.1 HIPÓTESIS DE LA FORMACIÓN DE LAS CORRIENTES CIRCUMPOLARES.....	4
II.1.2 ÚLTIMO MÁXIMO GLACIAL EN PENÍNSULA ANTÁRTICA Y LA CUENCA DE BRANSFIELD. ....	6
II.1.3 EL ALZAMIENTO DE LOS ANDES PATAGÓNICOS Y LA SOMBRA OROGÉNICA. ....	9
II.1.4 LA IMPORTANCIA DE COMPRENDER EL REGISTRO CLIMÁTICO EN SUDAMÉRICA. ....	10
II.1.5 FLUCTUACIONES GLACIALES DESDE LA ÚLTIMA GLACIACIÓN Y EL HOLOCENO EN EL PARQUE NACIONAL TORRES DEL PAINE. ....	19
<b>II.2. ISOTOPIA ESTABLE EN COMUNIDADES MICROBIANAS.....</b>	<b>21</b>
<b>II.3. REFERENCIAS.....</b>	<b>25</b>
<b>III. LA EVOLUCIÓN DEL GRAN PALEOLAGO TEHUELCHÉ.....</b>	<b>32</b>
<b>III.1. HIPÓTESIS, FUNDAMENTOS Y METODOLOGÍA. ....</b>	<b>32</b>
<b>III.2. LATE QUATERNARY LAKE LEVEL FLUCTUATIONS OF THE GREAT TEHUELCHÉ PALEOLAKE IN THE TORRES DEL PAINE NATIONAL PARK.....</b>	<b>33</b>
III.2.1 ABSTRACT .....	33
III.2.2 INTRODUCTION .....	34
III.2.3 GLACIATION IN PATAGONIA.....	36
III.2.4 STUDY AREA.....	37
III.2.5 METHODOLOGY.....	39
III.2.6 PALEOLACUSTRINE LEVELS.....	40
III.2.7 SEDIMENTARY DEPOSITS .....	47
III.2.8 DISCUSSION AND CONCLUSIONS .....	50
III.2.9 ACKNOWLEDGMENTS.....	53
III.2.10 REFERENCES.....	54
<b>IV. PALEOTERMOMETRÍA ISOTÓPICA DE OXÍGENO EN MICROBIALITAS.....</b>	<b>59</b>
<b>IV.1. HIPÓTESIS, FUNDAMENTOS Y METODOLOGÍA. ....</b>	<b>59</b>
<b>IV.2. PALEOCLIMATIC SIGNIFICANCE OF LACUSTRINE MICROBIALITES: A STABLE ISOTOPE CASE STUDY OF TWO LAKES AT TORRES DEL PAINE, SOUTHERN CHILE. ....</b>	<b>61</b>

IV.2.1	ABSTRACT .....	61
IV.2.2	INTRODUCTION .....	62
IV.2.3	GENERAL BACKGROUND .....	62
IV.2.4	METHODOLOGY .....	66
IV.2.5	LAKE WATER ISOTOPE CHARACTERISTICS .....	67
IV.2.6	DESCRIPTION AND PALAEO THERMOMETRY OF LAGO SARMIENTO THROMBOLITES ..	74
IV.2.7	DESCRIPTION AND PALAEO THERMOMETRY OF LAGUNA AMARGA STROMATOLITES	79
IV.2.8	INORGANIC VERSUS BIOLOGICALLY INDUCED PRECIPITATION .....	84
IV.2.9	DISCUSSION .....	85
IV.2.10	CONCLUSIONS.....	86
IV.2.11	ACKNOWLEDGMENTS.....	87
IV.2.12	REFERENCES.....	87

**V. DISCUSIÓN Y CONCLUSIONES..... 90**

<b>V.1.</b>	<b>DISCUSIÓN .....</b>	<b>90</b>
<b>V.2.</b>	<b>CONCLUSIONES.....</b>	<b>92</b>
V.2.1	REFERENCIAS.....	93

**ANEXOS**

**ANEXO I:** Geomorphologic and tectonic evolution of the Bransfield Basin, Antarctic Peninsula: insights from analogue models.....*i*

**ANEXO II:** La importancia de comprender el registro climático en Sudamérica.....*xiv*

**ANEXO III:** Glacio lacustrine evolution and modern microbilites at lago Sarmiento, del toro and Laguna Amarga.....*xxvi*

## ÍNDICE DE FIGURAS

- Fig. II-1:** Estructuras tectónicas mayores entre Sudamérica y la Antártica Occidental. El mapa enseña: la edad de las colisiones entre la dorsal de Phoenix y la fosa Antártica, las anomalías magnéticas del Mar de Wedell y el comienzo y cese de las distintas dorsales oceánicas (Modificado de Solari et al., 2008). ..... 4
- Fig. II-2:** Modelo paleo-geográfico de “Calce Apretado” modificado de Lawver et al. (1998) enseñando el desplazamiento hacia el sur de la Península Antártica la cual comienza no antes del Jurásico Tardío..... 5
- Fig. II-3:** Diagrama esquemático de la circulación oceánica actual en el sector del Mar de Scotia. Se enseña en naranja las Corrientes Circumpolares Antárticas, los círculos rojos muestran la posición media del Frente Polar, en azul se enseñan las corrientes profundas del Mar de Wedell (WSDW). En la figura B se destaca en azul las corrientes profundas que fluyen en dirección norte (SOBW) que presentaban similares características a las actuales WSDW (modificado de Barker, 2001). ..... 6
- Fig. II-4:** Reconstrucción de la extensión del hielo durante UMG y los principales paleo-drenajes de hielo en la Península Antártica (Anderson et al., 2000). ..... 7
- Fig. II-5:** Mapa de las principales formas glaciales, fallas y edificios volcánicos reconocidos en la Cuenca de Bransfield (Solari et al., 2008) ..... 8
- Fig. II-6:** Diagrama ilustrando el actual efecto de sombra de precipitaciones y los valores isotópicos a lo largo de los Andes Patagónicos Australes (Blisniuk et al., 2005). ..... 9
- Fig. II-7:** Mapa esquemático de la geometría presente de la zona de subducción y la migración de la Dorsal Oceánica formada entre la Placa de Nazca y Antártica. Las líneas grises indican la reconstrucción de la posición de la Dorsal de Chile hace 18, 14, 10 y 6 Ma (Blisniuk et al., 2005) ..... 9
- Fig. II-8:** Parámetros orbitales de la Tierra entorno al Sol considerados en los Ciclos de Milankovitch. A. La excentricidad se refiere a la forma en que la Tierra orbita entorno al Sol, varía de circular a elíptica (ciclo de 100.000 años y 413.000 años). B. La oblicuidad se refiere al ángulo de inclinación del eje de la Tierra relativo a la eclíptica y varía entre 21,1° y 24,5°. Un alto ángulo de inclinación aumenta el contraste estacional (inviernos más fríos y veranos más cálidos en ambos hemisferios). C. La presesión se refiere al bamboleo del eje de rotación que describe una trayectoria circular en el espacio con un periodo de 23.000 años. (Modificado de Zachos et al., 2001). ..... 10
- Fig. II-9:** Registro isotópico de  $\delta^{18}\text{O}$  de Groenlandia plotado en función de la profundidad en metros y el tiempo K años AP (Kilo años antes del presente, 1950 DC). Inter-estadios glaciales abruptos son numerados desde el 1 al 24 (Modificado de Dansgaard et al., 1993). ..... 11
- Fig. II-10:** Variación temporal del nivel del mar en dos escalas de tiempo diferentes (Lambeck y Chappell, 2001): A. Inferida de estratigrafía de secuencias sísmicas; B. Nivel relativo del nivel del mar de la Península de Huon. Inferidos desde la correlación temporal entre el alzamiento y arrecifes de coral fósiles para los pasados 13 ka AP y el nivel del mar promedio es estimado para el registro pre-LGM.. 12

<b>Fig. II-11:</b> Variabilidad espacial observada para el cambio relativo del nivel del mar desde el Último Máximo Glacial al presente en diferentes localidades (Lambeck y Champpell, 2001).	<b>13</b>
<b>Fig. II-12:</b> $\delta^{18}\text{O}$ (VSMOW) en testigos de hielo. Los rectángulos blancos representan períodos relativamente fríos, los rectángulos negros períodos relativamente más calidos y los rectángulos con gradientes blancos a negro períodos de transición. (a) Ajuste Promedio Ponderado (línea negra) de los valores de $\delta^{18}\text{O}$ pertenecientes al testigo de Groenlandia NGRIP (línea gris) (NGRIP dating group (2006), Vinther et al., 2006; Rasmussen et al., 2006; Andersen et al., 2006; Svensson et al., 2006) (d) Ajuste Promedio Ponderado (línea negra) de los valores de $\delta^{18}\text{O}$ pertenecientes al testigo de Antártica Dome C. (línea gris) (Stenni et al., 2006 ; Stenni et al., 2001 ; Schwander et al., 2001 ; Stenni et al., 2003). Notar que tanto las culminaciones de la Última Glaciación como la regresión fría pre-holocena (anterior a los ca. 11600 años AP) ocurren primero en el testigo de Antártica y después en el de Groenlandia.	<b>14</b>
<b>Fig. II-13:</b> Reconstrucción glacial por McCulloch y colaboradores (2000):	<b>18</b>
<b>Fig. II-14:</b> Mapa geomorfológico glacial del Parque Nacional Torres del Paine, área que fue cubierta por los Campos de Hielo Sur Patagónico durante el último ciclo glacial (Marden, 1993).	<b>19</b>
<b>Fig. II-15:</b> Clasificación de los tipos de mineralización y los diferente tipos de procesos bióticos y abióticos. En la zona inferior se muestran los productos de la precipitación biótica (Dupraz et al., 2009).	<b>21</b>
<b>Fig. II-16:</b> Tipos de microbialitas, macro-micro estructura y sus ambientes de formación (Dupraz et al., 2009).	<b>23</b>
<b>Fig. II-17:</b> Imagen obtenida por microscopio atómico de las moléculas (tamaño 500x500 nm) que componen a la Sustancia Extracelular Polimérica (SEP). Notar los ángulos abruptos (k) en los polímeros (p) (Decho et al., 1999).	<b>24</b>
<b>Fig. III-1:</b> Ice core $\delta^{18}\text{O}$ (VSMOW) paleoclimate and discontinuous glacial advance records. Grey bands represent timing of the HRCC (Mayewski et al., 2004) and white rectangles represent cool periods. (a) Smoothed weighted average (black line) of NGRIP $\delta^{18}\text{O}$ (grey line) ice core paleoclimate proxy data (NGRIP, 2006; Vinther et al., 2006; Rasmussen et al., 2006; Andersen et al., 2006; Svensson et al., 2006).(d) Smoothed weighted average (black line) of Dome C $\delta^{18}\text{O}$ (grey line) ice core paleoclimate proxy data (Stenni et al., 2001, 2003, 2006; Jouzel et al., 2001; Schwander et al., 2001). (c) “Mercer and Aniya Type” Neoglacial advances events in Patagonia (Mercer, 1968, 1970, 1982; Aniya, 1995, 1996), Cold Reversal Period in Lake District in northwestern Chilean Patagonia (Hajdas et al., 2003; Moreno et al., 2001), Cold Reversal Period in Torres del Paine (Moreno et al., 2009) and synchronous Patagonian LGM deglaciation.	<b>35</b>
<b>Fig. III-2:</b> Torres del Paine Drainage Basin and moraines superimposed on a shaded relief image obtained from the Shuttle Radar Topographic Mapping Mission (SRTM 90 m resolution, UTM 19 °S/ WGS 84) digital elevation model.	<b>38</b>
<b>Fig. III-3:</b> Terraces at shores of Lago Sarmiento.	<b>40</b>

<b>Fig. III-4:</b> Aerial photograph of the eastern area of Lago Sarmiento showing the mapped paleo-lacustrine terraces and the legend for Figs.III-5, 6 and 7. ....	<b>41</b>
<b>Fig. III-5:</b> Aerial photograph showing the mapped paleo-lacustrine terraces : a. Central part of Lago Sarmiento; b. Western part of Lago Sarmiento and southern margin of Lago Nordenskjöld; c. Enlarge view of the watershed at the Laguna Paso spillway. ....	<b>42</b>
<b>Fig. III-6:</b> Aerial photograph indicating the extend of lacustrine terraces: a. Eastern part of Lago Nordenskjöld to Paine River; b. From Paine River to Laguna Amarga; c. Magnification of Laguna Amarga showing the local terraces. ....	<b>44</b>
<b>Fig. III-7:</b> Glacial moraine complexes, drainage system and regional terraces superimposed on a shaded relief image obtained from the Shuttle Radar Topographic Mapping Mission (SRTM 90 m resolution, UTM 19 ° S/ WGS 84) digital elevation model. ....	<b>45</b>
<b>Fig. III-8:</b> Terrace levels observed in the Del Toro Range, as well as peninsulas extending into Lago del Toro.....	<b>46</b>
<b>Fig. III-9:</b> Sedimentary deposits east of the moraine complexes of Lago del Toro and Lago Sarmiento. The numbers indicate the localities where sedimentary units are described. ....	<b>47</b>
<b>Fig. III-10:</b> Deposits along “El Canal”: a. Stratigraphic columns showing the main units; b. Flood deposits with angular fragments from the underlying alluvial deposits; c. Wave-rippled and contorted beds; d. Consolidated basal moraine overlying the Cerro Toro Formation and underlying the lacustrine sequence. From older to younger: Dcm1. Consolidated basal moraine Fl: Lacustrine sequence; Dcm2. Basal moraine; Sm. Alluvial deposits; Gmm. Flood deposits.....	<b>49</b>
<b>Fig. III-11:</b> Grey bands represent timing of the HRCC (Mayewski et al., 2004) and white rectangles represent cool periods. (a) “Mercer and Aniya Type” Neoglacier advances events in Patagonia (Mercer, 1968, 1970, 1982; Aniya, 1995, 1996), Cold Reversal Period in Lake District in northwestern Chilean Patagonia (Hajdas et al., 2003; Moreno et al., 2001), Cold Reversal Period in Torres del Paine (Moreno et al., 2009) and synchronous Patagonian LGM deglaciation. (b) Chronology of the moraines complexes of Torres del Paine; (c) Chronology of the terrace levels of the Great Tehuelche Paleolake. ....	<b>51</b>
<b>Fig. III-12:</b> Reconstruction of the Great Tehuelche Paleolake during the different glacial stages: a. Glacial and lake extension during Glacial Stage B; b. Glacial and lake extension during Glacial Stage D, c. Glacial and lake extension during Glacial Stage E; d. Small lake organization during Glacial Stage F. <b>52</b>	
<b>Fig. IV-1:</b> Shaded Relief of Shuttle Radar Topographic Mission Digital Elevation Model (SRTM-DEM) showing the Torres del Paine drainage basin (black line), the river (R) network and main lakes (L). ...	<b>64</b>
<b>Fig. IV-2:</b> Merged SRTM-DEM and bathymetric digital elevation model. Lakes with microbialites are demarcated with thick lines and the drainage basin by a dashed line. ....	<b>65</b>
<b>Fig. IV-3:</b> Monthly mean isotopic relationship between $\delta^{18}\text{O}$ and $\delta^2\text{H}$ (IAEA/WMO, 2006) compared with Lago Sarmiento and Laguna Amarga $\delta^{18}\text{O}$ and $\delta^2\text{H}$ surface water composition. ....	<b>68</b>
<b>Fig. IV-4:</b> Diagram of the water inflow and outflow in a closed basin. $\text{Cl}$ and $\text{Cl}_{\text{vi}}$ represent the chloride concentration of the lake water and the surface water inflow. ....	<b>69</b>

**Fig. IV-5:** Examples of terraces observed in Lago Sarmiento. In the magnification, each level is associated with a contact between the thrombolite color zones: light brown for T1a, white for T1b, gray for T1c and dark brown for T1d. .... 74

**Fig. IV-6:** a: Section of a thrombolite with a distinctive clotted structure; b. Magnified area of the previous thrombolite (black square) showing well-differentiated massive and porous calcite phases. 6c. Oxygen and carbon stable isotope data for massive and porous phases of Lago Sarmiento thrombolites. .... 75

**Fig. IV-7:** Thrombolite sample profile at the southern shore of Lago Sarmiento (655334 E, 4340059 S, UTM – 18S -WGS 84). Each paleo-level is indicated: T1a, T1b, T1c and T1d. The sample points are indicated with a star and the numbers represent the distance in meters from the top of the thrombolite deposit. For sample points 4, 12 and 20 m the gastropod median probability radiocarbon ages are indicated. .... 76

**Fig. IV-8:** Oxygen stable isotope composition and paleotemperature for the samples of the Lago Sarmiento profile. The different paleolake levels are labeled T1a, T1b, T1c and T1d (dashed lines) and the lake water level is indicated by an uninterrupted line. 8a. Oxygen stable isotope composition of the massive phases; 8b. Oxygen stable isotope composition of the porous phases; 8c. Temperature and error bar obtained from the porous calcite phases using the Hays and Grossman (1991) equation revised from O’Neil et al. (1969). Each temperature is indicated with a number to the right of the point. .... 77

**Fig. IV-9:** a: Landscape picture showing the seven terraces observed on the northern and southern slopes of Laguna Amarga; 9b. Georeferenced (18° S UTM/WGS84) aerial photograph showing the terrace levels, the microbialite communities and the spring location at Laguna Amarga. .... 79

**Fig. IV-10:** Stromatolite from the eastern shore of Laguna Amarga: a) Section of dome stromatolites showing the subdivision into eight portions; 11b:) Superficial carbonate crust; c) Filamentous cyanobacteria; d) Trapping and binding sand-sized detritus; e) Small crustaceans; f) Carbonate detritus surrounded by filamentous cyanobacteria; g) Portion divisions related to column indicating the main minerals detected by X-Ray diffraction. .... 81

**Fig. IV-11:** Isotope data of mainly inorganically controlled precipitation: stable isotopes of oxygen and carbon for Tanume (34°S), General Carrera (48°S) and Milodon (51°S) stalagmites, as well as the Torres del Paine waterfall carbonate crust and carbonate spring crust. Isotope data of biochemically induced precipitation: stable isotopes of oxygen and carbon for the Laguna Amarga and Sarmiento microbialites. .... 85

# **I. INTRODUCCION**

## **I.1. Introducción General.**

En el extremo sur de Sudamérica existen dos campos de hielos denominados Campos de Hielo Norte y Sur. Los Campos de Hielo son en su conjunto la segunda mayor masa de hielo en el hemisferio sur luego de Antártica. Durante el Pleistoceno los Campos de Hielo cubrieron el extremo austral de América del Sur y el estudio de los vestigios dejados por su posterior evolución hasta el presente, ha permitido obtener una de las cronologías glaciales más completas del planeta. La existencia actual de los Campos de Hielo en latitudes bajas templadas y con solo una elevación promedio de 2000 m s.n.m puede explicarse como el resultado de las altas precipitaciones resultantes de los Vientos Predominantes del Oeste (VPO) y los sistemas frontales. Es por ello que descifrar las fluctuaciones de los Campos de Hielo y el sistema hidrológico alrededor de él, son claves para comprender las variaciones climáticas en el planeta y las variaciones de los VPO.

Uno de los focos de la presente tesis fue desarrollar un método de investigación paleoclimático novedoso en el actual margen sur-este de Campos de Hielo Sur, consistente en la construcción de registros de paleotemperaturas lacustres por medio de isotópicos de oxígeno en organominerales. La importancia de establecer este método no solo radica en el aporte al conocimiento de la evolución paleoclimática Patagónica, sino también en el avance que puede significar contar con un método paleotermométrico cuantitativo en microbialitas para el estudio de la historia paleoclimática de nuestra planeta. Las microbialitas reinaban las aguas primigénias del planeta en condiciones ambientales muy extremas. Se cree que en el Arqueano existía una atmósfera caliente, polvorienta, rica en gases volcánicos tóxicos, los mares carecían de grandes cantidades de oxígeno y el planeta recibía intensos bombardeos de meteoritos. La vida se adaptó a dichas condiciones extremas y más aun, se cree que la actividad de los mantos microbios cambio las condiciones redox, liberando oxígeno e hidrógeno en los mares y la atmósfera. Desde una perspectiva astrobiológica, la investigación de las microbialitas y su ambiente extremo buscan comprender como la vida se puede gestar en otros planetas o lunas del Sistema Solar. En base a ello el presente estudio, por medio de las microbialitas obtuvo información cuantitativa y cualitativa de las características del medio en el cual se formaron.

### *I.1.1 Hipótesis del Gran Paleolago Tehuelche.*

Se postula que las fluctuaciones glaciares son determinantes en la evolución del sistema hidrológico existente al este de los Campos de Hielo y que la evolución de dicho sistema esta vinculada a variaciones en la intensidad y localización de los Vientos Predominantes del Oeste. Por lo cual, en el sector de Torres del Paine es posible refinar la cronología de eventos glaciares por medio del estudio de la evolución del sistema hidrológico y en particular la evolución de un paleolago proglacial denominado en este estudio como “Gran Paleolago Tehuelche”.

### *1.1.2 Hipótesis de Paleotermometría.*

Se postula que la evolución del sistema hidrológico en el Sector de Torres del Paine permitió la formación de un conjunto de lagos y lagunas endorreicas, en alguna de las cuales se formaron colonias de microbilitas y que ellas pueden ser utilizadas como paleotermómetros si: el fraccionamiento isotópico entre el agua y los carbonatos se produce en equilibrio y la composición isotópica del agua depende principalmente de la temperatura.

## **1.2. Objetivos.**

### *1.2.1 Objetivo General.*

Contribuir al conocimiento de la evolución paleoclimática Holocena y Pleistocena por medio del estudio de registros glaciolacustres existentes en el Parque Nacional Torres del Paine.

### *1.2.2 Objetivos Específicos.*

#### *a. Evolución del sistema hidrológico.*

Conocer la evolución del sistema hidrológico al este de las morrenas terminales existentes en el Parque Nacional Torres del Paine.

#### *b. Paleotermometría.*

Reconstruir la evolución hídrica y determinar las paleotemperaturas del agua durante el Holoceno en Lago Sarmiento y Laguna Amarga. Para determinar las paleotemperaturas se utilizó métodos geoquímicos, petrológicos, mediciones de isótopos estables y determinación de edades por radiocarbono.



## II. MARCO TEÓRICO.

En el presente marco se desarrollaron brevemente dos líneas teóricas: la primera relacionada con estudios paleoclimáticos y la segunda con estudios en microbialitas. Gran parte del marco teórico esta basado en un conjunto de publicaciones escritas (como autor principal o coautor) durante el desarrollo de la tesis.

Partes del enfoque de la línea paleoclimática fue publicado en diversas fuentes, algunas de las cuales se encuentran adjuntadas en los anexos. Sus títulos se detallan a continuación:

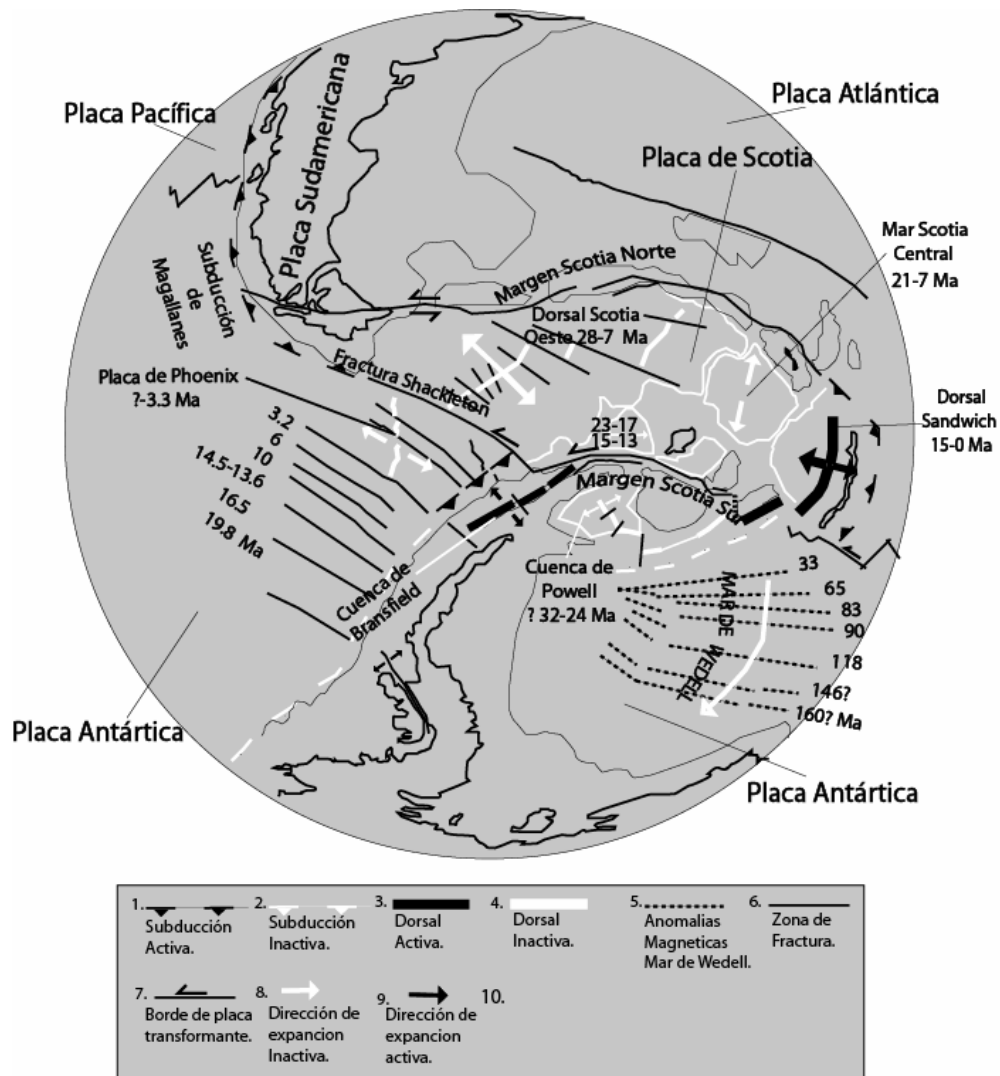
- En el Proyecto Anillo Antártico ARTG04 (2006): “Conexiones Geológicas entre Antártica Occidental y Patagonia desde el Paleozoico Tardío: Tectónica, Paleogeografía, Biogeografía y Paleoclima”.
- En la revista *Antartic Science*: Solari et al. (2008 a) narran la apertura del mar de Drake y se reconocieron formas glaciales en la Cuenca de Bransfield asociadas a las glaciaciones de la Península Antártica (En extenso en Anexo 1).
- En la revista de difusión científica *Eco-Engen* (Solari, 2008b, Ver anexo 2) se destaca la importancia de comprender el registro climático en Sudamérica.

El marco teórico de microbialitas esta enfocado a comprender su importancia como análogos de la vida primigenia del planeta Tierra, sus características macro-microscópicas, los factores ambientales que condicionan su crecimiento y su potencial como indicadores paleoclimáticos. Parte de dicho enfoque fue publicado en:

- En la guía titulada “Field Trip Guide of the International Geological Congress on the Southern Hemisphere, Geosur 2007” (Solari and Airo, 2007, ver Anexo 3).
- En el artículo de Airo et al. (2009) sometido a la revista *PALAIOS*, el cual se titula: *Environmental control on the morphological development of microbialites at Lago Sarimientto, Chile. Paleoclima.*

## II.1. Paleoclima

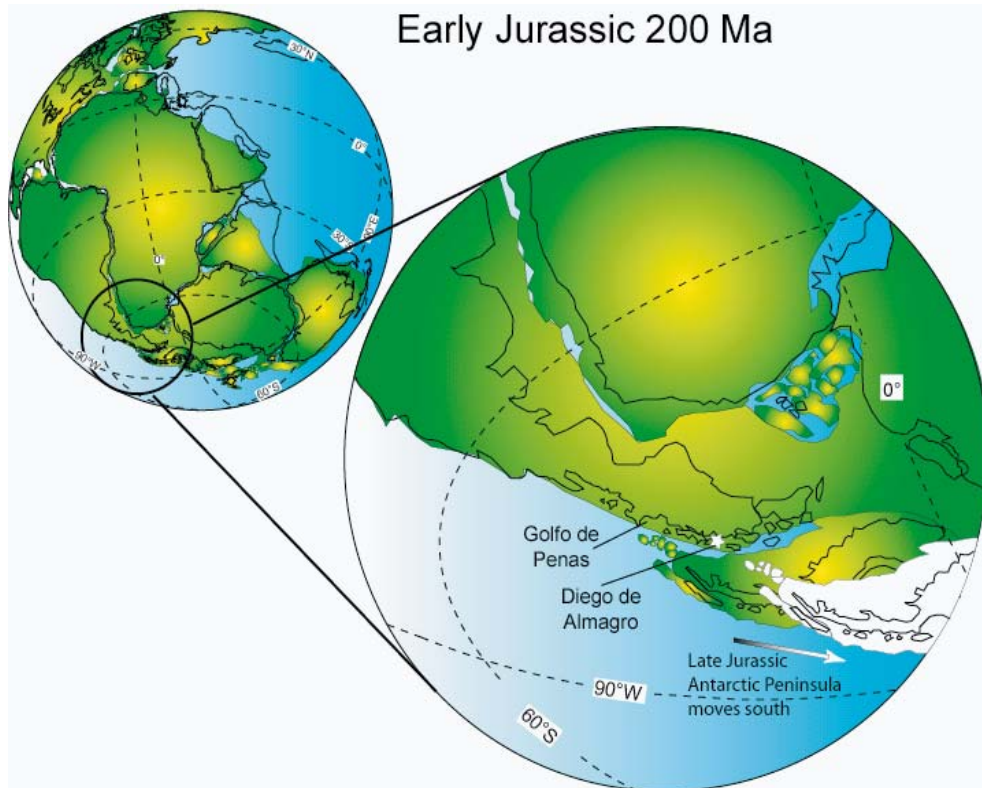
### II.1.1 Hipótesis de la Formación de las Corrientes Circumpolares



**Fig. II-1:** Estructuras tectónicas mayores entre Sudamérica y la Antártica Occidental. El mapa enseña: la edad de las colisiones entre la dorsal de Phoenix y la fosa Antártica, las anomalías magnéticas del Mar de Wedell y el comienzo y cese de las distintas dorsales oceánicas (Modificado de Solari et al., 2008).

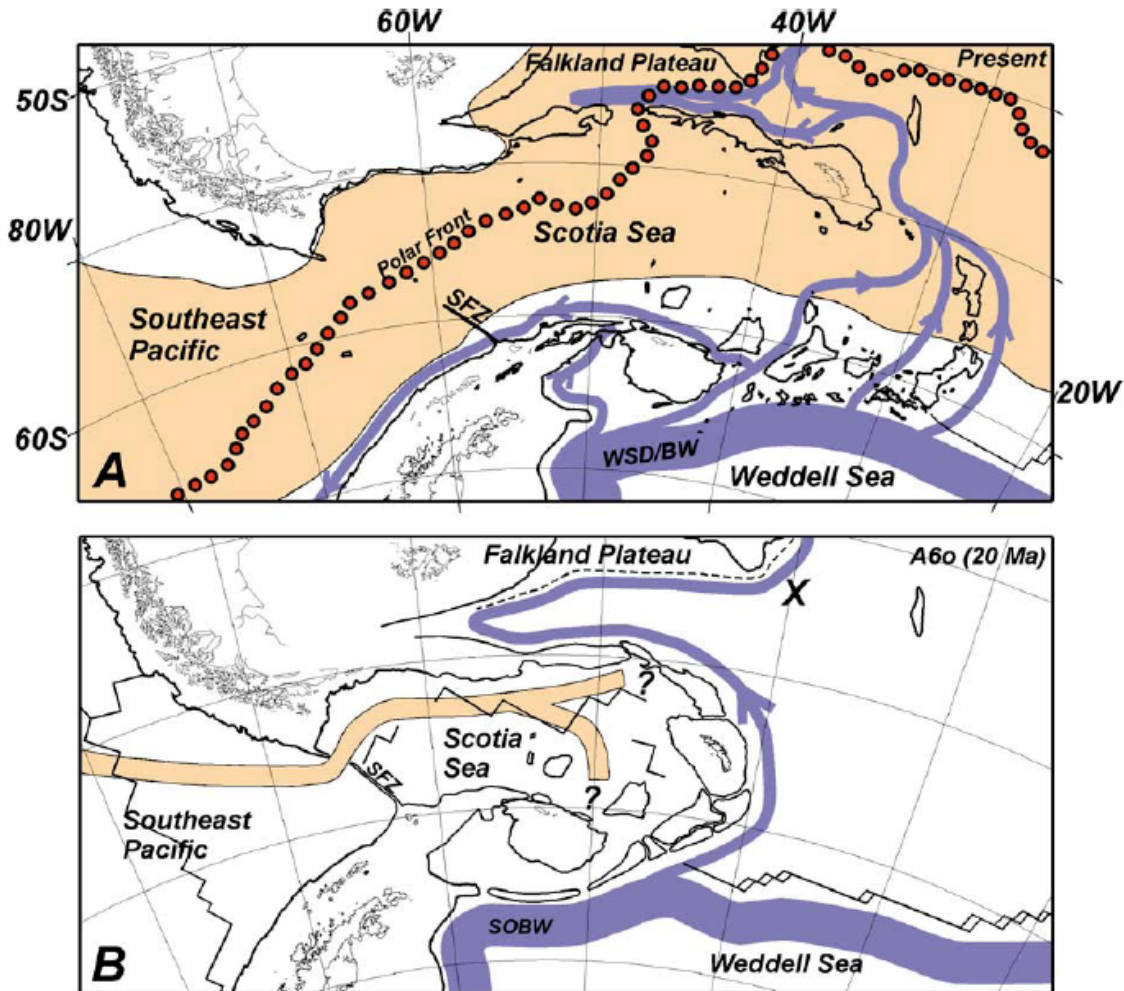
Muy probablemente antes de la ruptura de Gondwana, la Península Antártica (PA) se ubicaba al oeste de, y en continuidad con, el margen occidental de Patagonia. Miller (1983) fue el primero en presentar una reconstrucción paleo-geográfica de este tipo, idea retomada por Lawver et al. (1998). Estos últimos en lo que denominaron “modelo de calce apretado”, ubicaron la PA tan al norte como al oeste inmediato del Golfo de Penas (50°S, Fig. 2). Dicha hipótesis fue respaldada por Jökat et al. (2003) en reconstrucciones paleogeográficas basadas en la distribución de las anomalías magnéticas del Mar de

Weddell oriental y Atlántico sur. Ghidella et al. (2002) analizando las anomalías magnéticas del Mar de Wedell y del Mar de Scotia, produjeron una serie de mapas paleogeográficos indicando las variaciones en la posición relativa de la PA y Patagonia desde el Jurásico, que muestran la migración de la Península hacia el sur a partir de una posición ubicada al oeste de Patagonia. Los efectos e implicancias de esos modelos para la evolución geológica de la PA como la Patagonia, no han sido, hasta la fecha, investigados en detalle.



**Fig. II-2:** Modelo paleo-geográfico de “Calce Apretado” modificado de Lawver et al. (1998) enseñando el desplazamiento hacia el sur de la Península Antártica la cual comienza no antes del Jurásico Tardío.

La formación de la Placa de Scotia continúa con el distanciamiento entre Patagonia y Antártica, iniciado a partir del Jurásico. Barker (2001) sintetiza diversos datos (Tectonic Map (1985), Geosat y ERS-1 altimetría satelital-derivada de gravedad (Livermore et al., 1994) e interpretaciones (e.g. Barker et al., 1991; Dalziel, 1983; DeMeets et al., 1990), presentando un modelo paleotectónico a partir del Cenozoico para la expansión de los diferentes segmentos oceánicos y la reorganización de los segmentos continentales que conforman la Placa de Scotia. La configuración de los fragmentos a los 40 Ma posiblemente formó una barrera para las corrientes circumpolares oceánicas, que se completan luego de la disrupción tectónica de esta barrera. La disrupción de dicha barrera permitió la conexión de los océanos Pacífico y Atlántico y el establecimiento de una nueva barrera marina para la biota continental que había estado hasta ese entonces conectada.



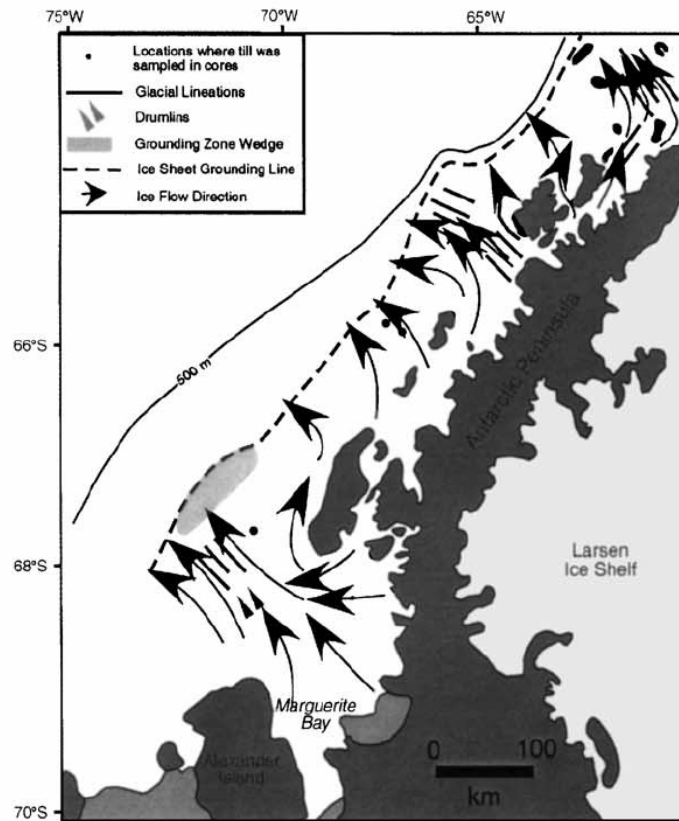
**Fig. II-3:** Diagrama esquemático de la circulación oceánica actual en el sector del Mar de Scotia. Se enseña en naranja las Corrientes Circumpolares Antárticas, los círculos rojos muestran la posición media del Frente Polar, en azul se enseñan las corrientes profundas del Mar de Wedell (WSDW). En la figura B se destaca en azul las corrientes profundas que fluyen en dirección norte (SOBW) que presentaban similares características a las actuales WSDW (modificado de Barker, 2001).

Como se ha mencionado, existe un modelo que explica las implicancias que produjo la apertura del Mar de Scotia en la re-configuración de las corrientes marinas. Sin embargo se desconoce cuales fueron los impactos de este cambio sobre las celdas de circulación atmosféricas y cual fue la magnitud, temporalidad y extensión de los cambios climáticos que implicó este cambio tectónico mayor a nivel global.

### II.1.2 Último Máximo Glacial en Península Antártica y la Cuenca de Bransfield.

Heroy et al. (2008) presenta datos sedimentológicos y dataciones de radiocarbono que acotan temporalmente el retroceso de la Plataforma de Hielo de la Península Antártica desde el Último Máximo Glacial. Sus estudios establecen que la deglaciación comenzó

entre 18.000 y 19.000 años AP coincidentemente con el incremento del nivel eustático del mar.

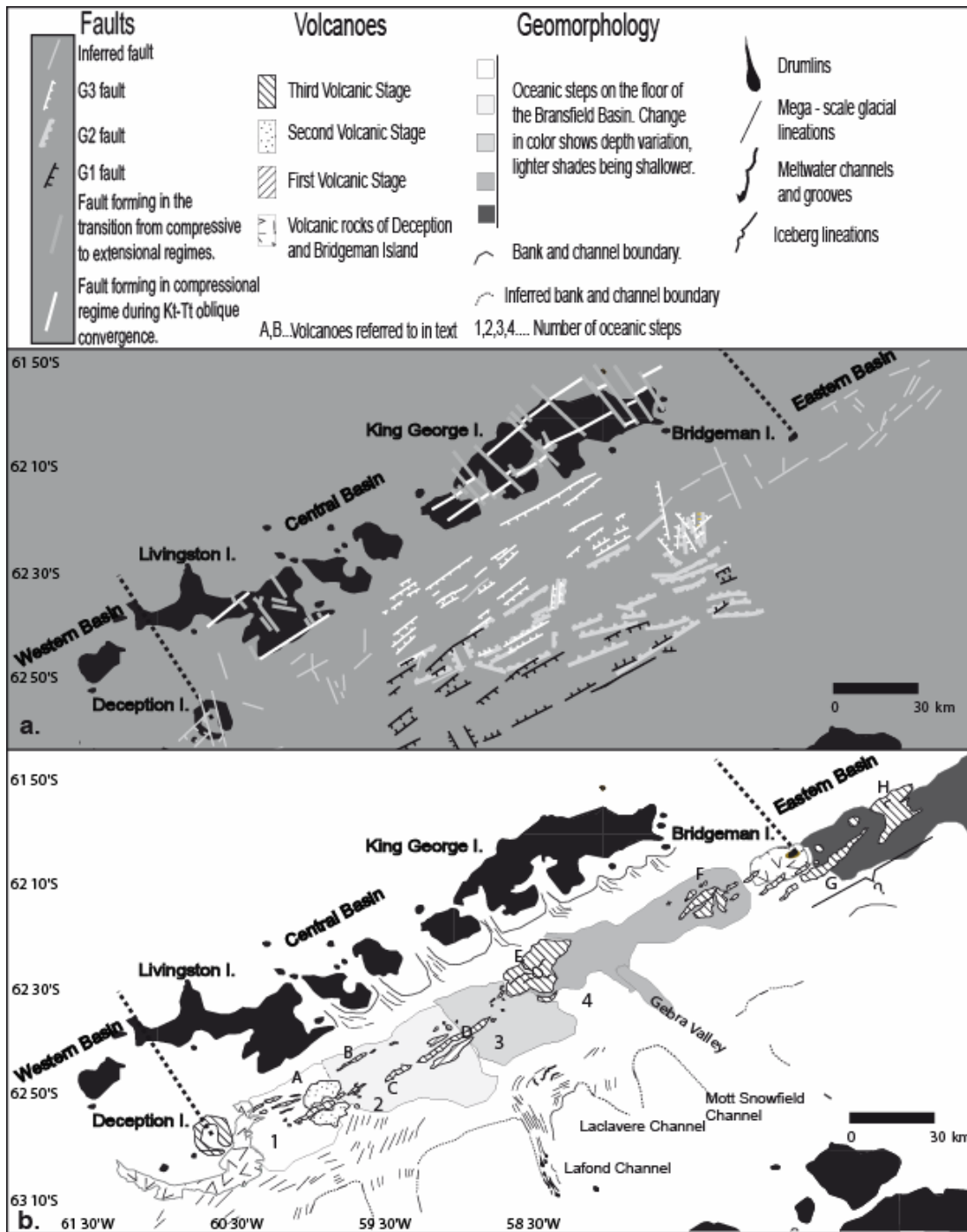


**Fig. II-4:** Reconstrucción de la extensión del hielo durante UMG y los principales paleodrenajes de hielo en la Península Antártica (Anderson et al., 2000).

La Cuenca de Bransfield es una cuenca elongada en dirección NE, localizada entre las Islas Shetland del Sur y el margen de la Península Antártica. La cuenca tiene aproximadamente 100 km de ancho y descansa entre las zonas de fractura de Hero y Shackleton. La Cuenca de Bransfield está dividida en 3 subcuencas: Subcuenca Este, Central y Oeste. Las cuencas presentan sedimentos hemipelágicos depositados durante periodos interglaciales, y sedimentos terrígenos y de erosión glacial en progradación durante periodos glaciales (Anderson 1999; Anderson et al., 2000).

Solari et al. (2008) caracterizaron y construyeron un mapa geológico de la subcuenca Central de Bransfield, en el cual se sintetizaron las principales evidencias glaciales, tectónicas y volcánicas (Fig. II-5). La subcuenca Central de Bransfield es una cuenca asimétrica de aproximadamente 150 km de ancho y 220 km de longitud. El margen norte de la subcuenca Central de Bransfield es empinado y presenta escarpes morfoestructurales relacionados a fallas extensionales. El margen sur de la subcuenca presenta una pendiente más suave y se observan amplios canales glaciales. En dichos canales es posible notar mega-lineamientos glaciales, drumlins y estrías de iceberg, producidas por el avance de los glaciares sobre la plataforma de la Península Antártica (Solari, 2003 y Solari et al., 2008 a). Datos obtenidos en testigos de depósitos glacio-marinos proximales al hielo fecharon el UMG cercano a 22,674 Cal ka AP (19055  $^{14}\text{C}$  años AP) e indicaron que el

hielo se retiró de la plataforma exterior de hielo hace 17,471 Cal ka AP (14.365 <sup>14</sup>C años AP) (Anderson et al., 2000).

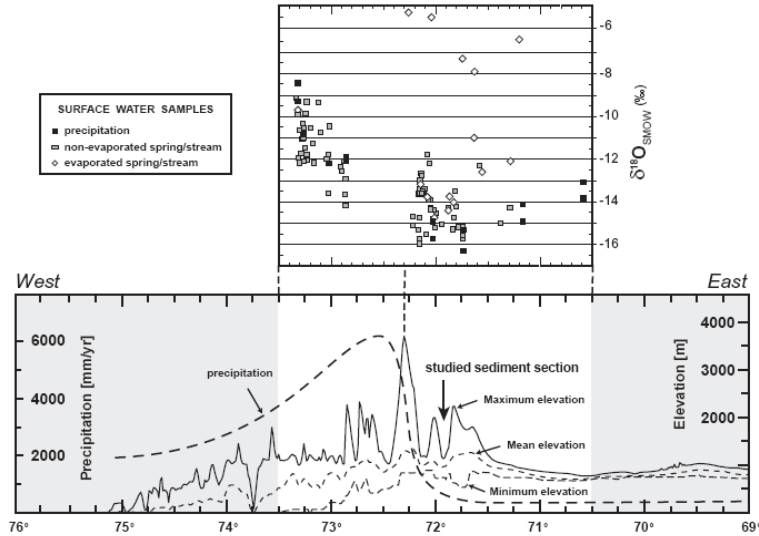


**Fig. II-5:** Mapa de las principales formas glaciales, fallas y edificios volcánicos reconocidos en la Cuenca de Bransfield (Solari et al., 2008)

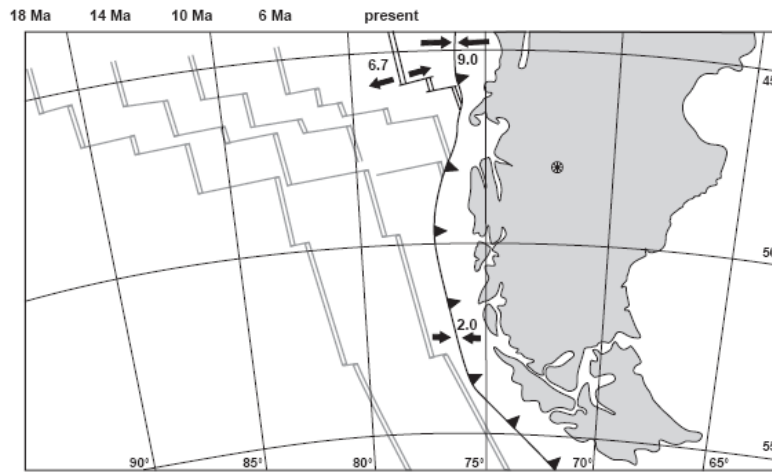


### II.1.3 El Alzamiento de los Andes Patagónicos y la Sombra Orogénica.

La gran altitud de los Andes Patagónicos es una pronunciada barrera morfológica para la circulación atmosférica de los Vientos Predominantes del Oeste (VPO) y causa una de las más drásticas sombras de precipitaciones en la Tierra.



**Fig. II-6:** Diagrama ilustrando el actual efecto de sombra de precipitaciones y los valores isotópicos a lo largo de los Andes Patagónicos Australes (Blisniuk et al., 2005).



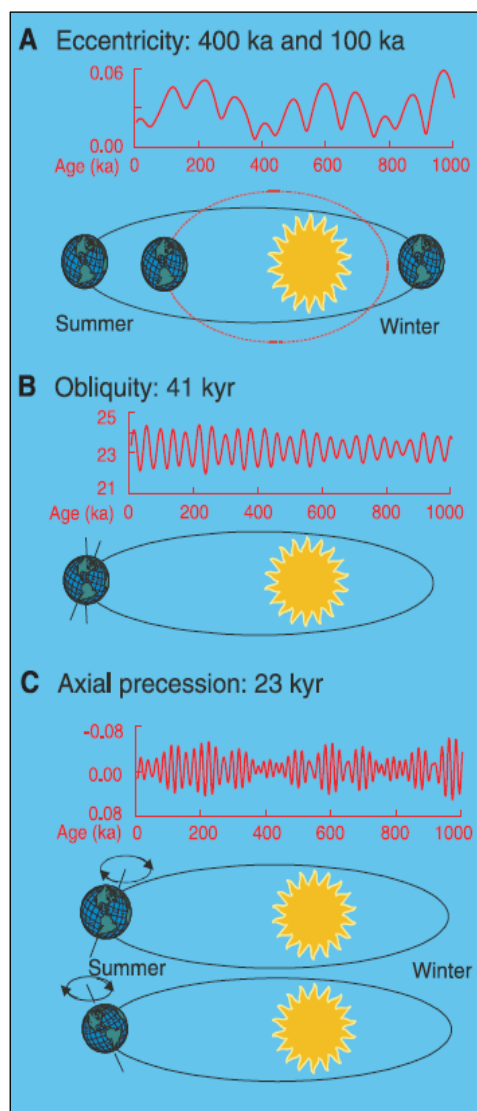
**Fig. II-7:** Mapa esquemático de la geometría presente de la zona de subducción y la migración de la Dorsal Oceánica formada entre la Placa de Nazca y Antártica. Las líneas grises indican la reconstrucción de la posición de la Dorsal de Chile hace 18, 14, 10 y 6 Ma (Blisniuk et al., 2005)

Los datos geológicos de isótopos estables de carbono y oxígeno adquiridos en nódulos de carbonatos pedogénicos analizados de la sección continental de Formación Santa Cruz presentados por Blisniuk et al. (2005) establecen la formación de la sombra de

precipitaciones de Patagónica producto del alzamiento de los Andes Patagónicos en el Mioceno. El rango de edad (dataciones Ar/Ar) de la formación Santa Cruz fluctúa entre 22 y 14 Ma. Hace ca. 16,5 Ma, los valores de  $\delta^{13}\text{C}$  se incrementa y los valores de  $\delta^{18}\text{O}$  decrecen, y además la depositación de la Formación Santa Cruz cesa a los ca. 14 Ma. Ambas evidencias, sugieren la intensificación de la aridez que produjo el cese de la depositación y el cambio isotópico son producidos por la formación de la sombra de precipitaciones luego del alzamiento resultado de la colisión de la Dorsal de Chile hace cerca de 14 Ma.

#### II.1.4 La importancia de comprender el registro climático en Sudamérica.

##### a. Variabilidad climática a escala global.

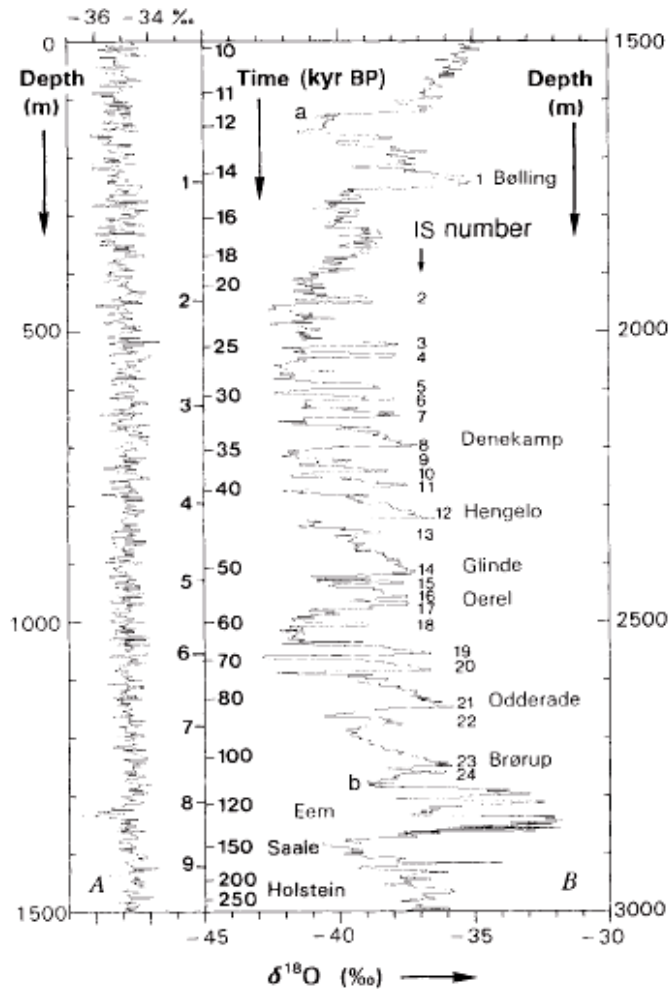


Considerando los parámetros orbitales de la Tierra entorno al Sol, Milankovitch (1930) postuló una explicación para los cambios climáticos terrestres. Él calculó la influencia combinada de la excentricidad (ciclo de 100.000 años y 413.000 años), la oblicuidad (ciclo de 41.000 años) y la precesión de los equinoccios (ciclo de 23.000 años) en la cantidad de radiación solar y calor recibida por la Tierra en latitudes altas, durante el último millón de años. Una importante modificación de la teoría orbital fue postulada por Davis y Bewer (2009). Estudios de registros isotópicos estables de oxígeno en testigos de sedimentos marinos, permiten suponer que las variaciones climáticas cíclicas observadas se pueden explicar por los cambios de calor cíclicos postulados en la teoría orbital de Milankovitch (Lambeck et al., 2001, Zachos et al., 2001).

**Fig. II-8:** Parámetros orbitales de la Tierra entorno al Sol considerados en los Ciclos de Milankovitch. A. La excentricidad se refiere a la forma en que la Tierra orbita entorno al Sol, varía de circular a elíptica (ciclo de 100.000 años y 413.000 años). B. La oblicuidad se refiere al ángulo de inclinación del eje de la Tierra relativo a la eclíptica y varía entre  $21,1^\circ$  y  $24,5^\circ$ . Un alto ángulo de inclinación aumenta el contraste estacional (inviernos más fríos y veranos más cálidos en ambos hemisferios). C. La presesión se refiere al bamboleo del eje de rotación que describe una trayectoria circular en el espacio con un periodo de 23.000 años. (Modificado de Zachos et al., 2001).



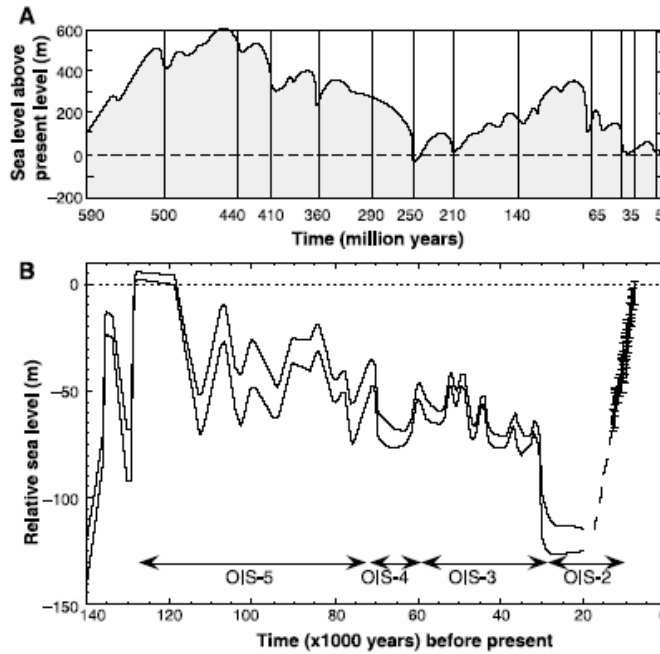
Recientemente, en testigos de hielo obtenidos en la Antártica (EPICA, 2004) y en Groenlandia (North Greenland Ice Core Project members, 2004) se pueden ver con claridad los ciclos cada 100.000 años previstos por la teoría orbital. Pero también se detectó cambios irregulares y abruptos en la composición isotópica estable de oxígeno, casi tan grandes como los relacionados a un periodo glacial e interglacial, pero en el plazo de unos pocos años. Estos son llamados cambios eventos tipo Dansgaard-Oeschger y Heinrich (de 500 a 1.000 y 1.000 a 4.500 años, respectivamente) y representan cambios de temperatura abruptos en lapsos de tiempo cortos (Dansgaard et al., 1993).



**Fig. II-9:** Registro isotópico de  $\delta^{18}\text{O}$  de Groenlandia ploteado en función de la profundidad en metros y el tiempo K años AP (Kilo años antes del presente, 1950 DC). Inter-estadios glaciales abruptos son numerados desde el 1 al 24 (Modificado de Dansgaard et al., 1993).

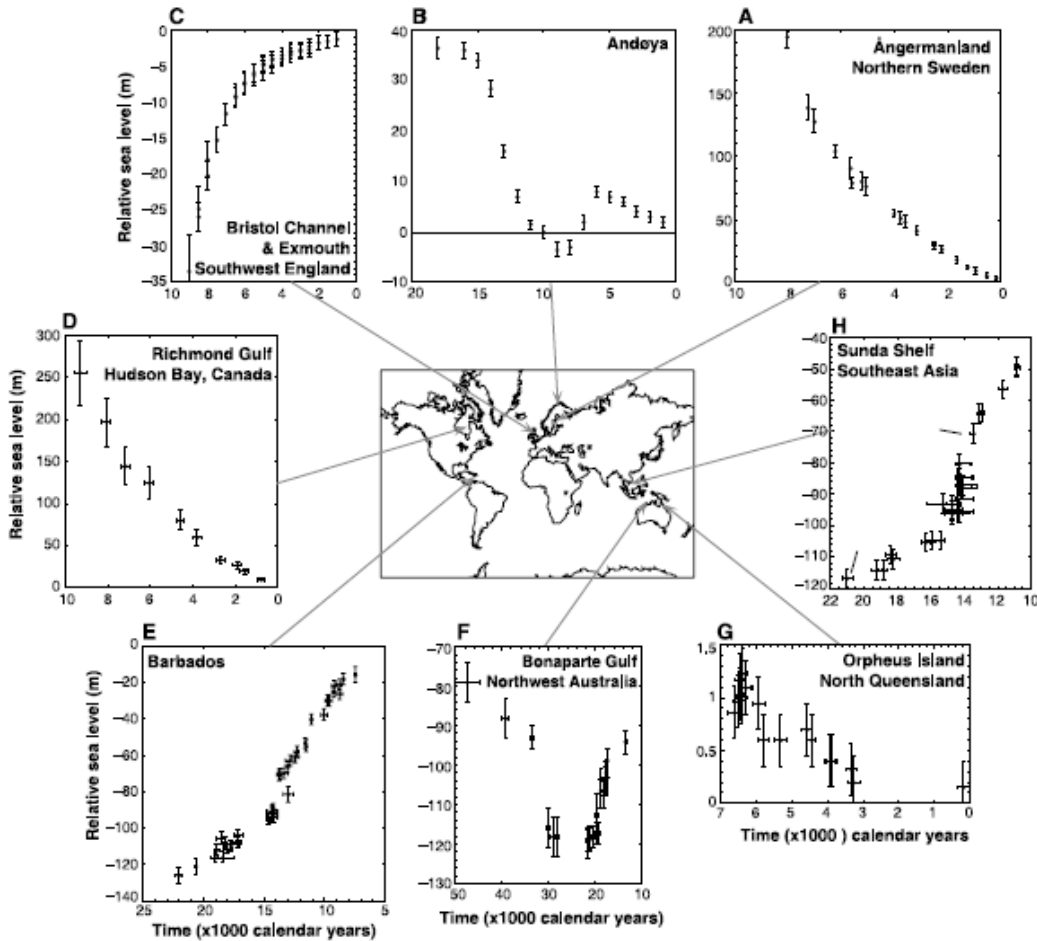
A lo largo del Cuaternario, el periódico intercambio de masas de agua entre el océano y los grandes casquetes de hielo ha sido la contribución dominante para el cambio de nivel del mar durante los últimos ciclos glaciales. Las edades glaciales corresponden a estadios bajos del nivel del mar y los interglaciales a niveles altos. Desde finales del

Pleistoceno hasta el presente se registran dos grandes estadios bajos del nivel del mar (OIS -2 y OSI6) que se correlacionan con los dos últimos máximos glaciales (Fig. II-10). Lambeck y Champpell (2001) sintetizaron las diferentes señales obtenidas para cambios del nivel del mar en variadas partes del mundo desde el último máximo glacial (LGM) hasta el presente (Fig. II-11).



**Fig. II-10:** Variación temporal del nivel del mar en dos escalas de tiempo diferentes (Lambeck y Chappell, 2001): A. Inferida de estratigrafía de secuencias sísmicas; B. Nivel relativo del nivel del mar de la Península de Huon. Inferidos desde la correlación temporal entre el alzamiento y arrecifes de coral fósiles para los pasados 13 ka AP y el nivel del mar promedio es estimado para el registro pre-LGM

A partir de las relaciones de alzamiento del arrecife y el estudio de muestras de corales fósiles sumergidos, en la Península de Huon, Papua Nueva Guinea, se obtuvo un registro del ascenso del nivel del mar desde el último ciclo hasta el presente. Pero hay que aclarar que muchas veces sobre impuesta a la señal global, existen cambios regionales y locales causados por el alzamiento y subsidencia de las zonas costeras o por climas regionales o locales. Dichos cambios glacio-hidro-isostáticos son la causa de la variabilidad espacial del nivel del mar ilustrada en la Fig. II-11 (Lambeck y Chappell, 2001).



**Fig. II-11:** Variabilidad espacial observada para el cambio relativo del nivel del mar desde el Último Máximo Glacial al presente en diferentes localidades (Lambeck y Champell, 2001).

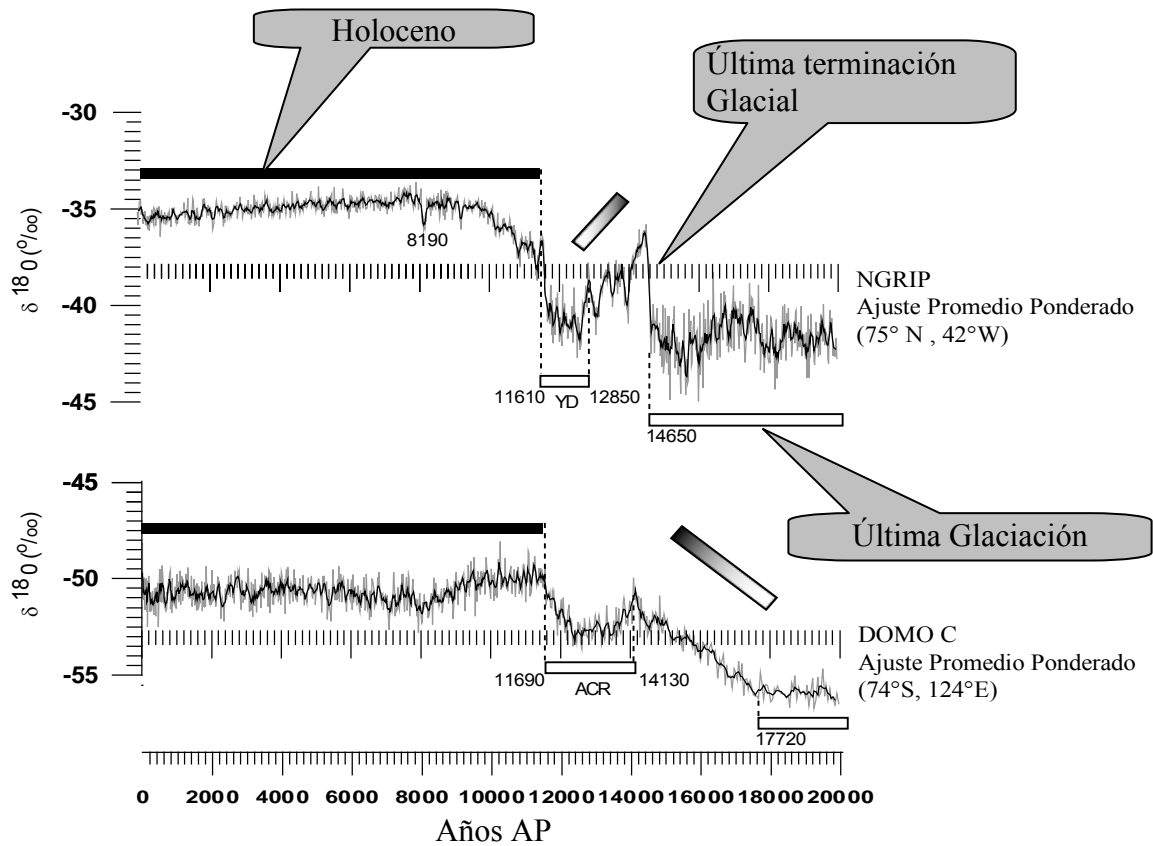
*b. Hipótesis inter-hemisféricas múltiples.*

Existen tres grandes grupos de tendencias para explicar el último de los bruscos cambios climáticos tipo Dansgaard-Oeschger (1 Bølling en Fig. II-9) que se observan tanto en las señales isotópicas marinas como de hielo. Estas hipótesis toman como base un cambio climático inter-hemisférico (McCulloch et al., 2000).

Un primer grupo plantea que cambios en el hemisferio norte dan pie a los cambios en el hemisferio sur. Se plantea que cambios de temperatura e insolación asociados al ciclo de insolación de Milankovitch generan aguas de fusión derivadas de las plataformas de hielo del Hemisferio Norte (Groenlandia), las cuales varían la densidad del agua superficial en el Océano Nor-Atlántico, afectando la producción del transporte de aguas oceánicas interhemisféricas y también modificando los patrones de transporte de calor globales a altas latitudes.

Un segundo grupo plantea que cambios en el Hemisferio Sur dan pie a los cambios en el Hemisferio Norte. Correlaciones recientes entre testigos de hielo en Antártica y Groenlandia (Sowers y Bender, 1995) indican que en el Testigo de Vostok (EPICA, 2004) la tendencia de calentamiento comienza antes de la culminación del Último Máximo Glacial en el Hemisferio Norte. Utilizando metano atmosférico atrapado en burbujas de aire se determinó que el evento de calentamiento Dansgaard – Oeschger (posterior al LGM) determinado en Groenlandia está retrasado en ca. 2000 Cal años (años calendario) de su contraparte en Antártica (Blunier et al., 1998). En adición, los testigos de Antártica revelan un evento de Inversión Fría Antártica (ACR,

Fig. II-12) que precede al equivalente Younger Dryas (YD, Fig. II-12) del Hemisferio Norte (Blunier et al., 1998).



**Fig. II-12:**  $\delta^{18}O$  (VSMOW) en testigos de hielo. Los rectángulos blancos representan períodos relativamente fríos, los rectángulos negros períodos relativamente más cálidos y los rectángulos con gradientes blancos a negro períodos de transición. (a) Ajuste Promedio Ponderado (línea negra) de los valores de  $\delta^{18}O$  pertenecientes al testigo de Groenlandia NGRIP (línea gris) (NGRIP dating group (2006), Vinther et al., 2006; Rasmussen et al., 2006; Andersen et al., 2006; Svensson et al., 2006) (d) Ajuste Promedio Ponderado (línea negra) de los valores de  $\delta^{18}O$  pertenecientes al testigo de Antártica Dome C. (línea gris) (Stenni et al., 2006 ; Stenni et al., 2001 ; Schwander et al., 2001 ; Stenni et al., 2003). Notar que tanto las culminaciones de la Última Glaciación como la regresión fría pre-holocena

(anterior a los ca. 11600 años AP) ocurren primero en el testigo de Antártica y después en el de Groenlandia.

El tercer grupo postula que los cambios climáticos ocurren sincrónicos en ambos hemisferios y se basa en el estudio de las fluctuaciones glaciares y cambios paleoecológicos asociados. Trabajos en la Región de los Lagos (Chile) y en Nueva Zelanda, permitieron a Denton y colaboradores (1999) tener un registro temporal de las fluctuaciones glaciares, las cuales permiten correlacionarlas con el evento Dansgaard-Oeschger en la región del Atlántico del Norte (Lowell et al., 1995; Denton et al., 1999). La buena correlación entre ambos “sets” implica una simetría interhemisférica de la estructura y del momento de la transición glacial-interglacial. Estas conclusiones se soportan en evidencia de eventos equivalentes del Younger Dryas en Ecuador (Clapperton et al., 1997) y Nueva Zelanda (Denton y Hendy, 1994; Ivy-Ochs et al., 1999). Análisis recientes de evidencias geomorfológicas glaciales en el Domo de Taylor en el flanco de la plataforma del Mar de Ross (Steig et al., 1998) soportan esta hipótesis de un cambio climático sincrónico interhemisférico.

c. *Campos de Hielo Sur.*

En el extremo sur de Sudamérica existen dos campos de hielos llamados Campos de Hielo Norte y Sur. Campos de Hielo Sur (CHS) es una meseta de hielo que se desarrolla en latitudes medias templadas entre los 48° y 51° S; se extiende a lo largo de los 73° 30' W, posee un área aproximada de 13.000 km<sup>2</sup> y una elevación que varía entre los 500 y 2.000 m con picos que alcanzan e incluso exceden los 3000 m (Carrasco et al., 2002).

CHS es la segunda gran masa de hielo en el hemisferio sur luego de Antártica. En ella, más de 48 glaciares se descargan en fiordos en el lado oeste y en lagos en el lado este (Carrasco et al., 2002). Los glaciares que nacen en los campos de hielo son templados con altas tasas de ablación y bajas velocidades de flujo.

Varios estudios indican que las grandes extensiones de hielo como Campos de Hielo Sur son sensibles al impacto del calentamiento global y al aumento de los gases de invernadero. El retroceso generalizado de CHS puede obedecer al calentamiento troposférico detectado al sur de Sudamérica en las últimas décadas (Ibarzabal et al., 1996).

La existencia particular de los CHS en condiciones de bajas latitudes templadas y en una topografía con una altura promedio de cerca de 2.000 m se puede explicar debido a:

a. La gran cantidad de días nublados (ca. 70%) y eventos de precipitación a lo largo del año, que son el resultado de los vientos predominantes desde el oeste (vientos promedio durante junio y julio) y a los sistemas frontales (Carrasco et al., 2002). La distribución espacial del régimen de precipitación está dada por una alta precipitación anual en el lado oeste cercana a 7.000 mm en la costa y 10.000 mm sobre los campos de hielo (D.G.A., 1987). Esa cantidad rápidamente decrece hacia el este de los Andes Patagónicos donde la precipitación media anual es menor a 400 mm (Carrasco et al., 1998; Ibarzabal et al., 1996).

b. La baja altitud de la línea de nieves que varía desde los 500 m cerca del Océano Pacífico a 1.500 m al este de la Cordillera de los Andes Patagónicos (Clapperton, 1994).

Datos adquiridos en diferentes estaciones meteorológicas en las vecindades de los CHS indican que el comportamiento de la temperatura revela diferencias en las estaciones cercanas a la costa, que son influidas por el Océano Pacífico, y las estaciones dentro del continente que experimentan una mayor variación de temperatura invernal-estival (Carrasco et al., 2002). El ascenso lineal de la temperatura cercana a la superficie durante los últimos 100 años en las vecindades de los CHS es entre 1,3 y 2,0°C basado en el período de homogenización entre los años 1933 y 1992 (Carrasco et al., 2002). Se utiliza el nivel de presión atmosférica de 850 hPa para el cálculo de la variación de temperatura anual, ya que se encuentra sobre los 1.350 m sobre el nivel del mar y la elevación promedio de campos de hielo es de 1.336 m (Casassa y Rivera, 1999). Re-análisis de los datos observados en la estación de Punta Arenas, permiten proyectar los datos desde el año 1977 hasta 1958, obteniendo un ascenso de la temperatura de 0,98° C desde 1958. El calentamiento de la atmósfera a 850 hPa (ca. de 1.350 m s.n.m) en Punta Arenas desde 1977 en verano e invierno por año es de  $-0,0224^{\circ}$  y  $0,0455^{\circ}\text{C yr}^{-1}$  (en 22 años  $-0,45^{\circ}$  y  $1^{\circ}\text{C}$ ), respectivamente. Esto indica que el calentamiento promedio anual es producido principalmente por el calentamiento de los inviernos (Carrasco et al., 2002).

d. *Síntesis cronológica de los eventos de glaciación en Patagonia*

Durante el Pleistoceno, el sector oeste del extremo austral de América del Sur estuvo cubierto por una gruesa capa de hielo, vestigio de los cuales actualmente existen en los grandes campos de hielo en Patagonia. Actualmente, los Campos de Hielo de Patagonia Norte descansan entre los 46°S y 48°S, mientras los Campos de Hielo de Patagonia Sur se extienden desde el Canal Baker hasta los 51°S cerca de Puerto Natales.

La cronología de las glaciaciones patagónicas es una de las más completas del planeta, y la comprensión de las glaciaciones ha experimentado significativos avances desde los pioneros estudios de Carl Caldenius (1932) y Charles Darwin (1842) (Ej. Mercer, 1976; Clapperton, 1993; Rabassa et al., 1990; Glasser et al., 2008a, 2008b). Rabassa et al. (2005) sintetizan el conocimiento respecto a la cronología glacial de Patagonia desde el Cenozoico tardío. La glaciación más antigua conocida tuvo lugar entre 7 y 5 Ma (Mioceno tardío – Pleistoceno temprano). Un mínimo de ocho (8) glaciaciones ocurrió en el Plioceno medio-tardío (Etapa Isotópica de Oxígeno 54 – 82). La Gran Glaciación Patagónica (GGP) se desarrolló entre 1.168 y 1.016 Ma (Etapa Isotópica de Oxígeno 30-34, Pleistoceno temprano). Luego de la GGP entre 14 y 16 estadios fríos (estadial) intercalados con sus correspondientes períodos calidos (interstadial) se desarrollaron en Patagonia, de ellos 13 complejos morrénicos han sido identificados.

Un avance glacial mayor ocurrió durante MIS 6 con una edad estimada de entre 150-140 ka BP (Singer et al., 2004; Kaplan et al., 2004; Douglass et al., 2006). Kaplan et al. (2005), basado en el evento stadial interpretado en los testigos de hielo de Antártico a los 75 ka infirió que en el Lago Buenos Aires existió un avance glacial durante MIS 4, pero fue obliterado por el avance ocurrido durante el UMG. El UMG ocurrió entre 30 y 16 ka (MIS 2) y se desarrolló con una amplia sincronía en todo Patagonia (Clapperton and

Seltzer, 2001) junto al desarrollo global de las plataformas de hielo (Mix et al., 2001). La actividad glacial durante este período es el foco de muchos estudios (Ej. Meglioli, 1992; Porter et al., 1992; Denton et al., 1999, Heusser, 2003; Harrison, 2004; Coronato et al., 2004; McCulloch et al., 2000, 2005; Kaplan et al., 2008a, 2008b).

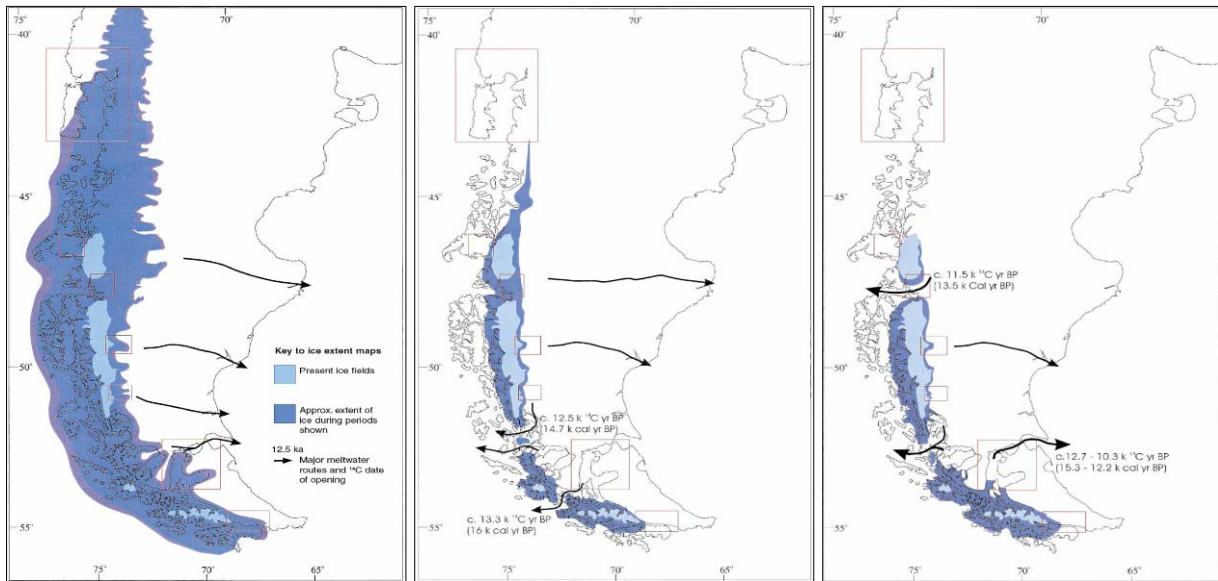
De acuerdo a McCulloch et al. (2000), la deglaciación del UMG ocurre de manera sincrónica en todo Patagonia cercana a los 17,500–17,150 ka AP. Fogwill et al. (2005) y posteriormente Moreno et al. (2009) concluyen que la máxima fase del reavance glacial en Torres del Paine fue entre los 14.8 y 12.6 ka AP ocurre en forma sincrónica con la RFA y que dichos resultados difieren notablemente con los establecidos en el la región de Los Lagos (Hajdas et al., 2003; Moreno et al., 2001), donde el enfriamiento mayor ocurre entre los 13.5 y 11.5 ka AP. Un calentamiento generalizado ocurre en Patagonia a partir de los 11.400 ka AP.

Glasser et al. (2004) realizaron una revisión del Holoceno en Patagonia y en ella establece dos tipos de cronologías para los avances neoglaciales: “Tipo Mercer y Aniya”. Mercer (1968, 1970, 1982) propuso tres avances neoglaciales: 5,413-4,687 Cal ka AP (4.700–4.200 <sup>14</sup>C años AP), 2,758-1,893 Cal ka AP (2.700–2.000 <sup>14</sup>C años AP) y la Pequeña Edad de Hielo desarrollada durante las tres últimas centurias. Aniya (1995, 1996) posteriormente obtuvo en Campos de Hielo Patagonico Sur cuatro avances neoglaciales: 3, 839 ka AP, 2,227 Cal ka AP, 1,455 – 1,286 Cal ka AP y la Pequeña Edad de Hielo desarrollada durante las tres últimas centurias.

*e. ¿Por qué estudiar el registro climático al sur de Sudamérica?*

Existen evidencias palinológicas (Moreno et al., 1999, Lumley y Switsur, 1993; McCulloch y Davies, 2001) que indican que en la zona austral de Sudamérica el calentamiento posterior al Último Máximo Glacial (LGM) se desarrolló en tres etapas (Fig. II.6). La primera ocurrió con posterioridad a la Última Terminación Glacial y se ha desarrollado entre los 17,500-17,150 Cal ka AP afectando a todas las latitudes (Fig. II.6a). La segunda ha ocurrido entre 15,650–15, Cal ka AP en la Región de los Lagos. La tercera etapa ocurre alrededor de los 11,450 Cal ka AP y se desarrolla principalmente al sur de la Región de los Lagos (McCulloch et al., 2000).

El registro climático de la porción sur de Sudamérica tiene el potencial de dilucidar las múltiples hipótesis que toman como base un cambio climático inter-hemisférico para explicar los cambios climáticos bruscos tipo Dansgaard-Oeschger. En el área se desarrolla la célula atmosférica de latitud media (Célula de Ferrel) y se da origen al cinturón de Vientos Predominantes del Oeste (VPO), los cuales responden a los cambios en su localización e intensidad en función del gradiente de presiones entre la zona de altas presiones subtropicales y bajas presiones subpolares. Se cree que durante los episodios glaciales, el núcleo de los VPO migró hacia el norte a latitudes de 45-50° S, brindando las condiciones de humedad y frío necesarias para que los Andes en la Región de los Lagos, cerca de la latitud 41°S, se glaciara (Hubbard, 1997; Denton et al., 1999). Al mismo tiempo, más al sur, en la Región de Magallanes (50-55°S) se redujo la caída de nieve y la expansión de los glaciares fue proporcionalmente menor (Hulton et al., 1994). Luego del último ciclo glacial, los VPO retornaron a su actual latitud.



**a.** **b.** **c.**  
**Fig. II-13:** Reconstrucción glacial por McCulloch y colaboradores (2000):

- Extensión glacial anterior al calentamiento que comienza ca. 17,500–17,150 Cal ka AP (14.600 y 14.300 C<sup>14</sup> AP). Datos basados en los perfiles de polen.
- Extensión glacial luego del calentamiento de los 15,650–15,350 Cal ka AP (14.600 y 14.300 C<sup>14</sup> años AP).
- Extensión glacial anterior al evento cálido que comienza ca. 11,450 Cal ka AP (10.000 C<sup>14</sup> años AP).

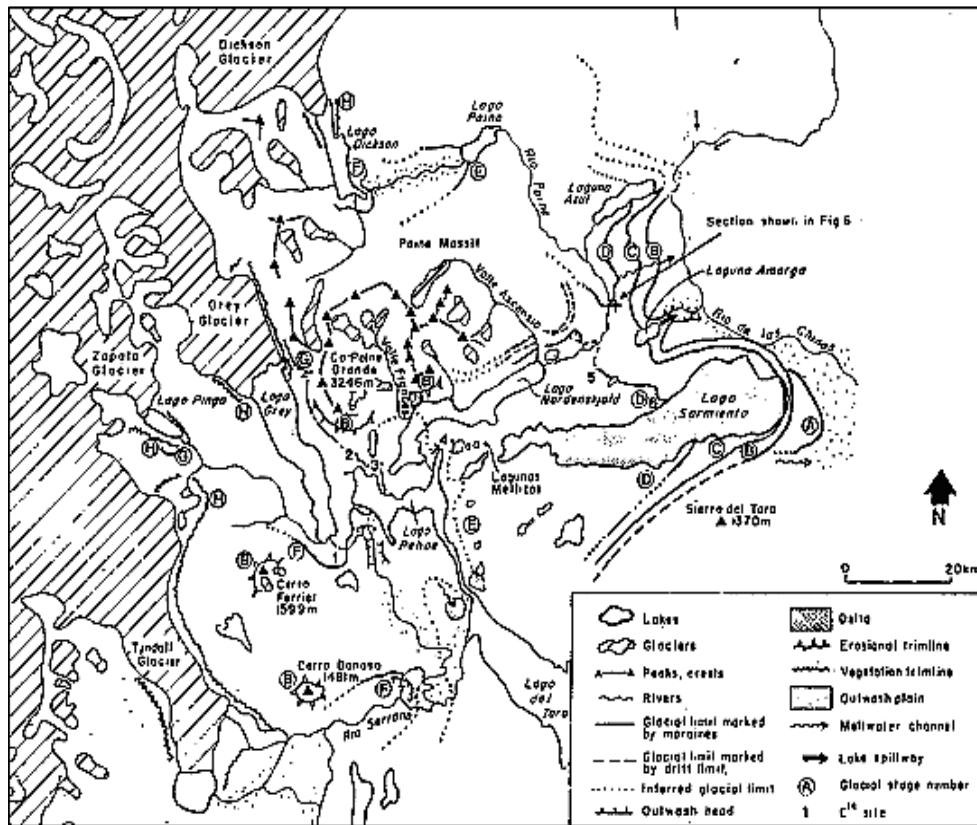
Comprender con mayor precisión la naturaleza y el tiempo de la migración de los VPO es clave para dilucidar las hipótesis inter-hemisféricas enunciadas en los párrafos anteriores. Una reconstrucción de la migración de los VPO solo es posible en la medida que se estructuren nuevos registros de las fluctuaciones glaciales y paleoecológicas que reflejen cambios latitudinales de la distribución de temperatura y precipitaciones.

En conclusión, un importante acierto que evoca un esfuerzo de la comunidad científico mundial, es comprender lo mejor posible los reajustes espaciales y temporales de las diferentes células atmosféricas y la circulación oceánica. Ello permitiría comprender mejor cómo la atmósfera y la hidrósfera se comportan frente a los cambios climáticos de primer orden impuestos por los fenómenos solares y orbitales terrestres y también frente a los enigmáticos cambios climáticos bruscos tipo Dansgaard-Oeschger.



## II.1.5 Fluctuaciones glaciales desde la Última Glaciación y el Holoceno en el Parque Nacional Torres del Paine.

Marden (1993) mapeó el paisaje glacial del área de Torres del Paine, diferenciando ocho ciclos glaciales (etiquetados como A, B, C, D, E, F, G y H de este a oeste en Marben y Clapperton, 1995) desde el margen sureste de los Campos de Hielo hasta las morrenas en la costa este del Lago Sarmiento (Fig. II-14). De los cinco primeros ciclos glaciales se obtuvieron edades por diferentes métodos (dendrocronología, tefrocronología y radiocarbono en partes basales de turbas, pantanos, turbas en hoyos glaciales o “kettles” y anillos de árboles).



**Fig. II-14:** Mapa geomorfológico glacial del Parque Nacional Torres del Paine, área que fue cubierta por los Campos de Hielo Sur Patagónico durante el último ciclo glacial (Marden, 1993).

El avance H que forma las morrenas más jóvenes, está asociado a la Pequeña Edad de Hielo. La edad del árbol más viejo detectado (*Nothofagus pumilio*) que pobló las morrenas fue estimada en 232 años (1.660 D.C.; Armesto, 1992).

La edad de control de las morrenas del avance G no ha sido obtenida, pero su edad relativa indica que es más antigua que la Pequeña Edad de Hielo y más joven que las morrenas del avance F (ca. 11,880 < F > 9,180 ka años AP). El avance G y F pueden correlacionarse con el Sistema Neoglacial Patagónico (Glasser et al., 2004). Marden y Clapperton (1995) determinaron que el avance E es consistente con una edad mínima de

control de ca. 9.755  $^{14}\text{C}$  años AP obtenida de la base de una turba sobre el límite del avance. Sedimentos con pómez re-trabajada encontrados en las capas superiores de una secuencia de delta asociada al avance E, permiten interpretar a Marden y Clapperton (1995) que el glaciar se estabilizó cerca del límite del avance E hace ca. 11.880 años AP. La edad del avance D no ha sido determinada con precisión por el método de radiocarbono, obteniendo un límite mínimo de 11,245 ka AP en la parte basal de un turbal sobre el límite de la morrena, pero gracias al método de del isótopo cosmogénico de  $^{10}\text{Be}$  se le asigna una edad entre 15-12 ka AP, lo cual es correlacionable con el periodo de Regresión Fría Antártico (Fodwill, 2005; Moreno et al., 2009).

Todas las muestras de radiocarbono tomadas en las partes basales de turbas no son mayores a 11,245 ka AP, por lo que Marden y Clapperton (1995) interpretaron que el área esteparia de Torres del Paine no fue colonizada por tórberas hasta después de los ca. 12 ka AP. No existen dataciones disponibles para el avance A, B y C pero se cree pertenecen a la Última Glaciación.



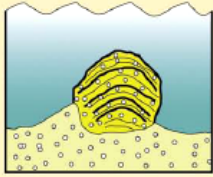
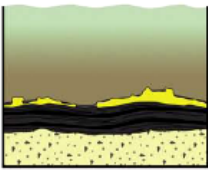
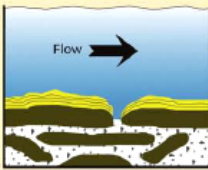
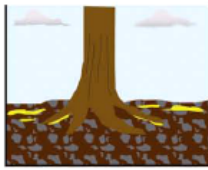
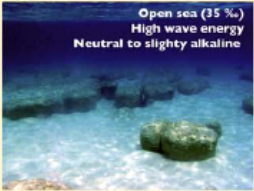
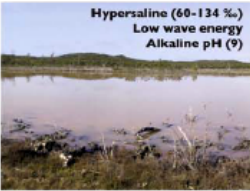







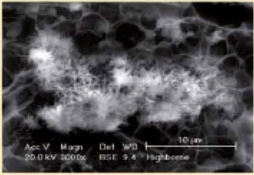
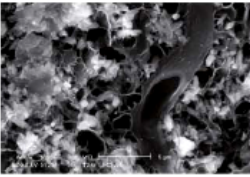
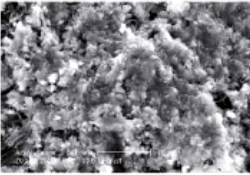

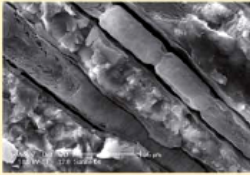

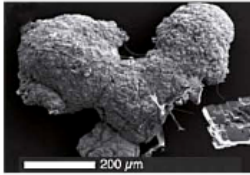
evidencias de vida en la Tierra (Schopf and Packer, 1987; Awramik, 2006; Nisbet y Sleep, 2001; Schidlowski, 1988; Hofmann et al., 1999) y han cambiado fuertemente las condiciones de la atmósfera y biosfera a lo largo del tiempo geológico, siendo las bases para la existencia de la vida moderna (Nisbet y Sleep, 2001; Grotzinger, 1990; Hoehler et al., 2004; Melezhik et al., 2005).

Las comunidades microbianas reinaban las aguas primigénias del planeta en condiciones ambientales muy extremas. Se cree que en el Arqueano existía una atmósfera caliente, polvorienta, rica en gases volcánicos tóxicos, los mares carecían de grandes cantidades de oxígeno y el planeta recibía intensos bombardeos de meteoritos. La vida se adaptó a dichas condiciones extremas y más aun se cree que la actividad de los mantos microbios cambio las condiciones redox, liberando oxígeno e hidrógeno en los mares y la atmósfera. La interpretación de los mantos microbianos fósiles y su rol potencial en alterar las condiciones geoquímicas ambientales de la Tierra es especulativa porque dichos mantos no se encuentran bien preservados (Dupraz et al., 2009).

La preservación de los tapetes microbianos en el registro fósil puede haberse mejorado a través de la precipitación de carbonato, resultando en la formación de mantos litificados, o microbialitas. Diferentes tipos de microbialitas pueden distinguirse en función del proceso de mineralización: biológicamente inducidas y biológicamente influenciadas (Fig. II-15). La mineralización biológicamente inducida resulta de la interacción entre la actividad biológica y el ambiente. La mineralización biológicamente influenciada se define como la mineralización pasiva en materiales orgánicos (de origen biogénicos o abiogénicos), cuyas propiedades influyen la morfología cristalina y la composición. Dupraz et al. (2009) propuso utilizar el termino organomineralización *sensu lato* como un termino que encierre y agrupe ambos tipos de mineralización. Componentes claves en la organomineralización son la alcalinidad (el metabolismo de los microbios y las condiciones ambientales impactan la concentración de carbonatos) y la Sustancia Extracelular Polimétrica (SEP).

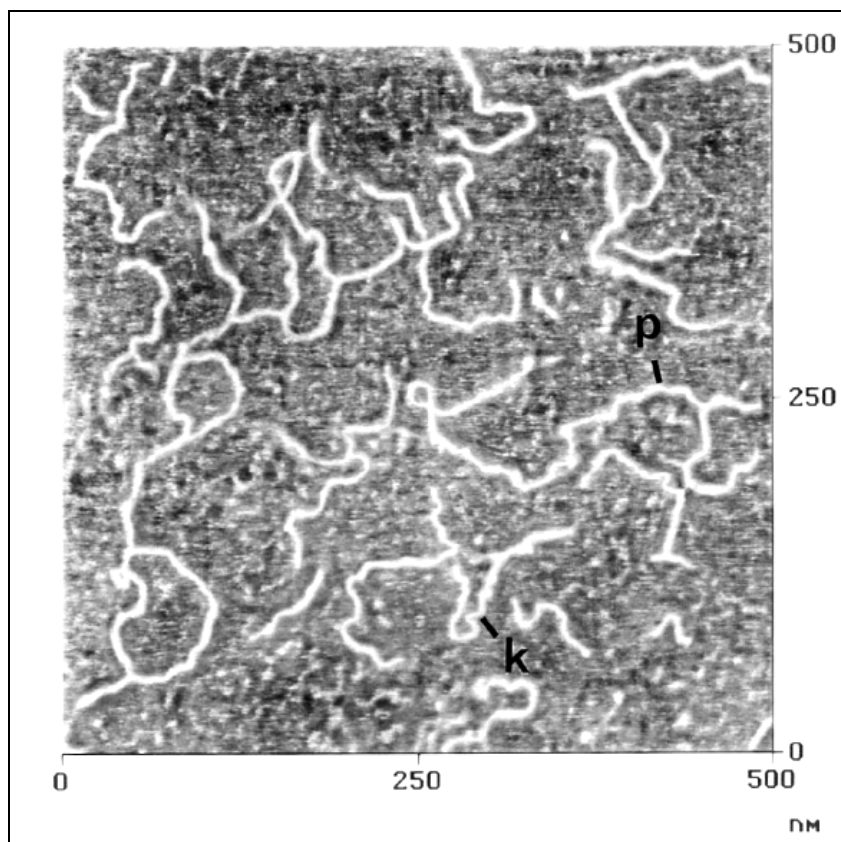
Las microbialitas se pueden clasificar en cuatro tipos generales en función de su fabrica interna: estromatolitos, trombolitos, dendrolitos y travertinos (Riding, 1991). Las microbialitas con laminación interna son estromatolitos, con una fábrica interna con coágulos son trombolitos, dendrítica son dendrolitos y una fabrica interna túpida son travertinos (Fig. II-16). Los trombolitos son frecuentemente asociados con una biota de conchas y cianobacterias filamentosas. Se cree que ellos probablemente tienen tasas de precipitación relativamente rápidas y capturan menor cantidad de sedimentos comparados con los estromatolitos (Kennard, 1994).

Las microbialitas vivientes son complejas colonias de microorganismos las cuales pueden incluir cianobacterias filamentosas fotosintéticas, microalgas eucarióticas, y microbios quicio – autotróficos y heterotróficos (Bauld, 1986). Las cianobacterias producen una Sustancia Extracelular Polimérica (Fig. II-17) la cual sirve para estabilizar físicamente la colonia de células microbianas dentro de ambientes de alta energía, concentrar los iones de  $\text{Ca}^{2+}$  y  $\text{Mg}^{2+}$  del agua que está alrededor, facilitar la retención de detritos y proveer un micro-ambiente químicamente protegido en el cual la precipitación biológicamente inducida de minerales alrededor de la célula puede llevarse a cabo (Decho et al., 2005).

	MARINE ENVIRONMENTS	HYPERSALINE LAKES	FRESHWATER ENVIRONMENTS	CONTINENTAL ENVIRONMENTS
	<p><b>HIGHBORNE CAY</b> COARSE-GRAINED STROMATOLITES</p> 	<p><b>ELEUTHERA</b> MG-CALCITE CRUST AT SURFACE OF MICROBIAL MAT</p> 	<p><b>SARINE RIVER</b> CALCITE CRUST ON SURFACE STONES</p> 	<p><b>IVORY COAST</b> CALCITE PRECIPITATION IN SOILS</p> 
<b>Environments</b>	<p>Open sea (35 ‰) High wave energy Neutral to slightly alkaline</p> 	<p>Hypersaline (60-134 ‰) Low wave energy Alkaline pH (9)</p> 	<p>Freshwater River current</p> 	<p>Oxalotrophic</p> 
<b>Dominant microbes</b>	<p>Schizothrix - Solentia Heterotrophs</p>	<p>Microcoleus - Phormidium Entophysalis - Gloeocapsa Heterotrophs</p>	<p>Phormidium - Oscillatoria</p>	<p>Heterotrophs (Oxalotrophic bacteria, Fungi)</p>
<b>Microbialite</b>	 <p>Open-Marine stromatolites - Laminated - Coarse grained</p>	 <p>Leiolite to thrombolite - Carbonate crust at the surface of microbial mat</p>	 <p>Travertine - Laminated - Micrite</p>	 <p>Carbonate crust/blocs - Micrite - sparite - Spherulite</p>
<b>SEM microstructure</b>	 	 	 	 
<b>Lithification process</b>	<p>↓</p> <p><b>EPS mineralization</b> <b>Sulfate reduction</b></p>	<p>↓</p> <p><b>EPS mineralization</b> <b>Sulfate reduction</b></p>	<p>↓</p> <p><b>Sheath and EPS mineralization</b> <b>Photosynthetic uptake of CO<sub>2</sub></b></p>	<p>↓</p> <p><b>EPS mineralization</b> <b>Heterotrophic bacteria activity</b> <b>(oxalotrophs)</b></p>

**Fig. II-16:** Tipos de microbialitas, macro-micro estructura y sus ambientes de formación (Dupraz et al., 2009).

En la SEP la precipitación de los cristales de tamaños micríticos, resulta del proceso de fotosíntesis que libera oxígeno y captura el  $\text{CO}_2$ , con el consecuente incremento del pH, lo cual induce la precipitación de carbonatos. Aunque este proceso es inducido por los microbios, la precipitación es inorgánica (Vasconcelos, 2005). Cuando la calcificación bio-inducida ocurre, aumenta el número de núcleos cristalinos, promoviendo la precipitación mineral en el micro-ambiente concentrado en iones de la SEP por nucleosíntesis.



**Fig. II-17:** Imagen obtenida por microscopio atómico de las moléculas (tamaño 500x500 nm) que componen a la Sustancia Extracelular Polimérica (SEP). Notar los ángulos abruptos (k) en los polímeros (p) (Decho et al., 1999).

Investigaciones en estromatolitos marinos de las Bahamas revelan una compleja asociación microbiana en la cual todos los microbios juegan un papel físico y químico en la acreción, laminación y litificación de las capas (Reid et al., 2000; Visscher et al., 1998). Por ejemplo, en los estromatolitos de *Highborne Cay* (Bahamas) las cianobacterias fotosintéticas, bacterias reductoras de sulfatos y bacterias anaeróbicas oxidantes de sulfuros producen la precipitación de  $\text{CaCO}_3$ , mientras que los microbios heterotróficos y las bacterias aeróbicas oxidantes de sulfuros disuelven el  $\text{CaCO}_3$  (Visscher et al., 1998)

El crecimiento de las microbialitas es controlado por la interacción entre los microorganismos y su ambiente, aunque la influencia relativa de cada factor permanece sin clarificar. Factores ambientales incluyen la profundidad del agua, temperatura, patrones de sedimentación, acción de las olas, corrientes, migración de las líneas de costa, luz solar, viento y química del agua (Logan et al., 1964; Ginsburg, 1991; Laval et al., 2000; Reid et

al., 2000). No obstante, luego de numerosos estudios en microbialitas, aun no se comprende a cabalidad como los factores biológicos y del ambiente influyen la formación de las microbialitas (Ginsburg, 1991).

El registro isotópico de oxígeno en carbonatos microbianos ha recibido la atención como potenciales inventarios de información paleoclimática y ambiental (Andrews et al., 1993; 1997; Casanova y Hillaire-Marcel, 1992; Vasconcelos et al., 2005; Teranes et al., 1999) y también ha generado considerable debate (Ver la revisión de Chafetz y Lawrence, 1994). La interpretación paleo-termométrica de la variación isotópica en lagos microbialíticos se basa necesariamente en el supuesto de que el fraccionamiento isotópico entre el agua y los carbonatos precipitados se produce en equilibrio, pero en condiciones naturales el equilibrio no siempre existe (Teranes et al., 1999; Kim and O'Neil, 1997). Por otro lado, existe tanto la temperatura como también la mezcla de agua que entra y sale puede controlar la signatura isotópica del lago.

### II.3. Referencias.

- Aniya, M., 1995. Holocene glacial chronology in Patagonia: Tyndall and Upsala Glaciers. *Arct. Alp. Res.* 27, 311–322.
- Aniya, M., 1996. Holocene variations of Ameghino Glacier, southern Patagonia. *Holocene* 6, 247–252.
- Airo, A., Ferrand, D., Lim, D.S., Christopher, M., Solari M.A., Lowe D.R., 2009. Environmental controls on the morphological development of microbialites at Lago Sarmiento, Chile. Submitted to *PALAIOS*.
- Andersen, K.K., Svensson, A., Johnsen, S.J., Rasmussen, S.O., Bigler, M., Röthlisberger, R., Ruth, U., Siggaard-Andersen, M.L., Steffensen, J.P., Dahl-Jensen, D., Vinther, B.M., Clausen, H.B., 2006. The Greenland Ice Core Chronology 2005, 15-42 ka, Part 1: Constructing the time scale, *Quaternary Science Reviews*, vol. 25, Shackleton special issue 24
- Anderson, J.B. 1999. Antarctic marine geology. Cambridge: Cambridge University Press, 287 pp.
- Anderson, J.B., Shipp, S.S., Lowe, A.L., Wellner, J.S., Mosola, A.B., 2002. The Antarctic Ice Sheet during the Last Glacial Maximum and its subsequent retreat history: a review. *Quaternary Science Reviews* 21, 49–70.
- Andrews J.E. Riding R., and Dennis P.F. 1993. Stable isotopic compositions of Recent freshwater cyanobacterial carbonates from the British Isles: local and regional environmental controls. *Sedimentology* 40, 303-314.
- Andrews J.E., Riding R, and Dennis P.F. 1997. The stable isotope record of environmental and climatic signals in modern terrestrial microbial carbonates from Europe. *Palaeogeography, Palaeoclimatology, Palaeoecology* 129, 171-189.
- Armesto J.J., Casassa I., Döllenz. O., 1992. Age structure and dynamics of Patagonian beech forest in Torres del Paine National Park, Chile. *Vegetatio*, 98, 13-22.
- Awramik, S. M., 2006. Respect for stromatolites. *Nature*, v. 441, p. 700-701.
- Barker, P.F., Dalziel, I.W.D., Storey, B.C., 1991. Tectonic development of the Scotia Arc region. In: Tingey, R.J. Ed. ,*Geology of Antarctica*. Oxford Univ. Press, Oxford, pp. 215–248.
- Barker P.F., 2001. Scotia Regional Tectonic Evolution: implication for the mantle flow and paleocirculation. *Earth-Science Review* 55 (2001), 1-39 pp.
- Bauld J., 1986. Benthic microbial communities of Australian saline lakes, in De Deckker., P., and Williamns, W.D., eds., *Limnology in Australia*: Melbourne, Commonwealth Scientific and Industrial Research Organization, and Dordrecht, Junk, p. 95-110.
- Blisniuk P.M., Stern L.A., Chamberlain C.P., Idleman B., Zeitler P.K. 2005. Andes Climatic and ecologic changes during Miocene surface uplift in the Southern Patagonian Andes. *Earth and Planetary Science Letters* 230, 125–142.

- Blunier T, Chappellaz J, Schwander J, Dällenbach A, Stauffer B, Stocker TF, Raynaud D, Jouzel J, Clausen HB, Hammer CV, Johnsen SJ. 1998. Asynchrony of Antarctic and Greenland climate during the last glacial period. *Nature* 394: 739–743.
- Bosak, T., Souza-Egipzy V., Corsetti F.A, Newman D.K., 2004. Micrometer-scale porosity as a biosignature in carbonate crust. *Geology*, v. 32, no 9, p. 781-784.
- Branchu, Ph. and Bergonzini, L., 2004. Chloride concentrations in Lake Tanganyika: an indicator of the hydrological budget?, *Hydrol. Earth Syst. Sci.*, v. 8, p. 256-265.
- Burne, R.V., and Moore, L.S., 1987, *Microbialites: Organosedimentary deposits of benthic microbial communities: Palaios*, v. 2, p. 241–254.
- Caldenius, C.C., 1932. Las glaciaciones cuaternarios en la Patagonia y Tierra del Fuego. *Geogr. Ann.* 14, 1–164 (English summary pages 144– 157).
- Carrasco, J.F., Casassa, G., y Rivera, A., 1998, *Climatología actual del Campo de Hielo Sur y posibles cambios por incremento del efecto invernadero*, *Anales del Instituto de la Patagonia, Serie Ciencias Naturales*, 26:119-128. a unique Natural Laboratory for Environmental and Climate Changes Studies. Edited by Gino Cassasa et al., Klumer, Academic/ Plenum Publishers, 2002.
- Carrasco, J.F., Casassa, G., y Rivera, A. 2002, *Meteorological and Climatological aspect of the Southern Patagonian Icefield. The Patagonian Icefield, a unique Natural Laboratory for Environmental and Climate Changes Studies*. Edited by Gino Cassasa et al., Klumer, Academic/ Plenum Publishers.
- Casassa, G and Rivera, A., 1999, *Topografic mass balance model for the Southern Patagonian Icefield*, *Abstract International Symposium on the Verification of Criospheric models, Bringing Data and Modeling Scientists Together*, 16-20 August 1999, Zurich, p.44.
- Casanova J., and Hillaire-Marcelo C. 1992. Late Holocene hydrological history of Lake tanganyika, East Africa, from isotopic data on fossil stromatolites. *Palaeogeography, Palaeoclimatology, Palaeoecology* 91, 35-48.
- Chafetz, H. and Lawrence, J.R., 1994. Stable isotopic variability within modern travertines. *Geogr. Phys. Quat.*, 48: 257-273.
- Coronato A, Martinez O, Rabassa J. 2004a. Pleistocene glaciations in Argentine Patagonia, South America. In *Quaternary Glaciations: Extent and Chronology. Part III: South America, Asia, Africa, Australia and Antarctica*, Ehlers J, Gibbard P (eds.) *Quaternary Book Series*. Elsevier: Amsterdam; 49–67.
- Clapperton, C., 1993. *Quaternary Geology and Geomorphology of South America* elsevier.
- Clapperton C., 1994, *The quaternary glaciation of Chile: a review*. *Revista de Historia Natural* 67: 369-383.
- Clapperton CM, Hall M, Mothers P, Hole MJ, Still JW, Helmens KF, Kuhry P, Gemmell AMD. 1997. A Younger Dryas ice cap in the equatorial Andes. *Quaternary Research* 47: 13–28.
- Clapperton C, Seltzer G. 2001. Glaciation during marine isotope Stage 2 in the American Cordillera. In *Interhemispheric Climate Linkages*, Markgraf V (ed.). Academic Press: San Diego, CA.
- Daansgard, W., S.J. Johnsen, H.B. Clausen, D. Dahl-Jensen, N.S. Gundestrup, C.U. Hammer, C.S. Hvidberg, J.P. Steffensen, A.E. Sveindjörnsdottir, J. Jouzel y G.Bond, 1993. Evidence for general inestabilty of past climate from 250 kyr ice-core record. *Nature*, 364, 218-220.
- Dalziel IWD 1983 *The evolution of the Scotia Arc: A Review*. In: Oliver RL, James PR, Jago JB (eds) *Antarctic Earth Science*. Australian Academy of Sciences, Canberra, pp 283-288.
- Darwin, Ch., 1842. On the distribution of erratic boulders and on the contemporaneous unstratified deposits of South America. *Trans. Geol. Soc. London*, 2nd.Ser. VI, 415–431.
- Davis B.A.S and Brewer S. 2009. Orbital forcing and role of the latitudinal insolation/temperature gradient. *Clim Dyn*, 32:143–165.
- Decho A. W., Visscher, P. T., Reid P. 2005. Production and cycling of natural microbial exopolymers (EPS) within a marine stromatolites. *Palaeogeography, Palaeoclimatology, Palaeoecology* 219, 71–86.
- Decho, A.W., Kawaguchi, T., 1999. Confocal imaging of natural in situ microbial communities and their extracellular polymeric secretions (EPS) using Nanoplast resin. *BioTechniques* 27, 1246–1251.
- DeMets, C., Gordon, R.G., Argus, D.F., Stein, S., 1990. Current plate motions. *Geophys. J. Int.* 101, 425–478.



- Denton GH, Heusser CJ, Lowell TV, Moreno PI, Andersen BG, Heusser LE, Schluöchter C, Marchant DR. 1999. Interhemispheric linkage of paleoclimate during the last glaciation. *Geografiska. Annaler* 81A(2): 107–153.
- Denton GH, Hendy CH. 1994. Younger Dryas age advance of Franz Josef glacier in the southern Alps of New Zealand. *Science* 264: 1434–1437.
- D.G.A., 1987, Balance Hídrico de Chile, dirección general de Aguas, Chile.
- Douglass DC, Singer BS, Kaplan MR, Mickelson DM, Caffee MW. 2006. Cosmogenic nuclide surface exposure dating of boulders on last-glacial and late-glacial moraines, Lago Buenos Aires, Argentina: interpretive strategies and paleoclimate implications. *Quaternary Geochronology* 1: 43–58
- Dupraz, C., Reid, R.P., Braissant, O., Decho, A.W., Norman, S.R., and Visscher, P.T. 2009. Processes of carbonate precipitation in modern microbial mats. *Earth-Science Review*. 96 (3), 141-162.
- EPICA community members, 2004, Eight glacial cycles from an Antarctic ice core. *Nature*, vol 429 , p. 623-628.
- Fogwill, C.J. and Kubik, P.W. 2005: A glacial stage spanning the Antarctic Cold Reversal in Torres del Paine (51°S), Chile, based on preliminary cosmogenic exposure ages. *Geogr. Ann.*, 87 A (2): 403–408.
- Friedman, I. and O'Neil, J.R., 1977. Compilation of stable isotope fractionation factors of geochemical interest. In: M. Fleischer (Ed), *Data of Geochemistry*, U.S. Geological Survey Professional Paper 440-KK, 6th Ed., Reston, VA.
- Glasser, N.F. and Jansson, K. 2008 a. The glacial map of southern South America. *Journal of Maps*, v2008, 175-196.
- Glasser, N.F., Harrison, S., Jansson, K. and Kleman, J. 2008 b. The glacial geomorphology and Pleistocene history of southern South America between 38oS and 56oS. *Quaternary Science Reviews*, 27(3-4), 365-390.
- Glasser, N.F., Harrison, S., Winchester, V., Aniya, M., 2004. Late Pleistocene and Holocene palaeoclimate and glacier fluctuations in Patagonia. *Global and Planetary Change* 43, 79–101.
- Ghidella ME, Yáñez G, LaBrecque JL. 2002. Revised tectonic implications for the magnetic anomalies of the Western Weddell sea, *Tectonophysics* 347: 65-86.
- Gibson J.J., Edwards T.W.D., Prowse T.D., 1999. Pan-derived isotopic composition of atmospheric water vapor and its variability in northern Canada. *Journal of Hydrology*, v. 217, p. 55–74.
- Ginsburg, R. N., 1991, Controversies about stromatolites: Vices and virtues. *Controversies in Modern Geology: Evolution of Geological Theories in Sedimentology, Earth History and Tectonics*. D. W. Müller, J. A. McKenzie and H. Weissert. London, Harcourt Brace Jovanovich, Publishers: p. 25-36.
- Grotzinger, J. P., 1990, Geochemical model for proterozoic stromatolite decline. *American Journal of Science* v. 290A, p. 80-103.
- Hajdas, I., Bonani, G., Moreno, P.I., and Ariztegui, D., 2003, Precise radiocarbon dating of lateglacial cooling in mid-latitude South America: *Quaternary Research*, v. 59, p. 70–78,
- Harrison S. 2004. The Pleistocene glaciations of Chile. In *Pleistocene Glaciations: Extent and Chronology*, Ehlers J, Gibbard P (eds.) INQUA/Elsevier: Amsterdam; 89–103.
- Hays, P.D. and Grossman, E.L., 1991. Oxygen isotopes in meteoric calcite cements as indicators of continental palaeoclimate. *Geology*, 19: 441-444.
- Heusser, C.J. 1987. FIRE history of Fuego – Patagonia.
- Heusser C.J. 2003. *Ice Age Southern Andes: A Chronicle of Palaeoecological Events*. Elsevier: Amsterdam.
- Hofmann H.J., Grey K., Hickman A.H., and Thorpe R. I., 1999. Origin of 3.45 Ga coniform stromatolites in Warrawoona Group, Western Australia. *GSA Bulletin*, v. 111, no. 8, p. 1256-1262.
- Hoehler T. M., Bebout B.M., and Des Marais D.J., 2004. The role of microbial mats in the production of reduced gases on the early Earth. *Nature*, v. 412, 19 JULY, p. 324-325.
- Hubbard AL. 1997. Modelling climate, topography and palaeoglacier fluctuations in the Chilean Andes. *Earth Surface Processes and Landforms* 22: 79–92.

- Hulton NRJ, Sugden DE, Payne A, Clapperton CM. 1994. Glacier modeling and the climate of Patagonia during the Last Glacial Maximum. *Quaternary Research* 42: 1–19.
- Ibarzabal y Donángelo, T., Hoffmann, J. A. J., and Naruse, R., 1996, Recent climatic change in southern Patagonian, *Bulletin of Glacier Research*, 14:29-36.
- Ivy-Ochs S., Schlüchter C., Kubik PW., Denton GH. 1999. Moraine exposure dates imply synchronous Younger Dryas advances in the European Alps and in the Southern Alps of New Zealand. *Geografiska Annaler* 81A(2): 313–323.
- Jokat W, Boebel T, König M, Meyer U (2003) Timing and geometry of early Gondwana breakup. *Journal of Geophysical Research* 108(B9), 2428, doi: 10.1029/2002JB001802: 1-15.
- Kaplan MR, Ackert RP, Singer BS, Douglass DC, Kurz MD. 2004. Cosmogenic nuclide chronology of millennial-scale glacial advances during O-isotope Stage 2 in Patagonia. *Geological Society of America Bulletin* 116: 308–321.
- Kaplan MR, Douglass DC, Singer BS, Ackert RP, Caffee MW. 2005. Cosmogenic nuclide chronology of pre-last glaciation maximum moraines at Lago Buenos Aires, 468 S, Argentina. *Quaternary Research* 63: 301–315.
- Kaplan, M.R., Moreno, P.I., Rojas, M. 2008 a. Glacial dynamics in southernmost South America during Marine Isotope Stage 5e to the Younger Dryas chron: a brief review with a focus on cosmogenic nuclide measurements. *Journal of Quaternary Science*, 23, 649-658.
- Kaplan MR, Fogwill CJ, Sugden DE, Hulton NRJ, Kubik PW, Freeman SPHT. 2008 b. Southern Patagonian and Southern Ocean climate during the last glacial period. *Quaternary Science Reviews* 27:284–294.
- Katz, H. R., 1963, Revision of Cretaceous Stratigraphy in the Patagonian Cordillera of Ultima Esperanza, Magallanes Province, Chile. *American Association of Petroleum Geologists Bulletin*, v. 47(3), p. 506-524.
- Kennard, J. M., 1994, Thrombolites and stromatolites within shale-carbonate cycles, Middle-Late Cambrian Shannon Formation, Amadeus Basin, Central Australia. *Phanerozoic Stromatolites II*. J. Bertrand-Sarfati and C. Monty. London, Kluwer Academic Publishers: 443-471.
- Kilian R., Hohner, M., Biester, H., Wallrade-Adams J. and Stern C.R. 2003. Holocene peat and lake sediment tephra record from the southernmost Chilean Andes (53-55°S). *Rev. geol. Chile*, jul. 2003, vol.30, no.1, p.23-37.
- Kim S. T. and O'Neil J. R. (1997) Equilibrium and nonequilibrium oxygen isotope effects in synthetic carbonates. *Geochim. Cosmochim. Acta* 61, 3461–3475.
- Lambeck, K. and Chappell, J., 2001. Sea Level Change through the Last Glacial Cycle. *Science*, Vol 292, 679-686.
- Lawver L A, Dalziel I W D, Gahagan L M (1998) A tight fit Early Mesozoic Gondwana, a plate reconstruction perspective. *Memoirs of the National Institute for Polar Research, Special issue*, 53: 214 -229, Tokyo.
- Laval, B., Cady, S. L., et al., 2000, Modern freshwater microbialite analogues for ancient dendritic reef structures. *Nature*, v. 407, p. 626-629.
- Livermore, R.L., McAdoo, D.C., Marks, K.M., 1994. Scotia Sea tectonics from high-resolution satellite gravity. *Earth Planet.Sci. Lett.* 123, 255–268.
- Logan, B. W., R. Rezak, et al. (1964). Classification and environmental significance of algal stromatolites. *Journal of Geology* v.72: p.68-83.
- Lowell TV, Heusser CJ, Andersen BG, Moreno PI, Hauser A, Heusser LE, Schlüchter C, Marchant DR, Denton GH. 1995. Interhemispheric correlation of Late Pleistocene glacial events. *Science* 269,1541–1549.
- Lumley SH, Switsur R. 1993. Late Quaternary chronology of the Taitao Peninsula, southern Chile. *Journal of Quaternary Science* 8: 161–165.
- Marden, C.J. 1993. Late Quaternary glacial history of the SouthPatagonian Icefield at Torres del Paine, Chile. Ph.D. Thesis, University of Aberdeen, 298.

- Marden C., and Clapperton C.M., 1995, Fluctuations of the South Patagonian Ice-field during the last glaciation and the Holocene, Department of Geography, University Of Aderdeen AB9 2UF, Scotlnd. Journal of Quaternary Science 10(3).
- McCulloch, R.D., 1994. Palaeoenvironmental evidence for the late-glacial in the Strait of Magellan, Sothern Patagonia. Unpublished PhD thesis, University of Aderdeen.
- McCulloch, R.D., Bentley, M.J., Purves, R.S., Hulton, N.R.J., Sugden, D.E. and Clapperton, C.M., 2000: Climatic inferences from glacial and palaeoecological evidence at the last glacial termination, southern South America. Journal of Quaternary. Science, 15: 409–417.
- McCulloch, R.D. and Davies, S.J., 2001: Late-glacial and Holocene palaeoenvironmental change in the central Strait of Magellan, southern Patagonia. Palaeogeography, Palaeoclimatology, Palaeoecology, 173: 143–173.
- McCulloch R.D., Fogwill C.J., Sugden D.E. 2005. Late glacial maxima, the Antarctic Cold Reversal and the Younger Dryas in the Strait of Magellan and Bahí'a Inu' til; a revised chronology. Geografiska Annaler 87: 289–312.
- Meglioli A. 1992. Glacial geology and chronology of southernmost Patagonia and Tierra del Fuego, Argentina and Chile. PhD dissertation, Lehigh University, Bethlehem, PA.
- Melezhic V.A., Fallik A. E., Hanski E.J., Kump L.R., Lepland A., Prave A.R., and Strauss H., 2005. Emergence of the biosphere during the Archean – Proterozoic transition: Challenges of future research. GSA Today, v. 15, no. 11, p.4- 11.
- Mercer, J.H., 1968. Variations of some Patagonian glaciers since the Late-Glacial. Am. J. Sci. 266, 91– 109.
- Mercer, J.H., 1970. Variations of some Patagonian glaciers since the Late-Glacial: II. Am. J. Sci. 269, 1 – 25.
- Mercer, J.H., 1976. Glacial history of Southernmost South America. Quaternary Research 6, 125–166.
- Mercer, J.H., 1982. Holocene glacier variations in southern Patagonia. Striae 18, 35– 40.
- Miller H , 1983. The position of Antarctica within Gondwana in the light of Palaeozoic orogenic development In: Oliver, RL, James, PR and Jago J.B. (eds), Antarctic Earth Science: 579-581; Canberra (Australian Academy of Sciences).
- Moreno PI., Lowell TV, Jacobson GL Jr, Denton GH. 1999. Abrupt vegetation and climate changes during the last glacial maximum and the last termination in the Chilean Lake District: a case study from Canal de la Puntilla (41°S). Geografiska Annaler 81A (2):285–311.
- Moreno, P.I., Jacobson, G.L., Lowell, T.V., and Denton, G.H., 2001, Interhemispheric climate links revealed by a late-glacial cooling episode in southern Chile: Nature, v. 409, p. 804–808.
- Moreno, P.I., Kaplan, M.R., François, J.P., Villa-Martínez, R., Moy, C.M., Stern, C.R., Kubik, P.W., 2009. Renewed glacial activity during the Antarctic cold reversal and persistence of cold conditions until 11.5 ka in southwestern Patagonia. Geology, 37(4), 375-378.
- Milankovitch, M. 1930. Mathematische Klimalhre und Astronomische Theorie der Klimaschwankungen, Gebruder Borntraeger, Berlin. 176 pp.
- Mix AC, Bard E, Schneider R. 2001. Environmental processes of the ice age: land, oceans, glaciers (EPILOG). Quaternary Science Reviews 20: 627–657.
- Nisbet E. G. & Sleep N. H., 2001. The habitat and nature of early life. Nature, v. 409, p. 1983-1991.
- NGRIP dating group, 2006. Greenland Ice Core Chronology 2005 (GICC05), IGBP PAGES/World Data Center for Paleoclimatology Data Contribution Series # 2006-118, NOAA/NCDC Paleoclimatology Program, Boulder CO, USA.
- North Greenland Ice Core Project members. 2004. High-resolution record of Northern Hemisphere climate extending into the last interglacial period. Nature, 431, 147- 151
- O'Neil, J.R., Clayton, R.N. and Mayeda, T.K., 1969. Oxygen isotope fractionation in divalent metal carbonates. J. Chem. Phys., 51:5547 5558.
- Patterson, W.P., Smith, G.R., and Lohmann, K.C. 1993. Continental paleothermometry and seasonality using the isotopic composition of aragonitic otoliths of freshwater fishes. In Continental climate change from isotopic records. Edited by P.A. Swart, K.C. Lohmann, J. McKenzie, and S. Savin. Monogr. No. 78, American Geophysical Union, Washington, D.C. pp. 191–202.

- Porter SC, Clapperton CM, Sudgen DE. 1992. Chronology and dynamics of deglaciation along and near the Strait of Magellan, southernmost South America. *Sveriges Geologiska Undersökning, Ser. Ca.* 81: 233–239.
- Rabassa J, Clapperton CM. 1990. Quaternary glaciations in the southern Andes. *Quaternary Science Reviews* 9: 153–174.
- Rabassa J., Coronato A.M., Salemme M. 2005. Chronology of the Late Cenozoic Patagonian glaciations and their correlation with biostratigraphic units of the Pampean region (Argentina). *Journal of South American Earth Sciences*, 20, 81–103.
- Rasmussen, S. O, K. K. Andersen, A. M. Svensson, J. P. Steffensen, B. M. Vinther, H. B. Clausen, M.-L. Siggaard-Andersen, S. J. Johnsen, L. B. Larsen, M. Bigler, R. Røthlisberger, H. Fischer, K. Goto-Azuma, M. E. Hansson and U. Ruth. 2006. A new Greenland ice core chronology for the last glacial termination, *J. Geophys. Res.*
- Reid, R. P., Visscher, P. T., Decho A. W., Stolz J. F., Beboutk B. M., Dupraz C., Macintyre I. G., Paerl H. W., Pinckney J. L., Prufert-Beboutk L., Steppe T. F. and DesMarais D. J. 2000. The role of microbes in accretion, lamination and early lithification of modern marine stromatolites. *Nature*, v. 406, p. 989-992.
- Riding, R., 1991, Classification of microbial carbonates. *Calcareous algae and stromatolites*. R. Riding. Berlin, Springer-Verlag: p. 21-51.
- Singer BS, Ackert RP, Guillou H. 2004. <sup>40</sup>Ar/<sup>39</sup>Ar and K-Ar chronology of Pleistocene glaciations in Patagonia. *Geological Society of America Bulletin* 116: 434–450.
- Solari, 2003. Modelamiento analógico de la evolución tectónica Pliocena y Cuaternaria de la Cuenca de Bransfield, Península Antártica. Memoria de Título de Geólogo, Universidad de Chile, Facultad de Ciencias Físicas y Matemáticas. 123 pp.
- Solari, M., Hervé, F., and Martinez, J., 2004. The presence of living stromatolites at Laguna Amarga, Torres del Paine National park, southernmost Chile. 2004 Denver Annual Meeting (November 7–10, 2004).
- Solari M and Airo A. 2007. Glacio lacustrine evolution and modern microbialites at lagos Sarmiento, del Toro and Laguna Amarga. Capítulo 3 en: the Field Trip Guide of the International Geological Congress on the Southern Hemisphere Punta Arenas, Chile 21/25 November 2007. Compiled and edited by Mauricio Calderón, Francisco Hervé and Marcelo Solari.
- Solari M., Hervé F., Martinod J., Ramirez L., Le Roux J., Palacios C. 2008a. Geomorphologic and tectonic evolution of the Bransfield Basin, Antarctic Peninsula: insights from analogue models. *Antarctic Sciences*.
- Solari M. 2008b. La importancia de comprender el registro climático en Sudamérica. *Ecoengen. Revista de Medio Ambiente – FACEA UCENTRAL*. N° 9. ISSN 0718-0454
- Schidlowski, M. A., 1988. 3,800 million-year old record of life from carbon in sedimentary rocks. *Nature* v. 333, p. 313–318.
- Schopf, J. W. and Packer, B. M. 1987. Early Archean (3.3 billion to 3.5 billion year old) microfossils from Warrawoona Group, Australia. *Science* v. 237, p. 70–73 .
- Schwander J., Jouzel J., Hammer C.U., Petit J.R., Udisti R., Wolff E., 2001. A tentative chronology for the EPICA Dome Concordia ice core. *Geophys. Res. Lett.*, 28 (22): 4243-4246.
- Sowers T, Bender M., 1995. Climate records covering the last deglaciation. *Science* 269: 210–214.
- Steig E.J, Brook E.J, White J.W.C, Sucher C.M, Bender M.L, Lehman S.J, Morse DL, Waddington E.D, Clow G.D. 1998. Synchronous climate changes in Antarctica and the North Atlantic. *Science* 282: 92–95.
- Stenni, B., V. Masson-Delmotte, S. Johnsen, J. Jouzel, A. Longinelli, E. Monnin, R. Rothlisberger, and E. Selmo. 2001. An Oceanic Cold Reversal during the last deglaciation. *Science*, 293: 2074-2077.
- Stenni, B., J. Jouzel, V. Masson-Delmotte, R. Rothlisberger, E. Castellano, O. Cattani, S. Falourd, S.J. Johnsen, A. Longinelli, J.P. Sachs, E. Selmo, R. Souchez, J.P. Steffensen, R. Udisti. 2003. A late-glacial high-resolution site and source temperature record derived from the EPICA Dome C isotope records (East Antarctica), *Earth Planet. Sci. Lett.*, 217: 183-195.

- Stenni, B.; Sachs, J.P.; Selmo, E.; Souchez, R.; Steffensen, J.P.; Udisti, R.; Jouzel, J.; Masson-Delmotte, V.; Rothlisberger, R.; Castellano, E.; Cattani, O.; Falourd, S.; Johnsen, S.J.; Longinelli, A. 2006. EPICA Dome C Stable Isotope Data to 44.8 KYrBP. IGBP PAGES/World Data Center for Paleoclimatology Data Contribution Series # 2006-112. NOAA/NCDC Paleoclimatology Program, Boulder CO, USA.
- Steig E.J, Brook E.J, White J.W.C, Sucher C.M, Bender M.L, Lehman S.J, Morse DL, Waddington E.D, Clow G.D. 1998. Synchronous climate changes in Antarctica and the North Atlantic. *Science* 282: 92–95.
- Stern, C. R., 1990, Tephrocronology of southernmost Patagonia. *National Geographic Research*, 6, 110-126.
- Svensson A, K,K, Andersen, M, Bigler, H,B, Clausen, D, Dahl-Jensen, S,M, Davies, S,J, Johnsen, R, Muscheler, S,O, Rasmussen, R, Röthlisberger, J,P, Steffensen, and B,M, Vinther, 2006. The Greenland Ice Core Chronology 2005, 15-42 ka, Part 2: Comparison to other records, *Quaternary Science Reviews*, vol, 25, Shackleton special issue 24.
- Tectonic Map of the Scotia Arc, 1985. 1:3000000. BAS Misc 3. British Antarctic Survey, Cambridge.
- Teranes, J.L., McKenzie J.A., Bernasconi S.M., Lotter A.F., and Sturm M. 1999. Study of oxygen isotopic fractionation during bio-induced calcite precipitation in eutrophic Baldeggersee, Switzerland. *Geochimica et Cosmochimica Acta*, Vol. 63, No. 13/14, pp. 1981–1989.
- Vasconcelos C, McKenzie J.A., Warthmann R, and Bernasconi S.M., 2005. Calibration of the  $\delta^{18}\text{O}$  paleothermometer for dolomite precipitated in microbial cultures and natural environments. *Geology* 2005 33: 317-320.
- Visscher P.T., Reid R.P., Bebout B.M., Hoefft S.E., Macintyre I.G., and Thompson J.A. Jr. 1998. Formation of lithified micritic laminae in modern marine stromatolites (Bahamas): The role of sulfur cycling: *American Mineralogist*, v. 83, p. 1482–1493.
- Vinther, B.M., H.B, Clausen, S.J, Johnsen, S.O, Rasmussen, K.K, Andersen, S.L, Buchardt, D, Dahl-Jensen, I.K, Seierstad, M,-L, Siggaard-Andersen, J.P, Steffensen, A.M, Svensson, J, Olsen, and J, Heinemeier, 2006, A synchronized dating of three Greenland ice cores throughout the Holocene, *Journ, Geophys, Res*, vol, 111, D13102, 2006, doi:10.1029/2005JD006921
- Wray JL (1977) *Calcareous Algae*. Elsevier, Amsterdam.
- Zachos, J., Pagani, M., Sloan, L., Thomas, E. and Billups, K. 2001. Trends, rhythms, and aberrations in global climate 65 Ma to present. *Science*, 292, 686–693.

### **III. La Evolución del Gran Paleolago Tehuelche**

#### **III.1. Hipótesis, Fundamentos y Metodología.**

Se postula que las fluctuaciones glaciares son determinantes en la evolución del sistema hidrológico existente al este de los Campos de Hielo y que la evolución de dicho sistema esta vinculada a variaciones en la intensidad y localización de los Vientos Predominantes del Oeste. Por lo cual, en el sector de Torres del Paine es posible refinar la cronología de eventos glaciares por medio del estudio de la evolución del sistema hidrológico y en particular la evolución de un paleolago proglacial denominado en este estudio como “Gran Paleolago Tehuelche”. Investigar y dilucidar la evolución del sistema hidrológico al este de las morrenas terminales existentes en el Parque Nacional Torres del Paine permite contribuir a conocer parte de la evolución paleoclimática del sector.

A continuación se detalla la metodología empleada para contribuir a conocer la evolución del sistema hidrológico del sector:

- a. Análisis geomorfológico por medio de observaciones de terreno y métodos de teledetección en fotos aéreas, imágenes satelitales y modelos digitales de elevación.
- b. Construcción y correlación de columnas estratigráficas en: margen este del lago El Toro, terrazas al norte de Cerro Castillo, el lago Porteño y al este del río Las Chinas.
- c. Dataciones de radiocarbono en lignitas y gastrópodos lacustres.

A continuación se presenta un artículo aceptado el 11 de junio del año 2010 por la revista *Andean Geology*. En él se presenta la evolución del sistema hídrico del Parque Nacional Torres del Paine, con mayor detalle se describe la metodología utilizada y el trabajo realizado para reconstruir la extensión y cronología de los glaciares y lagos desde el Último Máximo Glacial en el sector de estudio.

### **III.2. Late Quaternary lake level fluctuations of the Great Tehuelche Paleolake in the Torres del Paine National Park.**

M.A. Solari <sup>1\*</sup>, M. Calderón <sup>1</sup>, A. Airo <sup>2</sup>, J.P. Le Roux <sup>1</sup>, F. Hervé <sup>1</sup>

<sup>1</sup> *Departamento de Geología, Facultad de Ciencias Físicas y Matemáticas, Universidad de Chile, Casilla 13518, Correo 21, Santiago, Chile.*

<sup>2</sup> *School of Earth Sciences, Stanford University, 450 Serra Mall, Bldg. 320, Rm. 118 Stanford, CA 94305, USA.*

**Key words:** Patagonia, Last Glacial, Antarctic Cold Reverse, Younger Dries.

**Corresponding autor:** [msolari@cec.uchile.cl](mailto:msolari@cec.uchile.cl) (fax 56-2-6963050).

#### *III.2.1 Abstract*

##### *Abstract*

A suite of glacial moraines distributed from the eastern margin of the Torres del Paine Drainage Basin to near the present margin of the Patagonian Icefields, together with a set of regionally continuous lacustrine terraces are related to the past glacial fluctuations. The geomorphology, supported by lake sediment evidence, indicates the existence of a single proglacial paleolake in this area, here referred to as the Great Tehuelche Paleolake. This concept helps to clarify the chronology of glacial events and leads to a better understanding of the evolution of the hydrologic system in the Torres del Paine area. Glacial advances previously referred to as A, B and C occurred during the Last Glacial Maximum and fed the Great Tehuelche Paleolake with meltwater, allowing it to reach its maximum extension. The discovery of thrombolites at Laguna Amarga suggests that the drainage of the paleolake towards the Última Esperanza Fjord took place at 7113 Cal. yr BP, after the melting of an ice barrier that existed during the earlier glacial advance. This gave rise to the development of a complex fluvio-lacustrine hydrologic system that persists to the present day.

##### *Resumen*

Un grupo de morrenas glaciales están distribuidas desde el margen este de la Cuenca de Drenaje de Torres del Paine hacia el margen actual de los Campos de Hielo Patagónicos. Las morrenas se observan en conjunto con un grupo de terrazas lacustres regionales, las cuales están vinculadas a las fluctuaciones glaciales. La geomorfología y evidencias de sedimentos lacustres, indican la existencia de un único lago proglacial, referido en este estudio como Gran Paleolago Tehuelche. Este concepto ayuda a clarificar la cronología de los eventos glaciales y permite una mejor comprensión de la evolución del sistema hidrológico del sector de Torres del Paine. Los eventos glaciales, previamente referidos como Avance A, B y C ocurrieron durante el Último Máximo Glacial y alimentaron con aguas de fusión al Gran Paleolago Tehuelche, permitiéndole alcanzar su mayor extensión. El descubrimiento de trombolitos en Laguna Amarga sugiere que el desagüe del paleolago ocurrió hace 7113 Cal. años AP por el Seno de Última Esperanza y

que ocurrió producto de la fusión de una barrera glaciaria existente durante los avances glaciales anteriores. Luego del drenaje se desarrolló un complejo sistema hidrológico que persiste hasta el presente.

### *III.2.2 Introduction*

The Patagonian Ice Field fluctuation in the southern part of South America has considerable potential to contribute to the debate on interhemispheric abrupt climate change. The existence of the Patagonian Ice Field in a temperate, low latitude zone at an average elevation of only about 2,000 m a.s.l., can be explained by the high rainfall resulting from the predominantly westerly winds (June-July mean) and frontal systems (Carrasco et al., 2002; Carrasco et al., 1998; Ibarzabal and Donángelo et al., 1996). Therefore, deciphering the glacial fluctuations of the Patagonian Ice Field and the evolution of the hydrological system around their margins are key factors to understanding the fluctuation of the Westerlies and their relationship with global climatic events.

Studies of stable oxygen isotopes of foraminifers preserved in sediment samples from the Indian Ocean suggest that climatic variations causing the retreat of the ice caps and a rising of sea level are supported by the orbital theory of Milankovitch (Imbrie et al., 1984). In ice cores obtained from the Antarctic (EPICA, 2004) and Greenland (North Greenland Ice Core Project, 2004) it is also possible to observe these cycles as predicted by the orbital theory. However, the short, irregular and abrupt interglacial stadials also recorded in the ice cores occur on much shorter timescales than the variations explained by the orbital theory. These short stadials are of almost the same magnitude as those related to glacial or interglacial periods at a 100,000 yr scale, but represent intervals of only hundreds of years (Dansgaard et al., 1993).

Good examples of such abrupt changes include the global warming after the Last Glacial Maximum and the subsequent glacial readvance (Cold Reversal in Fig. III-1). Different hypotheses, generally based on inter-hemispheric climate changes, exist to try and explain why these climate variations occurred on earth.

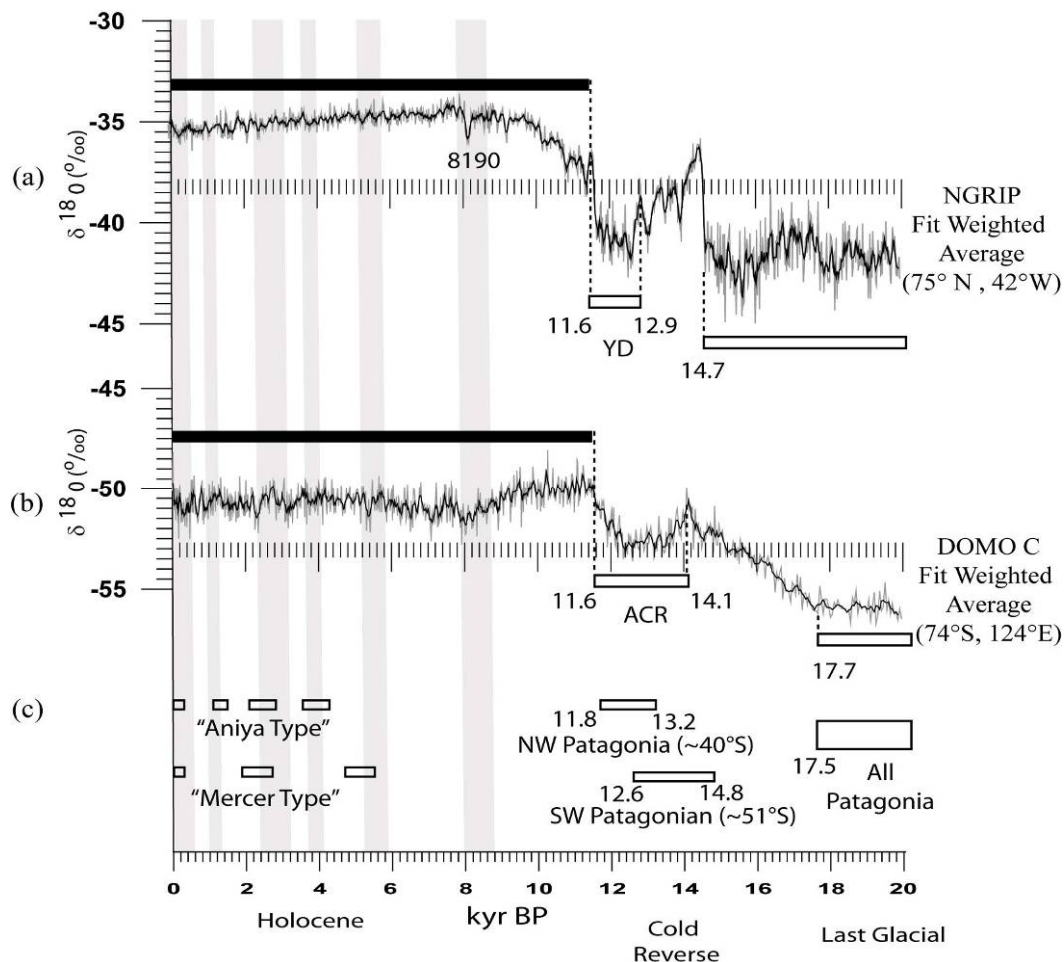
One line of hypotheses based on interhemispheric change postulates that changes in the Milankovitch insolation cycles (Imbrie et al., 1992) or ice rafting events (Bond et al., 1993; Macayeal, 1993; Bond and Lotti, 1995) could have produced variations in the density of the North Atlantic surface water, associated with changing temperature and glacial meltwater fluxes. These could have affected the turnover of the convection, thus linking ocean circulation between the Northern and Southern Hemispheres and modifying the patterns of global heat transfer to high latitudes. The hypothesis is partly supported by an analysis of oxygen isotopes from ice-sheet cores, which suggests that changes in Greenland may have preceded those in the Antarctic (Bender et al., 1994).

A second line of hypotheses based on ice cores from the Antarctic (EPICA, 2004), and Greenland (North Greenland Ice Core Project, 2004), suggests that climate variations in the Southern Hemisphere trigger changes in the Northern Hemisphere. Comparison of the ice cores suggests that the warming tendency after the Last Glaciation started first in Antarctica, from where it spread to Bolivia and then to Greenland. In addition, the ice cores from Antarctica reveal an abrupt inversion event (the Antarctic Cold Reverse or ACR) before the equivalent Younger Dryas (YD) event of the Northern Hemisphere (Blunier et al., 1998; Sowers and Bender, 1995).

A third line of hypotheses maintains that climate changes occurred simultaneously in both hemispheres. Studies by Denton et al. (1999) in the Lake District of Chile and in



New Zealand provided a record of glacial fluctuations that indicates a glacial event chronology simultaneous with the YD event of the North Atlantic region (Lowell et al., 1995; Denton et al., 1999). The good correlation between both sets of observations may indicate that the glacial-interglacial transition between both hemispheres occurred in phase. These conclusions are supported by evidence of events equivalent to the YD in Ecuador (Clapperton et al., 1997) and New Zealand (Denton and Hendy, 1994; Ivy-Ochs et al., 1999). Ice core analysis of the Taylor Dome and the Ross Sea Shelf in Antarctica (Steig et al., 1998) supports the hypothesis of simultaneous interhemispheric climate changes.



**Fig. III-1:** Ice core  $\delta^{18}\text{O}$  (VSMOW) paleoclimate and discontinuous glacial advance records. Grey bands represent timing of the HRCC (Mayewski et al., 2004) and white rectangles represent cool periods. (a) Smoothed weighted average (black line) of NGRIP  $\delta^{18}\text{O}$  (grey line) ice core paleoclimate proxy data (NGRIP, 2006; Vinther et al., 2006; Rasmussen et al., 2006; Andersen et al., 2006; Svensson et al., 2006). (b) Smoothed weighted average (black line) of Dome C  $\delta^{18}\text{O}$  (grey line) ice core paleoclimate proxy data (Stenni et al., 2001, 2003, 2006; Jouzel et al., 2001; Schwander et al., 2001). (c) “Mercer and Aniya Type” Neoglacil advances events in Patagonia (Mercer, 1968, 1970, 1982; Aniya, 1995, 1996), Cold Reversal Period in Lake District in northwestern Chilean Patagonia (Hajdas et al., 2003; Moreno et al., 2001), Cold Reversal Period in Torres del Paine (Moreno et al., 2009) and synchronous Patagonian LGM deglaciation.

According to Denton and Karlen (1973) Holocene global glacier fluctuations can be identified at 9,000–8,000, 6,000–5,000, 4,200–3,800, 3,500–2,500, and 1,200–1,000 yrs, and also since 600 yr BP (grey bands in Fig. III-1). Mayewski et al. (2004) examined about 50 globally distributed paleoclimate records that validated the six periods of significant Holocene rapid climate change (HRCC). Most of the climate change events in these globally distributed records are characterized by polar cooling, tropical aridity, and major atmospheric circulation changes, although during the most recent interval (600–150 yr BP), polar cooling was accompanied by increased moisture in some parts of the tropics.

In this paper we examine climate changes in Chilean Patagonia during the Holocene, in order to contribute to the evaluation of the different scenarios outlined above.

### *III.2.3 Glaciation in Patagonia*

During the Pleistocene, the western part of southernmost South America was buried beneath a thick ice cap, the remnants of which still remain in the form of large ice fields in Patagonia. Presently, the Northern Patagonian Ice Field (NPI) lies between about 46° and 48°S, whereas the Southern Patagonia Ice Field (SPI) stretches from the southern shores of the Baker Channel almost to Puerto Natales at about 51°S.

The chronology of Patagonian glaciations is among the most complete in the world and our understanding of the different has made significant progress in the past decade, following the pioneering work of Caldenius (1932), Mercer (1976), Clapperton (1993), Rabassa et al. (1990), and Glasser et al. (2008a, 2008b). Rabassa et al. (2005) synthesized the existing knowledge of the chronology of the Late Cenozoic Patagonian glaciations: The oldest known glaciations took place between approximately 7 and 5 Ma (latest Miocene–earliest Pliocene), while during the middle-late Pliocene, a minimum of 8 glaciations occurred (Oxygen Isotopic Stages 54–82). The Great Patagonian Glaciations (GPG) developed between 1.168 and 1.016 Ma (Oxygen Isotopic Stages: 30–34; early Pleistocene), followed by 14–16 cold (glacial/stadial) events with their corresponding warm (interglacial/interstadial) equivalents. Thirteen post-GPG moraines have been identified.

The available evidence indicates that a major glacial advance occurred during MIS 6 with a best age estimate of ca. 150–140 ka (Singer et al., 2004; Kaplan et al., 2004; Douglass et al., 2006). Kaplan et al. (2005), based on the Antarctic ice core peak in the glacial-age dust concentration at ca. 75 ka, inferred that a major MIS 4 glacial advance or event occurred at Lago Buenos Aires, but was obliterated by the more extensive MIS 2 glacial advances. The LGM occurred between ca. 30 and 16 ka (during MIS 2), being broadly synchronous across Patagonia (Clapperton and Seltzer, 2001) and with the ‘global’ ice sheet LGM (Mix et al., 2001). The glacial activity during this period has therefore been the focus of many studies (eg. Meglioli, 1992; Porter et al., 1992; Denton et al., 1999; Heusser 2003; Harrison 2004; Coronato et al. 2004; McCulloch et al., 2000, 2005; Sugden, 2005; Wenzens, 2005; Kaplan et al., 2008a, 2008b).

According to McCulloch et al. (2000), deglaciation of the LGM occurred synchronously at 14,600–14,300 14C yr BP (17,500–17,150 Cal yr BP). Moreno et al. (2009) concluded that the maximum phase of the southwestern Patagonian readvance (ca. 14.8–12.6 ka) coincided with the ACR in the European Project for Ice Coring in Antarctica (EPICA) Dome C record (Stenni et al., 2003) and that the results differ markedly from those reported for northwestern Patagonia (~40°S) (Hajdas et al., 2003; Moreno et al.,

2001), where moderate cooling between 14.6 and 13.5 ka was followed by an intensification that lasted until ca. 11.5 ka. A warming step occurred at ca. 10,000 14C yr BP (11,400 Cal yr BP) throughout Patagonia, achieving Holocene temperature levels.

Glasser et al. (2004) undertook a major revision of the Holocene, mentioning two types of Neoglacial advance, namely the “Mercer and Aniya Type”. Mercer (1968, 1970, 1982) proposed three Neoglacial advances: at 4,700–4,200 14C yr BP (5,413–4,687 Cal yr BP), at 2,700–2,000 14C yr BP (2,758–1,893 Cal yr BP) and during the Little Ice Age of the last three centuries. Aniya (1995, 1996) later obtained radiocarbon dates from moraines on the eastern side of the Southern Patagonian Ice Field and recognized four Holocene advances with maxima at 3,600 (3,839 Cal yr BP), 2,300 (2,227 Cal yr BP), 1,600–1,400 (1,455 – 1,286 Cal yr BP) 14C yr BP and again during the LIA.

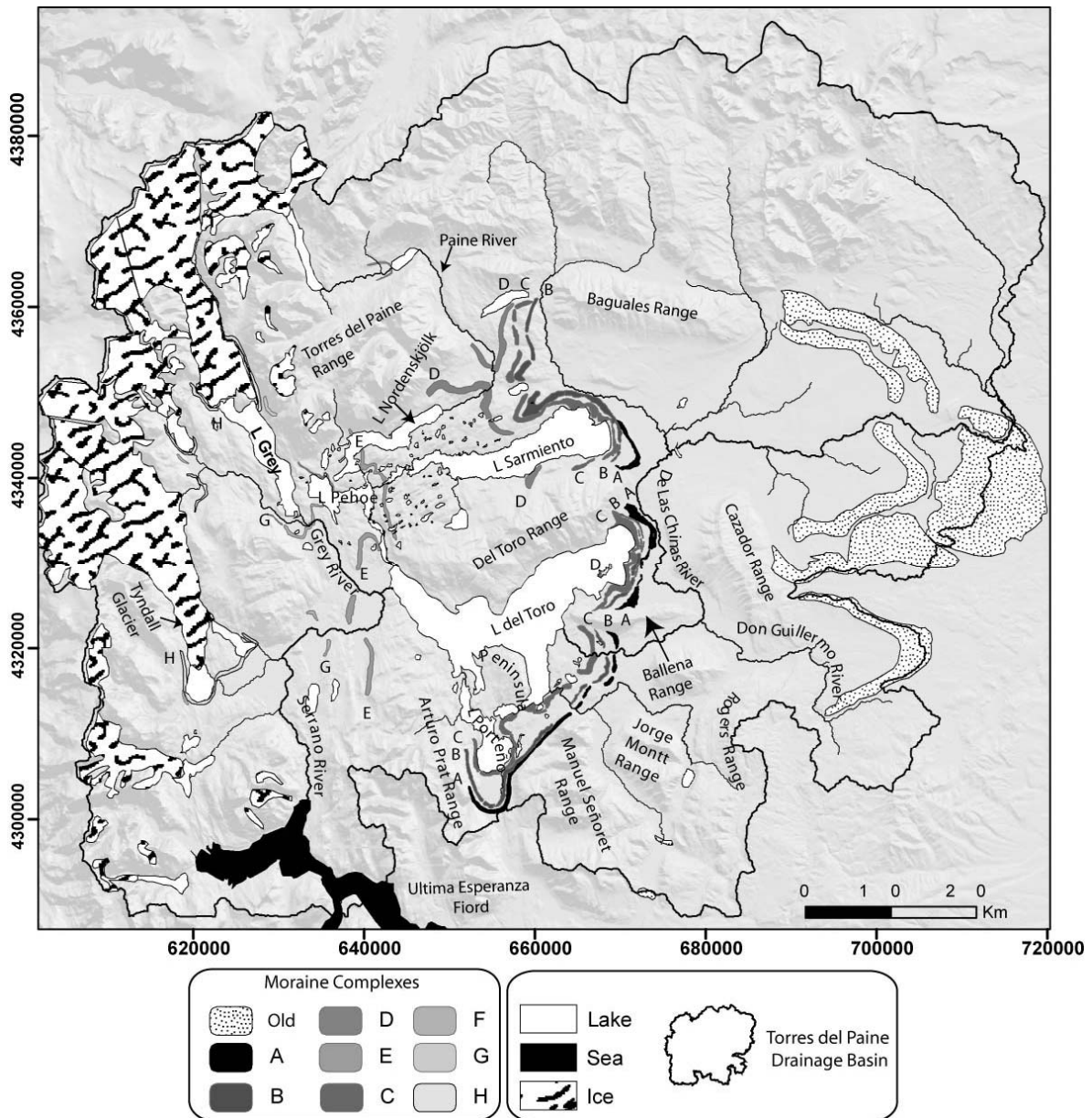
### *III.2.4 Study area*

The study area is defined by the Torres del Paine Drainage Basin (TPDB), covering an area of 8,767 km<sup>2</sup> and enclosing a complex hydrological system (Solari et al. 2010). On the western side of the TPDB, meltwater from the SPIF lobes developed a system composed of proglacial lakes feeding various rivers. The Paine River flows into Lago Nordenskjöld, which in turn drains into Lago Pehoe and then into Lago del Toro. The main outlet of Lago del Toro is the Serrano River. The Grey River links up with the Serrano River that flows into the Última Esperanza Fjord (Fig. III-2).

The TPDB as a whole had two possible outlets in the past, the first being along the Serrano River into the Última Esperanza Fjord, and the second along the Lago Porteño Valley.

Forming the eastern boundary of the TPDB as well as east of the Baguales and Cazador Ranges are widespread terminal moraines with multiples ridges, providing evidence of older glacial events in the Torres del Paine area.

Marden (1993) mapped the glacial landscape of the Torres del Paine district and determined 8 glacial stages (labelled from west to east A, B, C, D, E, F, G and H) from the Grey and Tyndall Glaciers to the recent terminal moraines along the coastline of Lake Sarmiento.



**Fig. III-2:** Torres del Paine Drainage Basin and moraines superimposed on a shaded relief image obtained from the Shuttle Radar Topographic Mapping Mission (SRTM 90 m resolution, UTM 19 °S/ WGS 84) digital elevation model.

Cosmogenic  $^{10}\text{Be}$  dating of erratics from the D moraine indicates a short-lived re-advance of Patagonian ice culminating at 12.6–14.8 kyr BP, coincident with the time of the Antarctic Cold Reverse (Fogwill, 2005; Moreno et al., 2009). The radiocarbon age of Glacial Advance E is  $9,755 \pm 95$   $^{14}\text{C}$  yr BP, based on dating of the basal part of a peat bog occurring within its limits (Marden and Clapperton, 1995). Two minimum radiocarbon ages for Advance F were obtained:  $8,750 \pm 170$   $^{14}\text{C}$  yr BP from basal organic bog sediments inside the moraine limits (Marden and Clapperton, 1995) and  $9,180 \pm$   $^{14}\text{C}$  yr BP obtained from basal organic sediments close to the inferred advance limits (Stern, 1990). An age control for Advance G has not been obtained, but it may be correlated with the Patagonian neoglacial advances (Glasser et al., 2004). The age of Advance H was determined by

studying the annual ring patterns of trees that colonised the moraines in the vicinity of Grey Glacier (Armesto et al., 1992). The age of the oldest tree (*Nothofagus pumilio*) was estimated at 232 yr, and it appears that the most extensive phase of Advance H at the Grey Glacier culminated at ca. 1,600-1,700 AD, apparently associated with the Little Ice Age (Marden and Clapperton, 1995).

Following the Marden (1993) study that defines the margins of the different glacial events in Torres del Paine, this paper aims to decipher part of the evolution of the hydrological system related to the past climate change.

### *III.2.5 Methodology.*

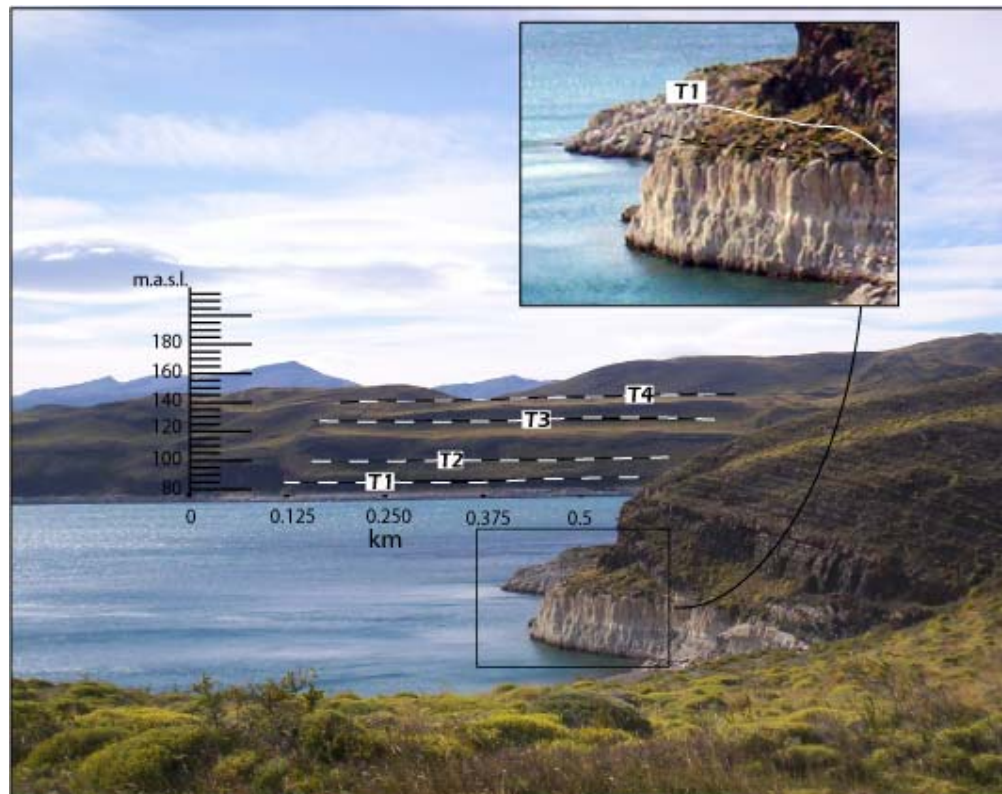
During five separate field excursions we mapped the geomorphology and distribution of Quaternary deposits at a scale of 1:10,000, which was supplemented by the Shuttle Radar Topography Mission Digital Elevation Model (SRTM DEM ) data (USGS, 2000) and aerial photographs. We also described and measured stratigraphic columns and collected samples for radiocarbon dating,

The radiocarbon ages were determined using a 0.5 MeV accelerator mass spectrometer at the Center for Applied Isotope Studies at the University of Georgia and was converted to calendar years using the software Calib 5.01 (Stuiver et al., 2005). For ages younger than 11 <sup>14</sup>C kyr BP calibration was in accordance with the Southern Hemisphere (McCormac et al., 2004) calibration curve and for ages older than 11 <sup>14</sup>C kyr BP it conformed to the Northern Hemisphere calibration curves (Reimer et al., 2009). Organic soil was collected in high density plastic bags at a depth of 10 cm below the surface. The  $\delta^{13}\text{C}$  values of the soil samples collected in glacial lake deposits are between -23.52 ‰ - 25.1‰  $\delta^{13}\text{C}$  PDB, consistent with the C3 land plant signature (Meyers et al., 1994). This suggests that the organic matter was derived from plants in the surrounding areas of the lake and that a reservoir effect does not exist.

In addition, radiocarbon ages were determined for trapped gastropod shells collected at a depth of about 7 cm in the external crust of the thrombolites, to prevent superficial contamination. The thrombolites formed when the lake was a closed basin, so that a reservoir effect produced by glacial meltwater is unlikely. However, the gastropods could potentially have a reservoir effect produced by dissolved, older carbonates from groundwater inflow.

### III.2.6 Paleolacustrine levels

#### a. Terraces between Lago Sarmiento to Laguna Amarga.

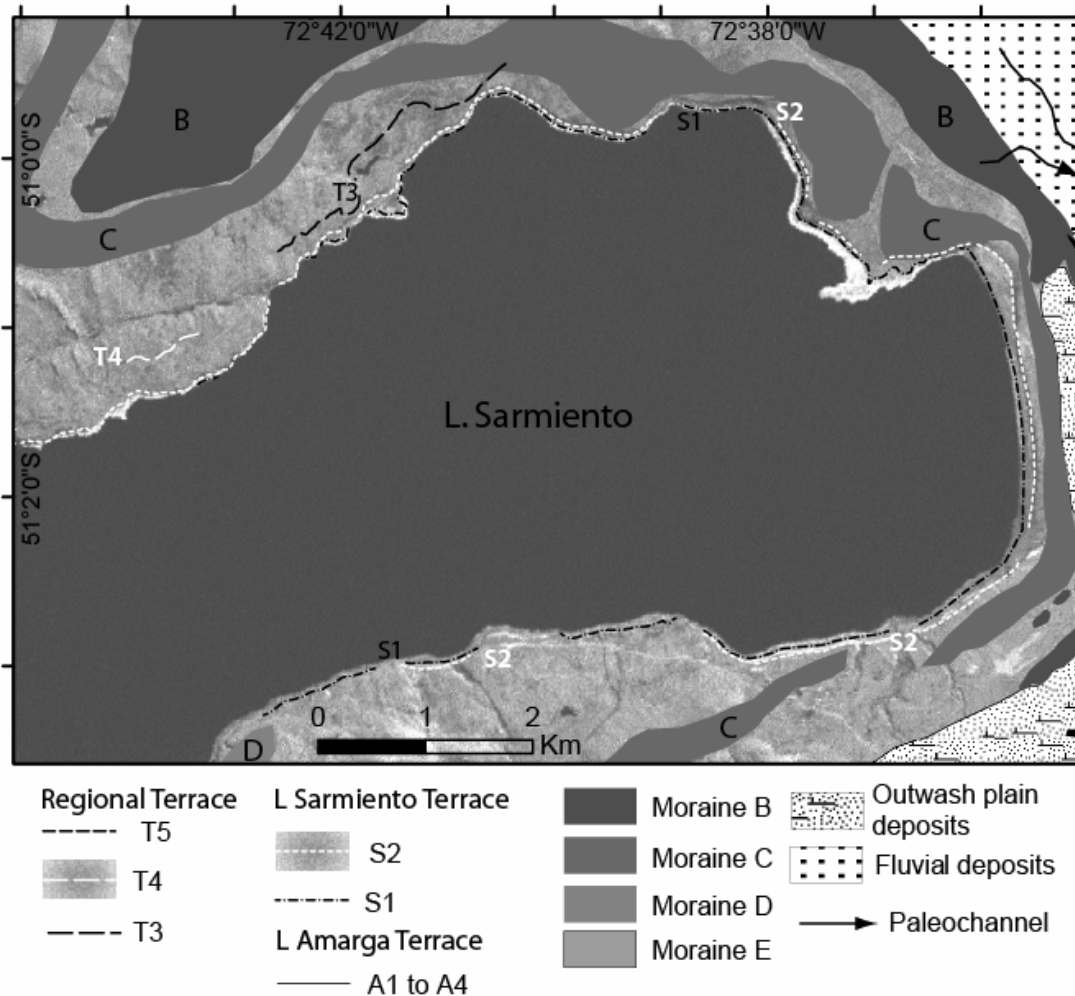


**Fig. III-3:** Terraces at shores of Lago Sarmiento.

Sarmiento Lake is an elliptical, closed basin with a surface area of 86.2 km<sup>2</sup> and a shoreline of 78.3 km, lying at an elevation of 75 m a.s.l. We recognized four terraces that in some areas eroded the Cerro Toro Formation and in others are covered by regolith. Terraces S1, S2, T3 and T4 range in elevation between 85-90, 105-110, 120-130, and 138-145 m a.s.l., respectively (Fig. III-3). Terraces T4 and T3 are recognised mainly on the northern and western slopes of the lake (Fig. III-5) and were not observed along the eastern shore (Fig. III-4). Terraces T4 and T3 were observed east of moraine E but not west thereof. Terraces S2 and S1 are also present at Lago Sarmiento Chico. A watershed at 86 m a.s.l between Lago Sarmiento and Sarmiento Chico (Fig. III-5b) can also be observed. On the western side of Lago Sarmiento Chico an outlet of the paleolake was developed at the S2 level (Fig. III-4b).

The S1 terrace (85-90 m a.s.l) is underlain by approximately 8 meters (from the lake level at ca. 77 m a.s.l) of carbonate deposits developed along almost the full extent of the coastline. These microbialite deposits are composed of sand, aragonitic gastropod shells and filamentous cyanobacteria enclosed by a clotted structure of calcite. The clotted structure, observed at field, hand sample and microscopic scale, define these bioherms as thrombolites. Gastropods shells collected from the top level (ca. 83 m a.s.l) at a depth of 7

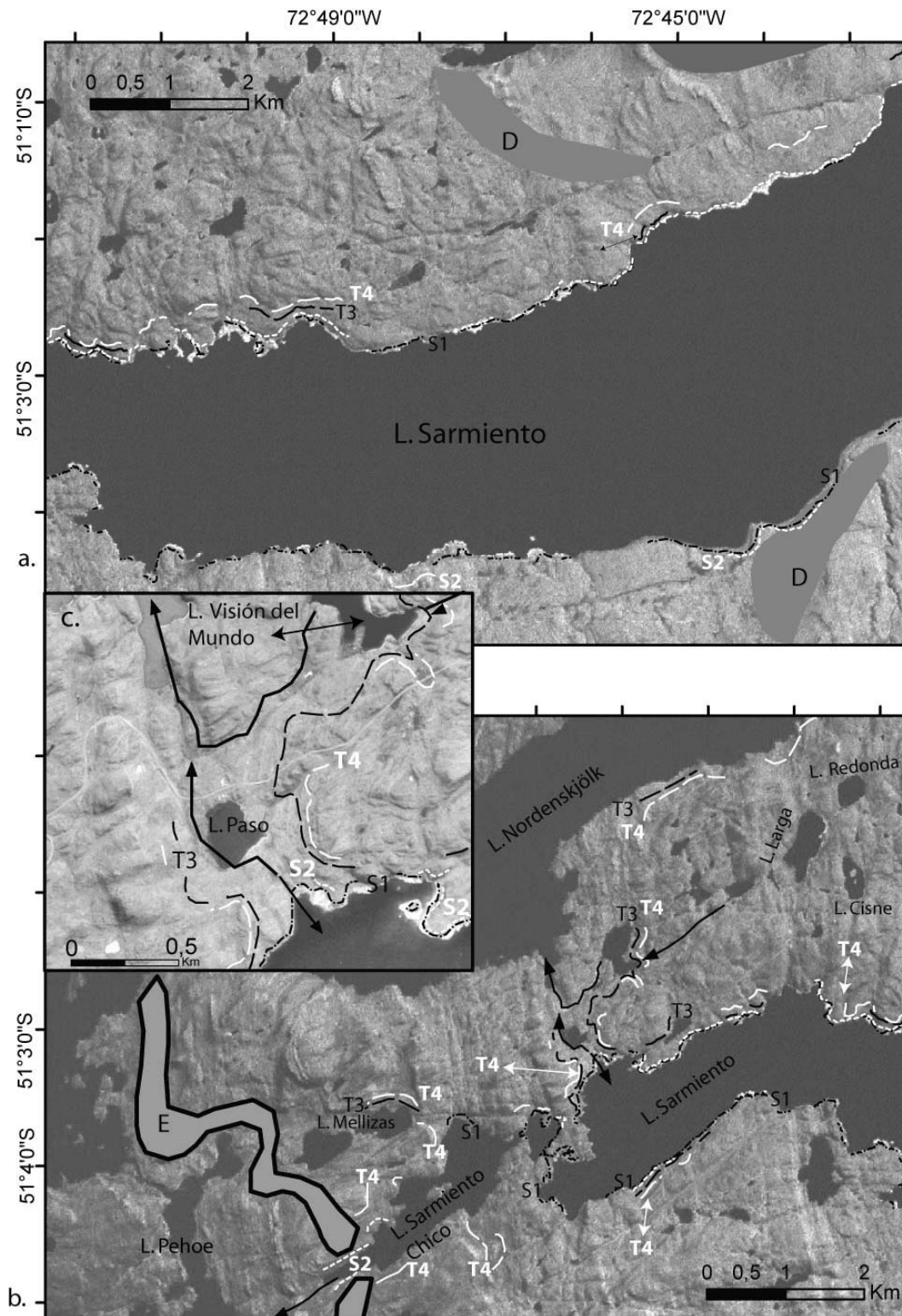
cm within the external crust of the thrombolites, yielded a median probability radiocarbon age of 1,215 Cal yr BP (1,341±52 14C yr BP) and represent an age reflecting the end of growth and precipitation at this level (Solari et al., 2010).



**Fig. III-4:** Aerial photograph of the eastern area of Lago Sarmiento showing the mapped paleo-lacustrine terraces and the legend for Figs.III-5, 6 and 7.

In the sector of Laguna Paso a lacustrine paleo-passage between the Lago Sarmiento and Nordenskjöld Basins can be observed at 115 m a.s.l, the upper limit of which is marked by the continuation of the T4 and T3 terraces observed on the eastern and western slopes of Laguna Paso (Fig. III-5c). It is possible to trace the S2 and S1 terraces uninterruptedly around Lago Sarmiento, but they do not continue northward into the Laguna Paso passage (Fig. III-4c). At a 115 m a.s.l watershed present in the Laguna Paso passage only the T3 and T4 terraces levels are observed.





**Fig. III-5:** Aerial photograph showing the mapped paleo-lacustrine terraces : a. Central part of Lago Sarmiento; b. Western part of Lago Sarmiento and southern margin of Lago Nordenskjöld; c. Enlarge view of the watershed at the Laguna Paso spillway.



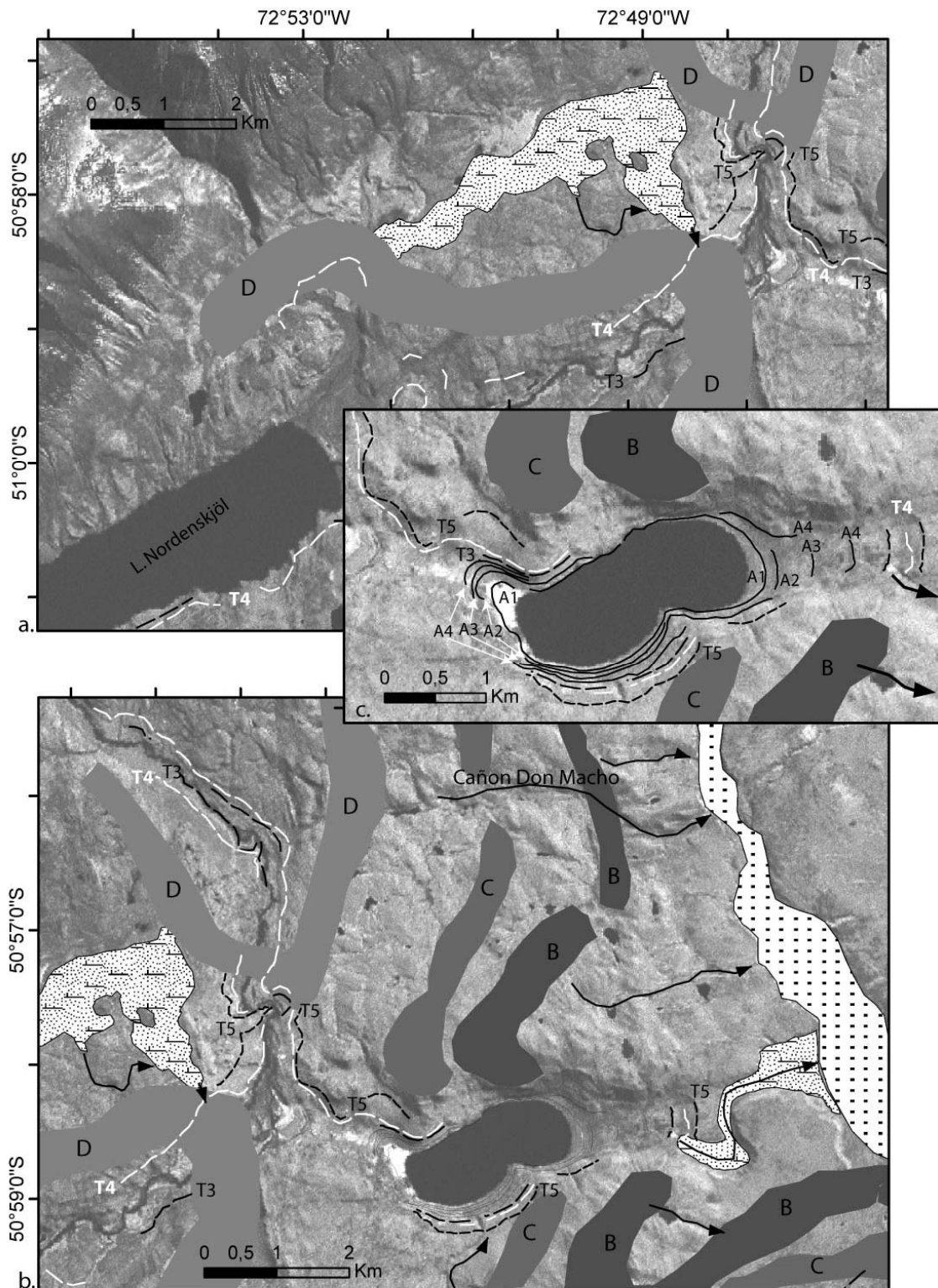
Terraces levels T4 and T3 represent an old proglacial lake level developed by meltwater from Glacial Advance E. These levels are observed at the 115 m a.s.l watershed and continue eastward into Lago Nordenskjöld. Terraces S2 and S1 delineate a single paleolake that included both Lago Sarmiento Chico and Lago Sarmiento. This paleolake drained westward into Lago Pehoe and the 86 m a.s.l watershed between Lago Sarmiento Chico and Lago Sarmiento indicates the elevation where this paleolake was formed and closed by at least 1,215 Cal yr BP.

Terraces T4 and T3 continue northward from Laguna Paso to the eastern shore of Laguna Visión del Mundo. They also stretch eastward to the southern shore of Lago Nordenskjöld, but can hardly be discerned along its northern shore (Figs.III-4b and 5a).

Terraces T3 and T4 continue from Lago Nordenskjöld eastward to the southern paleo-lobes of the moraine complex D. The T4 terrace was observed on both flanks of the Paine River valley and eroded the northern paleo-lobe moraine of the D Glacial Re-advance. Terrace level T5 (150 to 155 m a.s.l), was recognised east of the D moraine complex (Fig. III-6). Furthermore, at the margin of the D moraine complex north of the Paine Waterfall, deformed lacustrine deposits are in contact with diamictic moraine deposits, indicating that the D Re-advance terminated in a proglacial lake.

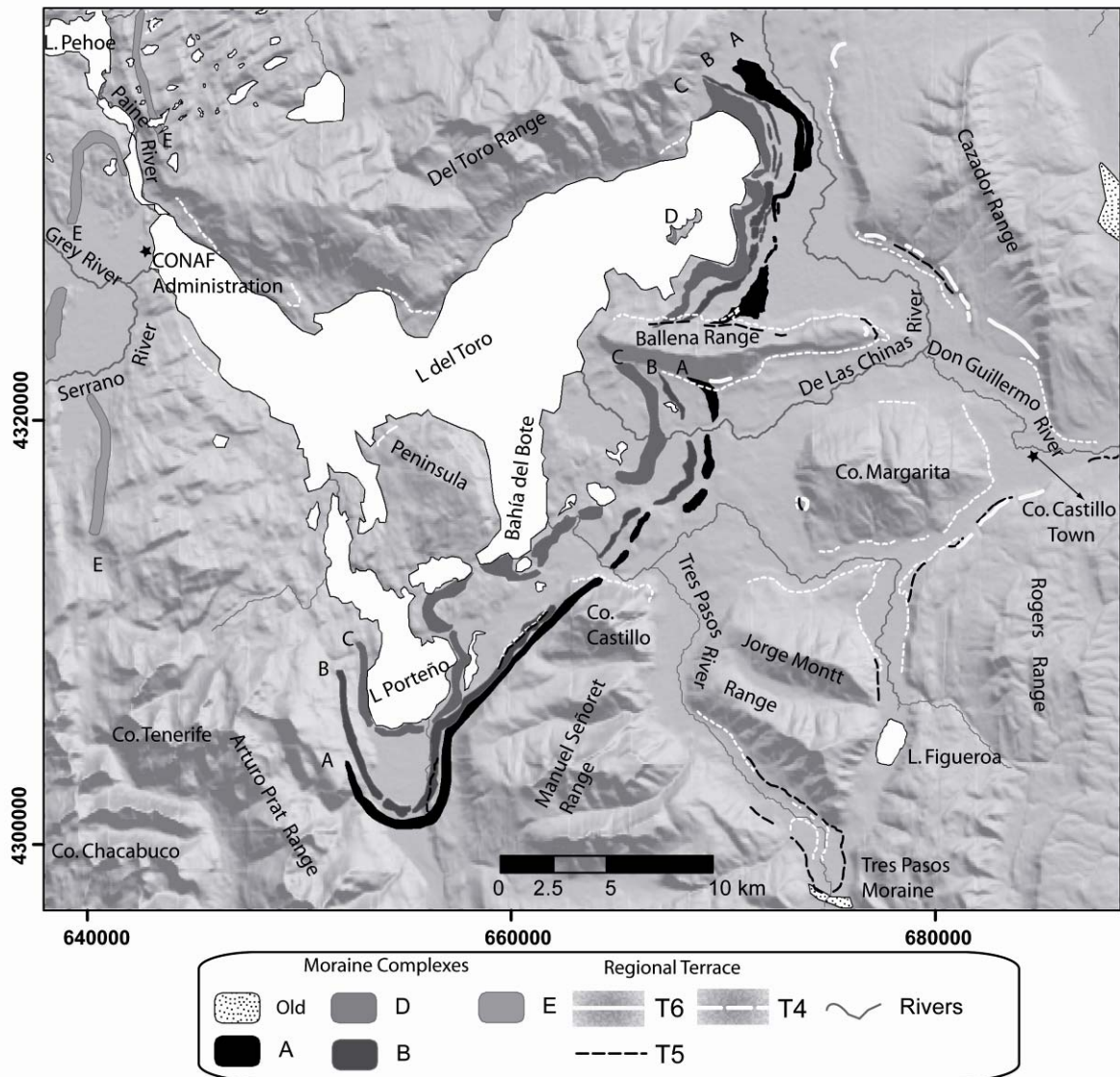
Seven terraces (A1, A2, A3, A4, T3, T4 and T5 in Fig. III-6) were observed along the slopes of Laguna Amarga. Terraces A1, A2, A3, A4, T3, T4 and T5 occur at mean altitudes of ca. 82, 90, 98, 108, 125, 138 and 150 m a.s.l, respectively.

Terraces T3 to T5 are regional levels and terraces A1 to A4 are local levels that formed when the water level dropped below the spillway between Laguna Amarga and the Paine River at 120 m a.s.l, when the lake became closed. In the Laguna Amarga Peninsula below terrace T3, a group of thrombolites are present with an internal clotted structure formed by calcite and gastropods. The latter yielded a median probability radiocarbon age of 7,113 Cal yr BP and represents the time when the water level dropped below the T3 elevation (< 120 m a.s.l).



**Fig. III-6:** Aerial photograph indicating the extend of lacustrine terraces: a. Eastern part of Lago Nordenskjöld to Paine River; b. From Paine River to Laguna Amarga; c. Magnification of Laguna Amarga showing the local terraces.

b. Terraces around Lago Del Toro



**Fig. III-7:** Glacial moraine complexes, drainage system and regional terraces superimposed on a shaded relief image obtained from the Shuttle Radar Topographic Mapping Mission (SRTM 90 m resolution, UTM 19 ° S/ WGS 84) digital elevation model.

The surface of Lago del Toro is at an elevation of ca.25 m.a.s.l., and covers an area of 195.1 and occupies a deep asymmetric basin south of the Toro Range. Well-developed terminal moraines were mapped along the eastern margin of Lago del Toro (Fig. III-7). The Peninsula and Ballena Ranges divided the ice sheets into three main lobes, namely the Lago del Toro, Bahía del Bote and Lago Porteño lobes. Due to the fact that the regional terrace level T5 related to Glacial Advance D (12,000–15,000 yr BP) was observed in the terminal moraines on the northern slopes of the Ballena Range, it can be deduced that the western moraine ridges of Lago del Toro are correlated with the C Moraine Complex exposed at Lago Sarmiento.

In the Lago del Toro lobe, Moraine Complex A reached 120 m.a.s.l and is composed of two well-defined ridges with erratic boulders on their surface. The B Moraine Complex has a maximum elevation of 90 m a.s.l and shows at least three main ridges. Moraine Complex C attains an elevation of 100 m a.s.l and is composed of two main ridges. On an island within Lago del Toro a terminal moraine is observed that reaches 65 m a.s.l and is correlated with the D stage.

East of the Lago del Toro terminal moraines occur on three levels of terraces with a regional extent. The highest of these (T6) lies at an elevation of 240 to 260 m a.s.l. and is always located east of the A Moraine Complex. It is very well preserved at the western limit of Sierra Cazador (Fig. III-8) and in the northern sector of Sierra Rogers. Above level T6 are whaleback structures which indicate glacial action that predates the formation of the T6 terrace. These older glacial events are probably related to the terminal moraines mapped at the source of the Don Guillermo River.



**Fig. III-8:** Terrace levels observed in the Del Toro Range, as well as peninsulas extending into Lago del Toro.

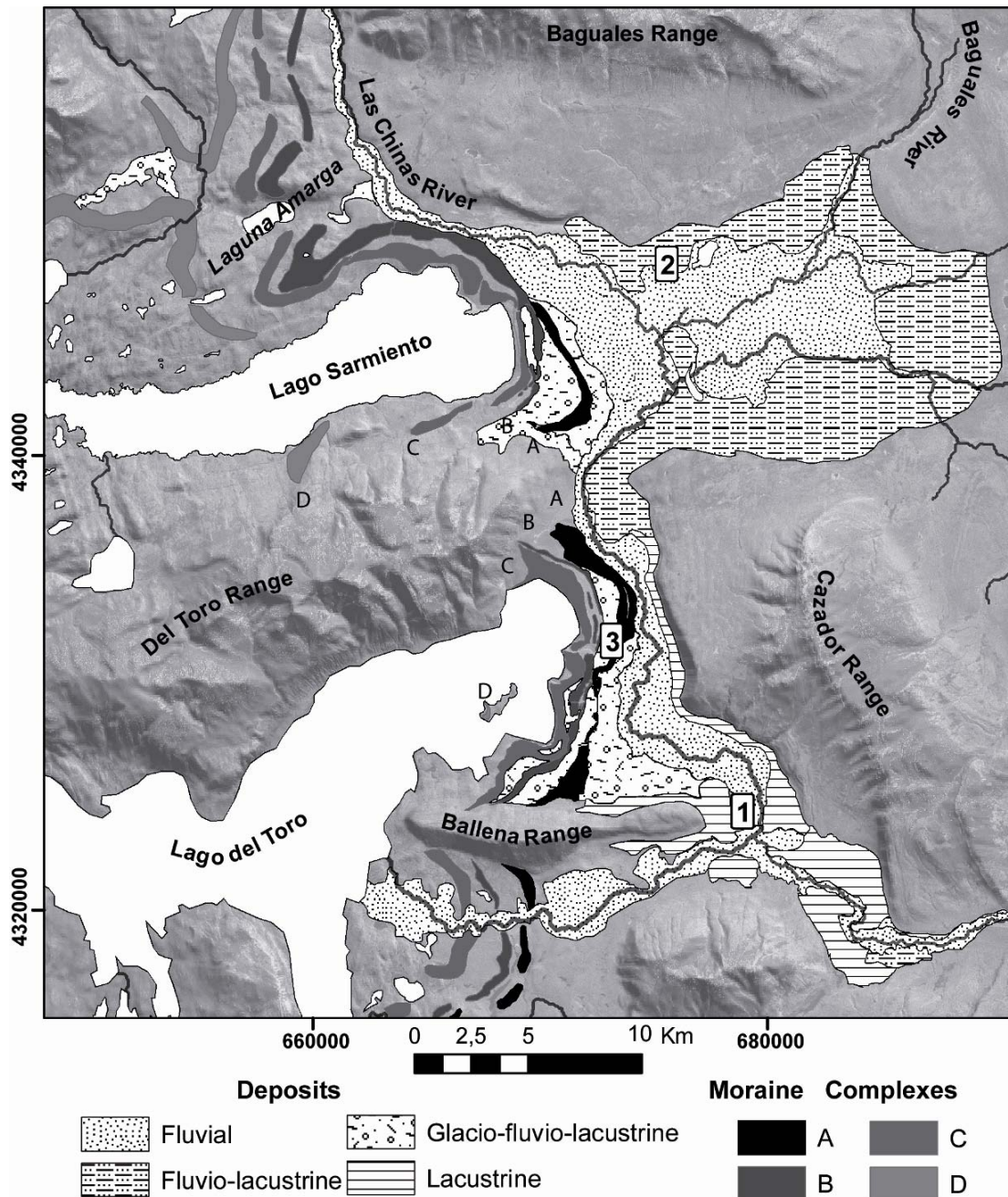
Terrace level T5, previously described in the Laguna Amarga sector and linked to Glacial Advance D, is present on both sides of the Tres Pasos River and the Tres Pasos moraine. Terrace T5 is again observed north of Lago Figueroa on the eastern flank of Sierra Jorge Montt, where it occurs at an elevation between 150 and 165 m a.s.l. It is particularly well preserved at the foot of the western slopes of Sierra Rogers.

Terrace T4 lies at an elevation between 135 and 145 m a.s.l. At the foot of Sierra Cazador this terrace extends from near the town of Cerro Castillo to the extreme northern part of the range. Along the northern shore of Lago el Toro it forms small peninsulas extending into the lake. In front of the CONAF Administration Building, T4 is also



observed immediately southeast of the E Glacial Advance, from where it disappears towards the west.

### III.2.7 Sedimentary deposits



**Fig. III-9:** Sedimentary deposits east of the moraine complexes of Lago del Toro and Lago Sarmiento. The numbers indicate the localities where sedimentary units are described.

#### a. Fluvial deposits

The activity of the Las Chinas, Baguales and Don Guillermo Rivers during part of the Holocene eroded the underlying deposits and formed wide alluvial plains. The Las Chinas River descends for almost 100 km from the Baguales Range, where it has an almost

straight reach and is capable of transporting gravels and cobbles included in a fine to coarse arenaceous matrix, On the plains opposite Lago Sarmiento up to where it flows into Lago del Toro, the Las Chinas River initiates a meandering path. On its alluvial plain exhumed meanderbelt deposits of silt and fine to medium sand are also preserved.

*b. Lacustrine deposits*

Lacustrine deposits recognized west of the Cazador Range add new evidence about the existence of an extensive lake to the east of the terminal moraines. These poorly consolidated deposits are composed of a finely stratified succession of sandstones and siltstones with dropstones and occasional load structures. The light to dark grey sandstone beds are fine to coarse, with planar and trough cross-stratification (troughs reaching up to 40 cm in width), sub-horizontal stratification or massive bedding. They frequently contain siltstone lenses. The siltstone beds are white or light grey to light brown, finely laminated or massive, and contain occasional sandstone lenses.

*c. Fluvio-lacustrine deposits*

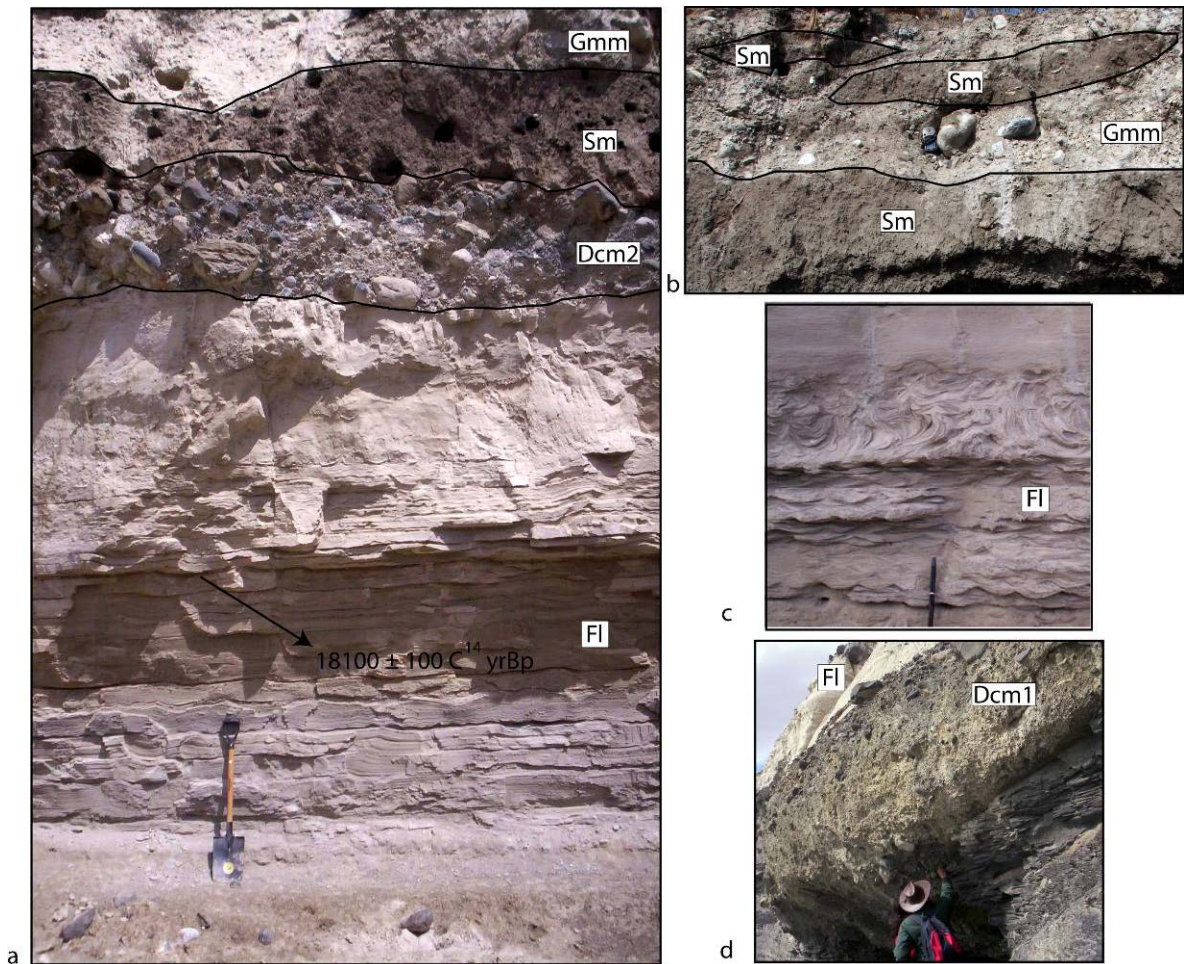
Between the Sierra Baguales and Cazador Ranges fluvio-lacustrine deposits were recognized, especially in drainage channels near the confluence of the Las Chinas and Baguales Rivers (locality 2 in Fig. III-9). Here profiles up to 4 m thick are exposed, which consist of (from bottom to top):

- Clast-supported gravels with an arenaceous matrix. The polymictic clasts, which vary between 1 and 90 cm in diameter, are rounded with a median sphericity and poor sorting.
- The gravel unit is concordantly overlain by silts and finely stratified, grey to brown sands. Gravel lenses within the sand show occasional planar cross-beds. Gravel lenses with 0.5–8 cm, subrounded, polymictic clasts within a sandy matrix also cross-cut the bedding within the sand-silt unit, forming wedge-shaped structures reminiscent of the stone polygons typical of permafrost areas.
- Concordantly overlying the sand-silt unit is a brown soil profile composed of clays, silts and fine, massive sand. Occasional bone fragments of *Lamae guanicoe* were also observed, one of which was dated at  $878,9 \pm 42$   $^{14}\text{C}$  yr BP (793 Cal yrs BP).

*d. Glacio-fluvio-lacustrine deposits at El Canal*

In the El Canal drainage channel, located on the eastern side of Lago El Toro (location 3 in Fig. III-9), lacustrine, glacial and fluvial deposits discordantly overlie the Cretaceous marine deposits of the Cerro Toro Formation. A generalized column for these deposits shows that they are composed (from base to the top) of the following units (nomenclature from Eyles et al., 1983):

- Dcm1: A well-consolidated, clast- to matrix-supported basal moraine up to 4.2 m thick. The clasts are polymictic and angular with a poor sphericity, reaching up to 1 m in diameter, whereas the matrix is composed of white silt. Eroded clasts of the underlying Cerro Toro Formation are also present.
- Fl: A lacustrine succession generally more than 10 m thick, well exposed over the whole length of the channel. It is composed of white to grey silts and laminated sands, frequently varved, with wave ripples. Within the laminated strata are dark brown silts with a high organic matter content (Fig. III-10), that have been radiocarbon-dated  $18,100 \pm 100$   $^{14}\text{C}$  yr BP ( $21,493$  Cal yr BP). Along El Canal a shear stress zone showing contorted, laminated or wave-rippled silt to silty clay units also occurs.



**Fig. III-10:** Deposits along “El Canal”: a. Stratigraphic columns showing the main units; b. Flood deposits with angular fragments from the underlying alluvial deposits; c. Wave-rippled and contorted beds; d. Consolidated basal moraine overlying the Cerro Toro Formation and underlying the lacustrine sequence. From older to younger: Dcm1. Consolidated basal moraine Fl: Lacustrine sequence; Dcm2. Basal moraine; Sm. Alluvial deposits; Gmm. Flood deposits.



The lacustrine succession displays a variety of glacial deformation structures, which are concentrated along two major thrust faults. These westward-dipping faults occur below the terminal moraine ridges of the C and B Moraine Complexes. The deformation structures include contorted laminated or wave-rippled silt to silty clay, recumbent folds in fine to very fine sandstone beds and low- to steep-angled reverse faults with cm-scale displacement.

Within the lacustrine succession two delta deposits are recognised, one overlying the other concordantly. The lower delta was dated in its uppermost beds at  $20,300 \pm 110$   $^{14}\text{C}$  yr BP (24,291 Cal yr Bp) and shows foresets onlapping towards the west, whereas the upper delta foresets onlap towards the east. The latter is interpreted to have formed by currents migrating from the Sierra Cazador sector towards Lago del Toro, as a result of the glacial retreat. On the other hand, the upper delta foresets are interpreted as a product of current migration towards the east in response to a glacial advance after 24,291 Cal yr BP.

- Dcm2: Basal moraine deposits discordantly overlying the lacustrine succession (Fig. III-10) are composed of clast- to matrix-supported gravels. The matrix is composed of white to grey silt, whereas the polymictic clasts are angular to subangular with a medium sphericity and poor sorting. They vary from millimeters to meters in diameter, some showing facets and striations. The deposits are linked to Glacial Advances A, B and C and dating shows that they are less than but close to 21,493 Cal yr BP. It seems very likely that the glacial advances occurred during the Last Glacial Maximum.
- Sm: Alluvial deposits discordantly overlie the basal moraine and are composed of brown, massive, fine-grained sands with plant roots. They have between 3% and 6% polymictic clasts varying in size between 7 cm and 3 mm, which are subrounded with a poor sphericity, generally forming subhorizontal flat pebbles. Within these deposits are bone fragments of *Lamae guanicoe*, one of which was dated at  $240 \pm 30$   $^{14}\text{C}$  yr BP, or a calibrated age of 200 Cal yr BP.
- Gmm: Flood deposits discordantly overlie the alluvial deposits. They are composed of gravels with matrix-supported cobbles. These poorly sorted deposits are massive with a white to brown matrix. Clasts vary in concentration between 5 and 40% and are subrounded and polymictic, with sizes ranging between 0.5 and 45 cm, but clasts derived directly from erosion of the underlying strata are between 25 cm and 330 cm in diameter. Tree bark fragments up to 40 cm long, as well as scarce clasts of travertine up to 10 cm long were also encountered. A piece of tree bark was dated at  $391 \pm 30$   $^{14}\text{C}$  yr BP, or a calibrated age of 200 Cal yr BP. This unit is interpreted as having been produced during a major flooding of the Las Chinas River.

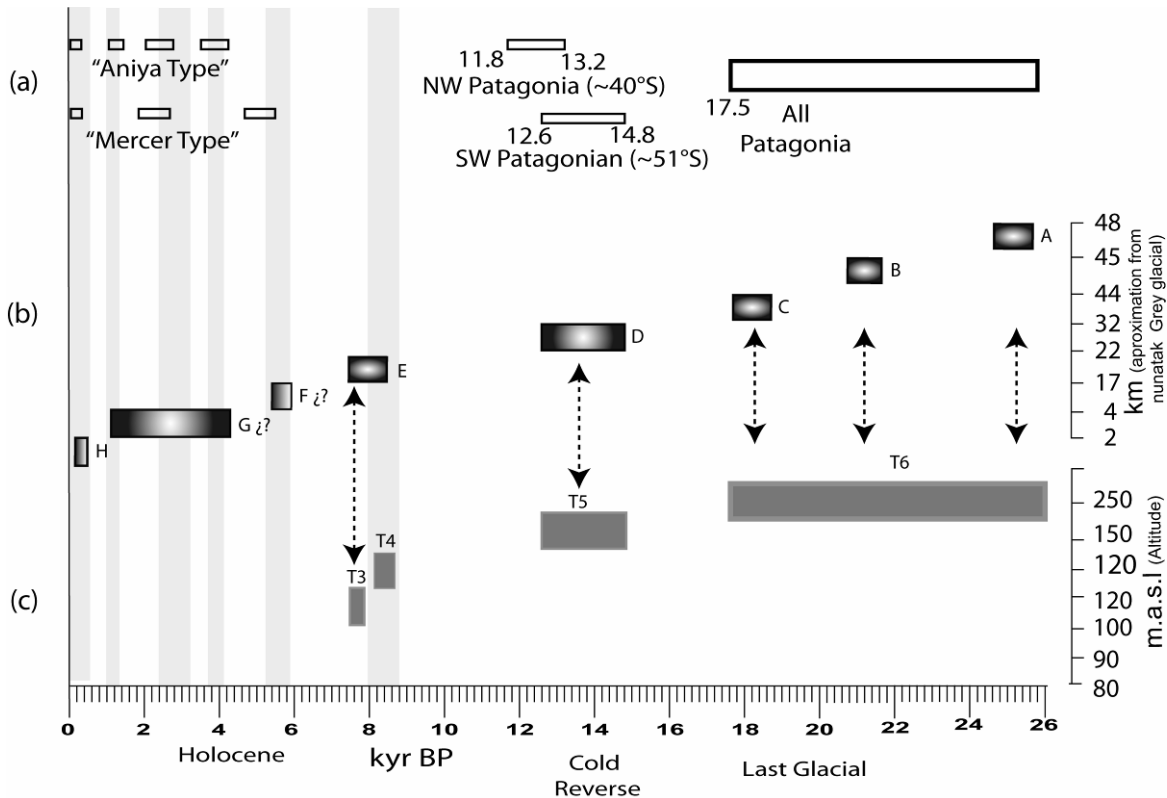
### III.2.8 Discussion and Conclusions

Evidence for older glacial events is provided by the terminal moraine located along the eastern boundary of the TPDB and in the Tres Pasos River area, as well as the consolidated basal moraine deposits that discordantly overlie the Cerro Toro Formation in the El Canal area. These moraine complexes were formed prior to the LGM and further investigation will be necessary to determine whether they formed during the MIS 6 and/or



during the Great Patagonian Glaciations (Early Pleistocene) as in Lago Buenos Aires (e.g. Ton-Tham et al., 1999; Singer et al., 2004).

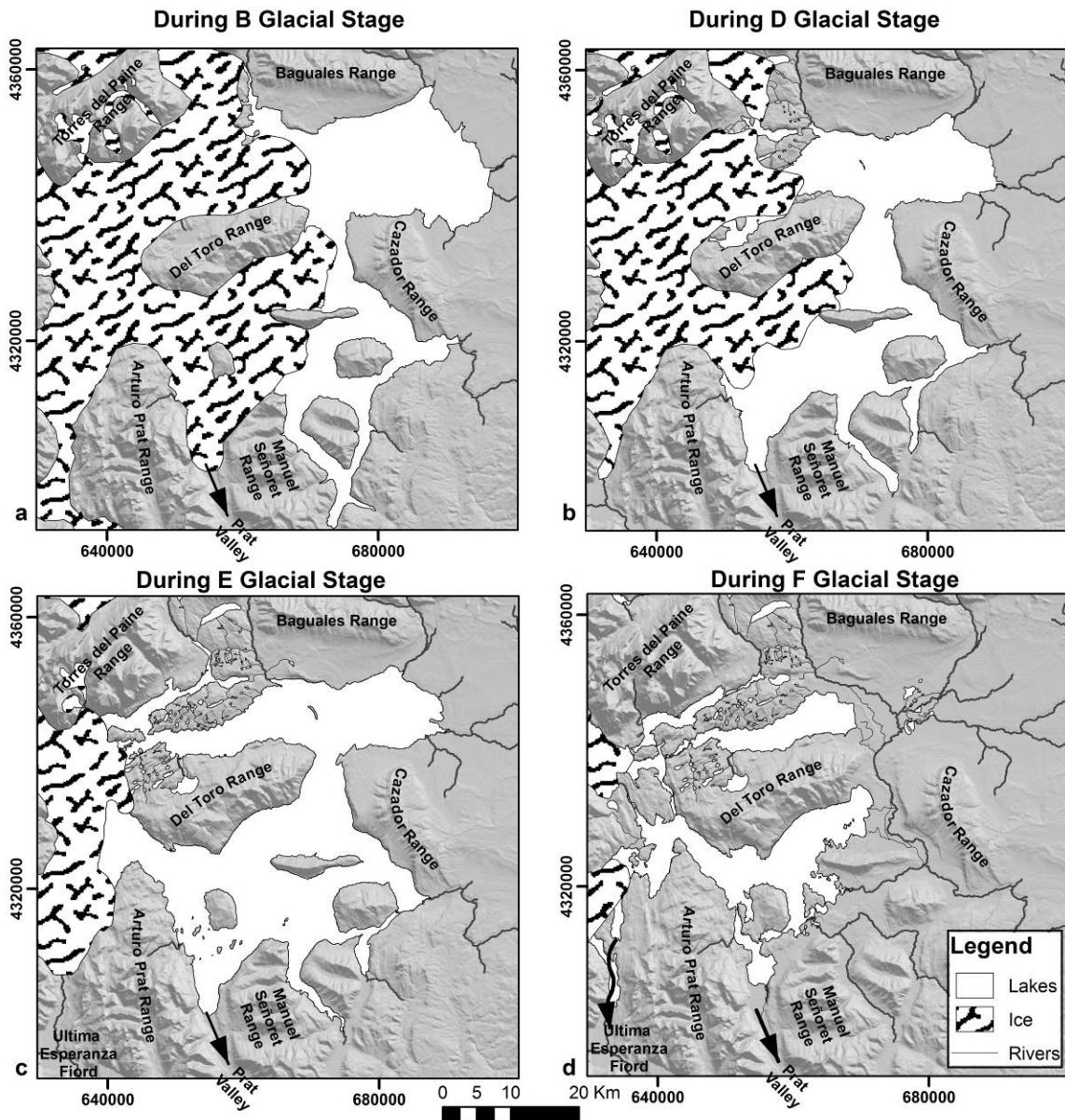
Based on their lateral continuation and location east of the terminal moraines of Glacial Stages E, D, C, B and A, four important, regionally extensive terrace levels are recognized, namely T6, T5, T4 and T3 (Fig. III-11). These observations support the existence of a single proglacial paleolake, which we call the Great Tehuelche Paleolake (GTP). This paleolake formed between the glacial mass and the topographic rise at the eastern margin of the TPDB. The Great Tehuelche Paleolake had an outlet towards the south along the Prat Valley between the Arturo Prat and Manuel Señoret Mountain Ranges.



**Fig. III-11:** Grey bands represent timing of the HRCC (Mayewski et al., 2004) and white rectangles represent cool periods. (a) “Mercer and Aniya Type” Neoglaciation advances events in Patagonia (Mercer, 1968, 1970, 1982; Aniya, 1995, 1996), Cold Reversal Period in Lake District in northwestern Chilean Patagonia (Hajdas et al., 2003; Moreno et al., 2001), Cold Reversal Period in Torres del Paine (Moreno et al., 2009) and synchronous Patagonian LGM deglaciation. (b) Chronology of the moraine complexes of Torres del Paine; (c) Chronology of the terrace levels of the Great Tehuelche Paleolake.

During the LGM, the GTP received extensive deposits and formed the highest paleolake level described so far. The T6 level varies in elevation between 240-260 m a.s.l and formed before and during Glacial Advances C, B and A (Fig. III-11). In the sector of El Canal, the eastward change in progradation of the upper delta is interpreted as reflecting the beginning of glacial advance after 24,291 Cal yr BP. Moraine Complex B developed at the eastern margin of Lago del Toro after 21,493 Cal yr BP, as evidenced by the intensive deformation that affected the lacustrine succession below the basal till. Glacial Advance C

was stable until about 17,500 yr BP, at which moment widespread deglaciation commenced in Patagonia. The T6 terrace level indicates an episode during which the Great Tehuelche Paleolake reached its maximum extent during the LGM, and its level varied as a function of the glacial fluctuation (Fig. III-12).



**Fig. III-12:** Reconstruction of the Great Tehuelche Paleolake during the different glacial stages: a. Glacial and lake extension during Glacial Stage B; b. Glacial and lake extension during Glacial Stage D, c. Glacial and lake extension during Glacial Stage E; d. Small lake organization during Glacial Stage F.

A new phase of the Great Tehuelche Paleolake developed at 12,600–14,800 yr BP during Glacial Re-advance D, at an altitude of 150-165 m a.s.l. The regional terrace level T5 on the northern flank of the Ballena Range extends west of the moraine ridges on the eastern shore of Lago del Toro and also formed a moraine ridge on an island

within this lake, so that the position of the terminal moraines of Glacial Advance D in this sector can be inferred to have been within Lago del Toro.

Terraces T4 and T3 are widespread in the area and are always observed east of Glacial Advance E, at an altitude that varies between 135-145 and 120-130 m a.s.l., respectively. They represent ancient proglacial lake levels, eroded mainly by meltwater from Glacial Advance E and forming the last stage of the GTP prior to its cessation by drainage (Fig. III-12). When the water level of the GTP dropped below the T3 elevation (< 120 m a.s.l.), Laguna Amarga became a closed lake with growing thrombolites that trapped gastropods dated at 7,113 Cal yr BP. This moment in time represents the retreat of Glacial Advance E and the restructuring of the GTP as a group of small lakes similar to the present configuration, as a result of the opening of a new lake outlet that drained towards the Última Esperanza Fjord (Fig. III-12). From this time on Laguna Amarga was a closed lake and the salinity of the lake increased because evaporation exceeded precipitation, enough to support the growth of thrombolites. A possible explanation for this salinity increase is that the glacial retreat reduced precipitation, generating more arid conditions.

We conclude that Glacial Advances E and F are younger than the ages previously proposed by Marden and Clapperton (1995). Glacial Advance E culminated at 7113 Cal yr BP, which closely approximates the glacial maximum of  $8.5 \pm 0.7$  kyr ( $^{10}\text{Be}$ ) dated by Douglas et al. (2005) in the Fachinal Moraine located at Lago General Carrera. However, it will be necessary to gather more regional evidence in Patagonia to establish a definite correlation with the 8000-9000 yr BP Northern Hemisphere cool interval. Glacial Advance F is younger than 7113 Cal yr BP and is probably synchronous with the older Neoglacial “Mercer Type” period, but further chronological evidence is necessary to assign a definite age to this glacial event.

The magnitude and position of the Westerlies is controlled by the subpolar low-pressure belt and the Southeast Pacific Anticyclone, potentially affecting both high- (southern) latitude and tropical Pacific forcing mechanisms (Cerveny, 1998). The delay recorded in the Los Lagos District with respect to the synchronous cold event in Antarctica and Torres del Paine (Fig. III-11), could be explained by a modification of the Westerlies caused by the strengthening of the Tropical Easterlies and the northward expansion of the subpolar low-pressure belt. Strengthening of the Tropical Easterlies is supported by an increase in summer precipitation from 14–11 k cal. yr BP in the Atacama Desert, as interpreted from pollen evidence by Maldonado et al. (2005). Lamy et al. (2004) also interpreted a northward displacement of the Antarctic Circumpolar Current (ACC) during the Cold Reverse Period (closely following upon the YD event), detected at site 1233 in the Los Lagos District.

### *III.2.9 Acknowledgments.*

We gratefully acknowledge financial support by the Comisión Nacional de Investigación y Tecnología (CONICYT) and the Project “Geological Connection between the Antarctic Peninsula and Patagonia” (ARTG-04) supported by the Programa Bicentenario de Ciencia y Tecnología (PBCT) of CONICYT and the Instituto Antártico Chileno (INACH). Thanks are also due to the Corporación Nacional Forestal (CONAF) for field support, in particular to the rangers. We would also like to thank D. Nieto for field support.

### III.2.10 References

- Andersen, K.K., Svensson, A., Johnsen, S.J., Rasmussen, S.O., Bigler, M., Röthlisberger, R., Ruth, U., Siggaard-Andersen, M.L., Steffensen, J.P., Dahl-Jensen, D., Vinther, B.M., Clausen, H.B., 2006. The Greenland Ice Core Chronology 2005, 15-42 ka, Part 1: Constructing the time scale, *Quaternary Science Reviews*, vol, 25, Shackleton special issue 24.
- Aniya, M., 1995. Holocene glacial chronology in Patagonia: Tyndall and Upsala Glaciers. *Arct. Alp. Res.* 27, 311–322.
- Aniya, M., 1996. Holocene variations of Ameghino Glacier, southern Patagonia. *Holocene* 6, 247–252.
- Armesto J.J., Casassa I., Dollenz. O., 1992. Age structure and dynamics of Patagonian beech forest in Torres del Paine National Park, Chile. *Vegetatio*, 98, 13-22.
- Bender M, Sowers T, Dickson ML, Orchardo J, Grootes J, Mayewski PA, Meese DA. 1994. Climate correlations between Greenland and Antarctica during the past 100,000 years. *Nature* 372: 663–666.
- Blunier T, Chappellaz J, Schwander J, Dällenbach A, Stauffer B, Stocker TF, Raynaud D, Jouzel J, Clausen HB, Hammer CV, Johnsen SJ. 1998. Asynchrony of Antarctic and Greenland climate during the last glacial period. *Nature* 394: 739–743.
- Bond G, Broecker W, Johnsen S, McManus J, Layberie L, Jouzel J, Bonani G. 1993. Correlations between climate records from North Atlantic sediments and Greenland ice. *Nature* 365: 143–147.
- Bond G, Lotti R. 1995. Iceberg discharges into the North Atlantic on millennial time scales during the last glaciation. *Science* 267:1005–1010.
- Caldenius, C.C., 1932. Las glaciaciones cuaternarios en la Patagonia y Tierra del Fuego. *Geogr. Ann.* 14, 1–164 (English summary pages 144–157).
- Carrasco, J.F., Casassa, G., y Rivera, A., 1998, Climatología actual del Campo de Hielo Sur y posibles cambios por incremento del efecto invernadero, *Anales del Instituto de la Patagonia, Serie Ciencias Naturales*, 26:119-128.
- Carrasco, J.F., Casassa, G., y Rivera, A. 2002, Meteorological and Climatological aspect of the Southern Patagonian Icefield. *The Patagonian Icefield, a unique Natural Laboratory for Environmental and Climate Changes Studies*. Edited by Gino Cassasa et al., Klumer, Academic/ Plenum Publishers.
- Cerveny R. S. 1998. *Climates of the Southern Continents: Present, Past and Future*, J. E. Hobbs, J. A. Lindsay, H. A. Bridgman, Eds. (Wiley, New York, 1998), pp. 107–134
- Coronato A, Martinez O, Rabassa J. 2004a. Pleistocene glaciations in Argentine Patagonia, South America. In *Quaternary Glaciations: Extent and Chronology. Part III: South America, Asia, Africa, Australia and Antarctica*, Ehlers J, Gibbard P (eds.) Quaternary Book Series. Elsevier: Amsterdam; 49–67.
- Clapperton CM, Hall M, Mothers P, Hole MJ, Still JW, Helmens KF, Kuhry P, Gemmell AMD. 1997. A Younger Dryas ice cap in the equatorial Andes. *Quaternary Research* 47: 13–28.
- Clapperton, C., 1993. *Quaternary Geology and Geomorphology of South America* elsevier.
- Clapperton C, Seltzer G. 2001. Glaciation during marine isotope Stage 2 in the American Cordillera. In *Interhemispheric Climate Linkages*, Markgraf V (ed.). Academic Press: San Diego, CA.
- Daansgard, W., S.J. Johnsen, H.B. Clausen, D. Dahl-Jensen, N.S. Gundestrup, C.U. Hammer, C.S. Hvidberg, J.P. Steffensen, A.E. Sveindjörnsdottir, J. Jouzel y G.Bond, 1993. Evidence for general instability of past climate from 250 kyr ice-core record. *Nature*, 364, 218-220.
- Denton, G.H., and W. Karlen. 1973. Holocene Climatic Variations-Their Pattern and Possible Cause. *Quaternary Research* 3: 155-205.
- Denton GH, Hendy CH. 1994. Younger Dryas age advance of Franz Josef glacier in the southern Alps of New Zealand. *Science* 264: 1434–1437.
- Denton GH, Lowell TV, Heusser CJ, Moreno PI, Andersen BG, Heusser LE, Schlüchter C, Marchant DR.. 1999. Interhemispheric linkage of paleoclimate during the last glaciation. *Geografiska Annaler* 81: 107–153

- Douglass DC, Singer BS, Kaplan MR, Mickelson DM, Caffee MW. 2006. Cosmogenic nuclide surface exposure dating of boulders on last-glacial and late-glacial moraines, Lago Buenos Aires, Argentina: interpretive strategies and paleoclimate implications. *Quaternary Geochronology* 1: 43–58.
- EPICA community members (2004), Eight glacial cycles from an Antarctic ice core, *Nature*, 429, 623–628.
- Eyles, N., Eyles, C.H., Miall, A.D., 1983. Lithofacies types and vertical profile models, an alternative approach to the description and environmental interpretation of glacial diamict and diamictite sequences. *Sedimentology* 30, 393–410.
- Fogwill, C.J. and Kubik, P.W. 2005: A glacial stage spanning the Antarctic Cold Reversal in Torres del Paine (51°S), Chile, based on preliminary cosmogenic exposure ages. *Geogr. Ann.*, 87 A (2): 403–408.
- Glasser, N.F. and Jansson, K. 2008 a. The glacial map of southern South America. *Journal of Maps*, v2008, 175–196.
- Glasser, N.F., Harrison, S., Jansson, K. and Kleman, J. 2008 b. The glacial geomorphology and Pleistocene history of southern South America between 38oS and 56oS. *Quaternary Science Reviews*, 27(3–4), 365–390.
- Hajdas, I., Bonani, G., Moreno, P.I., and Ariztegui, D., 2003, Precise radiocarbon dating of lateglacial cooling in mid-latitude South America: *Quaternary Research*, v. 59, p. 70–78.
- Harrison S. 2004. The Pleistocene glaciations of Chile. In *Pleistocene Glaciations: Extent and Chronology*, Ehlers J, Gibbard P (eds.) INQUA/Elsevier: Amsterdam; 89–103.
- Heusser C.J. 2003. *Ice Age Southern Andes: A Chronicle of Palaeoecological Events*. Elsevier: Amsterdam.
- Hormes, A., Müller, B.J., Schluöchter, C., 2001. The Alps with little ice: evidence for eight Holocene phases of reduced glacier extent in central Swiss Alps. *Holocene* 11, 255–265.
- Ibarzabal y Donángelo, T., Hoffmann, J. A. J., and Naruse, R., 1996, Recent climatic change in southern Patagonian, *Bulletin of Glacier Research*, 14:29–36.
- Imbrie, J., J. D. Hays, D. G. Martinson, A. McIntyre, A. C. Mix, J. J. Morley, N. G. Pisias, W. L. Prell, and N. J. Shackleton, 1984. The orbital theory of Pleistocene climate: Support from a revised chronology, of the marine  $\delta^{18}O$  record, in *Milankovitch and Climate*, Part 1, edited by A. Berger, Reidel, Hingham, Massachusetts. 269–305.
- Imbrie J, Boyle EA, Clemens SC, Duffy A, Howard WR, Kukla G, Kutzbach J, Martinson DG, McIntyre A, Mix AC, Molfino B, Morley JJ, Peterson LC, Pisias NG, Prell WL, Raymo ME, Shackleton NJ, Toggweiler JR. 1992. On the structure and origin of major glaciation cycles: 1. Linear responses to Milankovitch forcing. *Paleoceanography* 7: 701–738.
- Ivy-Ochs S., Schluöchter C., Kubik PW., Denton GH. 1999. Moraine exposure dates imply synchronous Younger Dryas advances in the European Alps and in the Southern Alps of New Zealand. *Geografiska Annaler* 81A(2): 313–323.
- Jouzel, J., V. Masson, O. Cattani, S. Falourd, M. Stievenard, B. Stenni, A. Longinelli, S.J. Johnsen, J.P. Steffensen, J.R. Petit, J. Schwander, R. Souchez, and N.I. Barkov. 2001. A new 27 ky high resolution East Antarctic climate record. *Geophys. Res. Lett.*, 28 (16): 3199–3202.
- Lamy, F., Kaiser, J., Ninnemann, U., Hebbeln, D., Arz, H.W., and Stoner, J., 2004, Antarctic timing of surface water changes off Chile and Patagonian ice sheet response: *Science*, 304, 1959–1962.
- Lowell TV, Heusser CJ, Andersen BG, Moreno PI, Hauser A, Heusser LE, Schluöchter C, Marchant DR, Denton GH. 1995. Interhemispheric correlation of Late Pleistocene glacial events. *Science* 269, 1541–1549.
- Macayeal DR. 1993. Binge/purge oscillations of the Laurentide icesheet as a cause of the North Atlantic's Heinrich events. *Paleoceanography* 8: 775–784.
- Maldonado A, Betancourt J., Latorre C., Villagran C. 2005. Pollen analyses from a 50 000-yr rodent midden series in the southern Atacama Desert (25° 30' S). *Journal of Quaternary Science* 20(5), 493–507.
- Marden, C.J. (1993). Late Quaternary glacial history of the South Patagonian Icefield at Torres del Paine, Chile. Ph.D. Thesis, University of Aberdeen, 298.

- Marden, C.J. and Clapperton, C.M. (1995). Fluctuations of the South Patagonian Icefield during the last glaciation and the Holocene. *Journal of Quaternary Science*, 10, 197-210.
- Mayewski P.A., E.J. Rohling, J.C. Stager, W. Karlén, K. Maasch, L.D. Meeker, E. Meyerson, F. Gasse, S. Van Kreveld, K. Holmgren, J. Lee-Thorp, G. Rosqvist, F. Rack, M. Staubwasser, R.R. Schneider and E.J. Steig, 2004. Holocene climate variability, *Quaternary Research* 62,43–255.
- McCormac, F.G., Hogg, A.G., Blackwell, P.G., Buck, C.E., Higham, T.F.G., Reimer, P.J., 2004. SHCAL04 Southern Hemisphere Calibration, 0–11.0 Cal kyrBP. *Radiocarbon*, 46 (3), 1087–1092
- McCulloch R.D., Bentley M.J., Purves R.S., Sugden DE, Clapperton C-, Hulton N.R.J. 2000. Climatic inferences from glacial and palaeoecological evidence at the last glacial termination, southern South America. *Journal of Quaternary Science* 15: 409–418.
- McCulloch R.D., Fogwill C.J., Sugden D.E. 2005. Late glacial maxima, the Antarctic Cold Reversal and the Younger Dryas in the Strait of Magellan and Bahı́a Inu’ til; a revised chronology. *Geografiska Annaler* 87: 289–312.
- Meglioli A. 1992. Glacial geology and chronology of southernmost Patagonia and Tierra del Fuego, Argentina and Chile. PhD dissertation, Lehigh University, Bethlehem, PA.
- Mercer, J.H., 1968. Variations of some Patagonian glaciers since the Late-Glacial. *Am. J. Sci.* 266, 91– 109.
- Mercer, J.H., 1970. Variations of some Patagonian glaciers since the Late-Glacial: II. *Am. J. Sci.* 269, 1 – 25.
- Mercer, J.H., 1976. Glacial history of Southernmost South America. *Quaternary Research* 6, 125–166.
- Mercer, J.H., 1982. Holocene glacier variations in southern Patagonia. *Striae* 18, 35– 40.
- Moreno, P.I., Jacobson, G.L., Lowell, T.V., and Denton, G.H., 2001, Interhemispheric climate links revealed by a late-glacial cooling episode in southern Chile: *Nature*, v. 409, p. 804–808.
- Meyers, P.A., 1994. Preservation of elemental and isotopic source identification of sedimentary organic matter. *Chemical Geology*. 144, 289–302.
- Milankovitch, M. (1930), *Mathematische Klimahre und Astronomische Theorie der Klimaschwankungen*, Gebruder Borntraeger, Berlin. 176 pp
- Mix AC, Bard E, Schneider R. 2001. Environmental processes of the ice age: land, oceans, glaciers (EPILOG). *Quaternary Science Reviews* 20: 627–657.
- Moreno, P.I., Kaplan, M.R., François, J.P., Villa-Martínez, R., Moy, C.M., Stern, C.R., Kubik, P.W., 2009. Renewed glacial activity during the Antarctic Cold Reversal and persistence of cold conditions until 11.5 ka in southwestern Patagonia. *Geology*, 37(4), 375-378.
- North Greenland Ice Core Project members, 2004. High-resolution record of Northern Hemisphere climate extending into the last interglacial period. *Nature*, 431, 147-151.
- North Greenland Ice Core Project dating group, 2006. Greenland Ice Core Chronology 2005 (GICC05), IGBP PAGES/World Data Center for Paleoclimatology Data Contribution Series # 2006-118, NOAA/NCDC Paleoclimatology Program, Boulder CO, USA.
- Kaplan MR, Ackert RP, Singer BS, Douglass DC, Kurz MD. 2004. Cosmogenic nuclide chronology of millennial-scale glacial advances during O-isotope Stage 2 in Patagonia. *Geological Society of America Bulletin* 116: 308–321.
- Kaplan MR, Douglass DC, Singer BS, Ackert RP, Caffee MW. 2005. Cosmogenic nuclide chronology of pre-last glaciation maximum moraines at Lago Buenos Aires, 468 S, Argentina. *Quaternary Research* 63: 301–315.
- Kaplan, M.R., Moreno, P.I., Rojas, M. 2008 a. Glacial dynamics in southernmost South America during Marine Isotope Stage 5e to the Younger Dryas chron: a brief review with a focus on cosmogenic nuclide measurements. *Journal of Quaternary Science*, 23, 649-658.
- Kaplan MR, Fogwill CJ, Sugden DE, Hulton NRJ, Kubik PW, Freeman SPHT. 2008 b. Southern Patagonian and Southern Ocean climate during the last glacial period. *Quaternary Science Reviews* 27:284–294.
- Porter SC, Clapperton CM, Sugden DE. 1992. Chronology and dynamics of deglaciation along and near the Strait of Magellan, southernmost South America. *Sveriges Geologiska Undersökning, Ser. Ca.* 81: 233–239.

- Rabassa J, Clapperton CM. 1990. Quaternary glaciations in the southern Andes. *Quaternary Science Reviews* 9: 153–174.
- Rabassa J., Coronato A.M., Salemme M. 2005. Chronology of the Late Cenozoic Patagonian glaciations and their correlation with biostratigraphic units of the Pampean region (Argentina). *Journal of South American Earth Sciences*, 20, 81–103.
- Rasmussen, S. O, K. K. Andersen, A. M. Svensson, J. P. Steffensen, B. M. Vinther, H. B. Clausen, M.-L. Siggaard-Andersen, S. J. Johnsen, L. B. Larsen, M. Bigler, R. Röthlisberger, H. Fischer, K. Goto-Azuma, M. E. Hansson and U. Ruth. 2006. A new Greenland ice core chronology for the last glacial termination, *J. Geophys. Res.*, doi:10.1029/2005JD006079.
- Reimer, P. J., Baillie, M. G. L., Bard, E., Bayliss, A., Beck, J. W., Bertrand, C. J. H., Blackwell, P. G., Buck, C. E., Burr, G. S., Cutler, K. B., Damon, P. E., Edwards, R. L., Fairbanks, R. G., Friedrich, M., Guilderson, T. P., Hogg, A. G., Hughen, K. A., Kromer, B., McCormac, F. G., Manning, S. W., Ramsey, C. B., Reimer, R. W., Remmele, S., Southon, J. R., Stuiver, M., Talamo, S., Taylor, F. W., van der Plicht, J., and Weyhenmeyer, C. E. 2004a. IntCal04 Terrestrial radiocarbon age calibration, 26 - 0 ka BP. *Radiocarbon* 46, 1029-1058.
- Schwander J., Jouzel J., Hammer C.U., Petit J.R., Udisti R., Wolff E., 2001. A tentative chronology for the EPICA Dome Concordia ice core. *Geophys. Res. Lett.*, 28 (22): 4243-4246.
- Singer BS, Ackert RP, Guillou H. 2004. 40Ar/39Ar and K-Ar chronology of Pleistocene glaciations in Patagonia. *Geological Society of America Bulletin* 116: 434–450.
- Solari M.A., Hervé F., Le Roux J.P., Airo A., Sial A.N. 2010, in press. Paleoclimatic significance of lacustrine microbialites: A stable isotope case study of two lakes at Torres del Paine, southern Chile. *Palaeogeography, Palaeoclimatology, Palaeoecology*. doi:10.1016/j.palaeo.2010.07.016
- Sowers T, Bender M., 1995. Climate records covering the last deglaciation. *Science* 269: 210–214.
- Steig E.J, Brook E.J, White J.W.C, Sucher C.M, Bender M.L, Lehman S.J, Morse DL, Waddington E.D, Clow G.D. 1998. Synchronous climate changes in Antarctica and the North Atlantic. *Science* 282: 92–95.
- Stenni, B., V. Masson-Delmotte, S. Johnsen, J. Jouzel, A. Longinelli, E. Monnin, R. Rothlisberger, and E. Selmo. 2001. An Oceanic Cold Reversal during the last deglaciation. *Science*, 293: 2074-2077.
- Stenni, B., J. Jouzel, V. Masson-Delmotte, R. Rothlisberger, E. Castellano, O. Cattani, S. Falourd, S.J. Johnsen, A. Longinelli, J.P. Sachs, E. Selmo, R. Souchez, J.P. Steffensen, R. Udisti. 2003. A late-glacial high-resolution site and source temperature record derived from the EPICA Dome C isotope records (East Antarctica), *Earth Planet. Sci. Lett.*, 217: 183-195.
- Stenni, B.; Sachs, J.P.; Selmo, E.; Souchez, R.; Steffensen, J.P.; Udisti, R.; Jouzel, J.; Masson-Delmotte, V.; Rothlisberger, R.; Castellano, E.; Cattani, O.; Falourd, S.; Johnsen, S.J.; Longinelli, A. 2006. EPICA Dome C Stable Isotope Data to 44.8 KYrBP. IGBP PAGES/World Data Center for Paleoclimatology Data Contribution Series # 2006-112. NOAA/NCDC Paleoclimatology Program, Boulder CO, USA.
- Stern, C.R. (1990). Tephrochronology of southernmost Patagonia. *National Geographic Research*, 30, 304-314.
- Stuiver, M., Reimer, P. J., and Reimer, R. W. 2005. CALIB 5.0. [WWW program and documentation]
- Sugden, D.E., Bentley, M.J., Fogwill, C.J. Hulton, N.R.J., McCulloch, .D. and Purves, R.S. 2005: ‘Late-glacial glacier events in southernmost South America: a blend of ‘northern’ and southern’ hemispheric climatic signals?’ *Geografiska Annaler*, 87A(2): 273–288
- Svensson A, K,K, Andersen, M, Bigler, H,B, Clausen, D, Dahl-Jensen, S,M, Davies, S,J, Johnsen, R, Muscheler, S,O, Rasmussen, R, Röthlisberger, J,P, Steffensen, and B,M, Vinther, 2006. The Greenland Ice Core Chronology 2005, 15-42 ka, Part 2: Comparison to other records, *Quaternary Science Reviews*, vol, 25, Shackleton special issue 24.
- Ton-That, T., Singer, B., Mörner, N. and Rabassa, J. 1999. Datación de lavas basálticas por 40Ar/ 39Ar y geología glacial de la región del Lago Buenos Aires. *Revista de la Asociación Geológica Argentina* 54: 333-352.

- USGS, 2000. Shuttle Radar Topography Mission, 3 Arc Second scene SRTM\_fb03\_p230r096, Filled-Finished B, Global Land Cover Facility, University of Maryland, College Park, Maryland, 2000. Source for this data set was the Global Land Cover Facility, [www.landcover.org](http://www.landcover.org).
- Vinther, B.M., H.B. Clausen, S.J. Johnsen, S.O. Rasmussen, K.K. Andersen, S.L. Buchardt, D. Dahl-Jensen, I.K. Seierstad, M.-L. Siggaard-Andersen, J.P. Steffensen, A.M. Svensson, J. Olsen, and J. Heinemeier, 2006, A synchronized dating of three Greenland ice cores throughout the Holocene, *Journ, Geophys, Res*, vol, 111, D13102, 2006, doi:10.1029/2005JD006921
- Wenzens, G., 2005. Glacier advances east of the Southern Andes between the Last Glacial Maximum and 5,000 BP compared with lake terraces of the endorheic Lago Cardiel (49° S, Patagonia, Argentina). *Zeitschrift für Geomorphologie*, 49: 433-454.



## IV. Paleotermometría Isotópica de Oxígeno en Microbialitas.

### IV.1. Hipótesis, Fundamentos y Metodología.

Como se ha mencionado en el Capítulo I por medio del presente estudio se busca contribuir a conocer parte de la evolución paleoclimática en el sector del Parque Nacional Torres del Paine. Para lograr dicho objetivo se fijaron objetivos específicos, y uno de ellos fue reconstruir la evolución hídrica y determinar las paleotemperaturas del agua durante el Holoceno en el lago Sarmiento y la laguna Amarga.

El objetivo específico mencionado, no solo pretende aportar a cumplir el objetivo general, sino también a demostrar la hipótesis de que la evolución del sistema hidrológico en el Sector de Torres del Paine permitió la formación de un conjunto de lagos y lagunas endorreicas en las cuales se formaron colonias de microbialitas y que ellas pueden ser utilizadas como paleotermómetros si: el fraccionamiento isotópico entre el agua y los carbonatos se produce en equilibrio y la composición isotópica del agua depende principalmente de la temperatura.

Gracias a experimentos realizados para la precipitación de carbonatos a bajas temperaturas, diversos autores han podido establecer relaciones entre el fraccionamiento isotópico de oxígeno y la variación de la temperatura del fluido del cual precipita. De esta manera la temperatura depende del fraccionamiento de oxígeno en función de las siguientes ecuaciones:

$$1000 \ln \alpha_{\text{Dolomita-agua}} = 2.73 \times 10^6 T^{-2} + 0.26 \text{ (Vasconcelos, 2005).}$$

$$1000 \ln \alpha_{\text{Calcita-agua}} = 2.78 \times 10^6 T^{-2} - 2.89 \text{ (Friedman y O'Neil, 1997).}$$

$$1000 \ln \alpha_{\text{Aragonito-agua}} = 18.56 \pm 0.32 \times 10^3 T^{-1} - 33.49 \pm 0.31 \text{ (} r=0.99 \text{) (Patterson et al., 1993)}$$

Donde  $\alpha_{A-B}$  es el factor de fraccionamiento entre las fases A y B:

$$\alpha_{\text{carbonato-agua}} = R_{\text{carbonato}} / R_{\text{agua}}$$

$$R_{\text{calcita}} = (\text{CaCO}^{18})^{1/3} / (\text{CaCO}^{16})^{1/3} = (\text{Isótopo pesado}) / (\text{Isótopo liviano}).$$

$$R_{\text{agua}} = (\text{H}_2\text{O}^{18}) / (\text{H}_2\text{O}^{16}) = (\text{Isótopo pesado}) / (\text{Isótopo liviano}).$$

El método se puede detallar en:

1. Estimar la magnitud del fraccionamiento del isótopo de oxígeno existente en el agua del lago Sarmiento y laguna Amarga por: los cambios de temperatura del agua, la precipitación directa sobre el lago, la evaporación directa sobre el lago, los escurrimientos superficiales de agua y las infiltraciones de aguas subterráneas.
2. Conocer las especies de carbonatos que precipitan (aragonito, calcita, dolomita, etc.) en los trombolitos y estromatolitos, por medio de difracción de rayos X.
3. Para utilizar las ecuaciones de paleotermómetros es necesario analizar isótopos estables de oxígeno en trombolitos, gastrópodos lacustres y agua de los lagos por medio de un espectrómetro de masa.
4. Para obtener la edad de los trombolitos es necesario realizar dataciones de  $^{14}\text{C}$  en las

conchas de gastrópodos muertos. En el caso de los estromatolitos fósiles, es necesario realizar dataciones de  $^{14}\text{C}$  de las fases orgánicas.

A continuación se presenta un artículo aceptado y publicado el año 2010 por la revista internacional *Palaeogeography, Palaeoclimatology, Palaeoecology*. En el artículo se evaluó como el equilibrio isotópico y las condiciones hidrológicas y mineralógicas locales pueden influenciar el uso de las microbialitas lacustres como indicadores paleoclimáticos. Para ello se escogió lago Sarmiento y laguna Amarga que comparten similares características regionales pero importantes diferencias particulares, permitiendo evaluar con mayor rigurosidad el potencial paleotermométrico de las microbialitas en estudio.

## **IV.2. Paleoclimatic significance of lacustrine microbialites: a stable isotope case study of two lakes at Torres del Paine, southern Chile.**

M.A. Solari<sup>a\*</sup>, F. Hervé<sup>a</sup>, J.P. Le Roux<sup>a</sup>, A. Airo<sup>b</sup>, A.N. Sial<sup>c</sup>

<sup>a</sup> Departamento de Geología, Facultad de Ciencias Físicas y Matemáticas, Universidad de Chile, Casilla 13518, Correo 21, Santiago, Chile.

<sup>b</sup> School of Earth Sciences, Stanford University, 450 Serra Mall, Bldg. 320, Rm. 118 Stanford, CA 94305, USA.

<sup>c</sup> NEG-LABISE, Dept. of Geology, Center of Technology and Geosciences, Federal University of Pernambuco, C.P. 7852, 50670-000 Recife, PE, Brazil.

**Keywords:** paleoclimate, climate change, isotopes, carbonate, thrombolites, stromatolites.

**Corresponding author:** msolari@cec.uchile.cl; fax 56-2-6963050.

### *IV.2.1 Abstract*

Two Patagonian lakes studied here, Lago Sarmiento and Laguna Amarga, are located within the orographic rain shadow formed to the east of the Southern Patagonian Ice Field in the Andes Range. Major thrombolite colonies are present in Lago Sarmiento, whereas widespread stromatolites occur in Laguna Amarga. Based on the characterization of the hydrologic system of these two lakes, together with an estimation of the isotopic balance and an analysis of the equilibrium conditions between the water and biologically induced carbonates, it is concluded that the microbialites of Lago Sarmiento are better suited as paleotemperature indicators than those of Laguna Amarga. Lago Sarmiento thrombolites contain unique carbonate mineral species in which carbonate precipitation occurs close to isotopic equilibrium and where the variation in water temperature controls fractionation of the stable oxygen isotope.

The results indicate that at 1215 cal yr Bp the level of the lake was at 85 m a.s.l with a temperature close to 9.3°C, was at 82 m a.s.l. at 600 cal yr Bp with a temperature close to 8.5°C. This coincides with the timing of the Northern Hemisphere Medieval Warming Period. At 183 cal yr Bp the level of the lake was at 80 m a.s.l with a cooler temperature close to 7.7°C, representing a colder period coinciding with the timing of the Little Ice Age (LIA). An interesting outcome of this study is that it reinforces the idea that the  $\delta^{13}\text{C}$  signal in carbonate deposits can be an effective tool in distinguishing between inorganic and biologically induced precipitation.

### *IV.2.2 Introduction*

The stable isotope record of oxygen in microbial carbonates has generated considerable debate as potential inventories of paleoclimatic and paleoenvironmental information. To evaluate the isotopic equilibrium and establish how local hydrological and mineralogical conditions can influence the use of microbialite carbonates as paleoclimatic tools, we studied the hydrological system and microbial communities of Lago Sarmiento and Laguna Amarga in the Patagonian region of southern Chile.

Microbialites are organo-sedimentary deposits that accrete as a result of benthic microbial communities trapping and binding detrital sediment and forming nuclei for mineral precipitation (Burne and Moore, 1987). Dupraz et al. (2009) proposed that in carbonate microbialites, the key components of organo-mineralization (Perry et al., 2007) are microbial metabolism, the environmental conditions that impact calcium carbonate saturation, and an organic matrix comprised of extracellular polymeric substances (EPS).

EPS are produced by the cyanobacteria that compose the microbialites, which facilitate the trapping of detrital minerals and also provide a chemically protective microenvironment in which biologically induced mineral precipitation can take place around the cells (Decho et al., 2005). The latter process results from photosynthesis that liberates O<sub>2</sub> and traps the CO<sub>2</sub>, with a consequent rise in pH that induces the precipitation of carbonates (Burne and Moore, 1987). Although caused by the microbes, however, the precipitation of carbonate minerals can be considered as inorganic (Burne and Moore, 1987; Vasconcelos, et al., 2005).

The stable isotopic record of  $\delta^{18}\text{O}$  in microbial carbonates has received significant attention as potential inventories of paleoclimatic and environmental information (Andrews et al., 1993; 1997; Casanova and Hillaire-Marcelo, 1992; Vasconcelos et al., 2005; Teranes et al., 1999) and has also been the subject of considerable debate (see the review of Chafetz and Lawrence, 1994). The paleothermometric interpretation of isotopic variation in microbialite lakes is based on the assumption that the oxygen isotope fractionation between the water and precipitated carbonate is produced in equilibrium. However, equilibrium does not always exist (Teranes et al., 1999; Kim and O'Neil, 1997), while temperature variations and the water balance also control the oxygen isotopic fractionation of the lake water.

In order to evaluate the isotopic equilibrium and establish how local hydrological and mineralogical conditions can influence the use of microbialite carbonates as paleoclimatic tools, we studied the hydrologic system and microbial communities of Lago Sarmiento and Laguna Amarga.

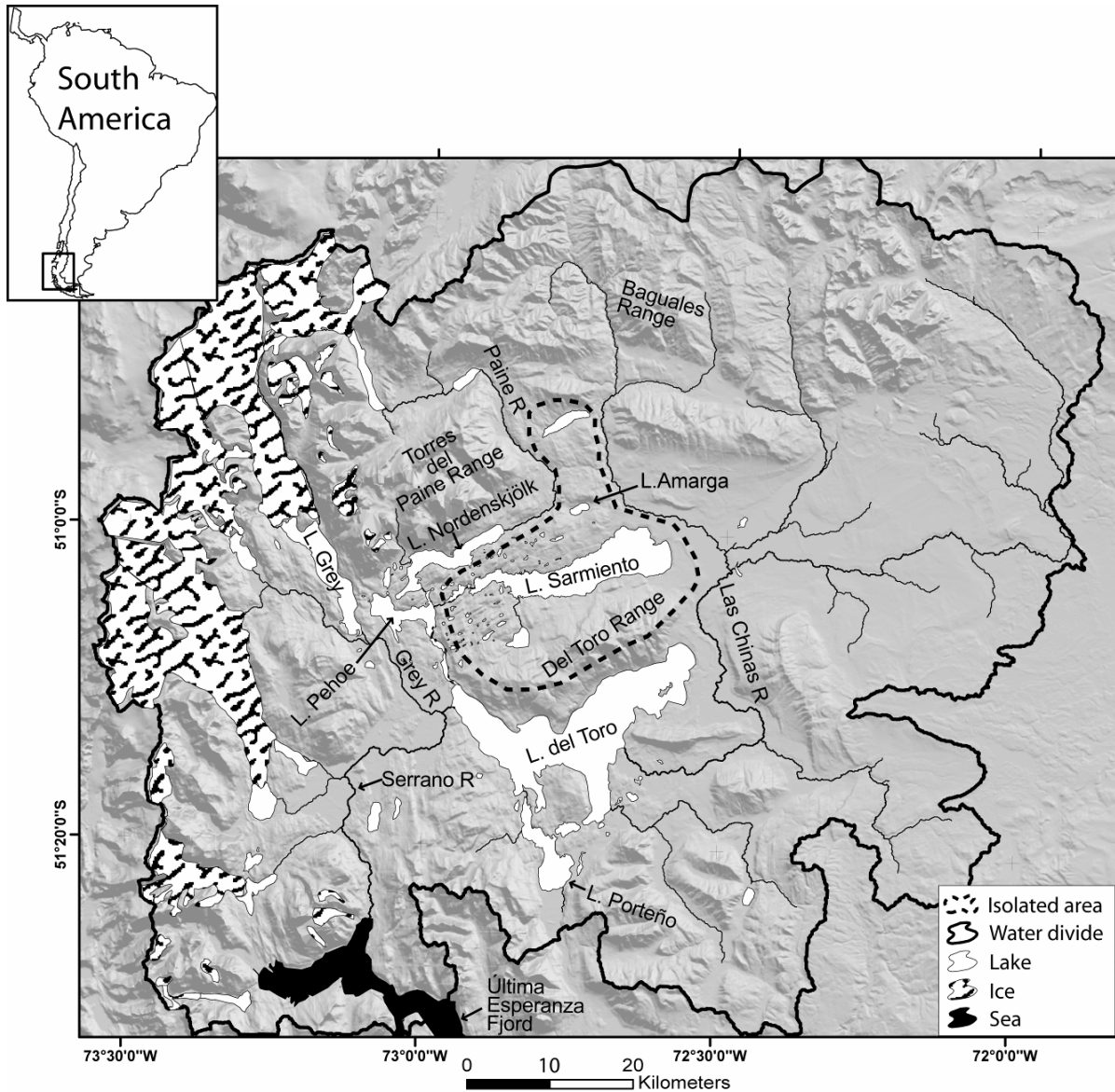
Lago Sarmiento and Laguna Amarga were selected because they have certain important common characteristics, which facilitate their comparison with respect to stable isotopes. These include the fact that both contain carbonate microbialite communities, that they experience the same regional climatic conditions, and that both lie within an isolated surface drainage basin where the underlying rocks are formed by the Cerro Toro Formation.

### *IV.2.3 General Background*

Lago Sarmiento and Laguna Amarga are enclosed by five moraine systems (Fig. IV. 2) labelled by Marden (1993) as A, B, C, D, and E. Of which A, B and C were correlated

with the last global glacial cycle (Marden and Clapperton, 1995) and recently investigation proposed that these glacial lobes are younger than 21,493 Cal yrs BP (Solari et al, 2010). Cosmogenic  $^{10}\text{Be}$  dating of erratics from the D moraine indicates a short-lived re-advance of Patagonian ice culminating at 12–15 kyr BP, coincident with the time of the Antarctic Cold Reversal (Fogwill and Kubik, 2005; Moreno et al., 2009). The lakes are developed over an area with sandstones, siltstones and conglomerates of the Cerro Toro Formation, a deep-marine succession thrust and folded into an approximately NNW-trending system (Fig. IV. 2).

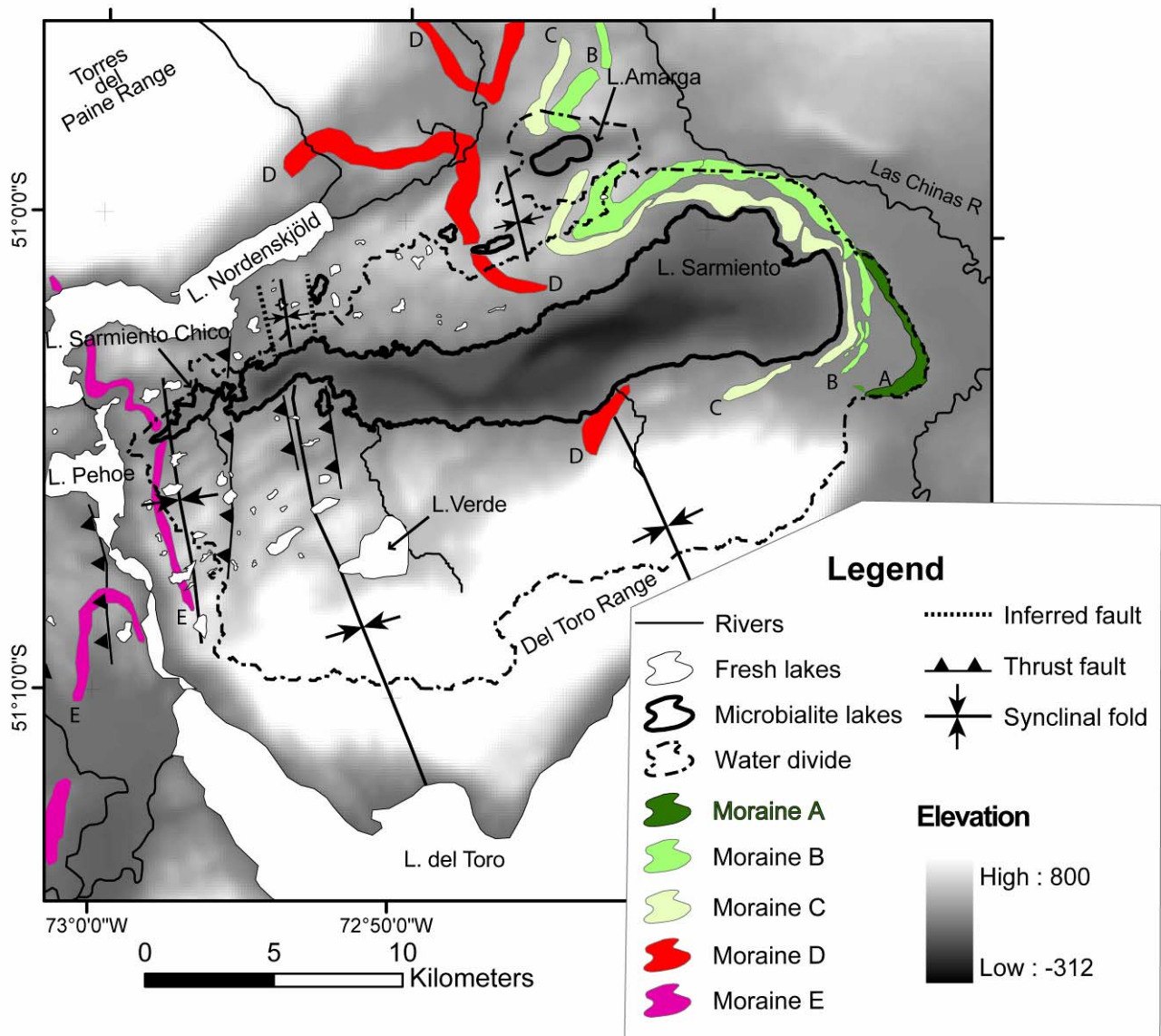
The two studied lakes form part of a hydrologic system, the Torres del Paine Drainage Basin (TPDB), developed to the east of the Southern Patagonian Ice Field (Fig. IV.1). The TPDB contains 5 closed lakes in addition to Lago Sarmiento and Laguna Amarga, all of which have carbonate microbialite communities (Microbialite Lakes in Fig. IV. 2). All these microbialites lakes are located in an isolated area disconnected from outside rivers and sources of glacial meltwater (demarcated by stippled line in Fig. IV. 1), so that their main source of water is rainfall resulting from the predominantly westerly winds. The precipitation has a spatial distribution reaching 10,000 mm per year over the ice field itself, but decreasing to 7,000 mm along its western flank (D.G.A., 1987) and less than 400 mm on its eastern side (Carrasco et al., 1998; Carrasco et al., 2002; Ibarzabal et al., 1996).



**Fig. IV-1:** Shaded Relief of Shuttle Radar Topographic Mission Digital Elevation Model (SRTM-DEM) showing the Torres del Paine drainage basin (black line), the river (R) network and main lakes (L).

Lago Sarmiento and Laguna Amarga are located in a semi-arid steppe region. The wind speed is characterized by an annual average of 27 km/h (1987-1988) and reaches a maximum of 100 km/hr during spring and summer. The average yearly precipitation (1983-1988) and evaporation (1983-1988), obtained from a meteorological station located near the administration office of the Torres del Paine National Park, is 639 mm and 839 mm, respectively. The lowest rainfall is observed at the end of winter (May) and mid-spring (September-October), whereas the highest precipitation is recorded during summer and autumn. The average air temperature (1983-1988) is 7°C, with a seasonal maximum variation between -1°C in winter and 13.8°C in summer (Campos et al., 1994; 1996).

Lago Sarmiento ( $51^{\circ}03'00''\text{S}$ ;  $72^{\circ}45'01''\text{W}$ ) receives an important contribution of water from Laguna Verde, has a maximum depth of 312 m and its altitude is 77 m a.s.l.. It is a sub-saline, alkaline lake with a mean salinity of 1.9 mg/l, a pH of 8.3 to 8.7, and a mean surface water temperature varying between  $6.2^{\circ}\text{C}$  in winter and  $12.2^{\circ}\text{C}$  in summer (Campos et al., 1994). *Cyanophyceae* predominate amongst the phytoplankton, *Merismopedia tenuissima* being the most abundant species (Campos et al., 1994). Massive, dead carbonate microbialites are exposed along the shoreline of Lago Sarmiento and up to 8 m above the present lake surface as a result of a drop in the water level (Campos et al., 1994; Soto et al., 1994). Similar microbialites are actively growing under the water surface of the lake, consisting of non-laminated, clotted calcium carbonate classified as thrombolites (Airo et al., submitted).



**Fig. IV-2:** Merged SRTM-DEM and bathymetric digital elevation model. Lakes with microbialites are demarcated with thick lines and the drainage basin by a dashed line.

The maximum depth of Laguna Amarga (50° 58' 27" S; 72° 44' 55" W) is 4.1 m and its altitude is 80 m a.s.l. (Campos et al., 1996). The average pH of the lake is 9.1, whereas the salinity and temperature average 26.1 mg/l and 11.7 °C, respectively (Campos et al., 1996). Physio-chemical conditions are reflected by a phytoplankton community dominated by *Cyanophyceae* aff. *gloescaspa* and *Artemia* (Campos et al., 1996).

In total, seven lakes with carbonate microbialite communities are developed in an isolated basin of the Torres del Paine National Park. These lakes have common characteristics that provide the essential conditions for microbialite communities to develop: (1) an area that is isolated from rivers, a condition which prevents dissolution because of river water input; (2) being closed lakes in an area where the mean annual evaporation is higher than the mean annual precipitation, a condition which leads to the concentration of ions; (3) the underlying rocks of the basin are formed by the Cerro Toro Formation, a marine succession that provides carbonates to the lake water through leaching.

#### *IV.2.4 Methodology*

##### *a. Isotopes, mineralogy, geochemistry and radiocarbon age*

Water samples were collected under the protocol specified in Clark and Fritz (1997) and were analyzed in the laboratory of the *Comisión Chilena de Energía Nuclear* (CCHEN). Carbon and oxygen isotopic compositions were determined at NEG-LABISE, Federal University of Pernambuco, Brazil, using the conventional digestion method (McCrea, 1950). Powdered samples were dissolved with H<sub>3</sub>PO<sub>4</sub> at 25°C to release the CO<sub>2</sub>. The δ<sup>13</sup>C and δ<sup>18</sup>O values were measured in cryogenically cleaned CO<sub>2</sub> (Craig, 1957) in a triple collector SIRA II mass spectrometer. The C and O isotopic data are reported as a deviation with reference to V-PDB and V-SMOW, respectively. Borborema Skarn Calcite (BSC), calibrated against international standards, was used as the reference gas and the reproducibility of the measurements was better than 0.1‰. The values obtained for the standard NBS-20 in a separate run against BSC yielded δ<sup>13</sup>C<sub>V-PDB</sub> = -1.05, and δ<sup>18</sup>O<sub>V-SMOW</sub> = -4.22. These results are in close agreement with the values reported by the US National Bureau of Standards (-1.06 and -4.14, respectively).

Minerals were identified by X-ray diffractometry and chemical compositions by X-ray fluorescence in the external laboratory of the *Servicio Nacional de Geología y Minería* (SERNAGEOMIN). The radiocarbon chronology was determined from gastropod shells at the Center for Applied Isotope Studies (CAIS) at the University of Georgia, using a CAIS 0.5 MeV mass spectrometer, which was calibrated for the Southern Hemisphere (McCormac et al., 2004).

##### *b. Variation in lake surface and volume*

The water surface variation of the lakes between October of 1986 and 1999 was determined by analysing Landsat TM (Nasa Landsat Program, 1986) and Landsat ETM (Nasa Landsat Program, 1999) satellite images. The software package ArcMap Version 9.2



was used to integrate the bathymetric curves of the lakes published in Campos et al. (1994; 1996) with the Shuttle Radar Topographic Mission Digital Elevation Model (SRTM DEM ) data (USGS, 2000). With this integrated digital elevation model (Fig. IV. 2) it was possible to estimate the volume change related to the calculated surface variation.

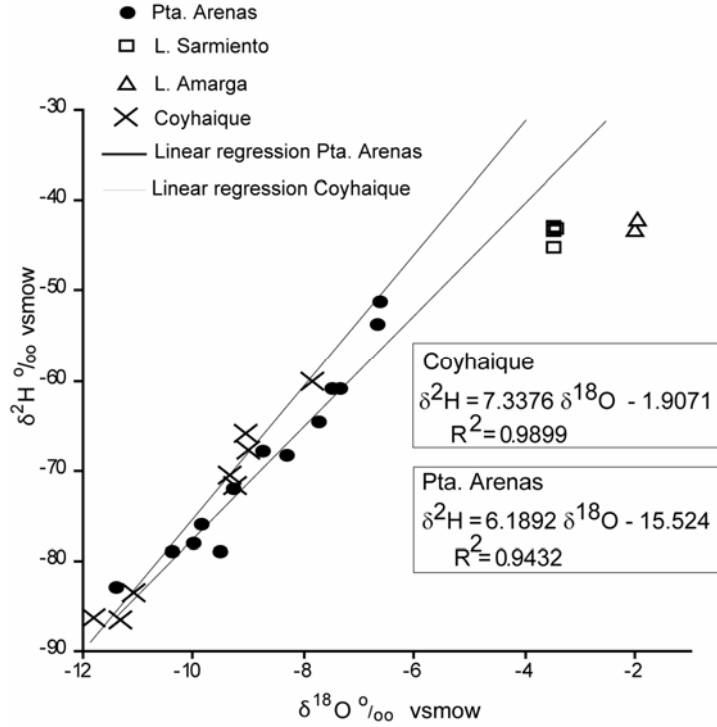
#### IV.2.5 Lake Water Isotope Characteristics

**Table 1:**  $\delta^{18}\text{O}$  and  $\delta^2\text{H}$  isotopic composition of the Lago Sarmiento and Laguna Amarga surface water.

Lake	UTM E	UTM N	Date Collected	Sample depth (cm)	Temperature (°C)	$\text{‰} \delta^{18}\text{O}$ (VSMOW)	$\text{‰} \delta^2\text{H}$ (VSMOW)
Sarmiento	655334	4340059	10 Jan 2007	20	9	-3.47	-42.9
Sarmiento	646459	4342206	10 Jan 2007	20	9	-3.44	-45.4
Sarmiento	667386	4346392	10 Jan 2007	20	9	-3.46	-43.4
Sarmiento	656516	4343694	6 Sep 2007	20	8.7	-3.43	-43.3
<b>Sarmiento Average</b>					8.9	-3.45	-43.75
Amarga	659205	4350730	12 Jan 2007	15	11	-2.01	-43.3
Amarga	656962	4350292	12 Jan 2007	15	11	-1.99	-43.1
Amarga	658351	4350379	12 Jan 2007	15	11	-1.95	-42.0
<b>Amarga Average</b>					11	-2	-42.8

#### a. Meteoric vs. lake water isotopy.

The meteorological stations located in Punta Arenas (53°S - 71.51°W, about 265 km south of Torres del Paine) and Coyhaique (45.35°S - 72.07°W, about 600 km north of Torres del Paine) are part of the Global Network of Isotopes in Precipitation (GNIP). We used the  $\delta^{18}\text{O}$  and  $\delta^2\text{H}$  in precipitation of the monthly average isotopic datasets (IAEA/WMO 2006), to calculate a linear relationship between  $\delta^{18}\text{O}$  and  $\delta^2\text{H}$  (meteoric lines, Fig. IV.3). The  $\delta^{18}\text{O}$  and  $\delta^2\text{H}$  contents of the lakes are closer to the Punta Arenas meteoric line than that of Coyhaique, which indicates a closer affinity with the Punta Arenas meteoric water. The  $\delta^{18}\text{O}$  and  $\delta^2\text{H}$  values of Laguna Amarga are more enriched than the values of Lago Sarmiento with respect to the meteoric line of Punta Arenas, indicating a higher fractionation produced by evaporation processes in Laguna Amarga.



**Fig. IV-3:** Monthly mean isotopic relationship between  $\delta^{18}\text{O}$  and  $\delta^2\text{H}$  (IAEA/WMO, 2006) compared with Lago Sarmiento and Laguna Amarga  $\delta^{18}\text{O}$  and  $\delta^2\text{H}$  surface water composition.

*b. Hydrologic, isotopic and saline balance approximation.*

The hydrologic balance of a closed lake can be expressed by the sum of the water inflow and outflow (e.g., Jones et al., 2007):

$$\frac{dV}{dt} = P + Si + Gi - So - E - Go \quad (\text{Eq. 1})$$

where  $V$  is lake volume;  $t$ , time;  $P$ , precipitation on the lake surface;  $Si$ , surface inflow from streams;  $So$ , surface outflow;  $Gi$ , ground water inflow;  $E$ , evaporation from the lake surface;  $Go$ , ground water outflow .

In addition to the water balance equation above (Eq.1), the stable isotope composition of the closed lake must also balance such that:

$$\delta^{18}\text{O}_{\frac{dV}{dt}} = P\delta^{18}\text{O}_P + Si\delta^{18}\text{O}_{Si} + Gi\delta^{18}\text{O}_{Gi} - So\delta^{18}\text{O}_{So} - E\delta^{18}\text{O}_E - Go\delta^{18}\text{O}_{Go} \quad (\text{Eq. 2})$$

where the values of  $\delta^{18}\text{O}_P$ ,  $\delta^{18}\text{O}_{Si}$ ,  $\delta^{18}\text{O}_{So}$ ,  $\delta^{18}\text{O}_{Gi}$ ,  $\delta^{18}\text{O}_{Go}$ ,  $\delta^{18}\text{O}_E$  and  $\delta^{18}\text{O}_{Go}$  are the isotope values of the lake surface precipitation, surface inflow, ground water inflow, surface outflow, lake surface evaporation, and ground water outflow, respectively (e.g., Gibson et al., 1999; Benson and Paillet, 2002).

The  $\delta^{18}\text{O}$  composition of newly formed water can be expressed by the simple mixing between the  $\delta^{18}\text{O}$  compositions of the component water phases (Clark and Fritz,

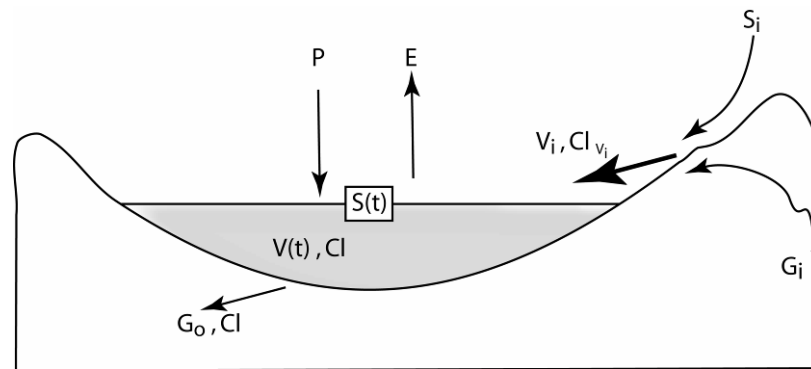
1997). An estimation of the  $\delta^{18}\text{O}$  variation in the lake in any year  $t$  can be expressed as the sum of the year  $t$  lake volume mixing between an initial  $t-1$  year  $\delta^{18}\text{O}$  mean annual lake water composition and the  $\delta^{18}\text{O}_{dV/dt}$  variation produced by the water inflow and outflow (Eq. 2):

$$\delta^{18}\text{O}(t) = \left(1 - \frac{dV/dt}{V(t)}\right) \delta^{18}\text{O}_{t-1} + \frac{\delta^{18}\text{O}_{dV/dt}}{V(t)} \quad (\text{Eq. 2})$$

3)

where  $\delta^{18}\text{O}(t)$  is the year  $t$  mean annual composition of the lake,  $\delta^{18}\text{O}(t-1)$  is the mean annual composition of the previous year,  $\delta^{18}\text{O}_{dV/dt}$  is the isotopic balance related to the water inflow and outflow between years  $t$  and  $t-1$ ,  $dV/dt$  is the water volume variation between years  $t$  and  $t-1$ , and  $V(t)$  is the lake water volume of year  $t$ .

To establish with some precision the hydrologic balance of the basin it is necessary to have an extended record of the different hydrologic and atmospheric parameters, which unfortunately does not currently exist for Lago Sarmiento and Laguna Amarga. However, to make up for a lack of data, Risacher et al. (1999) presented an approach for closed lakes in the north of Chile that allows their hydrologic balance to be estimated.



**Fig. IV-4:** Diagram of the water inflow and outflow in a closed basin.  $Cl$  and  $Cl_{v_i}$  represent the chloride concentration of the lake water and the surface water inflow.

A lake within a closed basin receives water from the drainage basin ( $G_i$  plus  $S_i$ ; Fig. IV. 4) and also from direct precipitation over the lake surface ( $P$ ). There is a loss of water from the lake by evaporation ( $E$ ) and groundwater infiltration ( $G_o$ ), but no loss of water from surface outflow ( $S_o$  is equal to zero). Eq. 1 can therefore be expressed as:

$$\frac{dV}{dt} = P + V_i - E - G_o \quad (\text{Eq. 4})$$

where  $V_i$  is the total volume of water inflow ( $G_i$  plus  $S_i$ ; Fig. IV. 4). In addition to the water balance equation (Eq. 4), the  $\delta^{18}\text{O}$  balance can be expressed as:

$$\delta^{18}O_{d/dt} = P\delta^{18}O_P + Vi\delta^{18}O_{Vi} - E\delta^{18}O_E - Go\delta^{18}O_{Go} \quad (\text{Eq. 5})$$

where  $\delta^{18}O_{Vi}$  represents simple mixing between the extreme values of  $\delta^{18}O_{Gi}$  and  $\delta^{18}O_{Si}$ :

$$\delta^{18}O_{Vi} = \frac{Gi\delta^{18}O_{Gi} + Si\delta^{18}O_{Si}}{Vi} \quad (\text{Eq. 6})$$

If the lake is permanent and the mean annual surface is stable from one year to the next, the inflow balances the outflow:

$$Vi + P = Go + E \quad (\text{Eq. 7})$$

Direct precipitation on and evaporation from the lake surface can be calculated by multiplying the lake surface ( $S(t)$ ) at year  $t$  and the average annual precipitation ( $Pm$ ) and average annual evaporation ( $Em$ ), respectively:

$$P = S(t) \times Pm \quad (\text{Eq. 8})$$

and

$$E = S(t) \times Em \quad (\text{Eq. 9})$$

To obtain the saline balance it necessary to assume dynamic equilibrium of the lake, i.e. that the concentration of the chemical components is stable and does not increase with time (Risacher et al., 1999). The ideal tracer should be highly soluble and should not participate in any mineral precipitation or biological processes, being only lost by infiltration. Chloride fulfills these conditions and is therefore commonly used as a tracer (Branchu and Bergonzini, 2004).

We assume that the chloride concentration can be estimated by the concentration of the surface inflow and that it is constant in time. Each year a certain quantity of chloride enters the lake, given by  $Vi \times Cl_{Vi}$  ( $Cl_{Vi}$  is the mean chloride concentration of the inflow), while another quantity is lost, given by  $Go \times Cl$  ( $Cl$  being the mean chloride concentration of the lake or groundwater outflow). If there is dynamic equilibrium, the saline balance is expressed by:

$$Vi \times Cl_{Vi} = Go \times Cl \quad (\text{Eq. 10})$$

The hydrologic and saline balance of the lakes proposed in Eqs. 7 and Eq. 8 can be solved by:

$$Go = \frac{E - P}{\frac{Cl}{Cl_{Vi}} - 1} \quad (\text{Eq. 11})$$

and

$$V_i = \frac{E - P}{1 - \frac{Cl_{Vi}}{Cl}} \quad (\text{Eq. 12})$$

*c. Lago Sarmiento.*

The drainage basin of Lago Sarmiento has an area of 378.52 km<sup>2</sup> (demarcated by the water divide in Fig. IV. 2) and includes many lakes. Lago Sarmiento is fed by a stream at its southern shore and some seasonal streams from the north, but the main inlet is a river sourced by Laguna Verde (Fig. IV. 2). The surface area of the lake in October 1986 occupied 83.96 km<sup>2</sup> and by October 1999 had decreased to 83.05 km<sup>2</sup>, with an annual linear variation of 0.07 km<sup>2</sup>. The volume variation was calculated from the surface variation as derived from the combined SRTM DEM and bathymetric digital elevation model (Fig. IV. 2). The volume of the lake water in October 1986 was 9.63 km<sup>3</sup> and by October 1999 had declined to 9.54 km<sup>3</sup>, with an annual linear decrease of 0.007 km<sup>3</sup> ( $\sim dV/dt$ ). As the annual variation is only 0.07 % of the 1986 volume, the lake level can be considered as quasi-stable from one year to the next (Eq. 7) and dynamic equilibrium can be assumed (Eq. 8).

**Table 2:** Lago Sarmiento and main surface inflow chloride concentrations. The coordinate system is in UTM 18S with a datum of WGS-84.

Samples	UTM N	UTM E	Description	Chloride (mg/l)
1	652143	4334446	Surface water at Laguna Verde shore	4
2	651192	4336632	Laguna Verde river	5,9
3	655467	4336632	Small Stream	2,1
4	656706	4339289	Small Stream	7,8

We assume that the chloride concentration of the water inflow is constant over time and can be estimated at 4.95 mg/l, which is the average concentration of the surface inlets (Table 2). Based on six surface water analyses of Campos et al. (1994) between 1988 and 1991, the lake has a mean chloride concentration of 256.7 mg/l. Using these chloride values, the average annual precipitation and evaporation determined by Campos et al. (1994), and the lake surface water of October 1986 in Eqs. 8, 9, 11 and 12, we obtain the values of  $P$ ,  $E$ ,  $Go$  and  $V_i$ , respectively.

$$P = 53650440 \text{ m}^3$$

$$E = 70442440 \text{ m}^3$$

$$Go = 330170 \text{ m}^3$$

$$Vi = 17122170 \text{ m}^3$$

Combining Eqs. 5 and 3:

$$\delta^{18}\text{O} (t) = \left(1 - \frac{dv/dt}{V(t)}\right) \delta^{18}\text{O}_{t-1} + \frac{P\delta^{18}\text{O}_P + Vi\delta^{18}\text{O}_{Vi} - E\delta^{18}\text{O}_E - Go\delta^{18}\text{O}_{Go}}{V(t)} \quad (\text{Eq. 13})$$

and using the October 1986 values of  $P$ ,  $E$ ,  $Go$ ,  $Vi$ , the lake water volume and the annual linear volume variation, we obtain :

$$\delta^{18}\text{O} (1986) = 0.9993\delta^{18}\text{O}_{1985} + 0.0055\delta^{18}\text{O}_P + 0.00178\delta^{18}\text{O}_{Vi} - 0.007\delta^{18}\text{O}_E - 0.00003\delta^{18}\text{O}_{Go}$$

The factor estimated above that multiplies the values of  $\delta^{18}\text{O}_{P,Vi,E}$  and  $Go$ , allows us to infer that the year-to-year fractionation produced in Lago Sarmiento by evaporation, precipitation, water inflow and outflow is insignificant compared to the previous  $\delta^{18}\text{O}$  mean annual lake water composition. This suggests that temperature variation is the most likely cause of year-to-year oxygen isotope fractionation in Lago Sarmiento.

#### *d. Laguna Amarga.*

Laguna Amarga is a shallow, E-W elongated, closed lake. The lake receives water from two springs with a pH of 7 and has a drainage basin area of 13.45 km<sup>2</sup>. The surface of the lake in October 1986 occupied 2.15 km<sup>2</sup> and in October 1999 had decreased to 2.00 km<sup>2</sup>, with an annual linear variation of 0.012 km<sup>2</sup>. The volume variation was calculated from the surface variation, which in turn was derived from the merged SRTM DEM - bathymetric digital elevation model (Fig. IV.2). The volume of the lake water in October 1986 was 0.006 km<sup>3</sup> and in October 1999 had decreased to 0.004 km<sup>3</sup>, with an annual linear decline of 0.00015 km<sup>3</sup>. As the annual decrease is 2.82% and 4.45% of the 1986 and 1999 volumes, respectively, the lake level cannot be considered as being stable from year to year (Eq. 7) and dynamic equilibrium therefore cannot be assumed (Eq. 8). In addition, the presence of a salt fringe around the coastline of the lake with chloride precipitates, eliminates the use of chloride as a tracer for the hydrologic budget.

Nevertheless, it is possible to calculate the direct precipitation and evaporation for the lake. Using the average annual precipitation and evaporation determined by Campos et al. (1994) and the lake surface area of October 1986 in Eqs. 8 and 9, the values of  $P$  and  $E$  were obtained:

$$P = 1373850 \text{ m}^3$$

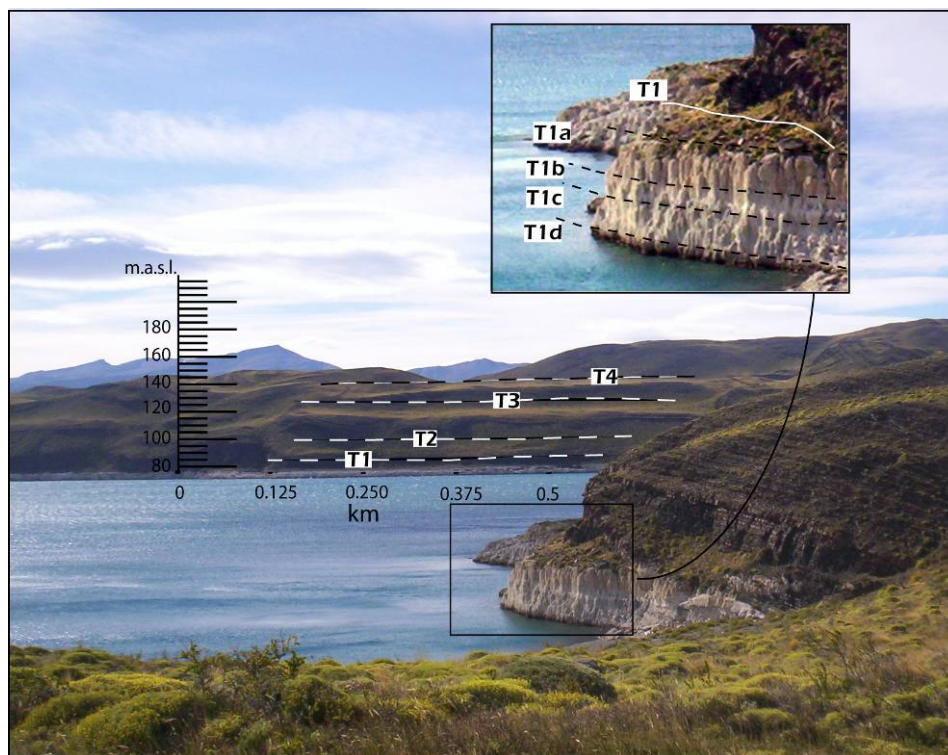
$$E = 1803850 \text{ m}^3$$

The precipitation ( $P$ ) and evaporation ( $E$ ) volume produce substantial fractionation from one year to the next in the lake. For this reason the isotopic fractionation of oxygen isotopes in Laguna Amarga is produced by a combination of direct precipitation and evaporation, as well as temperature variations.

#### IV.2.6 Description and Palaeothermometry of Lago Sarmiento Thrombolites

##### a. Description.

Four abrasion terraces (T1, T2, T3 and T4 in Fig. IV.5) lie above the present water level at ca. 77 m a.s.l. Terraces T4, T3, T2 and T1 occur at elevations of ca. 138, 121, 100, and 87 m a.s.l., respectively (Fig. IV.5). The lake becomes closed only when the water level drops below the junction between Lago Sarmiento and Lago Sarmiento Chico at 86 m a.s.l. Previously, the water of Lago Sarmiento discharged into Lago Sarmiento Chico and then into Lago Pehoe (see Fig. IV.2). Below the T1 terrace, 8 m of dead microbial build-up is exposed along a large part of the coastline. Under the water, living microbialites composed of gastropods with aragonite shells and cyanobacteria filaments enclosed by clotted calcite ( $\text{Mg}_{0.1}\text{Ca}_{0.9}\text{CO}_3$  determined by X-ray diffraction) and trapped sediments are observed.



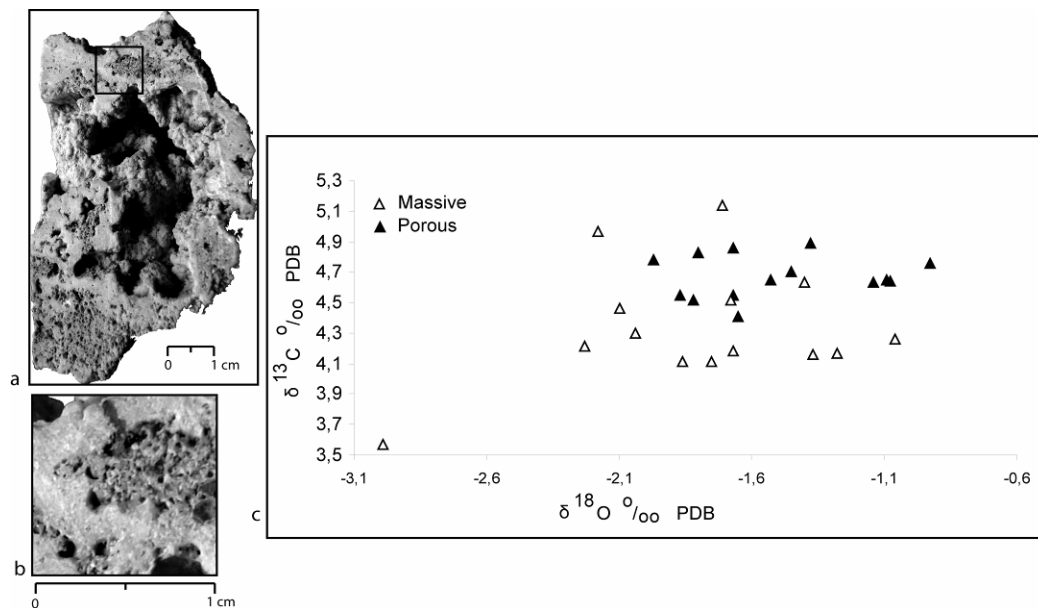
**Fig. IV-5:** Examples of terraces observed in Lago Sarmiento. In the magnification, each level is associated with a contact between the thrombolite color zones: light brown for T1a, white for T1b, gray for T1c and dark brown for T1d.

The distinctive clotted structure, observed at both microscopic and macroscopic scales (Fig. IV.7), classifies these deposits as thrombolites. In the thrombolites, zones of different colours separated by distinct contacts are observed. The contacts of the light brown, white, grey and dark brown colours of the thrombolite zones are interpreted as



resulting from four different lake levels, labelled T1a, T1b, T1c and T1d (magnification of Fig. IV.5 and Fig. IV.7). These levels have an average elevation of ca. 85, 82, 80, and 77.5 m a.s.l., respectively.

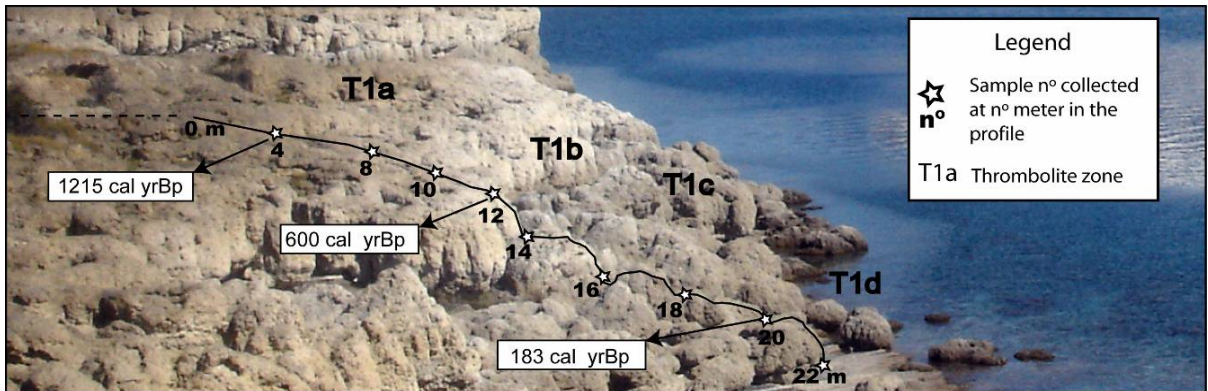
In hand samples and in thin sections it is possible to distinguish well differentiated phases of massive and porous calcite (Fig. IV.6b). The micrometer pores in the calcite can be interpreted as biosignatures related to the cyanobacteria activity (Bosak et al., 2004). The massive and porous phases of calcite show a  $\delta^{18}\text{O}$  distribution between -0.93 and -2.99‰  $\delta^{18}\text{O}$ , whereas, in nine samples out of thirteen, the massive phase is more negative in  $\delta^{13}\text{C}$  with respect to the porous phases (Fig. IV.6c). The more negative  $\delta^{13}\text{C}$  observed in the massive phases possibly reflects fractionation produced by recrystallization of previously porous phases.



**Fig. IV-6:** a: Section of a thrombolite with a distinctive clotted structure; b. Magnified area of the previous thrombolite (black square) showing well-differentiated massive and porous calcite phases. 6c. Oxygen and carbon stable isotope data for massive and porous phases of Lago Sarmiento thrombolites.

With the objective of characterizing the light brown, white, grey and dark brown thrombolite zones, a profile of 22 m was sampled from the water level to the top of the thrombolites along the southern shore of Lago Sarmiento (51° 04' 11.78" S and 72° 46' 58.28" O; Fig. IV.7). Along this profile, two samples at 4 and 8 m in the T1a level, three samples at 10, 12 and 14 m in the T1b level, three samples at 16, 18 and 20 m in the T1c level and one sample at 22 m in the T1d level were collected. Radiocarbon ages were determined for trapped gastropod shells collected at a depth of about 7 cm inside the external crust of the thrombolites and represent an age reflecting the end of growth and precipitation in each level. Median probability radiocarbon ages of 1215 (1340.89±52 C<sup>14</sup> yrBp), 600 (630.9±42 C<sup>14</sup> yrBp) and 183 (182.6±44 C<sup>14</sup> yrBp) cal yr Bp were obtained from samples of the T1a, T1b and T1c levels, respectively. Nevertheless, these data do not quantify a potential reservoir effect produced by dissolved old carbonates from

groundwater inflow and/or by old carbonates from remaining glacial water of the Lago Sarmiento proglacial stage. In the thrombolite profile the mean values of the  $\delta^{18}\text{O}$  in the massive and porous phases are  $-1.88$  and  $-1.70$ , respectively. The data of the massive phases have a standard deviation of  $0.27\text{‰}$   $\delta^{18}\text{O}$  and show a larger dispersion than the porous phases, which have a standard deviation of  $0.19\text{‰}$   $\delta^{18}\text{O}$ . For both phases the most depleted values are present in the T1a and T1b zones and the most enriched in the T1c zone (Fig. IV.8).



**Fig. IV-7:** Thrombolite sample profile at the southern shore of Lago Sarmiento (655334 E, 4340059 S, UTM – 18S -WGS 84). Each paleo-level is indicated: T1a, T1b, T1c and T1d. The sample points are indicated with a star and the numbers represent the distance in meters from the top of the thrombolite deposit. For sample points 4, 12 and 20 m the gastropod median probability radiocarbon ages are indicated.

*b. Paleothermometry.*

The paleothermometric interpretation of the  $\delta^{18}\text{O}$  variation in the thrombolites is necessarily based on the assumption that the oxygen isotope fractionation between the water and the precipitated carbonate is produced in equilibrium. Estimated equilibrium oxygen isotopic compositions for the carbonates precipitated in the thrombolite phases can be obtained using the mean isotopic composition of the Lago Sarmiento surface water, the ambient surface water temperature, and the well-established, temperature-dependent oxygen isotope equilibrium fractionation equation between calcite and water, from the Hays and Grossman (1991) equation as revised from O’Neil et al. (1969):

$$T(^{\circ}\text{C}) = 15.7 - 4.36(\Delta\delta^{18}\text{O}_{\text{C-W}}) + 0.12(\Delta\delta^{18}\text{O}_{\text{C-W}})^2 \quad (\text{Eq. 14})$$

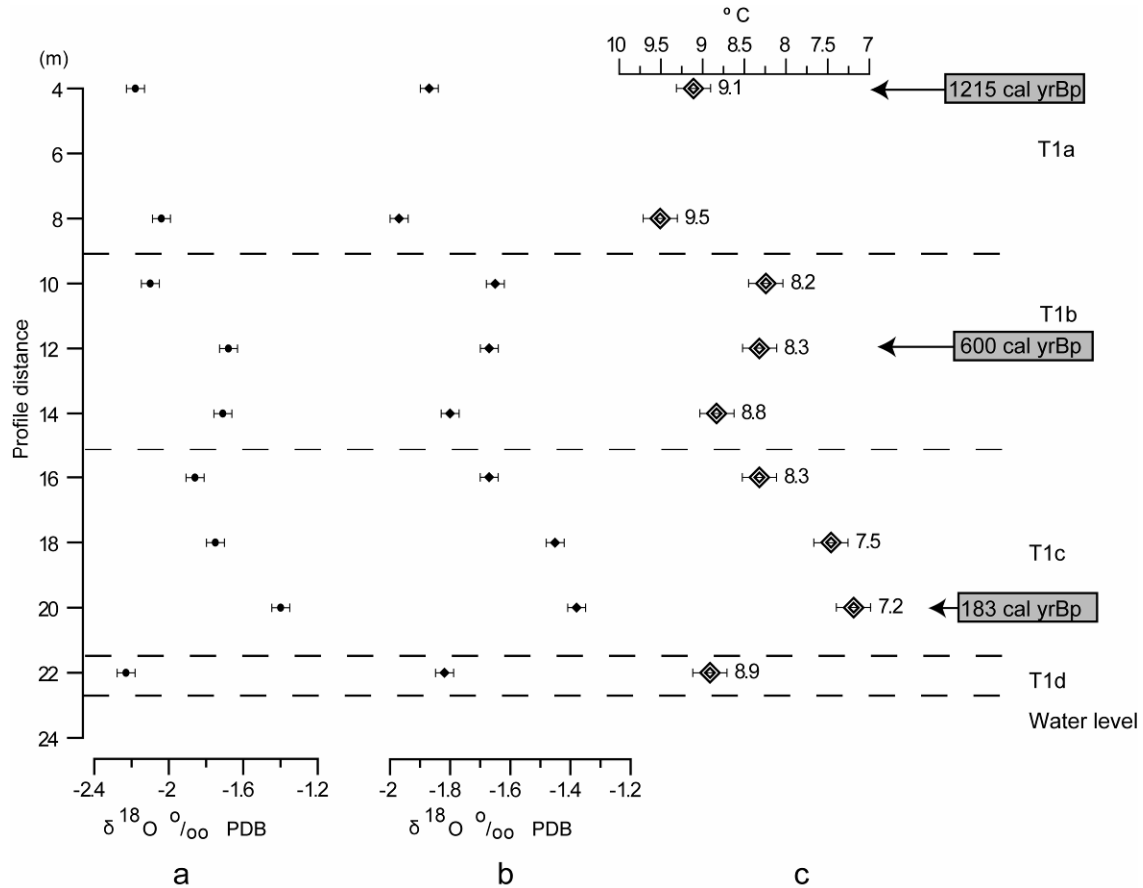
and

$$\Delta\delta^{18}\text{O}_{\text{C-W}} \approx \delta^{18}\text{O}_{\text{C}} - \delta^{18}\text{O}_{\text{W}} \quad (\text{Eq. 15})$$

where  $\delta^{18}\text{O}_{\text{C}}$  and  $\delta^{18}\text{O}_{\text{W}}$  refer to the oxygen isotopic composition of the calcite (VPDB) and lake water (VSMOW), respectively, and  $\Delta\delta^{18}\text{O}_{\text{C-W}}$  refers to the difference between  $\delta^{18}\text{O}_{\text{C}}$  and  $\delta^{18}\text{O}_{\text{W}}$ .

Solving the quadratic Eq. 14 and replacing the surface mean temperature of  $8.24^{\circ}\text{C}$  calculated from data collected every 20 minutes from April 1, 2003 to March 15, 2004, a hypothetical equilibrium  $\Delta\delta^{18}\text{O}_{\text{C-W}}$  of  $1.80\text{‰}$   $\delta^{18}\text{O}$  is obtained.

Using the mean isotopic composition of the water,  $-3.45\text{‰ } \delta^{18}\text{O}_{\text{VSMOW}}$  (Table 1), it is possible to calculate the  $\Delta\delta^{18}\text{O}_{\text{c-w}}$  for the massive and porous phases of sample 22 (Fig. IV. 7) that was collected within centimetres of the present lake level. The massive phase has a value of  $-2.23\text{‰ } \delta^{18}\text{O}_{\text{VPDB}}$  and yields a  $\Delta\delta^{18}\text{O}_{\text{c-w}}$  value of  $1.22\text{‰ } \delta^{18}\text{O}$ . The porous phase has a value of  $-1.82\text{‰ } \delta^{18}\text{O}_{\text{VPDB}}$  and a  $\Delta\delta^{18}\text{O}_{\text{c-w}}$  value of  $1.63\text{‰ } \delta^{18}\text{O}$ .



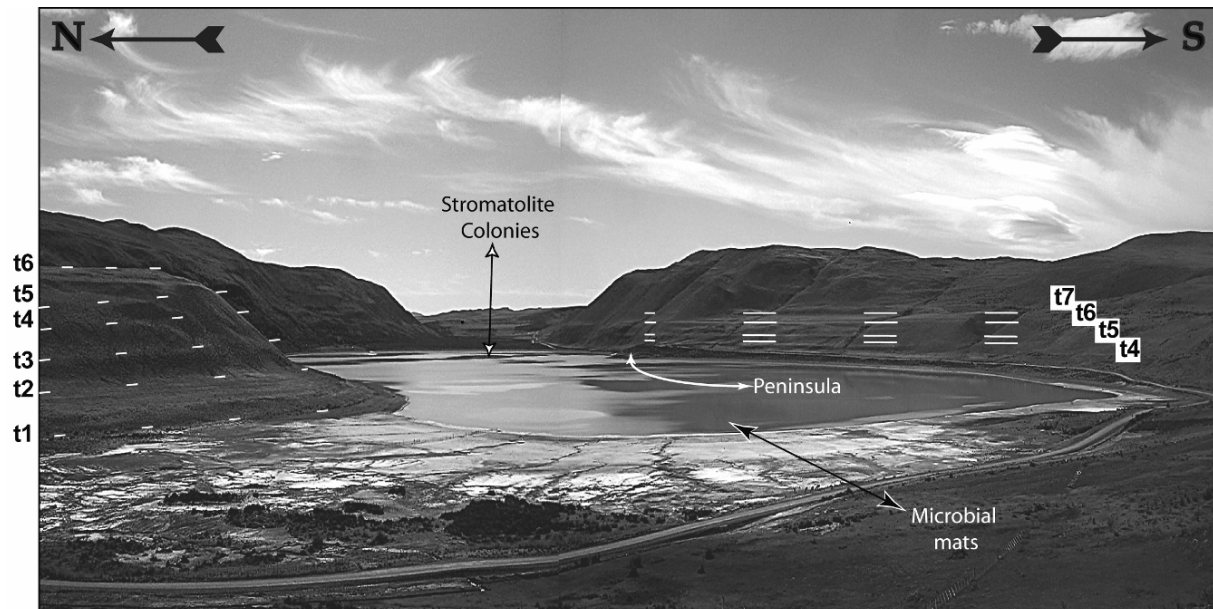
**Fig. IV-8:** Oxygen stable isotope composition and paleotemperature for the samples of the Lago Sarmiento profile. The different paleolake levels are labeled T1a, T1b, T1c and T1d (dashed lines) and the lake water level is indicated by an uninterrupted line. 8a. Oxygen stable isotope composition of the massive phases; 8b. Oxygen stable isotope composition of the porous phases; 8c. Temperature and error bar obtained from the porous calcite phases using the Hays and Grossman (1991) equation revised from O’Neil et al. (1969). Each temperature is indicated with a number to the right of the point.

The relatively close values obtained for the hypothetical equilibrium  $\Delta\delta^{18}\text{O}_{\text{c-w}}$  and the  $\Delta\delta^{18}\text{O}_{\text{c-w}}$  of the porous phases, indicate that these phases are close to equilibrium conditions, whereas the  $\Delta\delta^{18}\text{O}_{\text{c-w}}$  of the massive phases are far from the hypothetical equilibrium  $\Delta\delta^{18}\text{O}_{\text{c-w}}$ -value. For this reason we discard the massive phases for the paleothermometric interpretation of the  $\delta^{18}\text{O}$  variation in the thrombolites. The porous phases are the best candidates to calculate the surface water paleotemperature (Fig. IV.8),

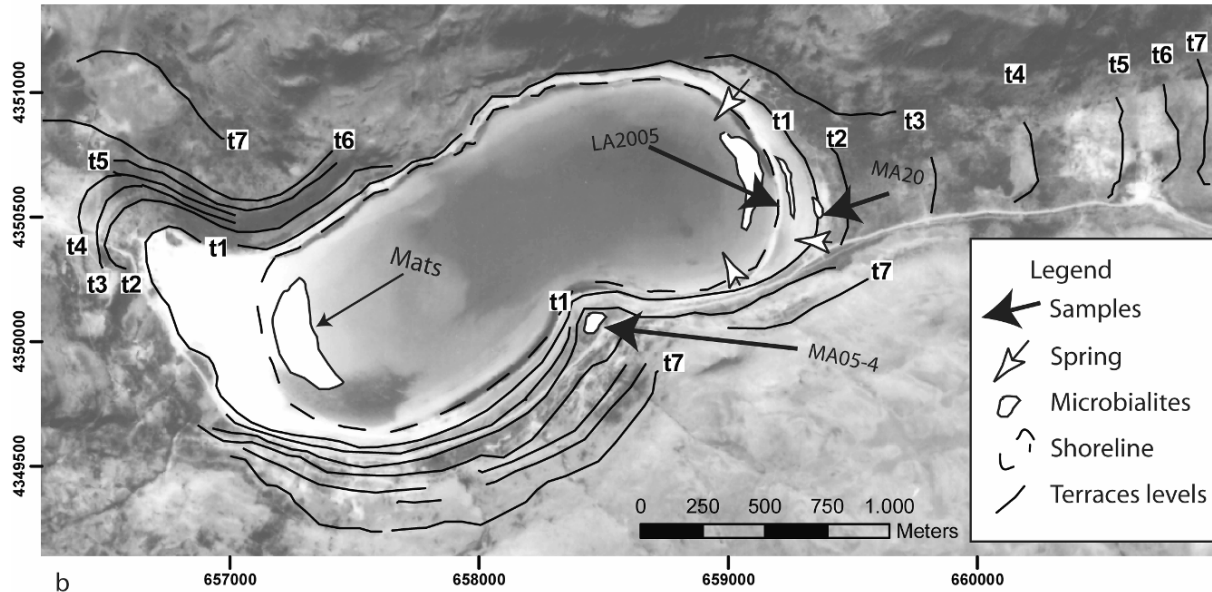
which is relative to the mean isotopic composition of the Lago Sarmiento water,  $-3.45\text{‰}$   $\delta^{18}\text{O}_{\text{VSMOW}}$  (Table 1). At 1215 cal yr Bp (median probability age) sample 4 indicates a temperature of  $9.1\text{ }^{\circ}\text{C}$  and the T1a level thus reflects a warm period with a mean temperature of  $9.3^{\circ}\text{C}$ . In the T1b level the temperature decreases to a mean of  $8.5^{\circ}\text{C}$  with respect to the T1a level and sample 12 at 600 cal yr Bp has a temperature of  $8.3^{\circ}\text{C}$ . At 183 cal yr Bp sample 20 indicates a relative temperature of  $7.2\text{ }^{\circ}\text{C}$  and the T1c level thus reflects a cold period with a mean temperature of  $7.7^{\circ}\text{C}$ .

IV.2.7 Description and Palaeothermometry of Laguna Amarga Stromatolites

a. Description



a



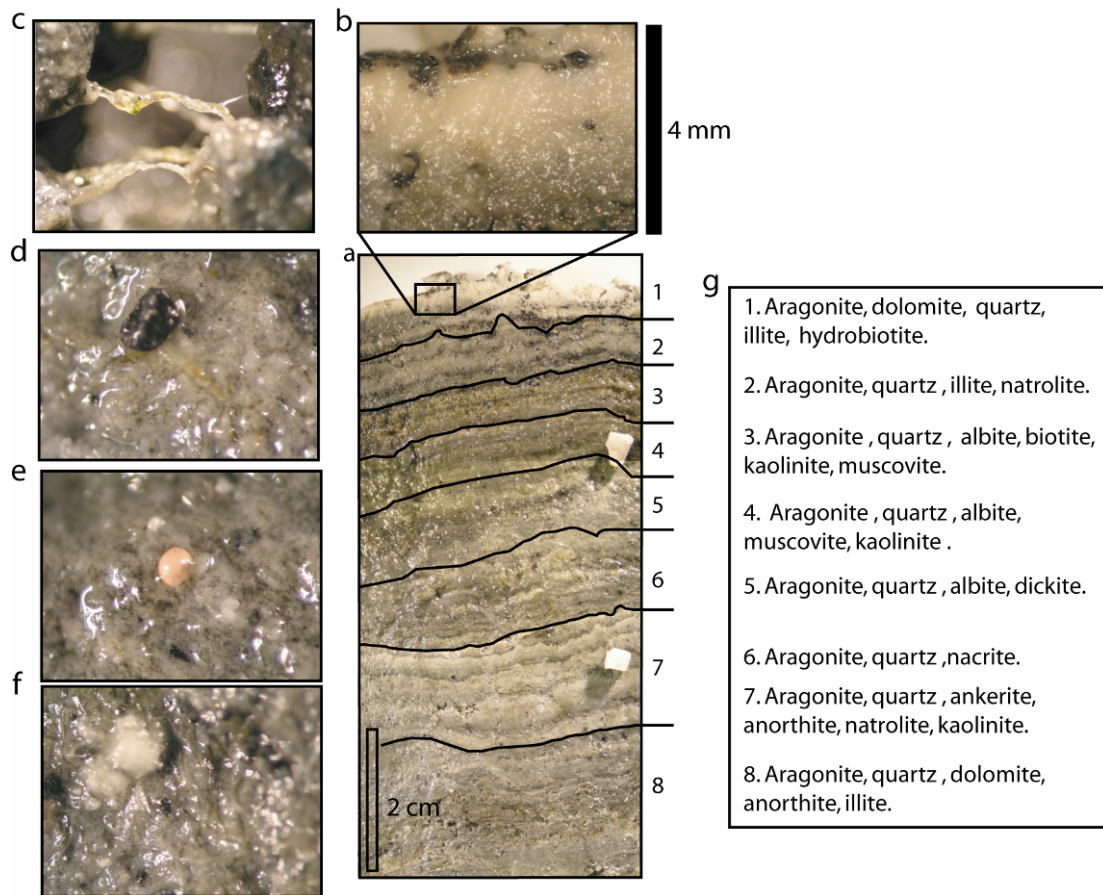
b

**Fig. IV-9:** a: Landscape picture showing the seven terraces observed on the northern and southern slopes of Laguna Amarga; 9b. Georeferenced (18° S UTM/WGS84) aerial photograph showing the terrace levels, the microbialite communities and the spring location at Laguna Amarga.

Seven terraces (t1, t2, t3, t4, t5, t6 and t7 in Fig. IV.9) are present along the slopes of Laguna Amarga (water level at 80 m a.s.l.). Terraces t1, t2, t3, t4, t5, t6 and t7 occur at altitudes of ca. 82, 90, 98, 108, 121, 138 and 150 m a.s.l., respectively. Below the t1 paleoshore level the lake receives water from springs that form a shallow stream, from which a laminated carbonate crust precipitates. Sample MA05-8 of the spring carbonates has a stable isotopic composition of  $-11.88\text{‰ } \delta^{18}\text{O}_{\text{VPDB}}$  and  $2.05\text{‰ } \delta^{13}\text{C}_{\text{VPDB}}$  (Table 3). Precipitation of the laminated carbonate crust is probably induced by the degasification of  $\text{CO}_2$ , evidenced by gas bubbles in the water and small (2-4 mm diameter) circular carbonate vents or domes over the crust. Along the western shore, desiccation cracks in silt deposits were detected between t1 and the present lake level.

A salt bed is developed around almost the entire shoreline, with crystals up to 0.8 cm. X-ray fluorescence determined the main chemical composition of the salt (in wt %): 49.84  $\text{SO}_3$ , 45.08  $\text{Na}_2\text{O}$ , 2.77  $\text{SiO}_2$ , and 1.12  $\text{Cl}$ . The X-ray diffraction analysis and the amount of  $\text{Na}_2\text{O}$  and  $\text{SO}_3$  confirm the presence of thenardite, but the existence of other undetermined salt species cannot be discarded.

The lake forms a habitat for colonies of modern microbialites, which are attached to the mud and sand of the lake bottom and covered by a few tens of centimetres of water. The stromatolites form a main colony at least 100 m long and 20 m wide, in which domal, bulbous and E-W elongated stromatolites compose a semi-coherent mat belt, extending for at least 300 m parallel to the shore. Some stromatolites with dome shapes pioneer the generation of colonies in other locations around the main stromatolite colony.



**Fig. IV-10:** Stromatolite from the eastern shore of Laguna Amarga: a) Section of dome stromatolites showing the subdivision into eight portions; 11b:) Superficial carbonate crust; c) Filamentous cyanobacteria; d) Trapping and binding sand-sized detritus; e) Small crustaceans; f) Carbonate detritus surrounded by filamentous cyanobacteria; g) Portion divisions related to column indicating the main minerals detected by X-Ray diffraction.

Sample LA2005 was taken under water, from a living dome-shaped stromatolite composed of a sequence of white and grey layers. The top layer of sample LA2005 is a homogeneous crust of carbonate with less than 1% detritus (Fig. IV.10b) and has a carbonate stable isotopic composition of 1.82 - 2.79 ‰  $\delta^{18}\text{O}_{\text{VPDB}}$  and 5.09 -5.16 ‰  $\delta^{13}\text{C}_{\text{VPDB}}$  (Table 3). In general, the layers are composed of a framework of filamentous cyanobacteria surrounded by an extracellular polymeric substance with carbonate precipitation (Fig. IV.10c). The grey layers trapped and bound more silt-sized detritus than the white layers, in which carbonate precipitation has concentrated. Commonly, it is possible to observe the presence of sand-sized detritus (Fig. IV.10d and f) and rare, small crustaceans (Fig. IV.10e).

To characterize the mineralogical composition, sample LA2005 (domed stromatolites) was divided into eight sections (labelled from 1 to 8 in Fig. IV.10a) and each section was analysed by X-ray diffraction. Aragonite is the primary carbonate mineral and dolomite and ankerite the secondary carbonates detected. All portions show the presence of low temperature silica that can be associated with the presence of detrital quartz in the layers. Diverse species of clay minerals (illite, natrolite, kaolinite and nacrite) and primary



rock forming silicates (albite, biotite, anorthite, muscovite and dickite) were detected (Fig. IV.10 g). These minerals are associated with trapped and attached detritus.

The organic fractions of the top and bottom layer of sample LA2005 have median probability radiocarbon ages of 1027 ( $1180 \pm 40$  C<sup>14</sup> yrBp) and 2955 ( $2892.91 \pm 59$  C<sup>14</sup> yrBp) cal yr Bp, respectively (Table 3). If assumed that the top layer is presently still growing, this layer represents an age close to 1082 yr with respect to the year 2005. The observed difference could be produced by a reservoir effect, a consequence of the accumulation of old carbonate that originated from dissolution of old carbonates from sedimentary rocks, and/or by the coexistence of more than one micro-organism type. Microbial associations can incorporate old carbon due a cycle that have the potential to produce the enrichment of old carbonates: the aerobic respiration of heterotrophic microbes and aerobic bacterial sulphide oxidation dissolve CaCO<sub>3</sub> previously precipitated by the cyanobacterial photosynthesis, bacterial sulphate reduction and anaerobic bacterial sulphide oxidation.

**Table 3:** Isotopes and radiocarbon age of Laguna Amarga microbialites.

Sample of Laguna Amarga	$\delta^{13}\text{C}$ VPDB ‰	$\delta^{18}\text{O}$ VPDB ‰	UTM E	UTM N	Radiocarbon age ( <sup>14</sup> C yr Bp)	Calibrated median probability age (Cal yr Bp)	Description
MA05-6	-5.69	-8.56	654702	4350046			Waterfall carbonate
MA05-7	-5.29	-7.36	654702	4350046			Waterfall carbonate
MA05-4	3.36	-1.74	658492	4350258	$6273.71 \pm 52$	7113	Thrombolite
MA019	3.03	-3.49	659461	4350701			Dead stromatolites
LA2005A	5.09	1.82	659205	4350730	$1180 \pm 40$	1027	Top white layer in living stromatolite
LA2005B	5.16	2.79	659205	4350730			Top white layer in living stromatolite
LA2005 Top Gray	4.2	-1.95	659205	4350730			Top gray layer in living stromatolite
LA2005 Bottom	4.07		659205	4350730	$2892.91 \pm 59$	2955	Bottom gray layer in living stromatolite
MA020-1	1.64	-3.6	659917	4350701	$641.27 \pm 40$	604	Dead microbial mat.
MA020-2	1.77	-3.67	659917	4350701			Dead microbial mat.
MA020-3	0.87	-5.65	659917	4350701			Dead microbial mat.
MA020-4	1.5	-4.22	659917	4350701			Dead microbial mat.
MA020-5	2.03	-3.21	659917	4350701			Dead microbial mat.
MA020-6	3.05	-2.86	659917	4350701	$409.74 \pm 42$	469	Dead microbial mat.
MA05-8	2.05	-11.88	659098	4350352			Carbonate spring crust
MAO 23-1	-0.28	-12.49	660658	4350559			Carbonate spring crust bottom
MA023-2	-0.17	-12.64	660658	4350559			Carbonate spring crust
MAO23-3	-0.13	-12.56	660658	4350559			Carbonate spring crust top



Sample MA020 was collected approximately 300 m east of the eastern shoreline at an elevation of ca.8 m above the present lake level, between the t1 and t2 paleoshore levels (Fig. IV.9). The sample is a dead microbial mat, 6 cm thick and covered by a white carbonate crust. The internal structure has a low degree of consolidation and shows 8 mm thick laminae, which are composed of dead filamentous cyanobacteria covered by brown-orange carbonate. MA020 was sampled at 1 cm resolution from the bottom to the top (MA020-1 to MA020-6 in Table 3), and the  $\delta^{18}\text{O}$  and  $\delta^{13}\text{C}$  composition of the carbonate fraction was analysed. The layers reflect an average of  $-3.86\text{‰}$   $\delta^{18}\text{O}_{\text{VPDB}}$  and  $1.81\text{‰}$   $\delta^{13}\text{C}_{\text{VPDB}}$ . The organic fraction of the top and bottom layers of sample MA020 have median probability radiocarbon ages of 468 ( $409.74\pm 43\text{ C}^{14}\text{ yrBp}$ ) and 604 ( $641.27\pm 40\text{ C}^{14}\text{ yrBp}$ ) cal yr Bp, respectively (Table 3).

When the water level drops below the sill between Laguna Amarga and the Paine River at an elevation of 125 m a.s.l, the lake becomes closed. Previously, the water discharged into the Paine River and then into Lago Nordenskjöld. In the Laguna Amarga Peninsula (Fig. IV.9), a group of thrombolites are present as isolated bodies only 8 to 15 cm high and 20 to 50 cm in diameter, with an internal clotted structure of calcite and gastropods. Sample MA05-4 was collected below terrace t4 at an elevation of ca. 23 m above the present lake level. It has a stable isotopic composition of  $-1.74\text{‰}$   $\delta^{18}\text{O}_{\text{VPDB}}$  and  $3.36\text{‰}$   $\delta^{13}\text{C}_{\text{VPDB}}$  and a gastropod was radiocarbon dated at 7113 cal yr Bp (Table 3).

Sample MA023 was collected 3 m above the lake level, below paleoshoreline t2 along the eastern shore, in the layered carbonate crust of the springs (Fig. IV.9b). The  $\delta^{18}\text{O}$  and  $\delta^{13}\text{C}$  composition was analyzed in three carbonate layers from the bottom to the top (MA023-1 to 2, respectively), obtaining an average of  $-12.56\text{‰}$   $\delta^{18}\text{O}_{\text{VPDB}}$  and  $-0.19\text{‰}$   $\delta^{13}\text{C}_{\text{VPDB}}$ .

#### b. Palaeothermometry.

In the case of Laguna Amarga, a problem in establishing a hypothetical equilibrium for the stromatolites is the existence of microscale multiple mineral phases: aragonite, dolomite and ankerite. However, if the aragonite and dolomite are chosen as primary and secondary representative carbonate of sample LA2005, respectively: the temperature-dependent oxygen isotope equilibrium fractionation equation between aragonite and water can be expressed by the Patterson et al. (1993) equation:

$$\Delta\delta^{18}\text{O}_{\text{A-W}} = 18.56 \pm 0.32 \times 10^3 \times T^{-1} - 33.49 \pm 0.31 \quad (\text{Eq. 16})$$

and the temperature-dependent oxygen isotope equilibrium fractionation equation between dolomite and water can be expressed by the Vasconcelos et al. (2005) equation:

$$\Delta\delta^{18}\text{O}_{\text{D-W}} = 3.06 \times 10^6 \times T^{-2} - 3.24 \quad (\text{Eq. 17})$$

where T is the temperature in degrees Kelvin.  $\delta^{18}\text{O}_{\text{A}}$ ,  $\delta^{18}\text{O}_{\text{D}}$  and  $\delta^{18}\text{O}_{\text{W}}$  refer to the oxygen isotopic composition of the aragonite (VSMOW) and lake water (VSMOW), respectively,

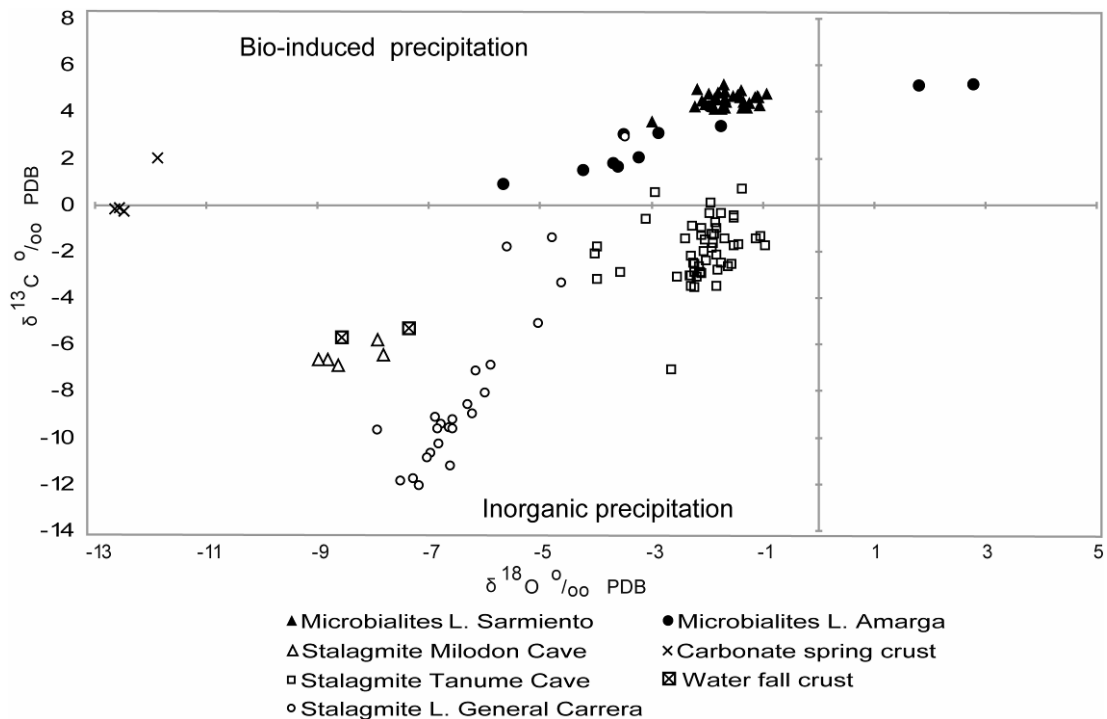
while  $\Delta\delta^{18}\text{O}_{\text{A-W}}$  refers to the difference between  $\delta^{18}\text{O}_{\text{A}}$  and  $\delta^{18}\text{O}_{\text{W}}$ , and  $\Delta\delta^{18}\text{O}_{\text{D-W}}$  to the difference between  $\delta^{18}\text{O}_{\text{A}}$  and  $\delta^{18}\text{O}_{\text{W}}$ .

With a temperature range between 9 and 12°C in Eq. 16, aragonite-water hypothetical equilibrium values of  $\Delta\delta^{18}\text{O}_{\text{A-W}} = 32.3 \pm 1.18$  and  $\text{‰}\delta^{18}\text{O}_{\text{VSMOW}} = 31.6 \pm 1.16$ , were obtained. Dolomite-water hypothetical equilibrium values of  $\Delta\delta^{18}\text{O}_{\text{D-W}} = 34.5$  and  $\text{‰}\delta^{18}\text{O}_{\text{VSMOW}} = 33.8$ , were also obtained for both temperatures. However, using the -2 ‰  $\delta^{18}\text{O}_{\text{VSMOW}}$  (Table 1) isotopic mean water composition of Laguna Amarga and the  $\delta^{18}\text{O}$ -value of the carbonate-enriched LA2005 A and B top white layers (Table 3), a carbonate-water calculated equilibrium of  $\Delta\delta^{18}\text{O}_{\text{Carbonate-W}} = 34.74$  and  $\delta^{18}\text{O}_{\text{VSMOW}} = 35.73\text{‰}$  were obtained for LA2005 A and B.

The different values obtained for the aragonite-water hypothetical equilibrium  $\Delta\delta^{18}\text{O}_{\text{A-W}}$  and the calculated equilibrium  $\Delta\delta^{18}\text{O}_{\text{Carbonate-W}}$  of the LA2005 A and B top white layers, indicate that the aragonite in these layers is far from the hypothetical equilibrium condition. The dolomite-water hypothetical equilibrium  $\Delta\delta^{18}\text{O}_{\text{D-W}}$  is close to the value of the calculated equilibrium  $\Delta\delta^{18}\text{O}_{\text{Carbonate-W}}$ -value of LA2005 A, but does not coincide with that of LA2005 B, indicating that the dolomite is closer to equilibrium conditions than the aragonite, but with a range of uncertainty. The existence of microscale multiple mineral phases detected by the analytical methods used here, therefore introduces some uncertainty in determining the equilibrium conditions, which means that the  $\delta^{18}\text{O}$ -value of the Laguna Amarga stromatolite layers cannot be used as a proxy for water paleotemperatures.

#### *IV.2.8 Inorganic versus biologically induced precipitation*

It is often difficult to determine biological influence on older and modern carbonate deposits. An interesting outcome of this study is that it reinforces, with new data, the  $\delta^{13}\text{C}$  tool proposed by Burne and Moore (1987) to distinguish between chemically and biologically induced precipitation of carbonates. Further investigation of stable isotopic data from a range of samples from a wider geographic area (stalagmites of the Tanume (34°S), General Carrera (48°S) and Milodon (51°S) caves, as well as a carbonate crust from a waterfall and spring near Torres del Paine) indicates that all of these have a significant amount of inorganically precipitated carbonate, without discarding minor biological control. The 0 ‰  $\delta^{13}\text{C}_{\text{VPDB}}$ -value of the inorganic carbonates reflects depleted  $^{13}\text{C}$  values in comparison with the isotopic signature of the microbialites, which are enriched in  $^{13}\text{C}$ . Consequently, the use of  $\delta^{13}\text{C}$  makes it possible to distinguish between inorganically and biochemically induced carbonates. The inorganic carbonate, in an environment influenced by minor microbiotic control, precipitates with a similar isotopic signature to that of the dissolved carbonate in the water from which it precipitated. However, in the microbialites, the extracellular polymeric substance provides a chemically protective microenvironment in which biologically induced precipitation of minerals around the cell can take place. Therefore, the enriched  $^{13}\text{C}$  carbonate signature of the biologically induced carbonate (Fig. IV.11), results from the preferential use of the lighter  $^{12}\text{C}$  isotope during photosynthesis. As a consequence,  $^{13}\text{C}$  is enriched in the surrounding extracellular polymeric substance.



**Fig. IV-11:** Isotope data of mainly inorganically controlled precipitation: stable isotopes of oxygen and carbon for Tanume (34°S), General Carrera (48°S) and Milodon (51°S) stalagmites, as well as the Torres del Paine waterfall carbonate crust and carbonate spring crust. Isotope data of biochemically induced precipitation: stable isotopes of oxygen and carbon for the Laguna Amarga and Sarmiento microbialites.

#### IV.2.9 Discussion

In the thrombolites of Lago Sarmiento it is possible to distinguish well differentiated phases of massive and porous calcite. The porous phases are the best candidates for calculating the surface water palaeotemperature, because they precipitated close to the hypothetical equilibrium condition of the water. In contrast, the massive phases do not precipitate in hypothetical equilibrium with the water. The massive phases are depleted in  $\delta^{13}\text{C}_{\text{VPDB}}$  with respect to the porous phases, indicating a closer affinity with inorganically controlled precipitation than the porous phases. These observations suggest that the massive phases form by re-crystallisation of the primary crystallization, induced by the cyanobacteria that form the porous phases. Therefore, the enriched  $^{13}\text{C}$  carbonate signature of the porous phases results from the preferential use of the lighter  $^{12}\text{C}$  isotope during photosynthesis of the cyanobacteria and enriched  $^{13}\text{C}$  in the surrounding extracellular polymeric substance. On the other hand, the depleted  $^{13}\text{C}$  carbonate signature of the massive phases and their none-equilibrium condition, result from crystallization from a concentrated solution in an environment without the presence of cyanobacteria.

Lago Sarmiento is an east-west elongated, closed basin with a high volume of water where the main inflow and outflow are linked to precipitation and evaporation caused by

the predominantly westerly winds. These characteristics mean that the lake is ideal for investigating long-term changes in the westerly winds during the Holocene. The surface area of Lago Sarmiento decreased from 1986 and 1999 due to changes in the precipitation and evaporation patterns, as reflected by a well recorded decrease in precipitation and glacial retreat around the Southern Patagonian Ice Field. Four different colour zones in the thrombolites are interpreted as reflecting four different lake levels. At 1215 cal yr Bp the level of the lake was at 85 m a.s.l with a temperature close to 9.3°C, and at 600 cal yr Bp the level dropped to 82 m a.s.l with a temperature close to 8.5°C. This warm lake period coincides with the timing of the Northern Hemisphere Medieval Warming Period, but more regional evidence is necessary to establish a definite correlation. At 183 cal yr Bp the level of the lake decreased further to 80 m a.s.l with a cooler temperature close to 7.7°C, representing a cold lake period coinciding with the timing of the Little Ice Age (LIA). This event was also detected by Armesto et al. (1992) in the vicinity of the Grey Glacier in the Torres del Paine area.

In Laguna Amarga the oldest thrombolites, dated at 7113 cal yr B, present a period when the glacial mass retreated and the lake water level dropped below the 125 m a.s.l. so that the lake became closed and the salinity and pH increased. The stromatolites began to grow after the thrombolites, in conditions of decreased water volume and higher salinity. The water in Laguna Amarga, with its living stromatolites, has a higher salinity than Lago Sarmiento, which contains living thrombolites. This suggests that salinity may be an important factor in determining the type of microbialite, the highest salinity favouring stromatolites and vice versa.

#### *IV.2.10 Conclusions*

It is important to have prior knowledge of the hydrologic balance of a lake in order to determine if temperature is the main variable producing oxygen isotope fractionation. Lago Sarmiento provides better conditions than Laguna Amarga for the use of microbialite carbonates as a paleoclimatic tool, and in particular for  $\delta^{18}\text{O}$  carbonate paleothermometry. In Lago Sarmiento, temperature variation is the most likely cause of the year-to-year oxygen isotope fractionation. On the other hand, in Laguna Amarga, evaporation and precipitation can produce substantial  $\delta^{18}\text{O}$  lake water fractionation from one year to the next, so that the isotopic water fractionation could be interpreted as a combination of direct precipitation and evaporation, as well as temperature variations.

Whereas the mineralogy of Lago Sarmiento thrombolites is mainly represented by calcite and the porous phases are close to equilibrium conditions, the Laguna Amarga stromatolites are formed by microscale organic matter and multiple mineral phases, which does not insure that measuring the isotopic composition in only one species of carbonates would establish a hypothetical equilibrium for this particular species.

The  $\delta^{13}\text{C}$  signal in carbonates deposits is an effective tool to distinguish between inorganic and biologically induced precipitation. Negative values of  $\text{‰ } \delta^{13}\text{C}_{\text{VPDB}}$  are characteristic of inorganic precipitation, whereas, positive values of  $\text{‰ } \delta^{13}\text{C}_{\text{VPDB}}$  are characteristic of biologically induced precipitation.

#### IV.2.11 Acknowledgments.

We gratefully acknowledge financial support by the *Comisión Nacional de Investigación y Tecnología* (CONICYT) and the Project “Geological Connection between the Antarctic Peninsula and Patagonia” (ARTG-04) supported by the *Programa Bicentenario de Ciencia y Tecnología* (PBCT) of CONICYT and the *Instituto Antártico Chileno* (INACH). In addition, we wish to thank A. Prieto, backed by financial support of Project FONDECYT 1070709, for the collection of water samples in the Lago Sarmiento area. Thanks are also due to the *Corporación Nacional Forestal* (CONAF) for field support, in particular to the rangers. We would also like to thank D. Nieto for field assistance and J. Martínez for laboratory support. In addition, we are grateful to the Laboratory of the *Servicio Nacional de Geología y Minería* (SERNAGEOMIN) and the X-Ray Diffraction Laboratory of the *Departamento de Física* of the *Universidad de Chile*, for analytical work.

#### IV.2.12 References

- Airo, A., Ferrand, D., Lim, D.S., Christopher, M., Solari M.A., Lowe D.R., 2009. Environmental controls on the morphological development of microbialites at Lago Sarmiento, Chile. Submitted to PALAIOS.
- Andrews, J.E. Riding, R., Dennis, P.F., 1993. Stable isotopic compositions of Recent freshwater cyanobacterial carbonates from the British Isles: local and regional environmental controls. *Sedimentology* 40, 303-314.
- Andrews, J.E., Riding, R., Dennis, P.F., 1997. The stable isotope record of environmental and climatic signals in modern terrestrial microbial carbonates from Europe. *Palaeogeography, Palaeoclimatology, Palaeoecology* 129, 171-189.
- Armesto, J.J., Casassa, I., Dollenz, O., 1992. Age structure and dynamics of Patagonian beech forest in Torres del Paine National Park, Chile. *Vegetatio*, 98, 13-22.
- Benson L., and Paillet F., 2002. HIBAL: a hydrologic–isotopic-balance model for application to paleolake systems. *Quaternary Science Reviews*, 21, 1521–1539.
- Bosak, T., Souza-Egipzy, V., Corsett, F.A., Newman, D.K., 2004. Micrometer-scale porosity as a biosignature in carbonate crust. *Geology*, 32 (9), 781-784.
- Branchu, P. and Bergonzini, L., 2004. Chloride concentrations in Lake Tanganyika: an indicator of the hydrological budget?, *Hydrol. Earth Syst. Sci.*, 8, 256-265.
- Burne, R.V., and Moore, L.S., 1987. Microbialites: Organo sedimentary deposits of benthic microbial communities. *PALAIOS*, 2, 241–254.
- Campos H., Soto, D., Steffen, W., Parra, O., Aguero, G., Zúñiga, L., 1994. Limnological studies of Sarmiento Lake (Chile): a subsaline lake from Chilean Patagonian. *Archiv fuer Hydrobiologie. Supplementband. Monographische Beitrage*, 99, 217-234.
- Campos H., Soto, D., Parra O., Steffen, W., Aguero, G., 1996. Limnological studies of Amarga Lagoon, Chile: a saline lake in Patagonian South America. *International Journal of Salt Lake Research*, 4, 301-314.
- Carrasco, J.F., Casassa, G., Rivera, A., 1998. Climatología actual del Campo de Hielo Sur y posibles cambios por incremento del efecto invernadero, *Anales del Instituto de la Patagonia, Serie Ciencias Naturales*. 26, 119-128.
- Carrasco, J.F., Casassa, G., Rivera, A., 2002. Meteorological and climatological aspect of the Southern Patagonian Icefield. In : Cassasa, G., Sepúlveda, F., Sinclair, R.(Eds), *The*

- Patagonian Icefield: A unique Natural Laboratory for Environmental and Climate Changes Studies. Klumer, Academic/ Plenum Publishers, New York, pp. 29-41.
- Casanova, J., and Hillaire-Marcelo, C., 1992. Late Holocene hydrological history of Lake Tanganyika, East Africa, from isotopic data on fossil stromatolites. *Palaeogeography, Palaeoclimatology, Palaeoecology* 91, 35-48.
- Chafetz, H. and Lawrence, J.R., 1994. Stable isotopic variability within modern travertines. *Geogr. Phys. Quat.*, 48, 257-273.
- Clark I.D. and Fritz P., 1997. *Environmental Isotopes in Hydrology*. I.D. Clark and P. Fritz, Lewis Publishers, New York (1997), pp. 0-328.
- Craig, H., 1957. Isotopic standards of carbon and oxygen and correction factors for mass-spectrometric analysis of carbon dioxide. *Geochim. Cosmochim. Acta* 12, 133– 149.
- Decho, A. W., Visscher, P. T., Reid, P., 2005. Production and cycling of natural microbial exopolymers (EPS) within a marine stromatolites. *Palaeogeography, Palaeoclimatology, Palaeoecology*, 219, 71– 86.
- D.G.A., 1987, *Balance Hídrico de Chile*, Ministerio de Obras Públicas, Transporte y Telecomunicaciones. Dirección General de Aguas. Chile.
- Dupraz, C., Reid, R.P., Braissant, O., Decho, A.W., Norman, S.R., and Visscher, P.T., 2009. Processes of carbonate precipitation in modern microbial mats. *Earth-Science Review*. 96 (3), 141-162.
- Fogwill, C.J., and Kubik, P.W., 2005. A glacial stage spanning the Antarctic Cold Reversal in Torres del Paine (51°S), Chile, based on preliminary cosmogenic exposure ages. *Geogr. Ann.*, 87 A (2), 403–408.
- Gibson J.J., Edwards, T.W.D., Prowse, T.D., 1999. Pan-derived isotopic composition of atmospheric water vapor and its variability in northern Canada. *Journal of Hydrology*, 217, 55–74.
- Hays, P.D. and Grossman, E.L., 1991. Oxygen isotopes in meteoric calcite cements as indicators of continental palaeoclimate. *Geology*, 19, 441-444.
- IAEA/WMO (2006). *Global Network of Isotopes in Precipitation*. The GNIP Database. The analysis was realized by the Laboratorio de Isótopos Ambientales, CCHEN, Santiago de Chile. Accessible at: <http://isohis.iaea.org>.
- Ibarzabal y Donángelo, T., Hoffmann, J. A. J., Naruse, R., 1996, Recent climatic change in southern Patagonian, *Bulletin of Glacier Research*, 14, 29-36.
- Jones M.D., Roberts, C.N., Leng, J.M., 2007. Quantifying climatic change through the last glacial–interglacial transition based on lake isotope palaeohydrology from central Turkey. *Quaternary Research*, 67, 463–473.
- Kim, S. T., and O’Neil, J. R., 1997. Equilibrium and nonequilibrium oxygen isotope effects in synthetic carbonates. *Geochim. Cosmochim. Acta* 61, 3461–3475.
- Marden, C.J., 1993, Late Quaternary glacial history of the South Patagonian Icefield at Torres del Paine, Chile. Ph.D. Thesis, University of Aberdeen, pp. 298.
- Marden, C.J., Clapperton, C.M., 1995, Fluctuations of the South Patagonian Icefield during the last glaciation and the Holocene. *Journal of Quaternary Science*, 10, 197-210.
- McCormac, F.G., Hogg, A.G., Blackwell, P.G., Buck, C.E., Higham, T.F.G., Reimer, P.J., 2004. SHCAL04 Southern Hemisphere Calibration, 0–11.0 Cal kyrBP. *Radiocarbon*, 46 (3), 1087–1092
- McCrea, J.M., 1950. On the isotopic chemistry of carbonates and a paleotemperature scale. *J. Phys. Chem.* 18, 849– 857.
- Moreno, P.I., Kaplan, M.R., François, J.P., Villa-Martínez, R., Moy, C.M., Stern, C.R., Kubik, P.W., 2009. Renewed glacial activity during the Antarctic cold reversal and persistence of cold conditions until 11.5 ka in southwestern Patagonia. *Geology*, 37(4), 375-378.
- NASA Landsat Program, 1986. Landsat TM, p230r96\_5t19861006, EarthSat-Orthorectified - Geocover, Geotiff, 10/06/1986. Source for this data set was the Global Land Cover Facility ([www.landcover.org](http://www.landcover.org)).

- NASA Landsat Program, 1999. Landsat ETM+, p230r096\_7x19991002, EarthSat-Orthorectified - Geocover, Geotiff, 10/02/1999. Source for this data set was the Global Land Cover Facility, [www.landcover.org](http://www.landcover.org).
- O'Neil, J.R., Clayton, R.N. Mayeda, T.K., 1969. Oxygen isotope fractionation in divalent metal carbonates. *J. Chem. Phys.*, 51, 5547-5558.
- Patterson, W.P., Smith, G.R., and Lohmann, K.C. 1993. Continental paleothermometry and seasonality using the isotopic composition of aragonitic otoliths of freshwater fishes. In: Swart, P.A., Lohmann, K.C., McKenzie, J., Savin S. (Eds), *Monogr. Continental climate change from isotopic records*. No. 78, American Geophysical Union, Washington, D.C. pp. 191–202.
- Perry RS, Mcloughlin N, Lynne BY, Sephtond M.A., Oliverb J.D., Perrye C.C., Campbelle K., Engelf M.H., Farmerg J.D., Brasiera M.D. and Staleyh J.T. 2007. Defining biominerals and organominerals: Direct and indirect indicators of life, *Sedimentary Geology*, 201, 157-179.
- Risacher, F., Alonso, H., Salazar, C. 1999. *Geoquímica de Aguas en Cuencas Cerradas: I, II y III Regiones - Chile*. Volumen I, Síntesis. S.I.T N° 51, Convenio de Cooperación DGA - UCN – IRD, pp. 1-89.
- Soto, D., Campos, H., Steffen, W., Parra, O. and Zuñiga, L. 1994. The Torres del Paine lake district (Chilean Patagonia): A case of potentially N- limited lakes and ponds. *Arch. Hydrobiol.Suppl.* 99, 181-197.
- Solari M.A., Le Roux J.P. and Hervé F. 2010. Holocene and last Glacial variability of the water levels of the Great Tehuelche Paleolake in the Torres del Paine National Park, Chilean Patagonia. *Andean Geology*, Accepted, 2010.
- Teranes, J.L., Mckenzie, J.A., Bernasconi, S.M., Lotter, A.F., Sturm, M. 1999. Study of oxygen isotopic fractionation during bio-induced calcite precipitation in eutrophic Baldeggersee, Switzerland. *Geochimica et Cosmochimica Acta*, 63 (13/14), 1981–1989.
- USGS, 2000. Shuttle Radar Topography Mission, 3 Arc Second scene SRTM\_fB03\_p230r096, Filled-Finished B, Global Land Cover Facility, University of Maryland, College Park, Maryland, 2000. Source for this data set was the Global Land Cover Facility, [www.landcover.org](http://www.landcover.org).
- Vasconcelos, C, McKenzie, J.A., Warthmann, R, Bernasconi, S.M., 2005. Calibration of the 18O paleothermometer for dolomite precipitated in microbial cultures and natural environments. *Geology*, 33, 317-320.

## **V. Discusión y Conclusiones.**

### **V.1. Discusión**

Evidencias de eventos glaciales antiguos están dadas por la existencia de extensas morrenas terminales, localizadas en el margen este de la Cuenca de Drenaje de Torres del Paine (CDTP) y en el sector de Tres Pasos. Otras evidencias se observan en el perfil sedimentario localizado en el “El Canal” (Lago del Toro), en él se reconocieron depósitos glaciales consolidados, los cuales sobreyacen en discordancia de erosión a los sedimentos marinos cretácicos de la Formación Cerro Toro. Aquellas morrenas terminales se formaron con anterioridad al UMG, posiblemente durante el estadio MIS6 y/o durante la Gran Glaciación Patagónica (Pleistoceno temprano), pero nuevas investigaciones deben realizarse para establecer una cronología certera.

Cuatro niveles de terrazas con continuidad regional fueron reconocidos y mapeados al este de los avances glaciales A, B, C, D y E. Los niveles de terrazas T6, T5, T4 y T3 soportan la existencia de un único lago proglacial, el cual hemos llamado el Gran Paleolago Tehuelche (GPT). El GPT se formó entre los glaciares y la topografía de altitud creciente hacia el este de la CDTP, además el paleolago poseía una zona de drenaje por el valle de Prat, ubicado entre las sierras montañosas de Prat y Señoret.

Durante el UMG, el GPT formó extensos depósitos lacustres y alcanzó el nivel lacustre de mayor altitud. El nivel T6 varía en elevación entre 240-260 m s.n.m y se estableció previamente y durante el avance A, B y C. En el perfil sedimentario de “El Canal” el cambio hacia el este del delta superior es interpretado como el comienzo del avance de los glaciales con posterioridad a 24.291 Cal años AP.

El avance B ocurrió posterior a los 21.493 Cal años AP, produciendo una intensa deformación en los sedimentos lacustres previamente depositados. El avance C estuvo estable hasta aproximadamente los 17.500 años AP, momento en el cual ocurrió la desglaciación sincrónica en Patagonia.

Una nueva fase del GPT se desarrolló durante el re-avance D entre los 12.600–14.800 años AP, a una altitud entre 150 y 165 m s.n.m y sincrónicamente con la Regresión Fría Antártica. Se reconoció en una isla en Lago del Toro una morrena terminal la cual se asocia a este re-avance.

Las terrazas T3 y T4 se presentan al este del Avance E y poseen una altitud de 135-145 y 120-130 m s.n.m, respectivamente. Ellas representan los últimos niveles del GPT alimentados por las aguas de fusión de los glaciares durante el avance E. Cuando el nivel del lago descendió bajo los 125 m s.n.m, laguna Amarga comenzó a ser una laguna cerrada, en la cual se desarrollaron trombolitos fechados en 7.113 Cal años AP. Esta edad representa el momento cuando el GPT fue reestructurado en un conjunto de lagos más pequeños, debido a la apertura de un gran drenaje hacia el Seno de Última Esperanza. El retroceso del Avance E produjo el desagüe del GPT producto de la desaparición de una barrera de hielo localizada en el sector de la Sierra Prat. Desde ese momento laguna Amarga comenzó a aumentar su salinidad, hasta que el incremento estableció las condiciones para el crecimiento de microbialitas. Se interpreta que la evaporación fue mayor que la



precipitación y que las condiciones de aridez se incrementaron producto del retroceso de la masa glaciaria, permitiendo que la salinidad se incrementara en la laguna.

Con posterioridad a la disrupción del GPT, lago Sarmiento también se vuelve a una cuenca cerrada en la cual se observan terrazas lacustres locales, que entregan importantes evidencias y aportan un conjunto de resultados de importancia paleoclimática regional. Lago Sarmiento posee una cuenca simétrica, alargada en dirección este-oeste, es una cuenca cerrada con un gran volumen de agua, donde los Vientos Predominantes del Oeste (VPO) modelan su principal aporte que son las precipitaciones y su principal salida que es la evaporación. Estas características son ideales para investigar el comportamiento de los VPO durante el Holoceno.

Es posible distinguir en los trombolitos del Lago Sarmiento una fase masiva y otra porosa de calcita. La fase porosa es la mejor candidata para calcular la paleotemperatura superficial del agua, porque dicha fase precipita cercana a las condiciones de equilibrio isotópico, en contraste con la fase masiva. La fase masiva está deprimida en  $\delta^{13}\text{C}_{\text{VPDB}}$  respecto a fase porosa, indicando una mayor afinidad con la precipitación inorgánica controlada respecto a la fase porosa que es biológicamente inducida. Dichas observaciones sugieren que la fase masiva se forma por un proceso de re-cristalización de la precipitación bio-inducida que forma la fase porosa. El enriquecimiento en  $^{13}\text{C}$  de los carbonatos de la fase porosa resulta de la utilización preferencial del isotopo liviano  $^{12}\text{C}$  por las cianobacterias durante el proceso de fotosíntesis y el consecuente enriquecimiento de  $^{13}\text{C}$  de la Sustancia Extracelular Polimérica que rodea a la célula. Por el contrario, la señal deprimida en  $^{13}\text{C}$  de la fase masiva y sus condiciones fuera del equilibrio, resultan de la cristalización a partir de una solución concentrada en un ambiente sin la presencia de cianobacterias.

En los trombolitos de Lago Sarmiento se observan con claridad 4 niveles lacustres en los cuales fue posible cuantificar la temperatura:

- Hace 1.215 Cal años AP el nivel del lago fue 85 m s.n.m con una temperatura cercana a 9,3°C, y hace 600 Cal años AP el nivel descendió a 82 m s.n.m con una temperatura cercana a los 8,5°C. Estos períodos cálidos en el lago coinciden temporalmente con el Período Cálido Medieval registrado ampliamente en el Hemisferio Norte, pero mayor cantidad de evidencias regionales son necesarias para establecer una correlación certera.
- Hace 183 Cal años AP el nivel del lago fue de 80 m s.n.m con una temperatura de 7,7°C, representando un periodo frío del lago coincidente con la Pequeña Edad Hielo. Este evento fue detectado por Armesto (1992) en las vecindades del glaciar Grey y en el glaciar Tyndall por Aniya (1995), en Torres del Paine.
- La superficie de lago Sarmiento disminuyó entre 1986 y 1999 debido a cambios en los patrones de precipitación y evaporación, muy probablemente relacionados a los efectos del cambio climático, los cuales han producido la disminución de casi la totalidad de los grandes glaciares en los Campos de Hielo Patagónicos, con excepción del glaciar Perito Moreno y Pio X.

La posición y magnitud de los VPO es controlada por la Celda Atmosférica de Bajas Presiones Subpolar y por el Anticiclón del Pacífico Sureste, permitiendo que existan mecanismos de forzamiento de altas latitudes y tropicales (Cerverny, 1998). El retraso registrado en la Región de los Lagos respecto a los eventos fríos sincrónicos en Antártica y Torres del Paine, se pueden explicar por la modulación de los VPO causada por el reforzamiento de los Vientos Tropicales del Este/ENSO y por la expansión hacia el norte de la Celda Atmosférica de Bajas Presiones Subpolar. El reforzamiento de los Vientos Tropicales del Este se soporta por el aumento de precipitaciones en el Desierto de Atacama entre los 14-11 k Cal años AP interpretadas a partir de evidencias polínicas por Maldonado et al. (2005). Por otro lado, Lamy et al. (2004) postuló la migración hacia el norte de las Corrientes Circumpolares Antárticas durante el período de regresión fría detectado en el sitio 1.233 en la Región de los Lagos. Esta hipótesis muy preliminar busca recalcar la necesidad de comprender en base a registros paleoclimáticos los reajustes espaciales y temporales de las diferentes células atmosféricas y la circulación oceánica, y con ello conceptualizar y modelar como la atmósfera y los océanos se comportan e interactúan frente a la renovada teoría orbital de Milankovitch (1930) propuesta por Davis and Bewer (2009).

## V.2. Conclusiones

Extensos depósitos lacustres y los niveles de terrazas T6, T5, T4 y T3 corroboran la hipótesis (planteada al comienzo de esta tesis) sobre la existencia de un único gran lago proglacial, el cual evolucionó en función de las fluctuaciones glaciares registradas por los avances A, B, C, D y E hasta el momento de su drenaje hace 7.113 Cal años AP.

La presente investigación produjo importantes modificaciones y avances a la cronología de los eventos glaciales registrados en Torres del Paine:

- Los eventos glaciales A, B y C se formaron durante la Última Glaciación. El avance glacial A se estableció cercano a los 24.291 Cal años AP y el avance B se estableció en el margen de Lago del Toro con posterioridad a los 21.493 Cal años AP.
- Los avances E y F son más jóvenes que las edades previamente asignadas por Marden and Clapperton (1995). El avance E se encuentra en retroceso hace 7.113 Cal años AP, pero una mejor cronología en Torres del Paine y en Patagonia son necesarias para establecer una correlación potencial con el evento frío registrado entre 8.000 y 9.000 años AP en el Hemisferio Norte. El avance F es más joven que 7.113 Cal años AP y también es necesario una buena cronología para establecer a cual de los eventos neoglaciales “Tipo Mercer y/o Aniya” potencialmente puede corresponder.

En el caso de la segunda hipótesis de la tesis, que planteaba que las microbialitas lacustres pueden ser utilizadas como paleotermómetros, se produjo un hecho interesante de destacar. Se ha demostrado que la hipótesis era correcta solo para el caso de los trombolitos de Lago Sarmiento y no para los estromatolitos de Laguna Amarga, dado que Lago

Sarmiento presenta mejores condiciones que Laguna Amarga para el uso de las microbialitas como paleotermómetros:

- Para la determinación de las temperaturas fue muy importante conocer el balance hídrico, ya que gracias a ello se estableció que en lago Sarmiento, la variación de la temperatura es la causa principal para producir el fraccionamiento isotópico de un año a otro. Por otro lado, en Laguna Amarga la evaporación, precipitación y temperatura producen un fraccionamiento de  $\delta^{18}\text{O}$  de magnitud considerable.
- Mientras que la mineralogía de los trombolitos de Lago Sarmiento está representada por calcita y la fase porosa está cercana a las condiciones de equilibrio, en Laguna Amarga los estromatolitos están conformados por materia orgánica y múltiples fases minerales, las cuales no aseguran que la composición isotópica sea medida en una especie mineral y con ello establecer el equilibrio hipotético para esa especie en particular.

Un resultado inesperado y muy importante de la tesis fue que la señal de  $\delta^{13}\text{C}$  en carbonatos es una herramienta efectiva para distinguir el proceso que produce su precipitación. Valores negativos de  $\text{‰ } \delta^{13}\text{C}_{\text{VPDB}}$  son característicos de la precipitación inorgánica y valores positivos son característicos de la precipitación biológicamente inducida.

### V.2.1 Referencias

- Aniya, M., 1995. Holocene glacial chronology in Patagonia: Tyndall and Upsala Glaciers. *Arct. Alp. Res.* 27, 311–322.
- Armesto, J.J., Casassa, I., Dollenz, O., 1992. Age structure and dynamics of Patagonian beech forest in Torres del Paine National Park, Chile. *Vegetatio*, 98, 13-22.
- Cerveny R. S. 1998. Climates of the Southern Continents: Present, Past and Future, J. E. Hobbs, J. A. Lindesay, H. A. Bridgman, Eds. (Wiley, New York, 1998), pp. 107–134
- Davis B.A.S and Brewer S. 2009. Orbital forcing and role of the latitudinal insolation / temperature gradient. *Clim Dyn*, 32:143–165.
- Hajdas, I., Bonani, G., Moreno, P.I., and Ariztegui, D., 2003, Precise radiocarbon dating of lateglacial cooling in mid-latitude South America: *Quaternary Research*, v. 59, p. 70–78.
- Lamy, F., Kaiser, J., Ninnemann, U., Hebbeln, D., Arz, H.W., and Stoner, J., 2004, Antarctic timing of surface water changes off Chile and Patagonian ice sheet response: *Science*, 304, 1959–1962.
- Maldonado A, Betancourt J., Latorre C., Villagran C. 2005. Pollen analyses from a 50 000-yr rodent midden series in the southern Atacama Desert (25° 30' S). *Journal of Quaternary Science* 20(5), 493–507.
- Marden, C.J., Clapperton, C.M., 1995, Fluctuations of the South Patagonian Icefield during the last glaciation and the Holocene. *Journal of Quaternary Science*, 10, 197-210.
- Milankovitch, M. (1930), *Mathematische Klimahre und Astronomische Theorie der Klimaschwankungen*, Gebruder Borntraeger, Berlin. 176 pp

**Anexo I:**

**Artículo: “Geomorphologic and tectonic evolution of the Bransfield Basin, Antarctic Peninsula: insights from analogue models”.**

# Geotectonic evolution of the Bransfield Basin, Antarctic Peninsula: insights from analogue models

M.A. SOLARI<sup>1\*</sup>, F. HERVÉ<sup>1</sup>, J. MARTINOD<sup>2</sup>, J.P. LE ROUX<sup>1</sup>, L.E. RAMÍREZ<sup>1</sup> and C. PALACIOS<sup>1</sup>

<sup>1</sup>Department of Geology, Universidad de Chile, PO Box 13518, Correo 21, Santiago, Chile

<sup>2</sup>IRD, LMTG, Université Toulouse 3, 14 Avenue Edouard Belin, 31400, Toulouse, France

\*msolari@cec.uchile.cl

**Abstract:** The Bransfield Strait, located between the South Shetland Islands and the north-western end of the Antarctic Peninsula, is a back-arc basin transitional between rifting and spreading. We compiled a geomorphological structural map of the Bransfield Basin combining published data and the interpretation of bathymetric images. Several analogue experiments reproducing the interaction between the Scotia, Antarctic, and Phoenix plates were carried out. The fault configuration observed in the geomorphological structural map was well reproduced by one of these analogue models. The results suggest the establishment of a transpressional regime to the west of the southern segment of the Shackleton Fracture Zone and a transtensional regime to the south-west of the South Scotia Ridge by at least *c.* 7 Ma. A probable mechanism for the opening of the Bransfield Basin requires two processes: 1) Significant transtensional effects in the Bransfield Basin caused by the configuration and drift vector of the Scotia Plate after the activity of the West Scotia Ridge ceased at *c.* 7 Ma. 2) Roll-back of the Phoenix Plate under the South Shetland Islands after cessation of spreading activity of the Phoenix Ridge at  $3.3 \pm 0.2$  Ma, causing the north-westward migration of the South Shetland Trench.

Received 8 May 2007, accepted 26 September 2007

**Key words:** back-arc basin, Bransfield Strait, Scotia Plate, South Shetland Islands

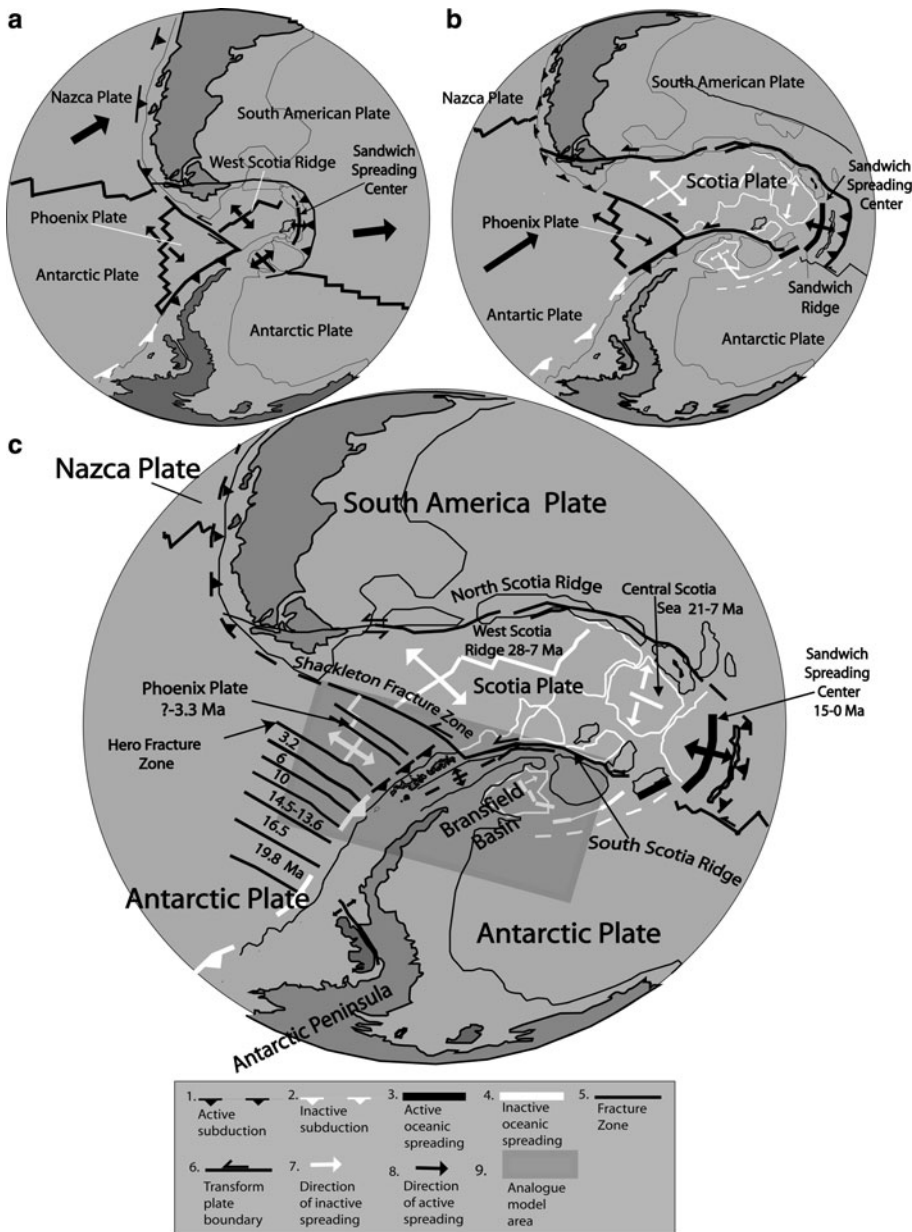
## Introduction

The Bransfield Strait lies between the South Shetland Islands and the north-western part of the Antarctic Peninsula (Fig. 1). In the north-east it is bounded by the South Scotia Ridge, a transform boundary (Galindo-Zaldívar *et al.* 1996) that connects the South Sandwich Arc with the Shackleton Fracture Zone and forms the southern boundary of the Scotia Plate (Pelayo & Wiens 1989, Barker *et al.* 1991). North-west of the South Shetland Islands is the South Shetland Trench that developed by south-eastward subduction of the Phoenix Plate, which is now considered by many to be extinct and overthrust by the Antarctic Plate from the south-east (Barker & Dalziel 1983, Larter & Barker 1991, Maldonado *et al.* 1994).

The Bransfield Basin is preserved as a remnant of the past subduction process, and is generally considered to represent a back-arc rift (Barker 1982, Larter & Barker 1991, Barker & Austin 1998). However, the exact nature of the basin has been a matter of debate. Although some neo-volcanic edifices within the basin are composed of enriched mid-ocean ridge basalt, which suggests nascent seafloor spreading (Gambôa & Maldonado 1990, Keller *et al.* 1991, 1992, Acosta *et al.* 1992, Keller & Fisk 1992), this might also be attributed to arc crustal extension without actual seafloor spreading (Barker & Austin 1998, Barker *et al.* 2003). Geochemical data, in fact, seem to indicate a bimodal composition, with a transition from mid-ocean

ridge basalt-like to arc-like volcanic rocks and a relatively small contribution by subducted material (Petersen *et al.* 2004). Normal faulting of the arc crust also suggests that the Bransfield Strait is in transition from intra-arc rifting to oceanic spreading (Barker & Austin 1994, Lawver *et al.* 1995, Prieto *et al.* 1998, Taylor *et al.* 1999, Barker *et al.* 2003). Pelayo & Wiens (1989) also noted that large normal fault events in the Bransfield Basin and along the South Scotia Ridge have greater depths and seismic moments than earthquakes associated with mid-ocean ridge spreading, indicating that the mechanical process of extension in these areas is notably different.

Whereas many authors believe that the opening of the Bransfield Basin results predominantly from roll-back of the South Shetland Trench (Barker 1982, Larter & Barker 1991, Barker & Austin 1998, Anderson 1999, Barker *et al.* 2003), González-Casado *et al.* (1999, 2000) related the basin opening to a sinistral simple-shear couple between the Scotia and Antarctic plates. They argued that the widening of the Bransfield Basin and insufficient trench roll-back cause compression in the South Shetland Islands. Regional strain analysis by the latter authors indicated that the main structures have a mean NE–SW strike, with a subordinate NW–SE direction and  $\sigma_3$  having a NE–SW orientation. The analysis of faults on Deception Island (Rey *et al.* 1995, Fernández-Ibáñez *et al.* 2005), on the other hand, indicates three main orientations:  $015^\circ$ ,  $080^\circ$ ,



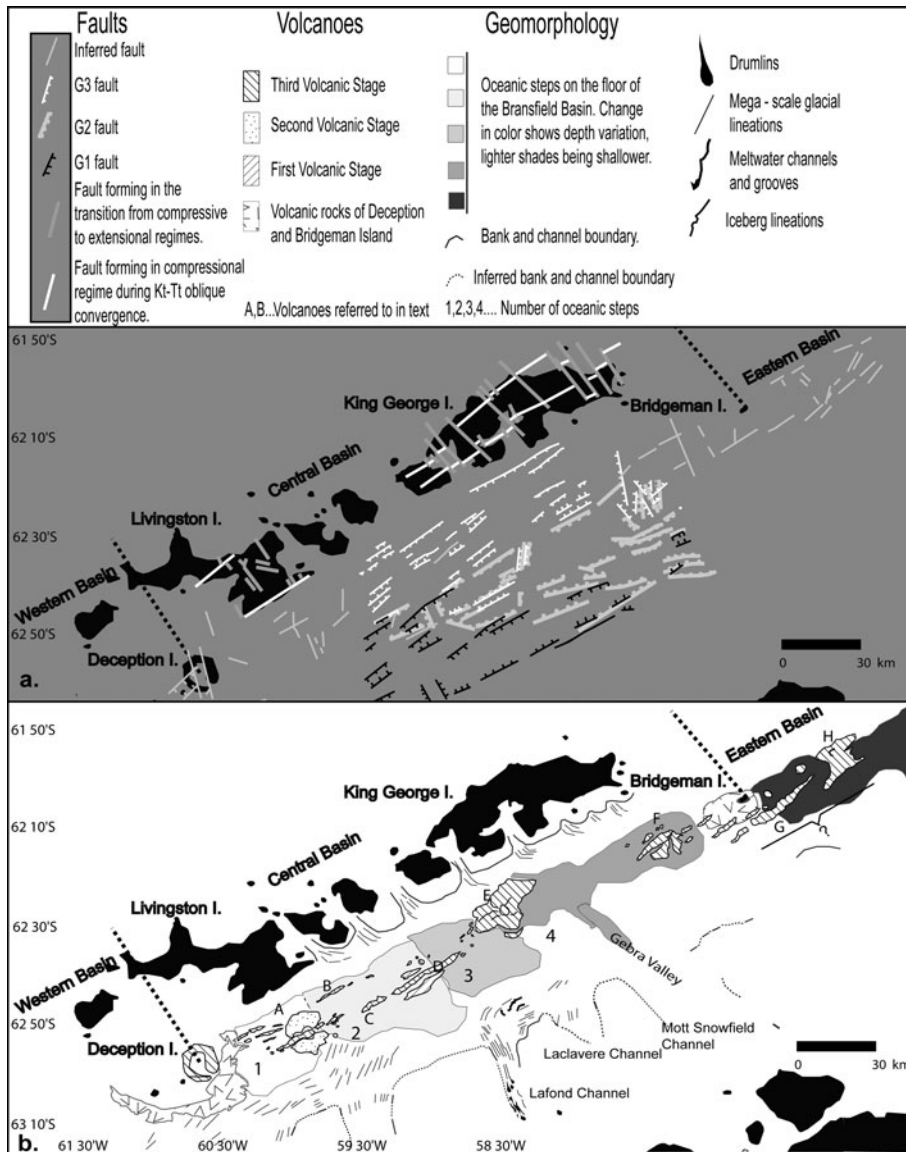
**Fig. 1.** Evolution of major tectonic features within and around the Scotia Plate. **a.** Tectonic plate configuration at 15 Ma, **b.** Tectonic plate configuration at 6 Ma (after Anderson 1999, Barker 2001). **c.** Present tectonic setting shows the age of the collision between the Phoenix Ridge and Antarctic Trench, and the beginning and cessation of spreading centre activities. The shadowed rectangle shows the experimental area.

and  $155^\circ$ . Apparently, most of these are steeply dipping normal faults with some horizontal and occasional reverse displacements, but the nature of the volcanic deposits and the absence of kinematic indicators make it difficult to identify the sense of displacement in most cases. Geomorphologic evidence, in the form of uplifted marine terraces and incised drainage, suggests tilt movement on some faults (Fernández-Ibáñez *et al.* 2005).

The Phoenix Ridge has been inactive since  $3.3 \pm 0.2$  Ma (Livermore *et al.* 2000), so that most authors have incorporated the Phoenix Plate into the Antarctic Plate (Galindo-Zaldívar *et al.* 1996, González-Casado *et al.* 2000, Barker *et al.* 2003, Fernández-Ibáñez *et al.* 2005). However, shallow normal faulting in the Bransfield Basin

(Prieto *et al.* 1998, Barker & Austin 1998), deformation of the trench sediments (Maldonado *et al.* 1994), and earthquakes as deep as 55 km localized near the south-western end of the Bransfield Basin (Pelayo & Wiens 1989) suggest that tectonic activity and possibly subduction could be continuing along the South Shetland Trench.

Considering the ambiguous field and petrographic evidence, as also reflected in the contradicting viewpoints outlined above, it is still not clear which processes are responsible for the opening of the Bransfield Basin, and to which extent this opening is influenced by the dynamics of the Phoenix and Scotia plates. In particular, it needs to be established whether active subduction is indeed continuing along the South Shetland Trench or whether the only active



**Fig. 2.** Bathymetry, tectonic and volcanic map of the Bransfield Basin. **a.** Fault systems are plotted with different line types to differentiate between the relative ages. **b.** Volcanic stages distinguished by different textures relative to age (after Birkenmajer 1982, Santanach *et al.* 1992, Gràcia *et al.* 1996, Canals *et al.* 1997, Prieto *et al.* 1998, Anderson 1999).

process since 3.2 Ma is one of trench roll-back due to thermal/gravitational sagging of the formerly subducting slab. It is also unclear whether the observed fault systems in the Bransfield Basin are related to extension because of back-arc or mid-ocean spreading, or to transtension along the South Scotia Ridge. Therefore, in an endeavour to understand the dynamic evolution of the Bransfield Basin since the Pliocene, we analysed the geomorphological and structural characteristics of the Bransfield Basin using analogue experimental models of the tectonic interaction between the Antarctic, Scotia, and Phoenix plates.

### Tectonic events associated with the opening of the Bransfield Basin

During the Cenozoic, the Pacific margin of the Antarctic Peninsula was affected by a series of progressive collisions

between the South Shetland Trench and segments of the Phoenix Ridge. This caused tectonic uplift of the arc and fore-arc (Barker 1982, Jeffers *et al.* 1991, Maldonado *et al.* 1994, Anderson 1999) (Fig. 1). Six unconformities in the sedimentary cover of the ocean floor represent the time when subduction ceased in the different oceanic segments (Herron & Tucholke 1976, Barker 1982). They were dated at 19.8, 16.5, 14.5, 10, 6.0, and 5.5–3.1 Ma, respectively.

The sequence of tectonic events associated with the opening and development of the Bransfield Basin can be summarized as follows:

- 1) Spreading of the West Scotia Ridge starting at 28 Ma (Fig. 1a) and finishing at 7 Ma (Fig. 1b) (Barker 2001),
- 2) Possible opening of the Bransfield Basin at a rate of  $1.1 \text{ mm yr}^{-1}$  during the Oligocene–Miocene (Sell *et al.* 2004),



**Table I.** Physical properties of the experimental material.

	Experiment 1	Experiment 2	Experiment 3
<b>Continental lithosphere</b>			
Density ( $\text{g cm}^{-3}$ )	1.26	1.26	1.44
Brittle layer thickness (mm)	10	10	10
Ductile layer thickness (mm)	40	40	40
Ductile layer viscosity (Pa s)	$6 \times 10^4$	$6 \times 10^4$	$1 \times 10^5$
<b>Oceanic lithosphere</b>			
Density ( $\text{g cm}^{-3}$ )	1.38	1.38	1.44
Brittle layer thickness (mm)	5	5	10
Ductile layer thickness (mm)	35	35	40
Ductile layer viscosity (Pa s)	$1 \times 10^5$	$1 \times 10^5$	$1 \times 10^5$
<b>Asthenosphere</b>			
Density ( $\text{g cm}^{-3}$ )	1.41	1.41	1.41
Thickness (mm)	100	100	100
Viscosity (Pa s)	460	460	460
Piston velocity ( $\text{cm h}^{-1}$ )	4.5	4.5	3

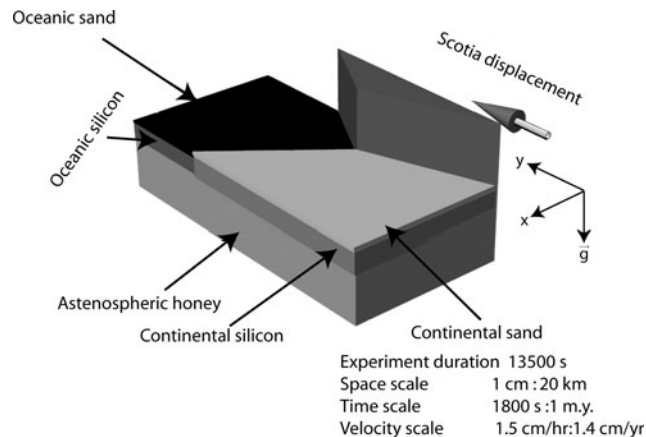
- 3) Activity of the Sandwich Spreading Center (Fig. 1b) from 15 Ma to the present (Vanneste *et al.* 2002),
- 4) Tectonic inversion in the Shackleton Fracture Zone at 7 Ma (Fig. 1), following the demise of the West Scotia Ridge (Livermore *et al.* 2000),
- 5) Simultaneous spreading extinction of the three remnant segments of the Phoenix Ridge (Fig. 1c), closely associated with the last ridge-trench collision of the Hero Fracture Zone (Fig. 1c) at *c.* 3.2–3.3 Ma (Anderson 1999, Livermore *et al.* 2000),
- 6) Extension of the Bransfield Basin for the past 2 Ma at an average full-rate of 2.5–7.5  $\text{mm yr}^{-1}$  (González-Ferrán 1991),
- 7) Formation of the axial volcanoes of the central Bransfield Basin 0.71 m.y.a. according to magnetic anomalies (Hardland *et al.* 1990, Canals *et al.* 1997) and a minimum full spreading rate of 0.83  $\text{mm yr}^{-1}$  (Canals *et al.* 1997).

### Bathymetry, volcanism, and structural features of the Bransfield Basin

The following overview was compiled from observations by different authors and the information is summarized in a geomorphologic structural map (Fig. 2).

The orientation of the longitudinal axis of the Bransfield Basin is approximately  $060^\circ$ . It is divided by volcanic complexes, forming the Deception and Bridgeman islands, into the western, central and eastern sub-basins (Gràcia *et al.* 1996, Lawver *et al.* 1996, Anderson 1999).

The western sub-basin is located between Boyd Strait and Deception Island (Fig. 2) and comprises the shallower part of



**Fig. 3.** Experimental assembly illustrating the differentiation between a continental and oceanic zone used in experiment 1. The width and length of the analogue area are 30 cm and 60 cm, respectively. The conical arrow shows the direction of piston movement.

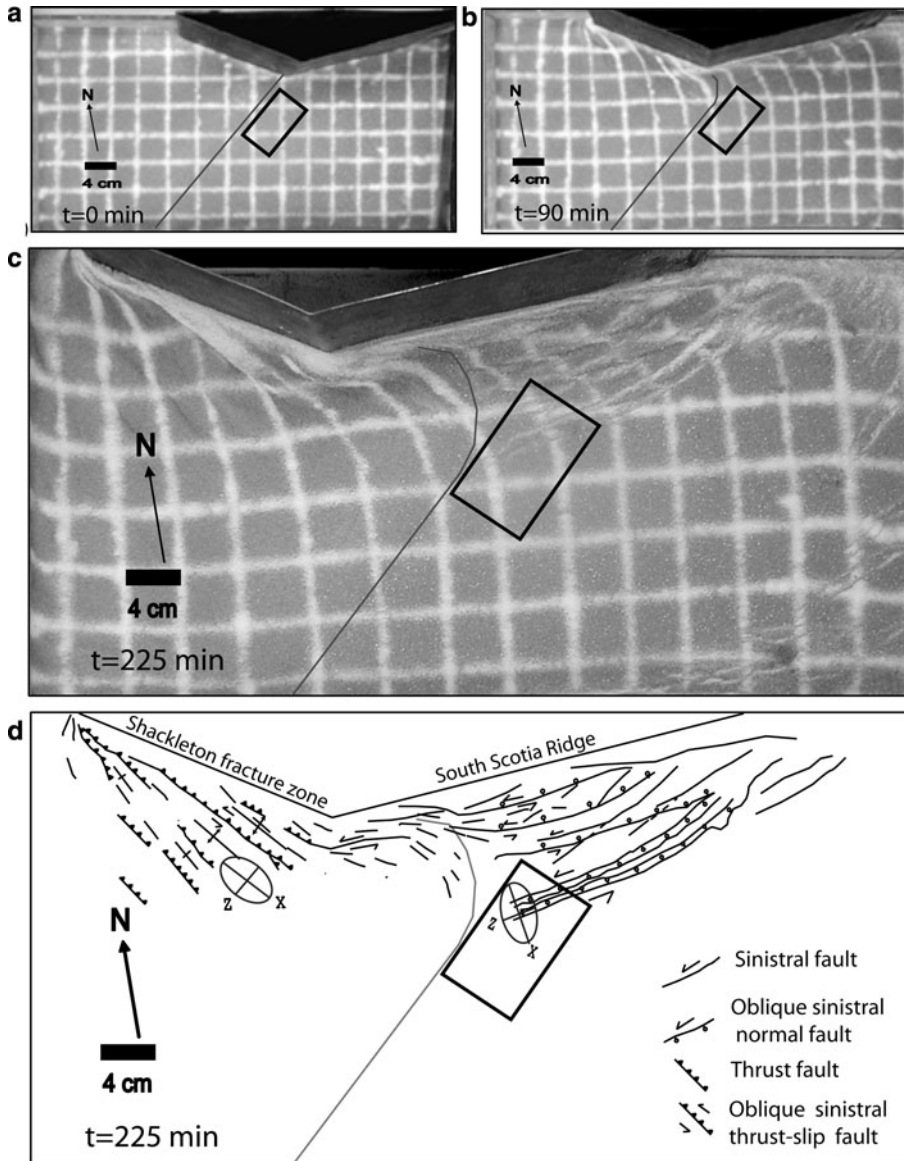
the Bransfield Basin, reaching maximum depths of 1250 m. Volcanism is not observed in this sub-basin (Anderson 1999).

The central sub-basin is asymmetric with a steep northern slope and a gentle southern slope. On the shelf, large glacial troughs with mega-glacial lineaments resulting from ice flow movement and erosion during the last glacial episode (Wellner *et al.* 2001, Canals *et al.* 2002) are present (Fig. 2). Four oceanic steps (1, 2, 3 and 4 in Fig. 2), spaced between 40 and 50 km apart and with depths that vary from west to east between 750 and 1950 m, segment the basin floor (Anderson 1999).

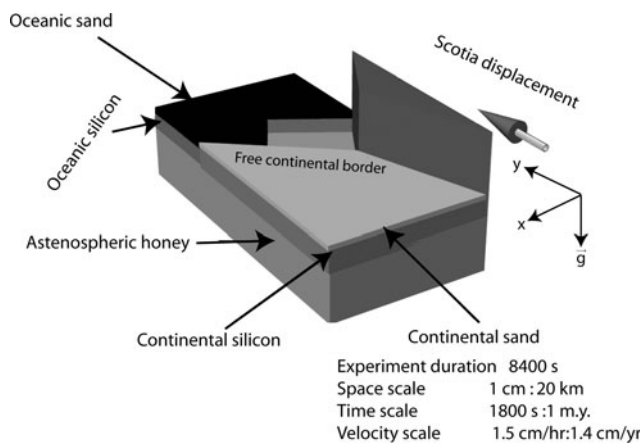
A line of conical and linear volcanic edifices labelled A–F, extend parallel to the basin axis, which trends at  $060^\circ$  (Gràcia *et al.* 1996). The latter authors distinguished three phases of volcanism. During the first phase a submarine volcanic edifice (D) began to form, followed by a conical submarine volcano (A). In the second phase, the previously formed conical volcano (D) was ruptured and separated by a linear volcanic edifice. Additional submarine volcanic edifices (B, C, F, and E) developed during the third phase, while continued extension in the volcano D area formed a thin belt of possible oceanic crust.

The central sub-basin is dominated by a main north-east and secondary north-west system of normal faults. The NE-trending faults define three graben systems parallel to the basin axis (Fig. 2). The orientation of these grabens and their associated deposits induced Prieto *et al.* (1998) to propose migration of the extensional grabens and associated depocentres from the Antarctic Peninsula margin to the South Shetland Island margin along three spatially and temporally differentiated trends, the first having an orientation of  $071^\circ$  (the graben system nearest to the Antarctic Peninsula), followed by  $064^\circ$  (the intermediate system), and finally  $053^\circ$  (the system nearest to the South





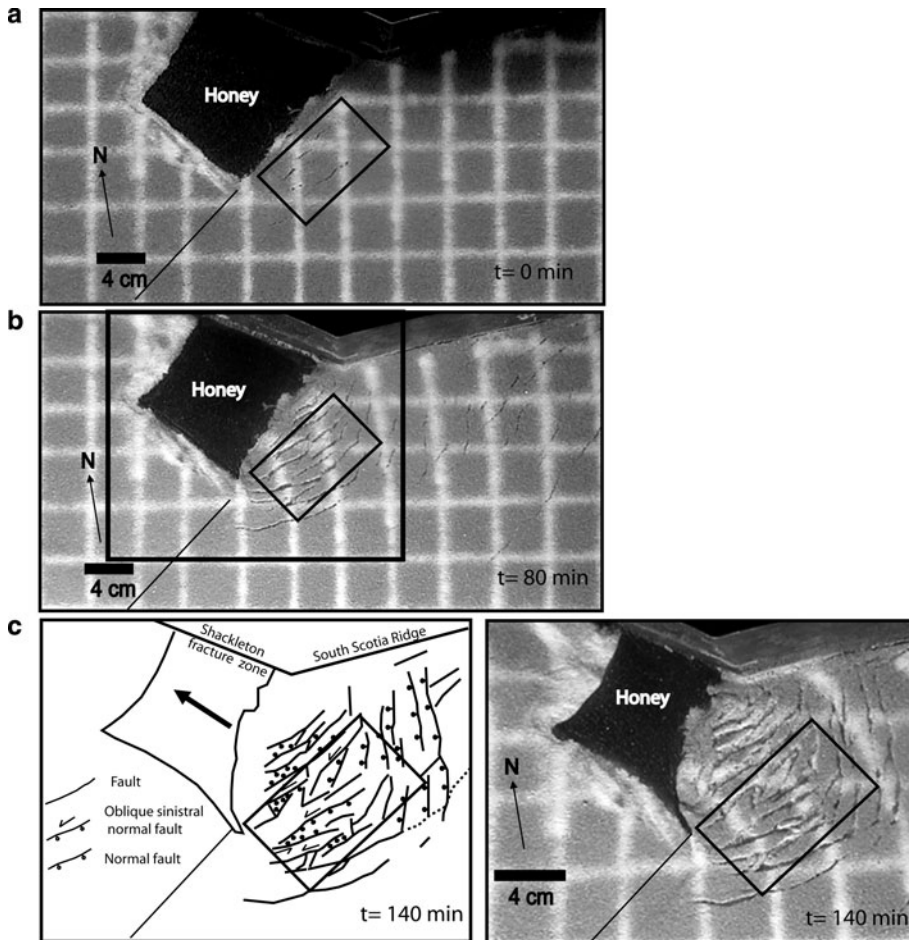
**Fig. 4.** Photographic sequence at **a.** 0, **b.** 90, and **c.** 225 min of experiment 1. **d.** Structural interpretation sketch at 225 min. This figure represents the shadowed rectangle of Fig. 1 and the box represents the Bransfield study area shown in Fig. 2. The grey line shows the limit between the continental and oceanic zones. Strain ellipsoids indicate maximum and minimum strain axes.



**Fig. 5.** Experimental assembly illustrating the differentiation between a continental and oceanic zone used in experiment 2.

Shetland Islands). The NW-trending secondary fault system is responsible for the morphological steps that deepen the basin from south-west to north-east (Prieto *et al.* 1998). On the King George and Livingston Islands of the central sub-basin,  $065^\circ$ -trending dextral strike-slip faults (Fig. 2) were formed by oblique convergence between the Phoenix and Antarctic plates (Birkenmajer 1982, Santanach *et al.* 1992) during the Late Cretaceous–Pliocene. The north-west strike-slip faults on King George and Livingston islands, spaced between 5 and 15 km apart, reflect a transition from compressional to extensional regimes produced by the cessation of spreading of the Phoenix Plate (Birkenmajer 1982, Santanach *et al.* 1992).

The eastern sub-basin lies between Bridgeman Island and the South Scotia Ridge (Figs. 1 & 2). This basin reaches a maximum depth of almost 2300 m. The northern slope of the basin is steep, between  $9^\circ$  and  $20^\circ$ , whereas its



**Fig. 6.** Photographic sequence of experiment 2 at **a.** 0, and **b.** 80 minutes, respectively. **c.** Photograph and structural interpretation sketch at 140 min of the enlarged area shown in Fig. 6b. This figure represents the shadowed rectangle of Fig. 1 and the box represents the Bransfield study area shown in Fig. 2.

southern slope is gentler (between  $5^\circ$  and  $13^\circ$ ) and irregular. The floor of the basin has an approximate width of 25 km and shows two oceanic steps divided by submarine volcano H (Fig. 2), which displays a complex geomorphology. This sub-basin is also characterized by four deep troughs displaying a rhombic shape, interpreted by Gràcia *et al.* (1996, 1997) to reflect NW–SE extension with a left-

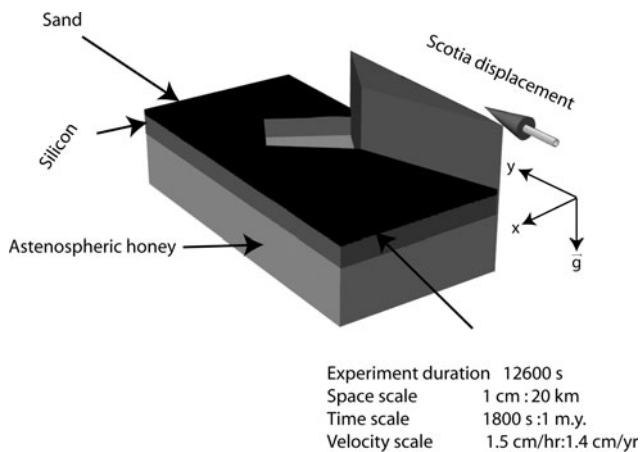
lateral strike-slip component probably related to the South Scotia Ridge.

### Analogue experimental models

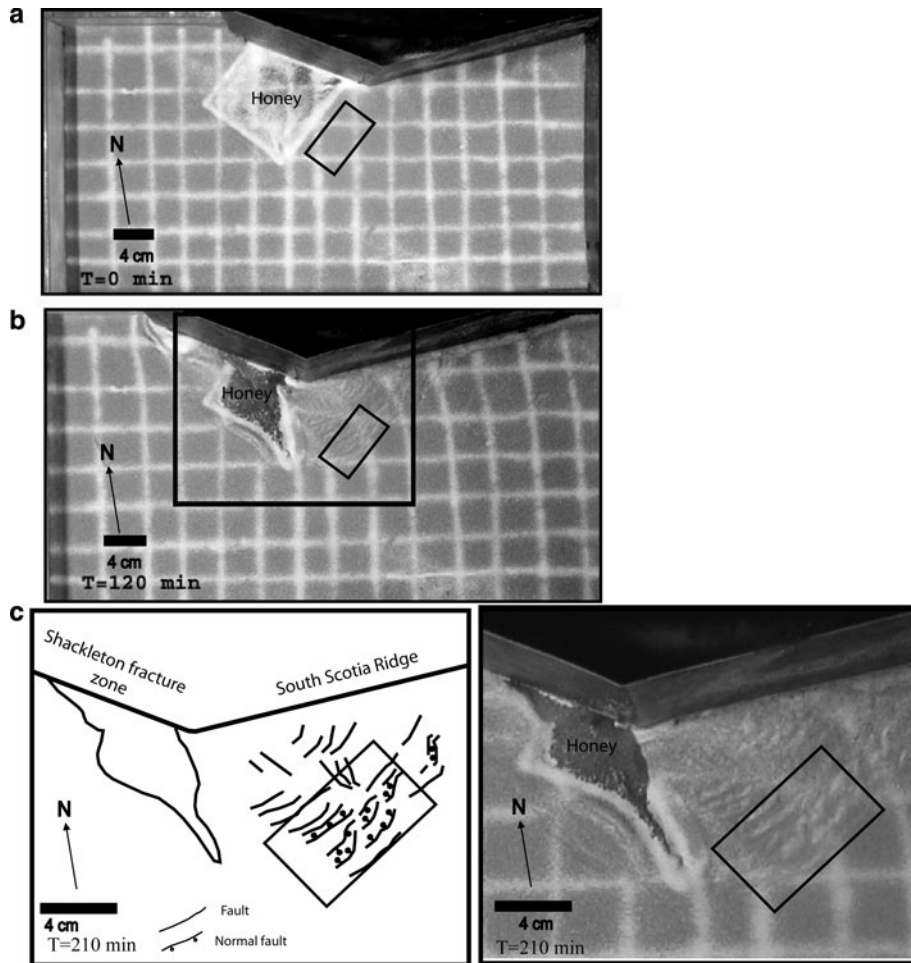
A series of experiments was carried out in order to understand how the regional dynamic evolution of the plates described above may have contributed to the development and opening of the Bransfield Basin. The aim of the experiments was to examine the causes of the deformation observed in the Bransfield Basin and in particular, the effect of the Scotia Plate motion on deformation in the Bransfield Basin area.

### Rheological, spatial and temporal analogies

The modelled area is a rectangle of approximately 1200 km by 600 km, corresponding to oceanic (ex-Phoenix Plate and part of the oceanic Antarctic Plate) and continental lithospheres (continental Antarctic Plate and associated shelves) (see Fig. 1). Analogue modelling was carried out within a rigid Plexiglas tank. The long side of the tank was parallel to the relative motion of the Scotia Plate with respect to the Antarctic Peninsula, i.e. approximately E–W.



**Fig. 7.** Assembly showing the layer configurations.



**Fig. 8.** Photographic sequence at **a.** 0, and **b.** 120 min of experiment 3. **c.** Photograph and structural interpretation sketch at 210 min of the enlarged area shown in Fig. 8b. This figure represents the shadowed rectangle of Fig. 1 and the box represents the Bransfield study area shown in Fig. 2.

The following assumptions were made to design the analogue models:

- 1) The mechanical behaviour of the continental and oceanic lithosphere is that of a brittle upper layer lying above a high-viscosity ductile layer. These layers are modelled using sand and silicon, respectively. Sand is a brittle material with a negligible cohesion and a  $30^\circ$  internal friction angle, which is suitable for reproducing at scale the mechanical properties of the brittle lithosphere (e.g. Davy & Cobbold 1991). Silicon putty is a Newtonian material with a high viscosity, close to  $1 \times 10^5$  Pa s. The analogues of the continental and oceanic lithospheres have different thicknesses, densities and viscosities (see Table I for a complete description of the physical parameters of the analogue experiments).
- 2) The asthenosphere is assumed to behave as a low-viscosity, ductile Newtonian fluid. It was modelled using honey, the viscosity of which is small compared to that of silicon.
- 3) Present-day deformation along the western part of the Scotia Plate is minor, so that we modelled the Scotia

Plate boundary as a rigid boundary, using a metal triangle that transmits stresses without being deformed. This rigid boundary was pushed at constant speed using a motor-driven piston, in order to reproduce the relative motion of the Scotia Plate with respect to Antarctica.

To model the deformation of 80 km thick lithospheric plates, the length scale factor is  $5 \times 10^{-7}$ , whereas the density scale factor is close to 0.4. From the simple scaling relations in Table I, we derived that 20 min in the experiments correspond to 1.5 m.y. in nature. The piston velocity was set to represent the relative motion of the Scotia Plate with respect to Antarctica ( $1.4 \text{ cm yr}^{-1}$ , Pelayo & Wiens 1989). Davy & Cobbold (1991) and Martinod *et al.* (2000) provide more details concerning scaling in this kind of experiment.

We also wanted to study how possible roll-back of the South Shetland Trench resulting from density contrasts between the continental lithosphere of the Antarctic Peninsula and the former Phoenix Plate section of the Antarctic Plate, could control the formation of the Bransfield Basin. To do so, we tested the effect of gravity spreading above the trench on the tectonics of the Antarctic Plate.



For convenience, we shall refer hereafter to regions of the experiment in terms of geographic locations, the northern boundary corresponding to the moving rigid plate.

### Model 1

Experiment 1 modelled the tectonic regime that developed in the study area resulting from the westward motion of the Scotia Plate. A continental (Antarctic Peninsula and associated shelves) and an oceanic (Antarctic Plate) zone were differentiated in the analogue model, in which the continental plate was more buoyant than the oceanic plate. The boundary between these zones had the same orientation as the Shetland subduction zone (Fig. 3). During the analogue experiment, the piston pushed a rigid structure modelling the Scotia Plate at constant speed ( $4.5 \text{ cm hr}^{-1}$ ). This rigid plate motion resulted in the superficial deformation of the sand/silicon layers. A square grid of passive sand markers enabled the visualization of surface deformation, which was surveyed using a digital camera.

Different stages of the experiment are shown in Fig. 4. Deformation concentrated near the triangle and propagated from north to south. The oceanic zone (western part of the model) was affected by transpressional deformation where folds and oblique sinistral thrust-slip faults appeared. The faults and fold axes trended between  $320^\circ$  and  $330^\circ$  (Fig. 4), corresponding to the axis of maximum extension (X). The angle between the maximum stretch axes and the eastern side of the triangle was almost perpendicular, implying a high deformation partition (Teyssier *et al.* 1995).

The continental zone was affected by a transtensional regime, where a set of  $078^\circ$ – $088^\circ$ -oriented oblique sinistral normal faults (Fig. 4) developed. Near the triangle, sinistral strike-slip faults were cut by a secondary system of  $058^\circ$ – $063^\circ$ -oriented strike-slip faults (Fig. 4). Grabens and horsts developed in the southern zone affected by transtensional deformation.

### Model 2

This experiment was done with a different geometry of sand/silicon plates to take into account the presence of the Phoenix Plate. As explained above, the Phoenix Plate subducted below the Antarctic Peninsula during the Miocene and Pliocene. The boundary between the Phoenix Plate and the Antarctic continent thus corresponds to a weak zone, despite the fact that the subduction velocity drastically decreased following the extinction of the Phoenix Ridge  $3.3 \pm 0.2 \text{ Ma}$  ago. Therefore, the limit between the Antarctic and Phoenix plates was considered to be a free boundary, so that the Antarctic continent could spread freely above the Phoenix oceanic plate. This approach has been used successfully to model the deformation of continental plates spreading above subduction zones, for

instance in the Aegean Sea (Hatzfeld *et al.* 1997, Gautier *et al.* 1999, Martinod *et al.* 2000). However, it must be stressed that this analogue model was limited in simulating roll-back in a passive rather than active way, i.e. there was no actual sinking of the oceanic crust relative to the continental crust. The experiment only reproduced buoyancy differences between the two types of crust, allowing the upper, less dense crust to extend over the lower, dense crust as if the latter were actively sinking.

Here, the sand-silicon layer modelled the Antarctic continental plate. To simulate the free boundary between the Antarctic and Phoenix plates, we removed the silicon-sand layer in a representative model area of the Phoenix Plate (Fig. 5). During the analogue experiment, the piston representing the Scotia Plate advanced at  $4.5 \text{ cm hr}^{-1}$  as in the previous experiment. As soon as the experiment started, fractures developed in the Bransfield area with an approximate  $065^\circ$  orientation (Fig. 6a). These fractures partly resulted from extension of the sand-silicon plate during spreading of the light material that modelled the continental lithosphere above the dense honey (Hatzfeld *et al.* 1997), and partly from the transtension produced by the migrating Scotia Plate. The direction of the extension was approximately perpendicular to the free continental boundary, which migrated towards the north-west. The oceanic free boundaries did not extend significantly because the buoyancy of the sand-silicon layer modelling the ocean was close to zero.

In the Bransfield area, a system of  $065^\circ$ -trending normal faults with a sinistral component of movement developed. They were segmented by a  $005^\circ$ – $010^\circ$ -striking secondary system of faults. It is interesting to note that in the Bransfield area (Fig. 6c), the main and secondary system of faults formed a discontinuous rift. After 20 min (equal to 0.67 m.y.) the main system of faults was clearly developing and after 80 min the entire main fault had been formed (Fig. 6b). The secondary system started as fractures at 40 min and developed into a clear normal fault before 80 min, equal to 2.7 m.y. Between 80 and 140 min the number of secondary faults and the extension of the main sinistral normal fault increased (Fig. 6c). The direction of extension at 0 min was  $325^\circ$  and rotated to  $316^\circ$  after 140 min, equal to 4.7 m.y.

### Model 3

In this analogue experiment, the sand-silicon layer was homogeneous with a density similar to that of the honey (Table I). It was used to model both the oceanic and continental Antarctica lithosphere. The buoyancy of the plate being close to zero, the spreading force occurring close to the free boundary modelling the Antarctica–Phoenix plates boundary was small. In this way, the magnitude of the extension produced by lithosphere–asthenosphere density contrasts in the free borders was

reduced. Extension in the central zone of this experiment mainly resulted from the constant speed motion of the rigid triangle that modelled the Scotia Plate (Fig. 7).

After 120 min, equal to 4 m.y., the developed structures were still very few (Fig. 8b). In the Bransfield area a diffuse extensional zone was characterized by  $060^{\circ}$ – $070^{\circ}$ -trending fractures.

After 210 min, equal to 7 m.y., extension increased in the Bransfield zone and in the southern part of the diffuse extensional zone a discontinuous system of normal faults trending  $060^{\circ}$ – $070^{\circ}$ , developed (Fig. 8c). The development of faults in experiment 3 was less extensive and slower than in experiment 2, whereas the secondary system of faults observed in experiment 2 did not reappear in experiment 3.

## Discussion

Experiment 1 did not reproduce all the structural features observed in the Bransfield Basin, but showed the development of transpressional and transtensional regimes close to the Shackleton Fracture Zone and South Scotia Ridge, respectively. The transtension observed in the Bransfield area (main NE–SW fault system, Fig. 4d) had a different orientation and extension was restricted to the eastern part of the Bransfield area (Fig. 4d), despite the fact that the density contrast between the oceanic and continental plate should have favoured extension on the continent, close to the continent-ocean boundary. Stresses arising from the buoyancy contrast between the continental and oceanic plate were not large enough to trigger extension of the continental plate in the Bransfield area.

The fact that experiment 1 did not exactly reproduce the structural setting of the Bransfield Basin is probably because it did not take into account the weak zone corresponding to the boundary between the Phoenix Plate and the Antarctic continent. Nevertheless, this experiment suggests that oblique continental rifting could have developed in the Bransfield area after 7 Ma due to the development of a transtensional regime, which concurs with field evidence. Pelayo & Wiens (1989) and Giner-Robles *et al.* (2003) concluded from seismic studies that left-lateral slip with a component of extension occurs along the South Scotia Ridge, which is supported by deformational structures in the eastern Bransfield sub-basin (Gràcia *et al.* 1996, Klepeis & Lawver 1996).

Transpression west of the southernmost sector of the Shackleton Fracture Zone, as shown by experiment 1, is also supported by field evidence (Pelayo & Wiens 1989). Multichannel seismic and long-range side scan sonar studies along the South Shetland Trench indicate the presence of an accretionary prism with a complex internal structure, the toe of which is overthrust above the youngest trench deposits. The thrust-bounded wedges are laterally and vertically segmented by normal faults (Maldonado

*et al.* 1994), suggesting that transpression may alternate with extension caused by roll-back of the oceanic crust.

In the case of experiment 3, the secondary N–S system of faults did not develop in the Bransfield area and an almost diffuse extension resulted. The absence of this secondary system of faults is attributed to the continental buoyancy of the plate having been close to zero and because the spreading force occurring close to the free boundary modelling the Antarctica–Phoenix plate boundary was small. However, the fact that a  $060^{\circ}$ – $070^{\circ}$  system of faults did develop as a result of the rigid triangle modelling the Scotia Plate, even in the absence of oceanic floor, indicates that transtension along the South Scotia Ridge was the dominant force in the development of this system.

Of the three models, experiment 2 bears the best resemblance to the structures actually occurring in the field. The main system of faults had an orientation of  $065^{\circ}$  that agrees with the ENE–WSW main fault system in the central and eastern Bransfield sub-basins. In particular, this strike is the same as that observed on King George and Livingston islands associated with the Ezcurra Phase (Birkenmajer 1982, Santanach *et al.* 1992), although the horizontal displacement produced by the experiments was sinistral, not dextral as reported by these authors. However, seismicity studies by Galindo-Zaldívar *et al.* (1996) indicate that the stress distribution in the Bransfield Strait is similar to that in the axial depression of the South Scotia Ridge, where an ENE–WSW fault system displays an active sinistral transtensional regime with transpressional sectors.

Of particular interest is that the  $065^{\circ}$  fracture set that initially developed in the experiments partially resulted from extension of the sand-silicon layer that modelled the buoyant continental lithosphere above the oceanic lithosphere. The direction of extension perpendicular to the free continental boundary and migration of the latter to the north-west closely resembles the situation in the Bransfield Basin. However, in the experiment only passive roll-back of ocean crust was simulated, which suggests that its effect was relatively minor and that the extension of the Bransfield Strait is related mainly to the west–north-westward migration of the Scotia Plate as suggested by González-Casado *et al.* (2000). In contrast with the latter authors, however, who consider the Phoenix Plate to be presently incorporated into the Antarctic Plate, experiment 3 indicates that the Phoenix Plate still exists as such and has a free boundary with the Antarctic continent. We contend that expansion of the buoyant continental crust is caused mainly by shearing and transtension along the South Scotia Ridge, but is facilitated by continued, albeit slow, roll-back of the Phoenix Plate. Barker *et al.* (2003) observed that the crustal thickness in the central sub-basin increases from north-east to south-west, which suggests that the Bransfield Basin is opening by north-east to south-west rift propagation within arc crust of the Antarctic Peninsula.

Older (*c.* 21 Ma) and thus denser oceanic crust to the north-east, compared with younger (*c.* 12 Ma) crust to the south-west (Larter & Barker 1991) would cause a somewhat higher rate of sinking in the north-east, in the process creating space for expansion of the continental crust caused by transtension along the South Scotia Ridge.

Barker *et al.* (2003) note that extension of the Bransfield Strait is focussed towards the trench side as shown by the asymmetric physiography of the basin floor, with a steep back-arc slope and gentler continental margin slope. They attribute this to subduction-related magmatism weakening the arc-back-arc crust along the trench side. However, this asymmetry could also be a result of purely sedimentary processes, with glacially derived sediments primarily being accumulated along the southern margin of the Bransfield Basin and much less along the northern margin, because the South Shetland Islands represent a much more reduced drainage basin. This is evident from the seismic and bathymetric studies of Prieto *et al.* (1998) and Canals *et al.* (2002). Based on our experimental results, we consider active subduction not to be taking place along the South Scotia Trench at present, but rather favour a process of passive subduction. In active subduction, the ocean floor expands horizontally and sinks beneath a stagnant continental plate, whereas passive subduction in our terminology refers to the situation where there is no active expansion of the oceanic crust but only roll-back, coupled with active extension of the continental crust above it due to transtension and pronounced density differences.

The secondary 005°–010° normal fault system that developed in experiment 3, forming a discontinuous rift with the main fault system, is also duplicated in the Bransfield Basin (Fig. 2). Individual NS-striking faults with downfaulting to the east are not uncommon, as for example associated with Costa Recta on Deception Island (Fernández-Ibáñez *et al.* 2005). Such faulting may also be manifested in the deepening of the whole Bransfield Basin towards the north-east. The N–S fault system may be partly attributed to the buoyancy of the continental crust in comparison with the oceanic crust, as modelled in experiment 2. Galindo-Zaldívar *et al.* (1996) noted that isostatic balance causes significant differences at the boundaries between oceanic and continental crust, with the development of scarps that highlight fault locations. There is ample evidence of tectonic uplift and prominent normal fault scarps in the Bransfield Strait. On Deception Island, Fernández-Ibáñez *et al.* (2005) described uplifted marine terraces and incised fluvial drainage associated with normal NNW–SSE striking faults, which may be due to continental/oceanic plate buoyancy differences. Muñoz-Martín *et al.* (2005) in fact identified continental and basic crust north and south of Deception Island, respectively, indicating a high density contrast in this area. Smith Island, on the other hand, may have resulted from uplift that followed a ridge crest-trench collision directly south-west

of the Hero Fracture Zone at 5.5 Ma (Maldonado *et al.* 1994) or, alternatively, from the subduction of a seamount, as this area is just landward of a seamount chain.

In conclusion, the analogue models of all three experiments suggest that opening of the Bransfield Basin is related to a combination of transtensional stress associated with the north-westward migration of the Scotia Plate, and slow roll-back of the Phoenix Plate, but dominated by the former process. Subduction is here seen as passive instead of active, i.e. induced by sinking of the oceanic plate without spreading at the Phoenix Ridge, which allows the continental crust of the Antarctic Peninsula to expand towards the north-west, creating the Bransfield Basin in the process.

### Acknowledgements

We are grateful to Drs John Anderson and Julia Wellner of Rice University, who actively encouraged the present study. The Chilean Ministry of Foreign Affairs and the Chilean Antarctic Institute (INACH) enabled the participation of one of us (MSO) as observer in the RVIB *Nathaniel B. Palmer* cruise (NBP0203) financed by the National Science Foundation (NSF). The Research Institute for Development of France (IRD) and the Geology Department of the University of Chile allowed the use of their laboratory facilities. Financial support by the Bicentennial Program of Science and Technology, backed by the National Research Corporation of Chile (CONICYT) and the World Bank, as well as INACH, of the project “Geological Connections Between Patagonia and Antarctica” (ARTG04) enabled the successful conclusion of this study. Jaime Martínez of the Chemical Laboratory at the University of Chile calculated the density of the products used in the experiments, and Rodrigo Fernández provided assistance in the field. Work on this paper started while one of us (JPLR) held a Fellowship at the Hanse Institute for Advanced Study in Delmenhorst, Germany. The logistical and financial support of the Institute is gratefully acknowledged.

We thank Marc de Batist and José-Manuel González-Casado for very thorough and instructive reviews, which helped us to improve this paper considerably.

### References

- ACOSTA, J., HERRANZ, P., SANZ, J.L. & UCHUPI, E. 1992. Antarctic continental margin: geologic image of the Bransfield Trough, an incipient ocean basin. In POAG, C.W. & DE GRACIANSKY, P.C., eds. *Geologic evolution of the Atlantic continental rises*. New York: Van Nostrand Reinhold, 49–61.
- ANDERSON, J.B. 1999. *Antarctic marine geology*. Cambridge: Cambridge University Press, 287 pp.
- BARKER, P.F. 1982. The Cenozoic subduction history of the Pacific margin of the Antarctic Peninsula: ridge crest-trench interactions. *Journal of the Geological Society of London*, **139**, 787–801.



- BARKER, P.F. & DALZIEL, I.W.D. 1983. Progress in geodynamics in the Scotia Arc region. In CABRÉ, R., ed. *Geodynamics of the eastern Pacific Region, Caribbean and Scotia arcs*. Washington, DC: American Geophysical Union, Geodynamic Series, vol. 9, 137–170.
- BARKER, P.F. 2001. Scotia Sea regional tectonic evolution: implications for mantle flow and palaeocirculation. *Earth-Science Reviews*, **55**, 1–39.
- BARKER, P.F., DALZIEL, I.W.D. & STOREY, B.C. 1991. Tectonic development of the Scotia Arc region. In TINGEY, R.J., ed. *Antarctic geology*. London: Oxford University Press, 215–248.
- BARKER, D.H.N. & AUSTIN, J.A. 1994. Crustal diapirism in Bransfield Strait, West Antarctica: evidence for distributed extension in marginal-basin formation. *Geology*, **22**, 657–660.
- BARKER, D.H.N. & AUSTIN, J.A. 1998. Rift propagation, detachment faulting and magmatism in the Bransfield Strait, Antarctic Peninsula. *Journal of Geophysical Research*, **103**, 24 017–24 043.
- BARKER, D.H.N., CHRISTESON, G.L., AUSTIN, J.A. & DALZIEL, I.W.D. 2003. Backarc basin evolution and cordilleran orogenesis: insights from new ocean-bottom seismograph refraction profiling in Bransfield Strait, Antarctica. *Geology*, **31**, 107–110.
- BIRKENMAJER, K. 1982. Late Cenozoic phases of the block-faulting on King George Island, South Shetland Island, (West Antarctica). *Bulletin de l'Académie Polonaise des Sciences, Série des Sciences de la Terre*, **30**, 21–32.
- CANALS, M., GRÁCIA, E., PRIETO, M.J. & PARSON, L.M. 1997. The Antarctic Region: geological evolution and processes. In RICCI, C.A., ed. *Proceedings of the VII International Symposium on Earth Sciences*. Siena: Terra Antarctica Publications, 669–673.
- CANALS, M., CASAMOR, J.L., URGELES, R., CALAFAT, A.M., DOMACK, E.W., BARAZA, J., FARRÁN, M. & DE BATIST, M. 2002. Seafloor evidence of a subglacial sedimentary system off the northern Antarctic Peninsula. *Geology*, **30**, 603–606.
- DAVY, P. & COBBOLD, P.R. 1991. Experiments on shortening of 4-layer model of the continental lithosphere. *Tectonophysics*, **188**, 1–25.
- FERNÁNDEZ-IBÁÑEZ, F., PÉREZ-LÓPEZ, R., MARTÍNEZ-DÍAZ, J.J., PAREDES, C., GINER-ROBLES, J.L., CASELLI, A.T. & IBÁÑEZ, J.M. 2005. Costa Recta beach, Deception Island, West Antarctica: a retreated scarp of a submarine fault? *Antarctic Science*, **17**, 418–426.
- GAUTIER, P., BRUN, J.P., MORICEAU, R., SOUKOUTIS, D., MARTINOD, J. & JOLIVET, L. 1999. Timing, kinematics, and cause of Aegean extension: a scenario based on a comparison with simple analogue experiments. *Tectonophysics*, **315**, 31–72.
- GALINDO-ZALDÍVAR, J., JABALOY, A., MALDONADO, A. & DE GALDEANO, C.S. 1996. Continental fragmentation along the South Scotia Ridge transcurrent plate boundary (NE Antarctic Peninsula). *Tectonophysics*, **258**, 275–301.
- GAMBÓA, L.A.P. & MALDONADO, P.R. 1990. Geophysical investigations in the Bransfield Strait and in the Bellinghousen Sea, Antarctica. In ST. JOHN, B., ed. *Antarctica as an exploration frontier: hydrocarbon potential, geology, and hazards*. American Association of Petroleum Geology, Studies in Geology, No. 31, 127–141.
- GINER-ROBLES, J.L., GONZÁLEZ-CASADO, J.M., GUMIEL, P., MARTÍN-VELÁZQUEZ, S. & GARCÍA-CUEVAS, C. 2003. A kinematic model of the Scotia Plate (SW Atlantic Ocean). *Journal of South American Earth Sciences*, **16**, 179–191.
- GONZÁLEZ-CASADO, J.M., LÓPEZ-MARTÍNEZ, J., GINER-ROBLES, J., DURAN, J.J. & GUMIEL, P. 1999. Análisis de la microfracturación en la Isla Decepción, Antártica Occidental. *Geogaceta*, **26**, 27–30.
- GONZÁLEZ-CASADO, J.M., GINER-ROBLES, J.L. & LÓPEZ-MARTÍNEZ, J. 2000. Bransfield Basin, Antarctic Peninsula: not a normal backarc basin. *Geology*, **28**, 1043–1046.
- GONZÁLEZ-FERRÁN, O. 1991. The Bransfield rift and its active volcanism. In THOMSON, M.R.A., CRAME, J.A. & THOMSON, J.W., eds. *Geological evolution of Antarctica*. New York: Cambridge University Press, 505–509.
- GRÁCIA, E., CANALS, M., FARRÁN, M., PRIETO, M.J., SORRIBAS, J. & GEBRA, T. 1996. Morphostructure and evolution of the central and eastern Bransfield Basin (NW Antarctic). *Marine Geophysical Research*, **18**, 429–448.
- GRÁCIA, E., CANALS, M., FARRÁN, M., SORRIBAS, J. & PALLAS, R. 1997. Central and Eastern Bransfield basins (Antarctica) from high-resolution swath-bathymetry data. *Antarctic Science*, **9**, 168–180.
- HARDLAND, W.B., ARMSTRONG, R.L., COX, A.V., CRAIG, L.E., SMITH, A.G. & SMITH, D.G. 1990. *A geological time scale 1989*. New York: Cambridge University Press, 263 pp.
- HATZFELD, D., MARTINOD, J., BASTET, G. & GAUTIER, P. 1997. An analog model for the Aegean to describe the contribution of gravitational potential energy. *Journal of Geophysical Research*, **102**, 649–659.
- HERRON, E.M. & TUCHOLKE, B. 1976. Sea floor magnetic patterns and basement structure in the southeastern Pacific. In HOLLISTER, C.D. & CRADDOCK, C., eds. *Initial Reports of the Deep Sea Drilling Project*, **35**, 263–278.
- JEFFERS, J.D., ANDERSON, J.B. & LAWVER, L.A. 1991. Evolution of the Bransfield Basin, Antarctic Peninsula. In THOMSON, M.R.A., CRAME, J.A. & THOMSON, J.W., eds. *Geological evolution of Antarctica*. New York: Cambridge University Press, 481–485.
- KELLER, R.A. & FISK, M.R. 1992. Quaternary marginal basin volcanism in the Bransfield Strait as a modern analogue of the southern Chilean ophiolites. In PARSON, L.M., MURTON, B.J. & BROWNING, P., eds. *Ophiolites and their modern oceanic analogues*. Geological Society Special Publication, No. 60, 155–169.
- KELLER, R.A., FISK, M.A., WHITE, W.M. & BIRKENMAJER, K. 1992. Isotopic and trace element constraints on mixing and melting models of marginal basin volcanism, Bransfield Strait, Antarctica. *Earth and Planetary Science Letters*, **111**, 287–303.
- KELLER, R.A., FISK, M.A. & WHITE, W.M. 1991. Geochemistry of Quaternary volcanism in the Bransfield Strait and South Shetland Islands: preliminary results. *Antarctic Journal of the United States*, **26**(5), 132–133.
- KLEPEIS, K.A. & LAWVER, L.A. 1996. Tectonics of the Antarctic-Scotia plate boundary near Elephant and Clarence islands, West Antarctica. *Journal of Geophysical Research*, **101**, 20 211–20 231.
- LARTER, R.D. & BARKER, P.F. 1991. Effects of the ridge crest-trench interaction on Antarctic-Phoenix spreading: forces on a young subduction plate. *Journal of Geophysical Research*, **96**, 19 583–19 607.
- LAWVER, L.A., KELLER, R.A., FISK, M.R. & STRELIN, J.A. 1995. Bransfield Strait, Antarctic Peninsula: active extension behind a dead arc. In TAYLOR, B., ed. *Backarc basins: tectonics and magmatism*. New York: Plenum, 315–342.
- LAWVER, L.A., SLOAN, B.J., BARKER, D.H.N., GHIDELLA, M., VON HERZEN, R.P., KELLER, R.A., KLINKHAMMER, G.P. & CHIN, C.S. 1996. Structure of the Bransfield Strait marginal basin, Antarctic Peninsula, based on multi-beam bathymetry: evidence for active extension. *GSA Today*, **6**, 1–6.
- LIVERMORE, R., BALANYA, J.C., MALDONADO, A., MARTÍNEZ, J.M., RODRÍGUEZ-FERNÁNDEZ, J., SANZ DE GALDEANO, C., GALINDO, J., JABALOY, A., BARNOLAS, A., SOMOZA, L., HERNÁNDEZ-MOLINA, J., SURIÑACH, E. & VISERAS, C. 2000. Autopsy on a dead spreading center: the Phoenix Ridge, Drake Passage, Antarctica. *Geology*, **28**, 607–610.
- MALDONADO, A., ALDAYA, F., BALANYA, J.C., GALINDO-ZALDÍVAR, J., JABALOY, A., LARTER, R.D., RODRÍGUEZ-FERNÁNDEZ, J., ROSSANOV, M. & SANZ DE GALDEANO, C. 1994. Cenozoic continental margin growth patterns in the north Antarctic Peninsula. *Terra Antarctica*, **1**, 311–314.
- MARTINOD, J., HATZFELD, D., BRUN, J.P., DAVY, P. & GAUTIER, P. 2000. Continental collision, gravity spreading, and kinematics of Aegea and Anatolia. *Tectonics*, **19**, 290–299.
- MUÑOZ-MARTÍN, A., CATALÁN, M., MARTÍN-DÁVILA, J. & CARBÓ, A. 2005. Crustal structure of Deception Island area (Bransfield Strait, Antarctica) from gravity and magnetic modelling. *Antarctic Science*, **17**, 213–224.
- PELAYO, A.M. & WIENS, D.A. 1989. Seismotectonic and relative plate motion in the Scotia Sea Region. *Journal of Geophysical Research*, **94**, 7293–7320.

- PETERSEN, S., HERZIG, P.M., SCHWARZ-SCHAMPERA, U., HANNINGTON, M.D. & JONASSON, I.R. 2004. Hydrothermal precipitates associated with bimodal volcanism in the Central Bransfield Strait, Antarctic. *Mineralium Deposita*, **39**, 358–379.
- PRIETO, M.J., CANALS, M., ERCILLA, G. & DE BATIST, M. 1998. Structure and geodynamic evolution of the Central Bransfield Basin (NW Antarctica) from seismic reflection data. *Marine Geology*, **149**, 17–38.
- REY, J., SOMOZA, L. & MARTÍNEZ-FRÍAS, J. 1995. Tectonic volcanic and hydrothermal event sequence on Deception Island (Antarctica). *Geo-Marine Letters*, **15**, 1–8.
- SANTANACH, R., PALLÁS, F., SÁBAT, F. & MUÑOZ, J.A. 1992. La fracturación en la Isla Livingston, Islas Shetland del Sur. In LÓPEZ-MARTÍNEZ, J., ed. *Geología de la Antártida Occidental*. Simposios T-III. Salamanca: III Congreso Geológico de España y VIII Congreso Latinoamericano de Geología, 141–151.
- SELL, I., POUPEAU, G., GONZÁLEZ-CASADO, J.M. & LÓPEZ-MARTÍNEZ, J. 2004. A fission-track thermochronological study of King George and Livingston Islands, South Shetland Islands (West Antarctica). *Antarctic Science*, **16**, 191–197.
- TAYLOR, B., GOODLIFFE, A.M. & MARTÍNEZ, F. 1999. How continents break up: insight from Papua New Guinea. *Journal of Geophysical Research*, **104**, 7497–7512.
- TEYSSIER, C., TIKOFF, B. & MARKLEY, M. 1995. Oblique plate motion and continental tectonics. *Geology*, **23**, 447–450.
- VANNESTE, L.E., LARTER, R.D. & SMYTHE, D.K. 2002. Slice of intra-oceanic arc: insights from the first multichannel seismic reflection profile across the South Sandwich island arc. *Geology*, **30**, 819–822.
- WELLNER, J.S., LOWE, A.L., SHIPP, S.S. & ANDERSON, J.B. 2001. Distribution of the glacial geomorphic features on the Antarctic continental shelf and correlation with substrate: implications for ice behavior. *Journal of Glaciology*, **47**, 397–411.



**Anexo II:**

**Artículo de difusión: “La importancia de comprender el registro climático en Sudamérica”.**

## La importancia de comprender el registro climático en Sudamérica

**Palabras clave:** Calentamiento global, registros en hielo, Sudamérica.

La importancia de ampliar y estudiar el registro climático de Sudamérica es clave para dilucidar uno de los cuestionamientos más importantes de la ciencia paleoclimática actual. Esta disciplina tiene como uno de sus focos comprender los cambios climáticos globales bruscos que podrían tener un insospechado efecto en la civilización moderna. El potencial de obtener buenos y amplios registros en Sudamérica es muy grande. Sin ir más lejos, en el extremo sur de Sudamérica existen dos campos de hielo llamados Campos de Hielo Norte y Sur, los cuales gracias a que su sistema hidrológico (lagos, ríos y glaciales) es muy sensible a los cambios climáticos globales (ya que registra de manera excepcional las fluctuaciones climáticas) y son un foco de interés mundial para realizar estudios climáticos y paleoclimáticos.

**Key word:** Global warming, Ice Record, South American.

The importance of widening and studying the South American climatic record is key to elucidate one of the most important questions of paleoclimatology in the present. This discipline is focused in understanding sudden climatic changes that may have unexpected effects in our modern civilization. The chance of getting good and complete records in South America is considerable. As a matter of fact, in the very south of the continent there are two ice fields named North and South, which, due to their hydrological system (lakes, rivers, glaciers), are very sensitive to global climatic changes (since they record in an exceptional way climatic variations) and are a focus of worldwide attention in the fields of climatic and paleoclimatic studies.



# La importancia de comprender el registro climático en Sudamérica

## Marcelo Solari

Candidato a Doctor en Ciencias, Mención en Geología.  
Departamento de Geología.  
Facultad de Ciencias Físicas y Matemáticas.  
Universidad de Chile.

### PALEOCLIMA A ESCALA GLOBAL

Considerando los parámetros orbitales de la Tierra en torno al Sol, Milankovitch (1930) postuló una explicación para los cambios climáticos terrestres. Él calculó la influencia combinada de la excentricidad (Figura 1A, ciclo de 100.000 años y 413.000 años), la oblicuidad (Figura 1B, ciclo de 41.000 años) y la precesión de los equinoccios (Figura 1C, ciclo de 23.000 años) en la cantidad de radiación solar y calor recibida por la Tierra en diferentes latitudes, durante el último millón de años (Fig. 1). Posteriores estudios de registros isotópicos estables de oxígeno en testigos de sedimentos marinos permiten suponer que las variaciones climáticas cíclicas observadas se pueden explicar por los cambios de calor cíclicos postulados en la teoría orbital de Milankovitch (Lambeck *et al.*, 2003, Zachos *et al.* 2001).

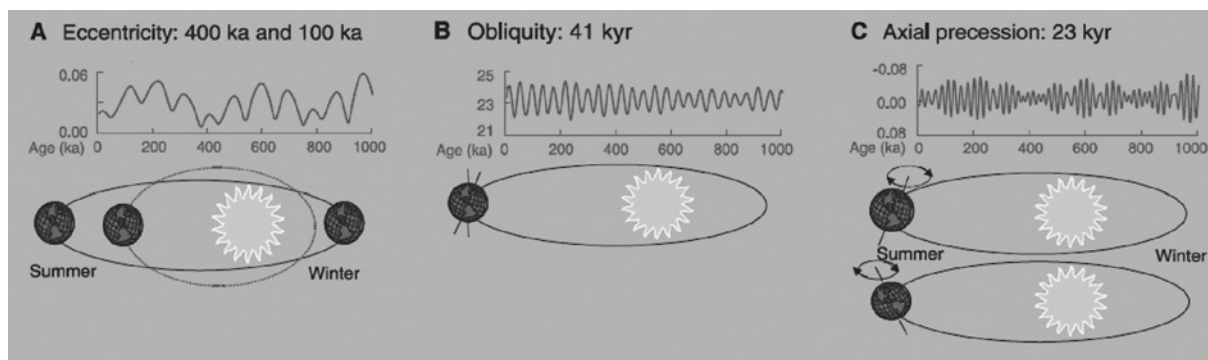


Fig. 1: Parámetros orbitales de la Tierra en torno al Sol considerados en los Ciclos de Milankovitch. A. La excentricidad se refiere a la forma en que la Tierra orbita en torno al Sol, varía de circular a elíptica (ciclo de 100.000 años y 413.000 años). B. La oblicuidad se refiere al ángulo de inclinación del eje de la Tierra relativo a la elíptica y varía entre  $21,1^{\circ}$  y  $24,5^{\circ}$ . Un alto ángulo de inclinación aumenta el contraste estacional (inviernos más fríos y veranos más cálidos en ambos hemisferios). C. La precesión se refiere al bamboleo del eje de rotación que describe una trayectoria circular en el espacio con un periodo de 23.000 años (Modificado de Zachos *et al.* 2001).

Recientemente, en testigos de hielo obtenidos en la Antártica (EPICA, 2004) y en Groelandia (North Greenland Ice Core Project members, 2004) se pueden ver con claridad los ciclos cada 100.000 años previstos por la teoría orbital. Pero también se detectó cambios irregulares y abruptos en la composición isotópica estable de oxígeno, casi tan grandes como los relacionados a un periodo glacial e interglacial (Fig. 2), pero en el plazo de unos pocos años. Estos son llamados cambios tipo Dansgaard-Oeschger (Dansgaard *et al.*, 1993) y representan cambios de temperatura abruptos en lapsos cortos.

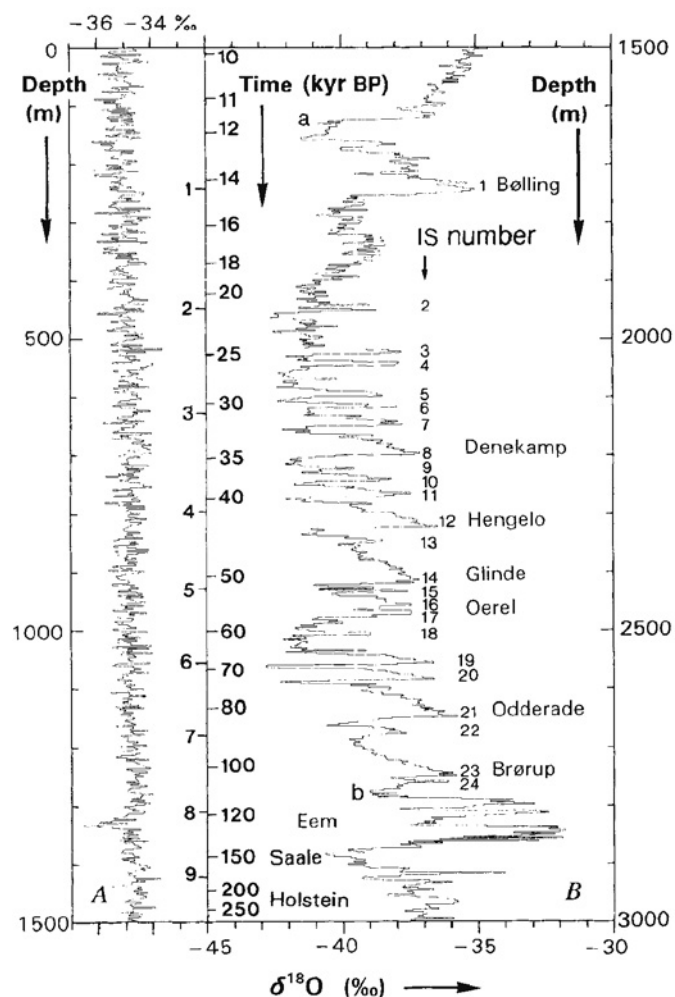


Fig. 2: Registro isotópico de oxígeno estable ploteado en función de la profundidad en metros y el tiempo KyrBp (Kilo años antes del presente, 1950 DC). Interstadios glaciales abruptos son numerados desde el 1 al 24 (Modificado de Dansgaard *et al.*, 1993).

Durante el Cuaternario el periódico intercambio de masas de agua entre el océano y los grandes casquetes de hielo ha sido la contribución dominante para el cambio de nivel del mar durante los últimos ciclos glaciales (Fig. 3). Las edades glaciales corresponden a estadios bajos del nivel del mar y los interglaciales a niveles altos. Lambeck y Champpeil (2001) sintetizaron las diferentes señales obtenidas para cambios del nivel del mar en variadas partes del mundo desde el último máximo glacial (LGM) hasta el presente (Fig. 4).

Desde finales del Pleistoceno hasta el presente se registran dos grandes estadios bajos del nivel del mar (OIS -2 y OIS6) que se correlacionan con los dos últimos máximos glaciales (Fig. 3).

A partir de las relaciones de alzamiento del arrecife y el estudio de muestras de corales fósiles sumergidos, en la península de Huon, Papúa Nueva Guinea, obtuvo un registro del ascenso del nivel del mar desde el último ciclo hasta el presente (Fig. 3 y 4). Pero hay que aclarar que muchas veces sobreimpuesta a la señal global, existen cambios regionales y locales causados por el alzamiento y subsidencia de las zonas costeras o por climas regionales o locales. Dichos cambios glacio-hidro-isostáticos son la causa de la variabilidad espacial del nivel del mar ilustrada en la Fig. 4 (Lambeck y Chappell, 2001).

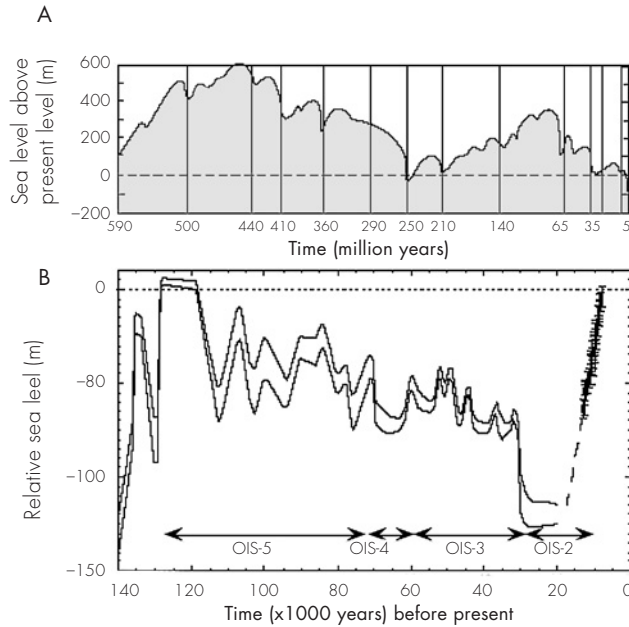


Fig. 3: Variación temporal del nivel del mar en dos escalas de tiempo diferentes (Lambeck y Chappell, 2001): A. Inferida de estratigrafía de secuencias sísmicas; B. Nivel relativo del nivel del mar península de Huon. Inferidos desde la correlación temporal entre el alzamiento y arrecifes de coral fósiles para los pasados 13000 AP y el nivel del mar promedio es estimado para el registro pre-LG.

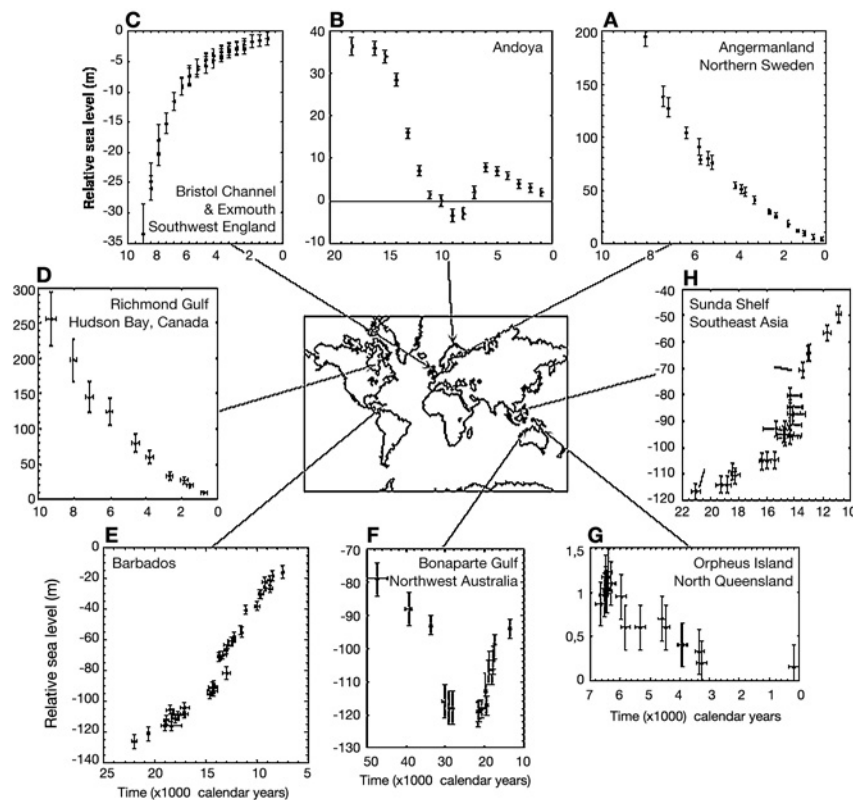


Fig. 4: Variabilidad espacial observada para el cambio relativo del nivel del mar desde el último máximo glacial al presente, diferentes localidades (Lambeck y Chappell, 2001).

## HIPÓTESIS INTERHEMISFÉRICAS MÚLTIPLES

Existen tres grandes grupos de tendencias para explicar el último de los bruscos cambios climáticos tipo Dansgaard-Oeschger (1 Bølling en Fig. 2) que se observan tanto en las señales isotópicas marinas como de hielo. Estas hipótesis toman como base un cambio climático interhemisférico (McCulloch *et al.*, 2000).

Un primer grupo plantea que cambios en el hemisferio Norte dan pie a los cambios en el hemisferio Sur. Se plantea que cambios de temperatura e insolación asociados al ciclo de insolación de Milankovitch generan aguas de fusión derivadas de las plataformas de hielo del hemisferio Norte (Groenlandia), las cuales varían la densidad del agua superficial en el océano Nor-Atlántico, afectando la producción del transporte de aguas oceánicas interhemisféricas y también modificando los patrones de transporte de calor globales a altas latitudes.

Un segundo grupo plantea que cambios en el hemisferio Sur dan pie a los cambios en el hemisferio Norte. Correlaciones recientes entre testigos de hielo en Antártica y Groenlandia (Sowers y Bender, 1995) indican que en el Testigo de Vostok (EPICA) la tendencia de calentamiento comienza antes de la culminación del Último Máximo Glacial en el hemisferio Norte. Utilizando metano atmosférico atrapado en burbujas de aire se determinó que el evento de calentamiento Dansgaard-Oeschger (posterior al LGM) determinado en Groenlandia está retrasado en ca. 2.000 a Cal (años calendario) de su contraparte en Antártica (Blunier *et al.*, 1998). En adición, los testigos de Antártica revelan un evento de Inversión Fría Antártica (ACR, Fig. 5) que precede al equivalente Younger Dryas (YD, Fig. 5) del hemisferio Norte (Blunier *et al.*, 1998).

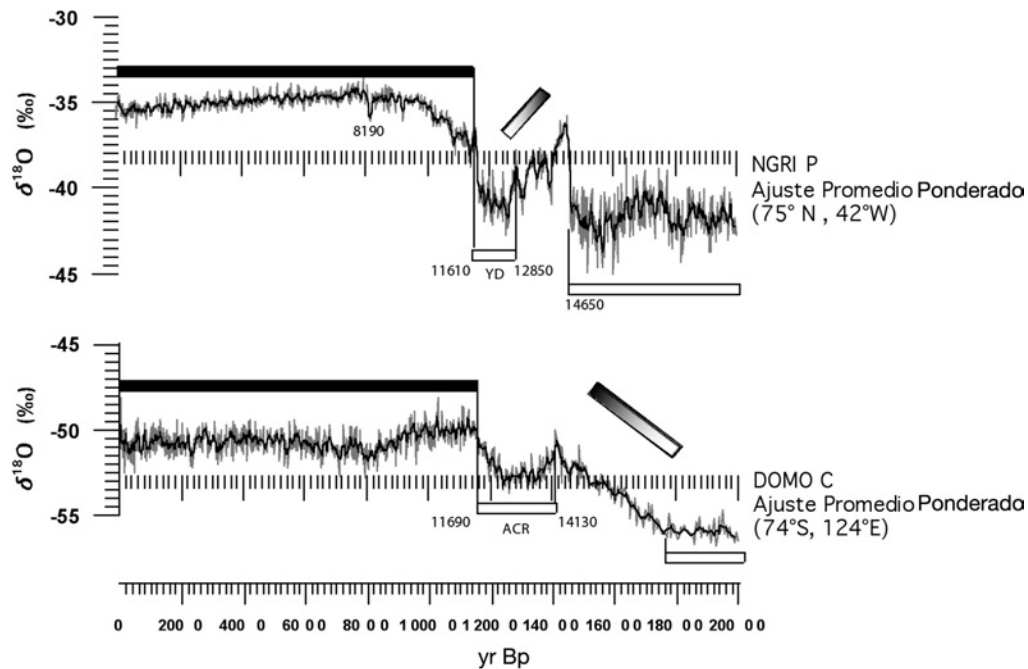


Fig. 5:  $\delta^{18}\text{O}$  (SMOW) en testigos de hielo. Los rectángulos blancos los sectores representan periodos relativamente fríos, los rectángulos negros periodos relativamente más cálidos y los rectángulos con gradientes blancos a negro periodos de transición. (a) Ajuste Promedio Ponderado (línea negra) de los valores de  $\delta^{18}\text{O}$  pertenecientes al testigo de Groenlandia NGRIP (línea gris) (NGRIP dating group (2006), Vinther *et al.*, 2006, Rasmussen *et al.*, 2006, Andersen *et al.*, 2006, Svensson *et al.*, 2006). (b) Ajuste Promedio Ponderado (línea negra) de los valores de  $\delta^{18}\text{O}$  pertenecientes al testigo de Antártica Dome C. (línea gris) (Stenni *et al.*, 2006, Jouzel *et al.*, 2001, Stenni *et al.*, 2001, Schwander *et al.*, 2001, Stenni *et al.*, 2003). Notar que tanto las culminaciones de la Última Glaciación como la regresión fría pre-Holocena (anterior a los ca. 11600 yrBp) ocurren primero en el testigo de Antártica que en el de Groenlandia.

El tercer grupo postula que los cambios climáticos ocurren sincrónicos en ambos hemisferios y se basa en el estudio de las fluctuaciones glaciares y cambios paleoecológicos asociados. Trabajos en la Región de Los Lagos (Chile) y en Nueva Zelandia permitieron a Denton y colaboradores (1999) tener un registro temporal de las fluctuaciones glaciares, las cuales permiten correlacionar con el evento Dansgaard-Oeschger en la región del Atlántico del Norte (Lowell *et al.*, 1995; Denton *et al.*, 1999). La buena correlación entre ambos sets implica una simetría interhemisférica de la estructura y momento de la transición glacial-interglacial. Estas conclusiones se soportan en evidencia de eventos equivalentes del Younger Dryas en Ecuador (Clapperton *et al.*, 1997) y Nueva Zelandia (Denton y Hendy, 1994; Ivy-Ochs *et al.*, 1999). Análisis recientes de evidencias geomorfológicas glaciales en el Domo de Taylor en el flanco de la plataforma del mar de Ross (Steig *et al.*, 1998) soportan esta hipótesis de un cambio climático sincrónico interhemisférico.

## CAMPOS DE HIELO SUR

En el extremo sur de Sudamérica existen dos campos de hielos llamados Campos de Hielo Norte y Sur. Campos de Hielo Sur (CHS) es un plató de hielo que se desarrolla en latitudes medias templadas entre los 48° y 51°S; se extiende a lo largo de los 73° 30' W, posee un área aproximada de 13.000 km<sup>2</sup> y una elevación que varía entre los 500 y 2.000 metros con picos que alcanzan e incluso exceden los 3.000 metros (Carrasco *et al.*, 2002).

CHS es la segunda gran masa de hielo en el hemisferio Sur luego de Antártica. En ella, más de 48 glaciares se descargan en fiordos en el lado oeste y en lagos en el lado este (Carrasco *et al.*, 2002). Los glaciares que nacen en los campos de hielo son templados con altas tasas de ablación<sup>1</sup> y bajas velocidades de flujo.

Varios estudios indican que las grandes extensiones de hielo como Campos de Hielo Sur son sensibles al impacto del calentamiento global y al aumento de los gases de invernadero. El retroceso generalizado de CHS puede obedecer al calentamiento troposférico detectado al sur de Sudamérica en las últimas décadas (Ibarzabal y Donángelo *et al.*, 1996).

La existencia particular de los CHS en condiciones de bajas latitudes templadas y en una topografía con una altura promedio de cerca de 2.000 metros se puede explicar debido a:

- a. La gran cantidad de días nublados (ca. 70%) y eventos de precipitación a lo largo del año, que son el resultado de los vientos predominantes desde el oeste (vientos promedio durante junio y julio) y a los sistemas frontales (Carrasco *et al.*, 2002). La distribución espacial del régimen de precipitación está dada por una alta precipitación anual en el lado oeste cercana a 7.000 mm en la costa y 10.000 mm sobre los campos de hielo (D.G.A, 1987). Esa cantidad rápidamente decrece hacia el este de los Andes Patagónico donde la precipitación media anual es menor a 400 mm (Carrasco *et al.*, 1998, Ibarzabal y Donángelo *et al.*, 1996).
- b. La baja altitud de la línea de nieves que varía desde los 500 metros cerca del océano Pacífico a 1.500 metros al este de la cordillera de los Andes Patagónica (Clapperton, 1994).

Datos adquiridos en diferentes estaciones meteorológicas en las vecindades de los CHS indican que el comportamiento de la temperatura revela diferencias en las estaciones cercanas a la costa, que son influenciadas por el océano Pacífico y las estaciones dentro del continente que experimentan una mayor variación de temperatura invernal-estival (Carrasco *et al.*, 2002). El ascenso lineal de la temperatura cercana a la superficie durante los últimos 100 años en las vecindades de los CHS es entre 1.3 y 2.0° C basado en el periodo de homogeneización entre los años 1933 y 1992 (Carrasco *et al.*, 2002). Se utiliza el nivel de

1. Ablación Glaciar: Pérdida de masa de hielo de un glaciar por sublimación, fusión y/o desmembramiento.



presión atmosférica de 850 hPa para el cálculo de la variación de temperatura anual, ya que se encuentra sobre los 1.350 metros sobre el nivel del mar y la elevación promedio de campos de hielo es de 1.336 metros (Casassa y Rivera, 1999). Reanálisis de los datos observados en la estación de Punta Arenas permiten proyectar los datos desde el año 1977 hasta 1958, obteniendo un ascenso de la temperatura de 0,98° C desde 1958. El calentamiento de la atmósfera a 850 hPa (ca. de 1.350 m.s.n.m.) en Punta Arenas desde 1977 en verano e invierno por año es de  $-0,0224^{\circ}$  y  $0,0455^{\circ}$  C yr<sup>-1</sup> (en 22 años  $-0,45^{\circ}$  y  $1^{\circ}$  C), respectivamente. Esto indica que el calentamiento promedio anual es producido principalmente por el calentamiento de los inviernos (Carrasco *et al.*, 2002).

### ¿POR QUÉ ESTUDIAR EL REGISTRO CLIMÁTICO AL SUR DE SUDAMÉRICA?

Existen evidencias palinológicas<sup>2</sup> (Moreno *et al.*, 1999, Lumley y Switsur, 1993, McCulloch y Davies, 2001) que indican que en la zona austral de Sudamérica el calentamiento posterior al Último Máximo Glacial (LGM) se desarrolló en tres etapas (Fig. 6). La primera ocurrió con posterioridad al evento glacial desarrollado entre los 14600-14300 C<sup>14</sup> yrBp (17500-17150 cal a) y afectó a todas las latitudes (Fig. 6 a). La segunda ocurrida entre 13000-12700 C<sup>14</sup> AP es clara en la Región de Los Lagos, mientras la tercera etapa ocurre alrededor de los 10000 C<sup>14</sup> yrBp (11450 cal. a) y se desarrolla principalmente al sur de la Región de Los Lagos (McCulloch *et al.*, 2000).

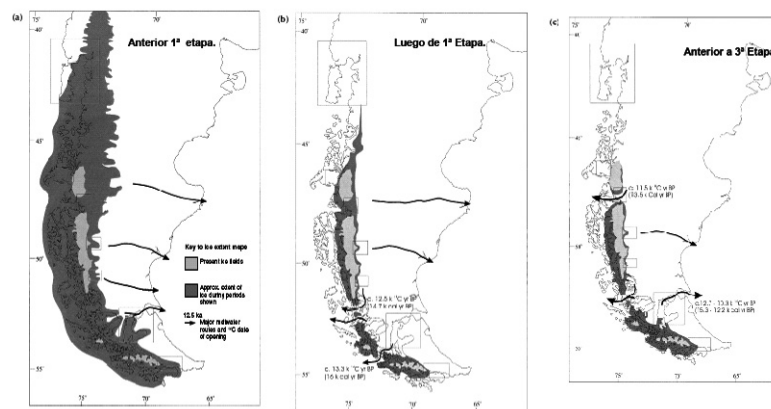


Fig. 6: Reconstrucción glacial por McCulloch y colaboradores (2000):  
 (a) Extensión glacial anterior al calentamiento que comienza ca. 14600 y 14300 C<sup>14</sup> AP. en los perfiles de polen.  
 (b) Extensión glacial luego del evento de los 14600 y 14300 C<sup>14</sup> AP.  
 (c) Extensión glacial anterior al evento cálido que comienza ca. 10000 C<sup>14</sup> AP.

El registro climático de la porción sur de Sudamérica tiene el potencial de dilucidar las múltiples hipótesis que toman como base un cambio climático interhemisférico para explicar los cambios climáticos bruscos tipo Dansgaard-Oeschger. En el área se desarrolla la célula atmosférica de latitud media (célula de Ferrel) y se da origen al cinturón de Vientos Predominantes del Oeste (VPO), los cuales responden a los cambios en su localización e intensidad en función del gradiente de presiones entre la zona de altas presiones subtropicales y bajas presiones subpolares. Se cree que durante los episodios glaciales el núcleo de los VPO migró hacia el norte a latitudes de 45-50° S, brindando las condiciones de humedad y frío necesarias

2. Palinología: Ciencia botánica que estudia el polen y esporas, vivas y fósiles. Permite desde una perspectiva ecológica contribuir a desarrollar interpretaciones paleoambientales.

para que los Andes en la Región de Los Lagos, cerca de la latitud 41° S, se glaciara (Hubbard, 1997; Denton *et al.*, 1999). Al mismo tiempo, más al sur, en la Región de Magallanes (50-55° S) se redujo la caída de nieve y la expansión de los glaciares fue proporcionalmente menor (Hulton *et al.*, 1994). Luego del último ciclo glacial los VPO retornaron a su actual latitud.

Comprender con mayor precisión la naturaleza y el tiempo de la migración de los VPO es clave para dilucidar las hipótesis interhemisféricas enunciadas en los párrafos anteriores. Una reconstrucción de la migración de los VPO solo es posible en la medida que se estructuren nuevos registros de las fluctuaciones glaciales y paleoecológicas que reflejen cambios latitudinales de la distribución de temperatura y precipitaciones.

En conclusión, un importante acierto que evoca un esfuerzo de la comunidad científico mundial, es comprender lo mejor posible los reajustes espaciales y temporales de las diferentes células atmosféricas y la circulación oceánica. Ello permitiría comprender mejor cómo la atmósfera y la hidrosfera se comportan frente a los cambios climáticos de primer orden impuestos por los fenómenos solares y orbitales terrestres y también frente a los enigmáticos cambios climáticos bruscos tipo Dansgaard-Oeschger.

## REFERENCIAS

- Andersen, K.K., Svensson, A., Johnsen, S.J., Rasmussen, S.O., Bigler, M., Röthlisberger, R., Ruth, U., Siggaard-Andersen, M.L., Steffensen, J.P., Dahl-Jensen, D., Vinther, B.M., Clausen, H.B., 2006. The Greenland Ice Core Chronology 2005, 15-42 ka, Part 1: Constructing the time scale, *Quaternary Science Reviews*, vol, 25, Shackleton special issue 24.
- Blunier T, Chappellaz J, Schwander J, Dällenbach A, Stauffer B, Stocker TF, Raynaud D, Jouzel J, Clausen HB, Hammer CV, Johnsen SJ. 1998. Asynchrony of Antarctic and Greenland climate during the last glacial period. *Nature* 394: 739-743.
- Carrasco, J.F., Casassa, G., y Rivera, A., 1998, Climatología actual del Campo de Hielo Sur y posibles cambios por incremento del efecto invernadero, *Anales del Instituto de la Patagonia, Serie Ciencias Naturales*, 26:119-128. a unique Natural Laboratory for Environmental and Climate Changes Studies. Edited by Gino Cassasa *et al.*, Klumer, Academic/ Plenum Publishers, 2002.
- Carrasco, J.F., Casassa, G., y Rivera, A., 2002, Meteorological and Climatological aspect of the Southern Patagonian Icefield. *The Patagonian Icefield*:
- Casassa, G and Rivera, A., 1999, Topografic mass balance model for the Southern Patagonian Icefield, *Abstract International Symposium on the Verification of Criospheric models, Bringing Data and Modeling Scientists Together*, 16-20 August 1999, Zurich, p.44.
- Clapperton C., 1994, The quaternary glaciation of Chile: a review. *Revista de Historia Natural* 67: 369-383.
- Clapperton CM, Hall M, Mothers P, Hole MJ, Still JW, Helmens KF, Kuhry P, Gemmell AMD. 1997. A Younger Dryas ice cap in the equatorial Andes. *Quaternary Research* 47: 13-28.
- EPICA community members, 2004, Eight glacial cycles from an Antarctic ice core. *Nature*, vol 429, p. 623-628.
- Denton GH, Heusser CJ, Lowell TV, Moreno PI, Andersen BG, Heusser LE, Schluöchter C, Marchant DR. 1999. Interhemispheric linkage of paleoclimate during the last glaciation. *Geografiska. Annaler* 81A(2): 107-153.
- Denton GH, Henty CH. 1994. Younger Dryas age advance of Franz Josef glacier in the southern Alps of New Zealand. *Science* 264: 1434-1437.
- D.G.A, 1987, Balance Hídrico de Chile, dirección general de Aguas, Chile.
- North Greenland Ice Core Project members. 2004. High-resolution record of Northern Hemisphere climate extending into the last interglacial period. *Nature*, 431, 147-151.
- Hubbard AL. 1997. Modelling climate, topography and palaeoglacier fluctuations in the Chilean Andes. *Earth Surface Processes and Landforms* 22: 79-92.

- Hulton NRJ, Sugden DE, Payne A, Clapperton CM. 1994. Glacier modeling and the climate of Patagonia during the Last Glacial Maximum. *Quaternary Research* 42: 1-19.
- Ibarzabal y Donángelo, T., Hoffmann, J. A. J., and Naruse, R., 1996, Recent climatic change in southern Patagonian, *Bulletin of Glacier Research*, 14:29-36
- Ivy-Ochs S., Schlüchter C., Kubik PW., Denton GH. 1999. Moraine exposure dates imply synchronous Younger Dryas advances in the European Alps and in the Southern Alps of New Zealand. *Geografiska Annaler* 81A(2): 313-323.
- Jouzel, J., V. Masson, O. Cattani, S. Falourd, M. Stievenard, B. Stenni, A. Longinelli, S.J. Johnsen, J.P. Steffensen, J.R. Petit, J. Schwander, R. Souchez, and N.I. Barkov. 2001. A new 27 ky high resolution East Antarctic climate record. *Geophys. Res. Lett.*, 28 (16): 3199-3202.
- Lambeck, K. and Chappell, J., 2001. Sea Level Change through the Last Glacial Cycle. *Science*, 292, 679-686.
- Lambeck K, Esat T.M., and Potter E.K. 2002. Links between climate and sea levels for the past three million years. *Nature*, 419, 199-206.
- Lowell TV, Heusser CJ, Andersen BG, Moreno PI, Hauser A, Heusser LE, Schlüchter C, Marchant DR, Denton GH. 1995. Interhemispheric correlation of Late Pleistocene glacial events. *Science* 269, 1541-1549.
- Lumley SH, Switsur R. 1993. Late Quaternary chronology of the Taitao Peninsula, southern Chile. *Journal of Quaternary Science* 8: 161-165.
- McCulloch, R.D., Bentley, M.J., Purves, R.S., Hulton, N.R.J., Sugden, D.E. and Clapperton, C.M., 2000: Climatic inferences from glacial and palaeoecological evidence at the last glacial termination, southern South America. *Journal of Quaternary Science*, 15: 409-417.
- McCulloch, R.D. and Davies, S.J., 2001: Late-glacial and Holocene palaeoenvironmental change in the central Strait of Magellan, southern Patagonia. *Palaeogeography, Palaeoclimatology, Palaeoecology*, 173: 143-173.
- Moreno PI., Lowell TV, Jacobson GL Jr, Denton GH. 1999. Abrupt vegetation and climate changes during the last glacial maximum and the last termination in the Chilean Lake District: a case study from Canal de la Puntilla (41°S). *Geografiska Annaler* 81A (2):285-311.
- Milankovitch, M. (1930), *Mathematische Klimahre und Astronomische Theorie der Klimaschwankungen*, Gebruder Borntraeger, Berlin. 176 pp.
- NGRIP dating group, 2006. Greenland Ice Core Chronology 2005 (GICC05), IGBP PAGES/World Data Center for Paleoclimatology Data Contribution Series # 2006-118, NOAA/NCDC Paleoclimatology Program, Boulder CO, USA.
- Schwander J., Jouzel J., Hammer C.U., Petit J.R., Udisti R., Wolff E., 2001. A tentative chronology for the EPICA Dome Concordia ice core. *Geophys. Res. Lett.*, 28 (22): 4243-4246.
- Sowers T, Bender M., 1995. Climate records covering the last deglaciation. *Science* 269: 210-214.
- Steig E.J, Brook E.J, White J.W.C, Sucher C.M, Bender M.L, Lehman S.J, Morse DL, Waddington E.D, Clow G.D. 1998. Synchronous climate changes in Antarctica and the North Atlantic. *Science* 282: 92-95.
- Stenni, B., V. Masson-Delmotte, S. Johnsen, J. Jouzel, A. Longinelli, E. Monnin, R. Rothlisberger, and E. Selmo. 2001. An Oceanic Cold Reversal during the last deglaciation. *Science*, 293: 2074-2077.
- Stenni, B., J. Jouzel, V. Masson-Delmotte, R. Rothlisberger, E. Castellano, O. Cattani, S. Falourd, S.J. Johnsen, A. Longinelli, J.P. Sachs, E. Selmo, R. Souchez, J.P. Steffensen, R. Udisti. 2003. A late-glacial high-resolution site and source temperature record derived from the EPICA Dome C isotope records (East Antarctica), *Earth Planet. Sci. Lett.*, 217: 183-195.
- Stenni, B.; Sachs, J.P.; Selmo, E.; Souchez, R.; Steffensen, J.P.; Udisti, R.; Jouzel, J.; Masson-Delmotte, V.; Rothlisberger, R.; Castellano, E.; Cattani, O.; Falourd, S.; Johnsen, S.J.; Longinelli, A. 2006. EPICA Dome C Stable Isotope Data to 44.8 KYrBP. IGBP PAGES/World Data Center for

Paleoclimatology Data Contribution Series # 2006-112. NOAA/NCDC Paleoclimatology Program, Boulder CO, USA.

- Svensson A, K.K, Andersen, M, Bigler, H,B, Clausen, D, Dahl-Jensen, S,M, Davies, S,J, Johnsen, R, Muscheler, S,O, Rasmussen, R, Röthlisberger, J,P, Steffensen, and B,M, Vinther, 2006. The Greenland Ice Core Chronology 2005, 15-42 ka, Part 2: Comparison to other records, Quaternary Science Reviews, vol, 25, Shackleton special issue 24.
- Vinther, B.M,, H.B, Clausen, S.J, Johnsen, S.O, Rasmussen, K.K, Andersen, S.L, Buchardt, D, Dahl-Jensen, I.K, Seierstad, M,-L, Siggaard-Andersen,J.P, Steffensen, A.M, Svensson, J, Olsen, and J, Heinemeier, 2006, A synchronized dating of three Greenland ice cores throughout the Holocene, Journ, Geophys, Res, vol, 111, D13102, 2006, doi:10.1029/2005JD006921
- Zachos, J., Pagani, M., Sloan, L., Thomas, E. and Billups, K. 2001. Trends, rhythms, and aberrations in global climate 65 Ma to present. Science, 292, 686-693.

**Anexo III:**

**Guía de excursión científica: “Glacio lacustrine evolution and modern microbilites at lago Sarmiento, del toro and Laguna Amarga”.**

# ***GEOSUR 2007***

## **FIELD GUIDE TO**

### **MAIN GEOLOGICAL FEATURES OF EXTRA ANDEAN PATAGONIA AND THE EASTERN SLOPE OF THE ANDES, INCLUDING PALI AIKE AND TORRES DEL PAINE NATIONAL PARKS, SOUTHERN CHILE**



#### **Field Trip Guide of the International Geological Congress on the Southern Hemisphere**

Punta Arenas, Chile  
21/25 November  
2007

Compiled and edited by  
Mauricio Calderón, Francisco Hervé and Marcelo Solari

**MAIN GEOLOGICAL FEATURES OF EXTRA ANDEAN PATAGONIA AND  
THE EASTERN SLOPE OF THE ANDES, INCLUDING PALI AIKE AND  
TORRES DEL PAINE NATIONAL PARKS, SOUTHERN CHILE**

CONTENTS

**DAY 1:** pages 1 – 8

THE PALI AIKE VOLCANIC FIELD AND MORRO CHICO VOLCANIC  
NECK IN SOUTHERNMOST CHILE

*Charles R. Stern*

**DAY 2:** pages 9 – 27

THE LATE CRETACEOUS MAGALLANES FORELAND BASIN IN  
THE ULTIMA ESPERANZA REGION

*Constantino Mpodozis*

**DAY 3A:** pages 28 – 43

THE TORRES DEL PAINE IGNEOUS COMPLEX AND ITS  
CONTACT AUREOLE

*Lukas P. Baumgartner, Jürgen Michel,  
Benita Putlitz, Julien Leuthold, Othmar Müntener,  
Martin Robyr and Bastien Darbellay*

**DAY 3B:** pages 44 – 53

GLACIO LACUSTRINE EVOLUTION AND MODERN MICROBIALITES  
AT LAGOS SARMIENTO, DEL TORO AND LAGUNA AMARGA

*Marcelo Solari and Alessandro Airo*

**DAY 4:** pages 54 – 55

GEOLOGICAL TRANSECT AT SENO ULTIMA ESPERANZA

*Creative Committee*

**References:** pages 56 – 60

This publication contains the description of the localities visited in the field excursions  
of the GEOSUR 2007 in eastern slope of the Patagonian Andes

*Compiled and edited by Mauricio Calderón, Francisco Hervé and Marcelo Solari  
Photo on the front page by Mark Fanning  
Printed in Santiago*



## GLACIO LACUSTRINE EVOLUTION AND MODERN MICROBILITES AT LAGOS SARMIENTO, DEL TORO AND LAGUNA AMARGA

**Marcelo Solari<sup>\*</sup> and Alessandro Airo<sup>\*\*</sup>**

<sup>\*</sup>Departamento de Geología, Universidad de Chile. Mail: msolari@cec.uchile.cl.

<sup>\*\*</sup>School of Earth Sciences, Stanford University. Mail: aairo@stanford.edu.

### Background

The Southern Ice Field (Campo de Hielo Sur) is a large ice plateau developed in a temperate mid-latitude area between 48° y 51° S, on both sides of 73° 30'W longitude. It covers an area of approximately 13,000 km<sup>2</sup>, at an elevation of between 500 and 2000 m, with only a few peaks exceeding 3000 m (Carrasco et al., 2002). More than 48 glaciers advance into fjords to the west and lakes to the east (Carrasco et al., 2002). The glaciers that arise in this ice shield are temperate with high rates of ablation and low flow velocities.

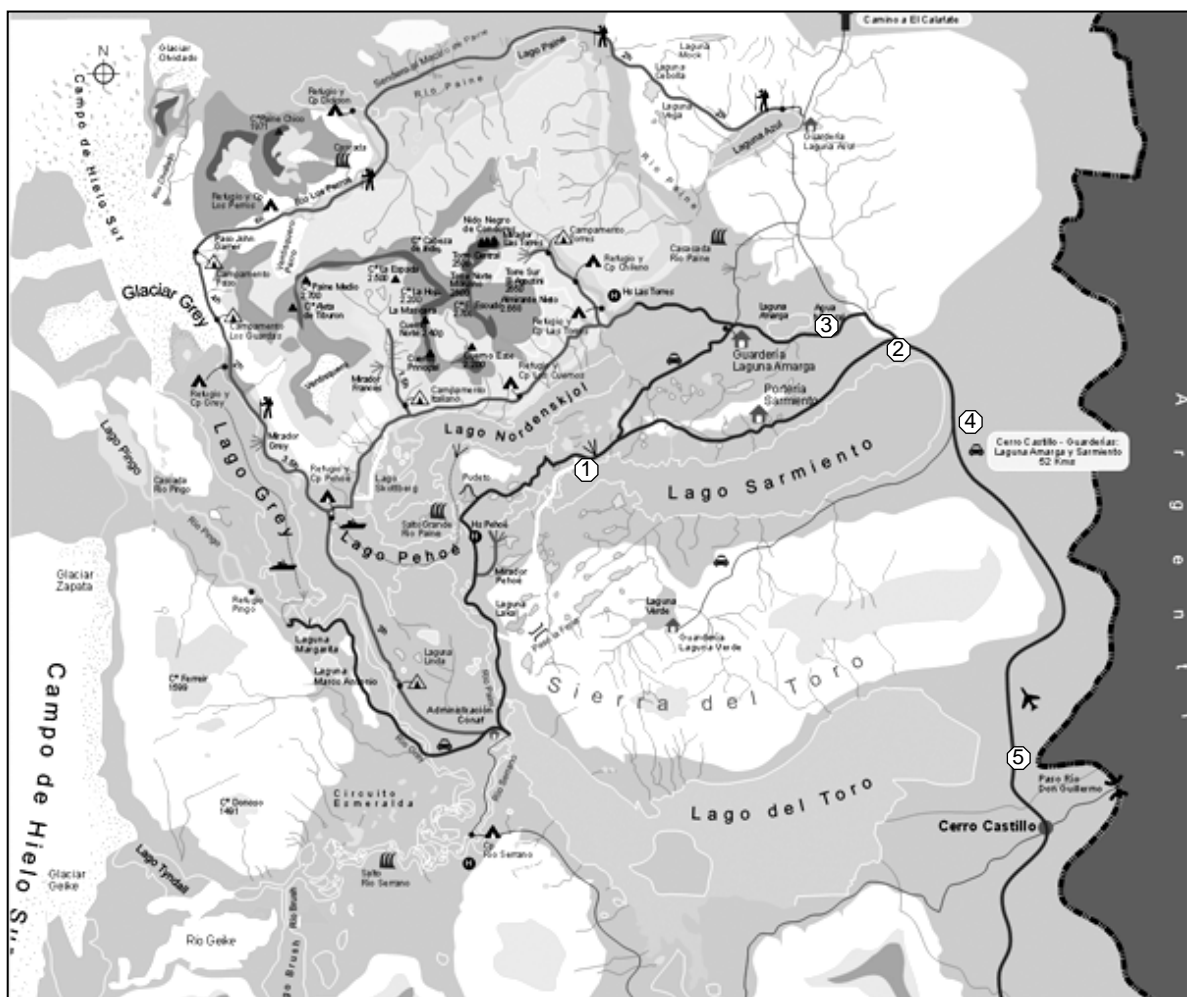


Figure 1: Map of the Torres del Paine National Park with the number of the field guide stops.

The existence of the Southern Ice Field in a temperate low latitude zone and an average elevation of only about 2000 m can be explained as follows: a. The high percentage of cloudy days (ca. 70%) and rainfall throughout the year resulting from the predominantly westerly winds (June-July mean) and frontal systems (Carrasco et al., 2002). The spatial distribution of the rainfall regime is characterized by a high annual precipitation of almost 7,000 mm along the western coastal flank and 10,000 mm over the ice shield itself (D.G.A, 1987). This quantity diminishes rapidly towards the east of the Patagonian Andes where the mean annual rainfall is less than 400 mm (Carrasco et



al., 1998; Ibarzabal y Donángelo et al., 1996); b. The low altitude of the snowline that varies from 500 m near the Pacific Ocean to 1500 m east of the Patagonian Andes (Clapperton, 1994).

The predominantly westerly winds are the main source of water and ice for the Southern Ice Field and the hydrological system developed to the east of the latter. Therefore, deciphering the glacial fluctuations of the Southern Ice Field and the variation of lake levels around their margins are key factors in understanding Holocene climatic variations (Solari et al., 2007, in preparation). In his seminal work Caldenius (1932) was able to trace the position of most major moraine systems throughout Patagonia and Tierra del Fuego, By teleconnecting glacial lake varves in Patagonia with the Swedish varve chronology of, he attempted to construct a temporal framework for these advances. Caldenius attributed the largest moraine limits to late-glacial stadial events, the Finiglacial, Gotiglacial and the Daniglacial. Subsequent work has demonstrated that, although the mapped limits are broadly correct, the chronology is unresolved between regions and individual lobes of the once-expanded Patagonian ice sheet.

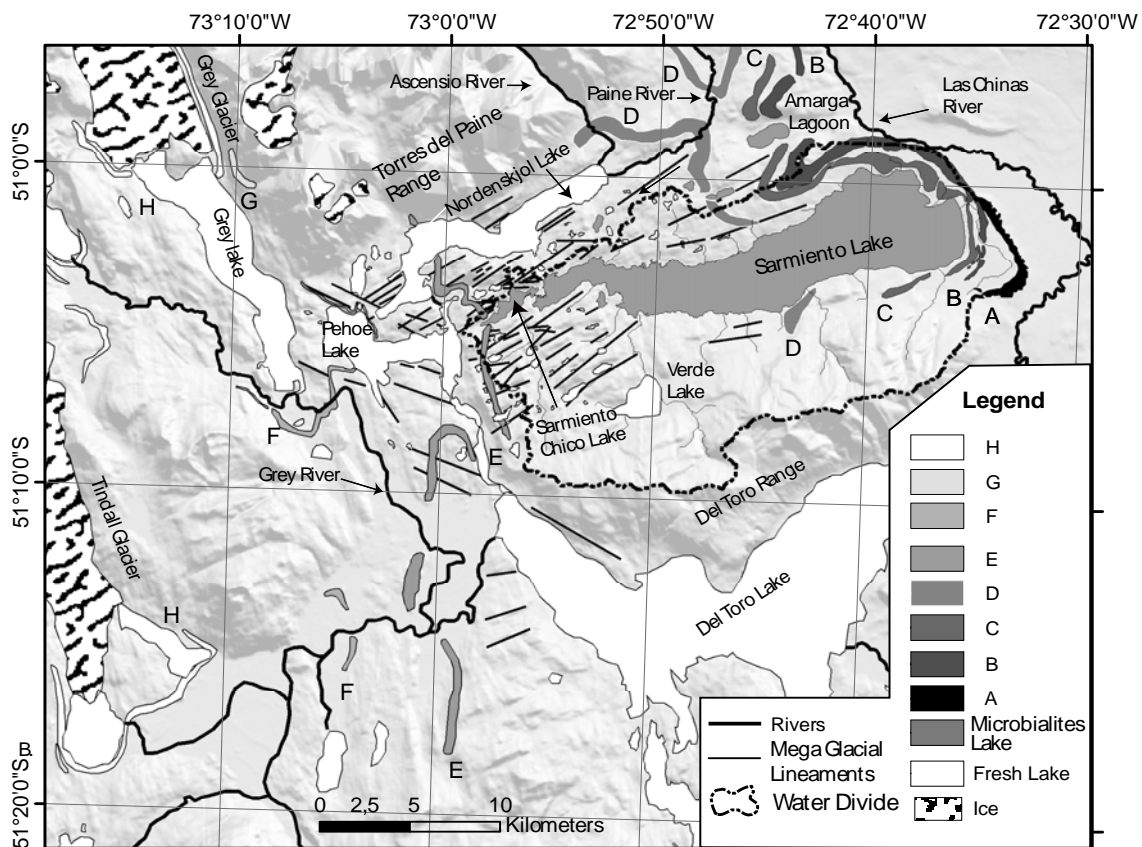


Figure 2: A. Georeferenced Mosaicking of digital elevation model (DEM) obtained from (SRTM) B. Shaded relief image was obtained from Shuttle Radar Topographic Mapping Mission (SRTM 90 m resolution) digital elevation model. The shaded relief show the moraines advanced, the microbialites lakes and the water divide of Sarmiento drainage basin area.

Marden (1993), mapped the glacial landscape of the Torres del Paine district and determined 8 glacial events (labeled from west to east A, B, C, D, E, F, G and H) from the Grey and Tyndall Glaciers to the recent terminal moraines along coastlines of Lakes Sarmiento and Toro (Figure 2). The outer limits (A, B and C) still have no direct dating in Torres del Paine, but they can be correlated with those in the Magellan region where they have been ascribed to the Last Glacial Maximum (LGM, 17–26 kyr) by both radiocarbon dating and cosmogenic exposure dating (McCulloch et al. 2005). Cosmogenic <sup>10</sup>Be dating from erratics of the D moraine indicate a short-lived re-advance of Patagonian ice culminating at 12–15 kyr BP with a mean age of 13.2 ± 0.8 kyr BP, coincident with the time of Antarctic Cold Reverse (ACR, Fogwill, 2005). The minimum radiocarbon age for advance E is 9755 ± 95 C<sup>14</sup> yr BP, based on the dating of the basal part of a peat bog occurring within its limits (Marden and Clapperton, 1995). Two minimum radiocarbon ages for advance F was obtained: 8750 ± 170 C<sup>14</sup> yr BP from basal organic bog sediments inside

the moraine limits (Marden and Clapperton, 1995) and  $9180 \pm C^{14}$  yr BP obtained from basal organic sediments close to the inferred advance limits (Stern, 1990). Age control for advance G has not been obtained, but the advance may be correlated (Marden and Clapperton, 1995) with the Patagonian neoglacial advances (Mercer, 1976). The age of advance H was determined by counting the annual rings of trees that colonised the moraines in the vicinity of Grey Glacier (Armesto et al., 1992). The age of the oldest tree (*Nothofagus Pumilio*) was estimated at 232 yr. It appears that the most extensive phase of advance H at the Grey Glacier culminated at ca. 1600-1700 AD and seems to be associated with the Little Ice Age (Marden and Clapperton, 1995).

### Stop 1. Paleo Lacustrine Lake Level of Lago Sarmiento.

Lago Sarmiento and Laguna Amarga is a present day closed basin with a W- E elongated axis and elliptical shape, enclosed by the moraines A,B,C,D,E (Figure 2) and developed over a depleted area composed by deformed rocks of the Cerro Toro Formation, a deep-marine stratigraphy sequence (ej. Beaubouef 2004).

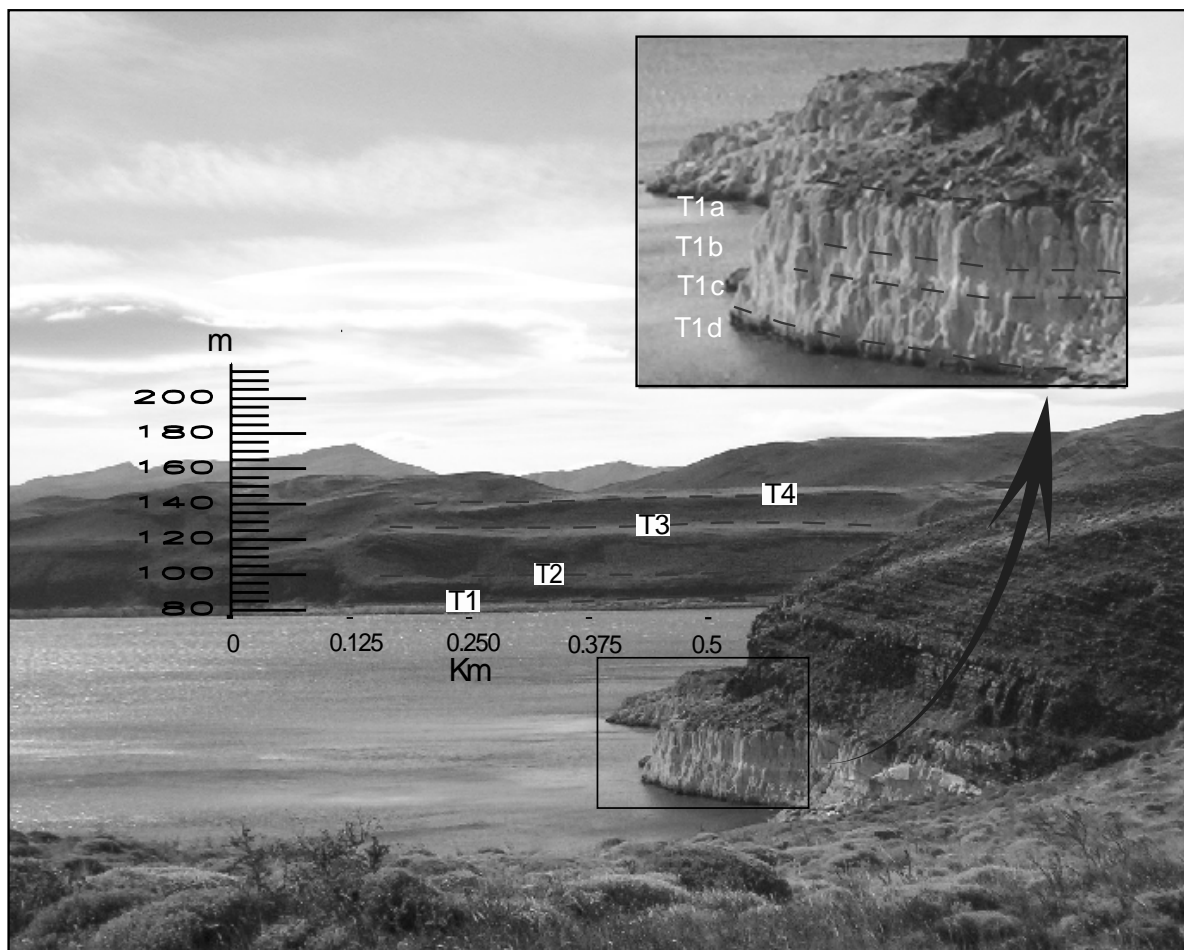


Figure 3: Terraces and change in the colors of the thrombolites give evidence for the fluctuation of the Lago Sarmiento level.

The drainage basin of Lago Sarmiento retains the water and allows no outflow to other bodies of water. The drainage basin has an area of 378, 5219 km<sup>2</sup> (water divide in Figure 2) and many lakes developed into then. Some inlets born From Del Toro Range and one important inlet are produced by Verde Lake that drains into the Lago Sarmiento (Figure 2).

Four abrasion terraces (T1, T2, T3 and T4 in Figure 3) arise along the whole perimeter of the Lago Sarmiento (Figure 4). The terraces T4, T3, T2 and T1 occur at altitude of ca. 138, 121, 100, 85 m.a.s.l., respectively (Solari et al., 2007). The T1 terrace is composed mostly by an eight-meter thick deposit of carbonates, well exposed along nearly the entire coast of the lake. This deposit is composed by sand, aragonite shells of gastropods and filamentous cyanobacterium enclosed by a

clotted calcite magnesian (Mg 0.1Ca 0.9 CO<sub>3</sub> determined through X-ray diffraction). The distinctive clotted structures, observed from macroscopic to microscopic scale, allow classifies these deposits as thrombolites (see below). Four different lake levels, labeled T1a, T1b, T1c and T1d (Figure 3), can be distinguished in the thrombolites. Radiocarbon ages of 1215, 600 and 183 yr (median probability age) were calculated for gastropods into the T1a, T1b and T1c levels, respectively (Solari et al., 2007, in preparation).

### **Microbialites Background**

For at least 3 billion years, microbes were the dominant terrestrial life forms and their build-ups, termed microbialites, provide much of what is known about the early evolution of life. Controversy still surrounds both the identification of microbial structures in the early geologic record and the role of biotic versus abiotic processes in forming putative microbialites of all ages (Schopf, 1993; Lowe, 1994; Brasier et al., 2002). Even where a biological role is strongly suspected, the mechanisms by which microbes influence or control the deposition of sediment and the large- and fine-scale structuring of microbialites remain unclear (Grotzinger and Knoll 1999). Without a clear understanding of how microbialite structure and morphology are related to the environmental and biological setting in which they form, it will not be possible to realize the full potential of microbialites as windows to past biospheres.

Microbialites are "organo-sedimentary deposits that have accreted as a result of a benthic microbial community trapping and binding detrital sediment and/or forming the locus of mineral precipitation" (Burne and Moore, 1987). They have been subdivided into four general types: stromatolites, thrombolites, dendrolites, and travertines (Riding, 1991). Internally laminated microbialites are classified as stromatolites, whereas all other types lack laminations and are classified based on internal fabric: thrombolites have a clotted fabric, dendrolites a dendritic fabric, and travertines a bushy fabric. Most fossil microbialites are stromatolites of Proterozoic age (2,500 to 543 Ma). The decline of microbialites in the late Proterozoic has been inferred to reflect the evolution of grazing animals (Garrett, 1970; Awramik, 1971; Walter and Heys, 1985).

Although the shape of microbialites is controlled by the interplay between benthic microbial communities and their environment, the extent to which each of these factors influences morphology remains unclear (Burne and Moore, 1987). Gebelein (1974) suggested that stromatolite microstructures are largely of biological origin whereas macrostructures are mainly the result of environmental conditions, a conclusion that has been supported by later studies that included thrombolites (Awramik and Vanyo, 1986; Kennard, 1994). Environmental factors include water depth, sedimentation patterns, wave action, currents, migrating shorelines, sunlight (heliotropism), and wind (Logan et al., 1964; Awramik and Vanyo, 1986; Ginsburg, 1991; Laval et al., 2000; Reid et al., 2000). It has also been proposed that changes of the ocean chemistry during Earth history have been responsible for the "evolution" of stromatolitic structures (Grotzinger, 1990). However, despite numerous studies on mostly ancient microbialites, there is not yet a clear understanding of how biological and/or environmental factors actually influences microbialite formation (Ginsburg 1991).

### **Stop 2. Modern thrombolitic microbialites at Lago Sarmiento**

Lago Sarmiento, one of the largest lakes of the Torres del Paine district, southern Chile, has a circumference of about 78, km, a surface of 86.2 km<sup>2</sup> and a maximum depth of 312 m. The region is cold steppe with an annual mean air temperature of 7°C and strong Patagonian winds. Lake water is subsaline (~2.5g NaCl/liter) and around pH 9, reflecting the lack of an outlet: its water chemistry is controlled mainly by input and evaporation. Massive carbonate microbialites are exposed along the shoreline of Lago Sarmiento up to 8 m above the shoreline as a result of a recent drop in water level (Campos, Soto et al. 1994) and similar living microbialites are actively forming within the lake. Internally, these microbialites are composed of non-laminated clotted calcium carbonate and are hence thrombolites. They represent one of the most spectacular occurrence of thrombolites known from modern settings and provide an opportunity to study and compare associated fossil and living microbialites.

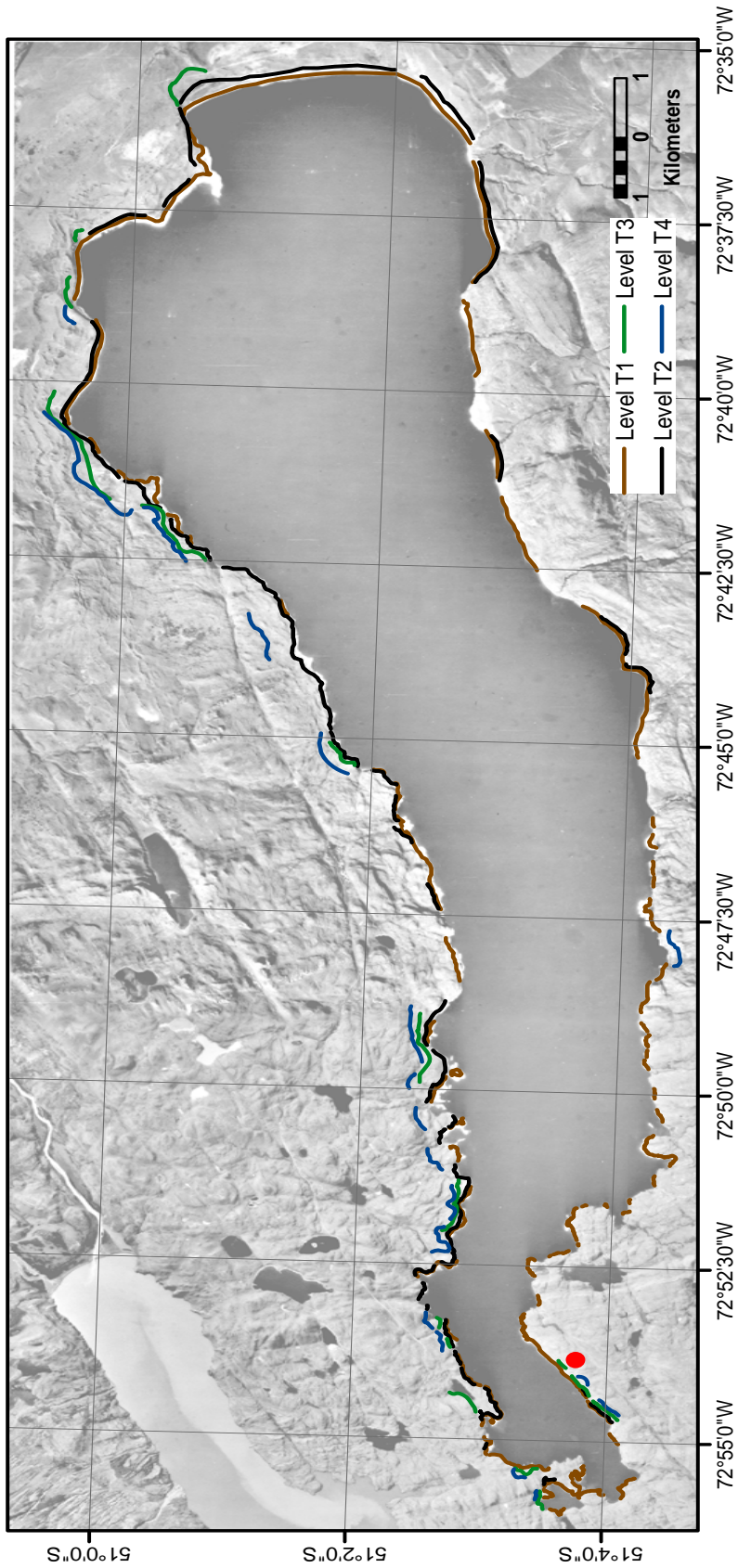


Figure 4: Map of the erosion terraces in the region of the Lago Sarmiento.

Microbialite growth at Lago Sarmiento occurs through carbonate precipitation driven by the photosynthetic activity of a microbial community attached to a solid surface (Airo et al., in preparation). Therefore, microbialite growth correlates with the long-term activity of its surficial microbial mat. Presuming nutrient supply not to be a limiting factor, it can be assumed that light availability and destruction of the mat determine the long-term activity of the mat and consequently also the build-up of the microbialite framework. The amount of available light is at first approximation a function of light attenuation with water depth and shadowing by adjacent obstacles or overlaying sediment. Mat degradation can be due to grazing organisms such as snails or due to physical destruction through sediment abrasion. Although snails are commonly found at the lake bottom, they rarely occur on smaller microbialites and have not been found on microbialites that are taller than 0.5m. Microbialite growth is strongly affected by sediment abundance, grain size, and mobility. Microbialites are rare to absent in areas lacking long-term solid surfaces, such as sandy beaches and stream inlets. In these areas, isolated microbialite build-ups have formed only locally on solid carbonate-cemented beach gravels, large boulders, and bedrock outcrops exposed high enough above the beach surface to not be affected by sediment coverage or abrasion.

### **Field Stop**

Field observations have shown that large-scale microbialite morphologies correlated to the local environmental conditions that were present during their formation (Airo et al., in preparation). In particular, it has been demonstrated that local topography, sediment coverage and abrasion, strong directional water agitation, and light availability take part in controlling the morphological development of microbialites at Lago Sarmiento.

For the field trip we will visit a peninsula located at the northeastern end of Lago Sarmiento. The eastern part of the lake is dominated by glacial deposits that formed during the last glacial cycle when the South Patagonian Ice-field extended through the basin now occupied by Lago Sarmiento. The peninsula is part of these deposits and presumably represents the remains of debris that accumulated between two former glacial lobes. Due to the shallowness and horizontal extent of the peninsula, it is the largest contiguous area of subaerial microbialite exposure at Lago Sarmiento. Furthermore, the subaerially exposed microbialites on the peninsula clearly demonstrate the relationship between their morphological development and their environmental conditions, such as sediment coverage and/or abrasion, strong directional water agitation, and light availability and directionality.

### **Stop 3: Stromatolites of Laguna Amarga.**

The glacial stages D, C and B were identified in the Laguna Amarga Area. The moraine complex B and C cross the Laguna Amarga and continues to the south until the Lago Sarmiento (figure 3). The moraine complex B have many small meltwater channels, but in the east side of the Amarga Basin a big spillway breached the moraine complex B. The drift stage D in the Paine River area is composed by two moraine complex. The southern part of the D complex beginning like a lateral moraine closely to the Ascensio River and continue like a terminal moraine to the middle portion of the Sarmiento (Figure 3). The northern part of the D complex is 1.5 km northward of the southern part of the D moraine complex and has an arc shape with the inflection point in the Valley of Paine River (Figure 2).

The Laguna Amarga, a closed lagoon located at 80 m.a.s.l., has a circumference of about 6.2 km, a surface of ca. 3.2 km<sup>2</sup> and a maximum depth of 4.1 m (Campos et al., 1996). The lagoon is alkaline with a mean pH of 9.1, a mean salinity of 26.1 mg/L and temperature of 11.7 °C, revealed also by the occurrence of a phytoplankton community dominated by Cyanophyceae Aff. *Gloescaspa* and *Artemia* (Campos et al., 1996).

Along the entire coast of the Laguna Anarga, a salt belt, with rare drying cracks (at the west coast), occurs. The lagoon is the habitat for the extensive colonies of modern layered microbialites or stromatolites (Solari et al., in preparation), adhered to the gravel and sand of the lagoon bottom (Figures 5-6). The stromatolites have a nodular, bulbous, layered and dome shapes and consist mostly of aragonite, silica, filamentous cyanobacterium, small crustaceans, sediments and carbonates sediments.





Figure 5: View of a stromatolite stratiform colony with a unique bulbous form over the water in the east shore of Laguna Amarga.

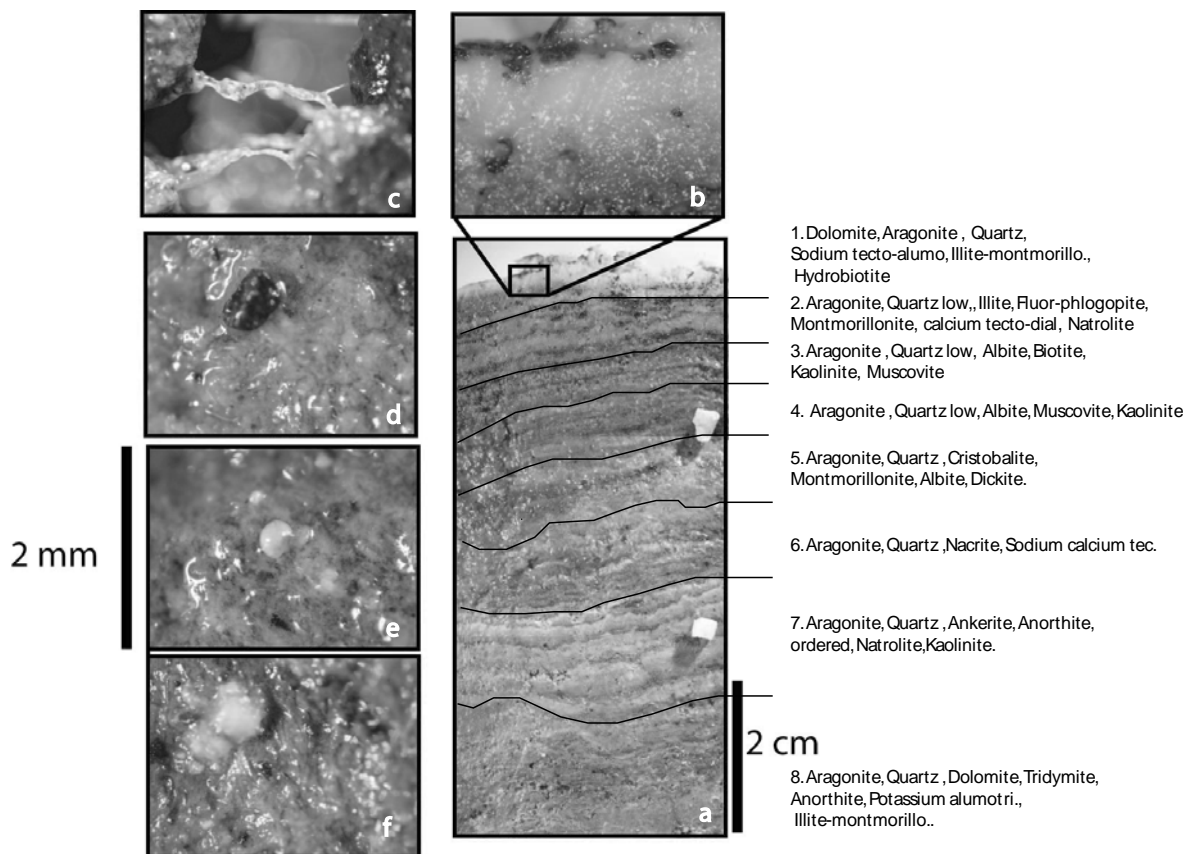


Figure 6: a) Cross section of dome stromatolite with a related column indicating the main minerals detected by XR diffraction. ; b) Superficial carbonate crust; b) Filamentous cyanobacterium c) Sediment d) Small crustacean e) Carbonate fragment rounded by filamentous cyanobacterium. (Solari et al., 2007 in preparation)

The lagoon received contributions of meteoric waters from springs with a Ph of 6.4-7.2. Two chemical measures realized in the water of spring (March 2005 and March 2006) and the meaning of the chemical water lakes dates, published by Campos et al. 1996, be evidence for an enrichment of anions and cations in the lake water respect the concentration detected in the spring water analyses.

**Stop. 4. View of the Lago Sarmiento Moraines**

The eastern shoreline of the Lago Sarmiento is surrounded by three moraines complexes (see limit A, B and C in Figure 7). The moraine complex A has a single convex ridge with 30 m of elevation which diverges from the moraine complex B. The ridge is cover by boulders and has a maximum altitude of ca. 160 m.a.s.l. with ca. 7, 8 km of longitude. The moraine complex B, with a maximum width of ca. 700 m, is composed in some places by six ridges. The outer ridge have 20 m height, is the largest and has a maximum altitude of ca. 150 m.a.s.l. Meltwater channels cut the moraines at different locations and are separated from the moraine complex A by an outwash plane. The moraine complex C consists, in some places, of three ridges that follow the shape of the moraine complex B.

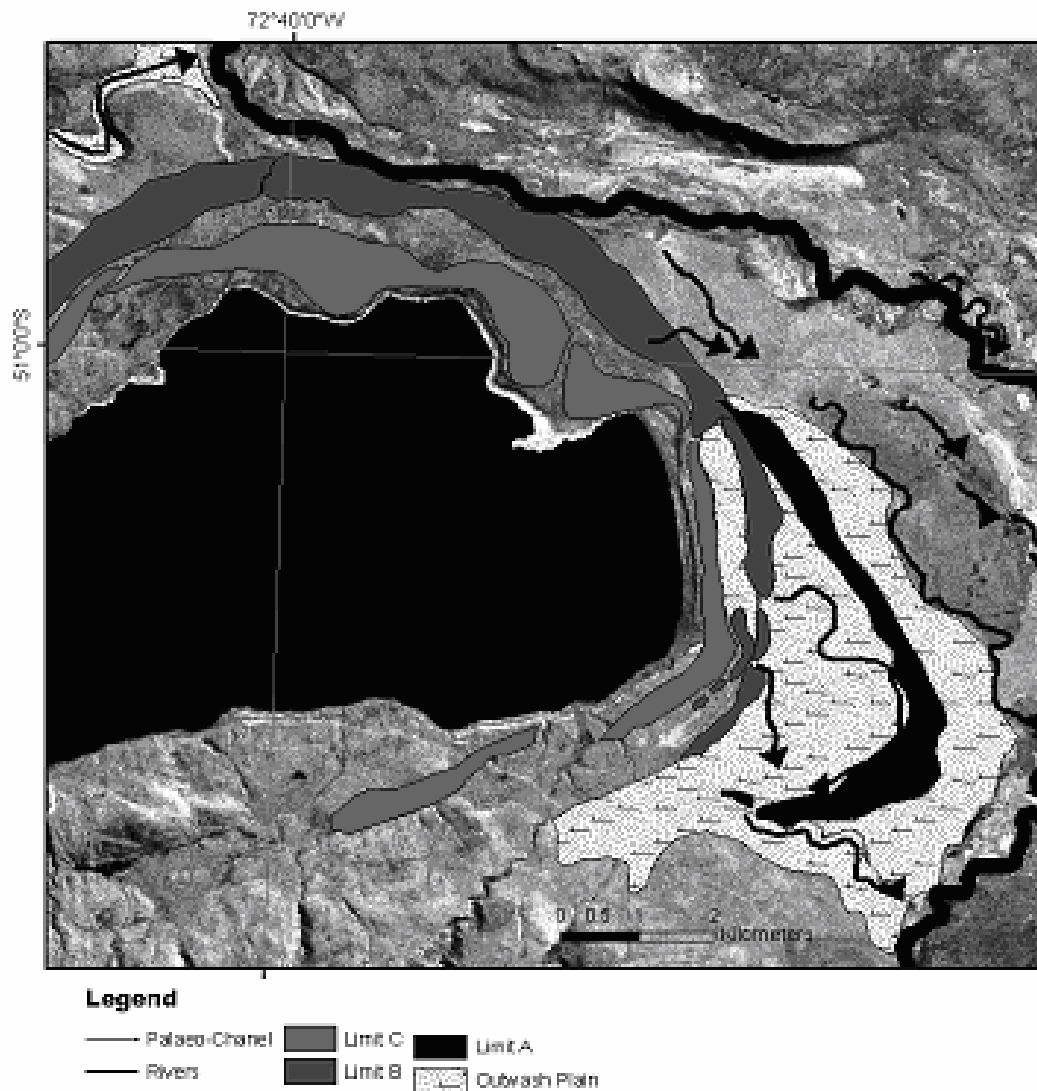


Figure 7: Moraines complex in the east coast of the Sarmiento Lake.

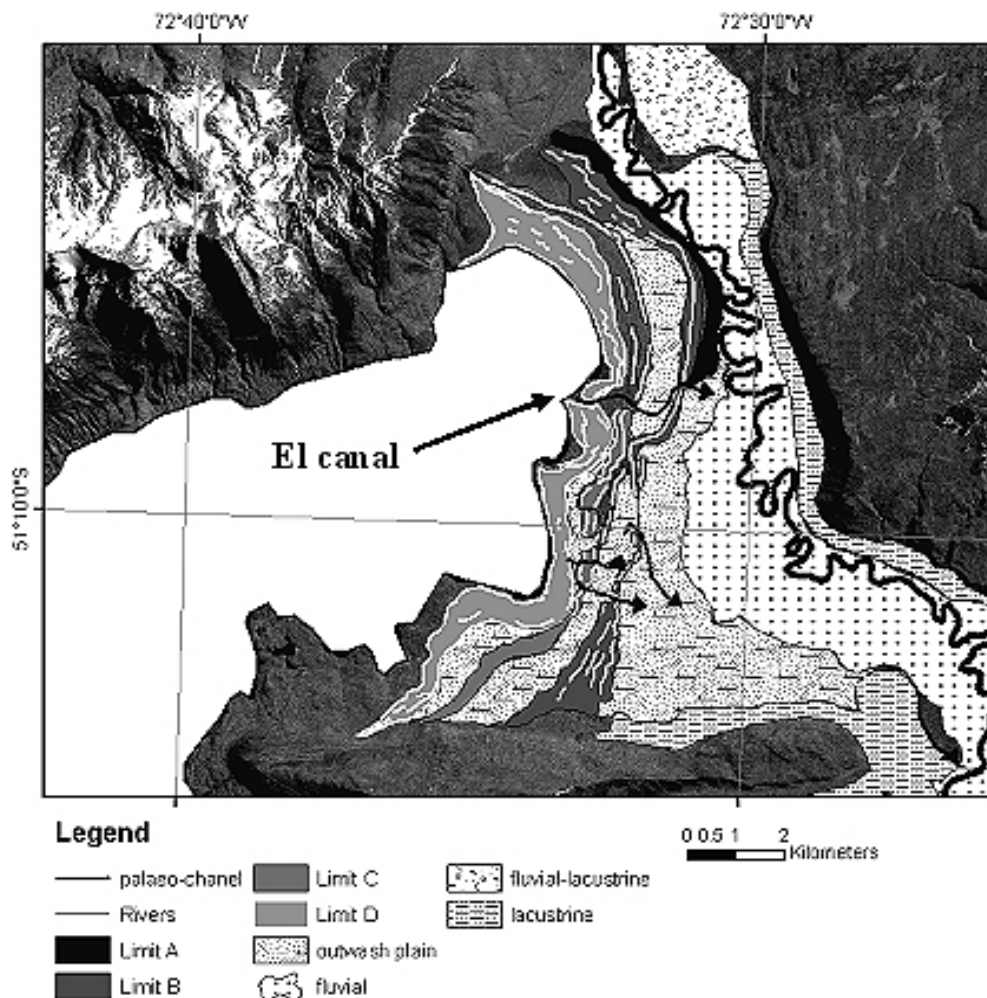


Figure 8: Quaternary deposits in the Lago del Toro. (Solari et al., in prep.)

Shear stress from the overlying glacier seems to have been displaced downward from the ground moraine into more fluid-rich horizons within the lacustrine sediments (Figure 9). This is shown by contorted beds occurring below or cross-cutting undeformed wave-rippled units. Other small-scale deformation structures include recumbent folds in fine to very fine sandstone beds, which locally form rolls or flame-like structures with amplitudes between 5 and 30 cm. Their axial planes dip towards the west. Small, low- to steep-angled reverse faults with cm-scale displacement are also associated with some of these structures.

Large-scale deformation structures consist of stacked thrust faults dipping between 3° and 25° towards the west (Figure 10). The fault planes are sharp with no apparent breccia, which can be attributed to the soft and fluid-rich nature of the sediments at the time of deformation. Below these fault zones are large-scale disharmonic folds in the ground moraine and coarser lake deposits. The folds are chaotic to horseshoe-shaped with multiple injections of sand into moraine along numerous shear planes.

The intensely faulted and sheared zones generally occur below the terminal moraine ridges that traverse the area. This may possibly be attributed to two processes at the glacier front: ablation releasing large volumes of meltwater that infiltrated the directly underlying sediments and provided lubrication for fault movement, or pressure release that enhanced brittle deformation of the underlying deposits.





Figure 9: Deformed layer of silt enclosed by undeformed laminated silt layers.

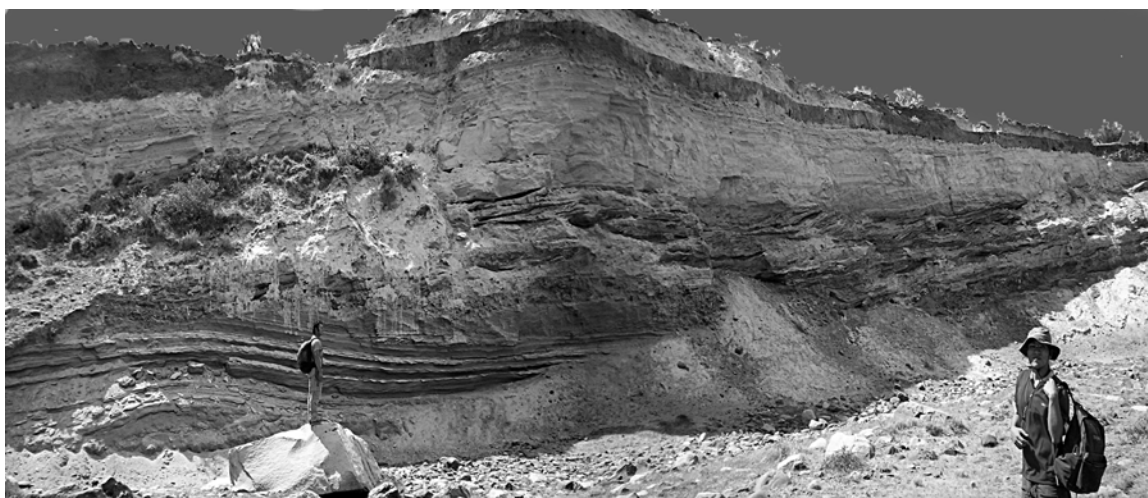


Figure 10: Thrust fault produced during a glacial advance.